

Polish Academy of Sciences  
University of Engineering and Economics in Rzeszów  
University of Life Sciences in Lublin  
Faculty of Production Engineering

# MOTROL

**COMMISSION OF MOTORIZATION AND ENERGETICS  
IN AGRICULTURE**

AN INTERNATIONAL JOURNAL  
ON OPERATION OF FARM  
AND AGRI-FOOD INDUSTRY MACHINERY

Vol. 16, No 8

LUBLIN – RZESZÓW 2014

**Editor-in-chief:** *Eugeniusz Krasowski*  
**Assistant Editor:** *Jerzy Grudziński*

### Associate Editors

1. Agricultural machinery: *Valeriy Dubrovin*, Kiev, *Mariusz Szymanek*, Lublin
2. Machinery of agri-food industry: *Leszek Mościcki*, Lublin
3. Energetics: *Iliia Nikolenko*, Simferopol, *Janusz Wojdalski*, Warszawa
4. Land management, urban planning, construction, architecture and geodesy:  
*Mykhailo Sukach*, Kiev, *Karol Noga*, Kraków, *Roman Kodaj*, Rzeszów,  
*Michał Proksa*, Rzeszów, *Lech Licholaj*, Rzeszów
5. Mathematical, statistics: *Andrzej Kormacki*, Lublin, *Rostislav Bun*, Lviv

### Editorial Board

<i>Dariusz Andrejko</i> , Lublin, Poland	<i>Ignacy Niedziolka</i> , Szczecin, Poland
<i>Andrzej Baliński</i> , Kraków, Poland	<i>Paweł Nosko</i> , Ługansk, Ukraine
<i>Volodymyr Bulgakow</i> , Kiev, Ukraine	<i>Çannadij Oborski</i> , Odessa, Ukraine
<i>Zbigniew Burski</i> , Lublin, Poland	<i>Yurij Osenin</i> , Ługansk, Ukraine
<i>Karol Cupiał</i> , Częstochowa, Poland	<i>Marian Panasiewicz</i> , Lublin, Poland
<i>Valeriy Dyadychev</i> , Ługansk, Ukraine	<i>Sergiy Pastushenko</i> , Mykolaiv, Ukraine
<i>Konstantin Dumenko</i> , Mykolayiv, Ukraine	<i>Vitaliy Ploskiy</i> , Kiev, Ukraine
<i>Dariusz Dzik</i> , Lublin, Poland	<i>Ivan Rohowski</i> , Kiev, Ukraine
<i>Stepan Epoyan</i> , Kharkiv, Ukraine	<i>Józef Sawa</i> , Lublin, Poland
<i>Sergey Fedorkin</i> , Simferopol, Ukraine	<i>Vjacheslav Shebanin</i> , Mykolayiv, Ukraine
<i>Jan Gliński</i> , Lublin, Poland	<i>Pavilas A. Sirvydas</i> , Kaunas, Lithuania
<i>Dmitriy Goncharenko</i> , Kharkiv, Ukraine	<i>Volodymyr Snitynskiy</i> , Lviv, Ukraine
<i>Aleksandr Holubenko</i> , Ługansk, Ukraine	<i>Stanisław Sosnowski</i> , Rzeszów, Poland
<i>LP.B.M. Jonssen</i> , Groningen, Holland	<i>Ludvikas Spokas</i> , Kaunas, Lithuania
<i>Stepan Kovalyshyn</i> , Lviv, Ukraine	<i>Jarosław Stryczek</i> , Wrocław, Poland
<i>Józef Kowalczyk</i> , Lublin, Poland	<i>Aleksandr Sydoruk</i> , Kiev, Ukraine
<i>Volodymyr Kravchuk</i> , Kiev, Ukraine	<i>Beata Ślaska-Grzywina</i> , Lublin, Poland
<i>Petro Kulikov</i> , Kiev, Ukraine	<i>Wojciech Tanaś</i> , Lublin, Poland
<i>Elżbieta Kusińska</i> , Lublin, Poland	<i>Viktor Tarasenko</i> , Simferopol, Ukraine
<i>Andrzej Kusz</i> , Lublin, Poland	<i>Çiorgiy Tayanowski</i> , Minsk, Bielarus
<i>Janusz Laskowski</i> , Lublin, Poland	<i>Leonid Tishchenko</i> , Kharkiv, Ukraine
<i>Nikolaj Lubomirski</i> , Simferopol, Ukraine	<i>Henryk Tylicki</i> , Bydgoszcz, Poland
<i>Kazimierz Lejda</i> , Rzeszów, Poland	<i>Denis Viesturs</i> , Ulbrok, Latvia
<i>Jerzy Merkiś</i> , Poznań, Poland	<i>Dmytro Voytiuk</i> , Kiev, Ukraine
<i>Ryszard Michalski</i> , Olsztyn, Poland	<i>Anatolij Yakovenko</i> , Odessa, Ukraine
<i>Aleksandr Morozov</i> , Simferopol, Ukraine	<i>Oleg Zaitsev</i> , Simferopol, Ukraine
<i>Janusz Mysłowski</i> , Szczecin, Poland	<i>Tadeusz Złoto</i> , Częstochowa, Poland

All the articles are available on the webpage: <http://www.pan-ol.lublin.pl/wydawnictwa/Teka-Motrol.html>

All the scientific papers positive evaluation by independent reviewers

Linguistic consultant: *Mykhailo Sukach*

Typeset: *Dmitro Mischuk*

Cover desing: *Hanna Krasowska-Kolodziej*

Photo on the cover: *Konstantin Dumenko*

Editorial Office address: Polish Academy of Sciences Branch in Lublin

Palac Czartoryskich Plac Litewski str. 2, 20-080 Lublin, Poland

e-mail: [eugenius.krasowski@up.lublin.pl](mailto:eugenius.krasowski@up.lublin.pl)

ISSN 1730-8658

© Copyright by Polish Academy of Sciences 2014

© Copyright by University of Life Sciences in Lublin 2014

© Copyright by University of Engineering and Economics in Rzeszów 2014

In co-operation with Kyiv National University of Construction and Architecture 2014

Edition 100 + 16 egz.

Publishing Office address: KNUCA

Povitroflotskyy prosp., 31, Kyiv, Ukraine, 03680

<http://www.knuba.edu.ua>

## The Principles of Discrete Modeling of Rod Constructions of Architectural Objects

*Petro Kulikov, Vitaliy Ploskiy, Volodymyr Skochko*

Kyiv National University of Construction and Architecture  
Povitroflotskiy prosp., 31, Kyiv, Ukraine, 03680, e-mail: vladimir-skochko@yandex.ru

**Summary.** This article describes the basic principles of rod spatial building constructions modeling by means of discrete geometry. The mathematical dependence that form the basis of this approach are the differential regularities between the geometric and physical parameters of the modeled constructions, as well as the parameters of the external loads which determine the final shape of the model.

**Key words:** geometric modeling, discrete model, mesh structure, rod constructions, differential regularities.

### INTRODUCTION

As is well known, the most common approach to the projecting of any building construction can be conditionally divided into three stages:

1) determination of the shape of future construction;

2) calculation of the internal efforts, acting in the construction as a result of action of different loadings;

3) selection of structural elements that could be able to withstand the load acting therein. Only after that, it is possible to carry out the architectural and construction drawings.

Very often, the disadvantage of this approach is the need for frequent repeating of the first and second stages in order to clarify the shape, since the architect, which invents the concept of a new nonstandard construction, not always can to predict appearance in it of excess tensions. These tensions may cause a malfunction of the whole construction, and even its destruction. Partially described disadvantage is a consequence of the rapid development of numerical methods for

calculation of building constructions. Numerical methods allow us to define the internal forces in constructions and even entire buildings of almost any complexity level (including underground constructions). As a result, the architects more and more neglect the preliminary analysis of designed shapes and rely on engineering solutions of constructors.

However, require special attention spatial rod constructions. In recent years, exactly rod construction form the basis for designing of most large-span erection truss as well as shell coatings and steel cable roof. Moreover, they are successfully used as load-bearing skeletons of buildings and structures. Obviously, that engineering of rod structures requires a special responsibility and accuracy in performing the calculations.

That is why in the design of rod constructions it makes sense to perform the operations of pre-shaping taking into account the external influences that will act on these construction. Apart from external loads, must be taken into account the expected internal forces in the rods of the model.

As an effective tool to perform this pre-shaping can be used the methods of geometric modeling. The modeling process in this

case reduces to constructing of a discrete geometric model of the rod construction taking into account all the external loads and boundary conditions, as well as of its subsequent analysis and correction.

PURPOSE OF WORK

Separate methods of discrete geometric modeling (such as static-geometrical method [1]) allow us to obtain the desired shape of rod constructions based on information about their topology, the value of nodal loads and features of allocation of internal forces in the elements of the model. However, the resulting shape of the model do not always correspond to the expected outward appearance, as it is often the architects have to observe the features of space-planning solutions of the design object and the style of already existing buildings. In consequence of this the shape of the model must be adjusted "by hand", which entails the impossibility of the use of geometric modeling methods and the need to use one of the well-known numerical methods (such as finite element method, finite difference method, and others [2–7]) to further define the internal forces in the system.

All of the above defines the main goals of this work:

- 1) to introduce universal algorithm of rod constructions forming providing the possibility of local changes in its geometry, using the same modeling methodology,
- 2) to demonstrate the mathematical regularities necessary for the implementation of this algorithm.

ANALYSIS OF MAIN PREVIOUS RESEARCHES

One of the most variative and suitable for shaping of rod constructions methods of discrete modeling is a static-geometrical method (SGM). SGM based on constructing of interpretative models of multi-unit non-extensible or non-compressible elastic threads and nets. The main idea is that vector loads  $P_i$  ( $i=1,2,\dots,n$ ), which are put in nodal points,

define the shape of discrete model (Fig. 1).

It is assumed directly proportional relationship between the length of the individual straight line segments of threads or nets  $\delta_{i,j}$  and the absolute values of internal forces in them  $R_{i,j}$ :

$$R_{i,j}/\delta_{i,j} = \pm k_{i,j}, (i, j = \overline{0, n+1}; i \neq j), (1)$$

where:  $\pm k_{i,j}$  – adopted proportionality coefficient («+» – stretching, «-» – compression).

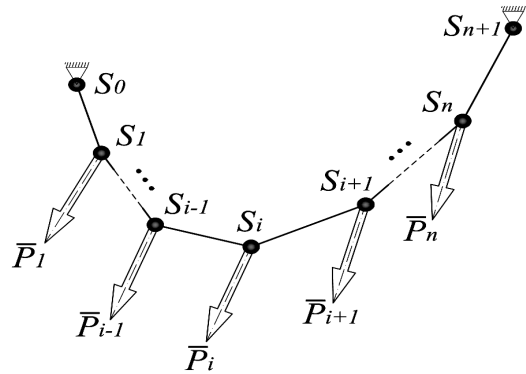


Fig. 1. The multi-unit elastic thread

The vector equation of static equilibrium of the  $i$ -th node of two-dimensional elastic thread with  $n$  free loaded nodes is as follows (Fig. 2):

$$\bar{R}_{i,i-1} + \bar{R}_{i,i+1} + \bar{P}_i = 0. (2)$$

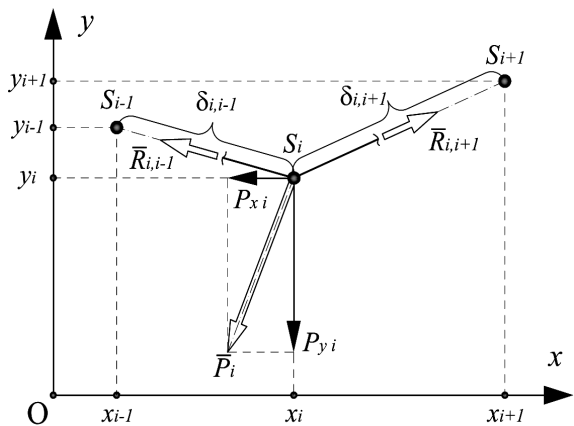


Fig. 2. The equilibrium of the  $i$ -th node which cut out from multi-unit elastic thread

In the projections, the system of equilibrium equations of SGM for the  $i$ -th node of multi-unit thread with the same for all segments coefficients  $+k$  has the following form:

$$-2 \cdot s_i + s_{i-1} + s_{i+1} = -P_{s_i}/k, \quad (3)$$

where:  $s$  – generalizing designation of coordinates.

Forming process basically boils down to the selection of the external loads. Typically, load vectors have a formal mathematical sense and are the parameters of variation.

However, the method does not require the formalization of these parameters and, if necessary, they may correspond to the actual physical vector quantities.

This approach was suggested to use in [8]. This eliminates the need to establish a constant coefficient of proportionality, and it can be changed in each element of discrete model.

If we know the laws or properties of the investigated process or object, it can be interpreted by a set of vertices, which correspond to the parameters of the process or object in specific points of the space and form a grid. Then the equilibrium state of  $i$ -th vertex of the grid, which connected to its other  $n$  vertices, in accordance with the SGM can be described by the following system of equations:

$$-\left(\sum_{j=1}^n k_{i,j}\right) \cdot s_i + \sum_{j=1}^n k_{i,j} \cdot s_j = -P_{s_i}. \quad (4)$$

This system can be used for static and dynamic processes and objects modeling, since the coefficient  $k_{i,j}$  and the components of the external influence  $P_{s_i}$  may be the non-linear functions not only on the coordinates of vertices of the grid, but also on additional parameters, for example, measures such as time. In [8] was proposed to use a generalized form of SGM for modeling of heat and mass exchange process occurring during the heating of the porous building materials with electrocutation, as well as for the numerical modeling of the elements of stress-strain state of building structures, which are under the influence of external loads.

However, it should be noted that in the above-mentioned work the solutions of practical problems have been implemented on the basis of the control of parameters  $k_{i,j}$  using

additional discrete models, which characterize the current physical state of the model in its different areas. In this approach hasn't been proposed to construct a unified geometric model of the area of the medium or object, allowing at the same time to describe the physical state of the elements of the model and the character of external influence on its nodes.

The mathematical regularities between the geometric and physical parameters of the network structures and the characteristics of acting on the nodes of model loads were presented in [9]. The influences of external loads, in accordance with [9], presented in the form of a vector field  $\bar{\mathfrak{S}}_i$ . In this case, the field  $\bar{\mathfrak{S}}_i$  must be a scalar and have a scalar potential  $\varphi_i$  at each point of the needed area of space:

$$\varphi_i = \varphi(s_i) = \zeta(x_i, y_i, z_i). \quad (5)$$

The values  $\bar{\mathfrak{S}}_i$  and  $\varphi_i$  are related by the following relationship:

$$\mathfrak{S}_{s_i} = \partial\varphi_i/\partial s_i. \quad (6)$$

The complete system of equations, which describe the static equilibrium of the  $i$ -th node of 3-dimensional network structure, and deformed-stress state the acceding to this node bonds is as follows:

$$\begin{cases} \sum_{j=1}^n (x_j - x_i) \cdot R_{i,j}/\delta_{i,j} + \mathfrak{S}_{x_i} = 0, \\ \sum_{j=1}^n (y_j - y_i) \cdot R_{i,j}/\delta_{i,j} + \mathfrak{S}_{y_i} = 0, \\ \sum_{j=1}^n (z_j - z_i) \cdot R_{i,j}/\delta_{i,j} + \mathfrak{S}_{z_i} = 0, \\ \sum_{j=1}^n R_{i,j} \cdot \delta_{i,j} - \varphi_i + G_i = 0, \\ \sum_{j=1}^n R_{i,j}/\delta_{i,j} - (d/2) \cdot \rho_i(x_i, y_i, z_i) = 0, \end{cases} \quad (7)$$

where:  $\rho_i(x_i, y_i, z_i)$  – distribution function of the density of the field sources,

$d$  – constant of that reflects empirical prop-

erties of the environment in which is located a rod structure, in the case when it interprets the physical process,

$G_i$  – constant of integration.

This system can be written in a more convenient form, if the relations of effort and bond lengths will be replaced by parameters of the state of bonds (or rigidity parameters of bonds)  $\mathfrak{K}_{i,j}$ :

$$\mathfrak{K}_{i,j} = R_{i,j} / \delta_{i,j}. \quad (8)$$

Here we intentionally replace the coefficient  $k_{i,j}$  to state parameter  $\mathfrak{K}_{i,j}$ , since the first one is the constant in the process of influence on the construction by various loads, while the second one can change its value, as in the real working conditions of rod constructions.

As a result of this replacement, the system (7) takes the following form:

$$\left\{ \begin{array}{l} \sum_{j=1}^n (x_j - x_i) \cdot \mathfrak{K}_{i,j} + \mathfrak{S}_{x_i} = 0, \\ \sum_{j=1}^n (y_j - y_i) \cdot \mathfrak{K}_{i,j} + \mathfrak{S}_{y_i} = 0, \\ \sum_{j=1}^n (z_j - z_i) \cdot \mathfrak{K}_{i,j} + \mathfrak{S}_{z_i} = 0, \\ \sum_{j=1}^n \delta_{i,j}^2 \cdot \mathfrak{K}_{i,j} - \varphi_i + G_i = 0, \\ \sum_{j=1}^n \mathfrak{K}_{i,j} - (h/2) \cdot \rho_i(x_i, y_i, z_i) = 0. \end{array} \right. \quad (9)$$

The system (9) is important because it gives an opportunity not only to find the position of free nodes of rod constructions, but also allows to use additional characteristics of the field of external influence (such as the scalar potential  $\varphi_i$  and the density of the field sources  $\rho_i$ ) to correct positions of the nodes and rigidity parameters of rods.

## PARAMETRIC EQUATIONS OF THE RODS

It is obvious that control of the shape of the rod construction should be carried out by

the system solution.

To allow adjustment of the model shape is necessary that the quantity of equations containing parameters of variation, corresponds to the amount of rods of the model. A method of producing of parametric equations depend on whether the quantity of rods exceeds the quantity of its nodes in the model [10]. Besides, there are two types of parametric equations describing the state of the two types of rods:

1) the rods, which connect the two free (loaded) node of the model (I type),

2) the rods, which connect one free and one fixed (basic or reference) node of the model (II type).

If the number of nodes in the model exceeds the number of its rods, parametric equations have the form:

1) for the rod  $S_a S_b$  of I type:

$$\begin{aligned} & \sum_{i=1}^{m-1} \delta_{a,i}^2 \cdot \mathfrak{K}_{a,i} + 2 \cdot \delta_{a,b}^2 \cdot \mathfrak{K}_{a,b} + \\ & + \sum_{j=1}^{n-1} \delta_{b,j}^2 \cdot \mathfrak{K}_{b,j} - (\varphi_a + \varphi_b) + D_{a,b} = 0, \end{aligned} \quad (10)$$

2) for the rod  $S_a S_{ref}$  of II type:

$$\begin{aligned} & \sum_{i=1}^{m-1} \delta_{a,i}^2 \cdot \mathfrak{K}_{a,i} + 2 \cdot \delta_{a,ref}^2 \cdot \mathfrak{K}_{a,ref} - \varphi_a + \\ & + (R_{x_{ref}} \cdot x_{ref} + R_{y_{ref}} \cdot y_{ref} + R_{z_{ref}} \cdot z_{ref}) + \\ & + D_{a,ref} = 0, \end{aligned} \quad (11)$$

where:  $m$  and  $n$  – number of nodes adjacent to the  $a$ -th and  $b$ -th (or  $ref$ -th) nodes.

If the number of nodes in the model is less than the amount of its rods, parametric equations have the form:

1) for the rod  $S_a S_b$  of I type:

$$\begin{aligned} & \sum_{i=1}^{m-1} [(\delta_{i,a}^2 + (x_i - x_a) \cdot x_b + \\ & + (y_i - y_a) \cdot y_b + (z_i - z_a) \cdot z_b) \cdot \mathfrak{K}_{a,i}] + \\ & + \sum_{j=1}^{n-1} [(\delta_{j,b}^2 + (x_j - x_b) \cdot x_a + \\ & + (y_j - y_b) \cdot y_a + (z_j - z_b) \cdot z_a) \cdot \mathfrak{K}_{b,j}] + \end{aligned} \quad (12)$$

$$\begin{aligned}
 & + (\mathfrak{S}_{x_b} \cdot x_a + \mathfrak{S}_{y_b} \cdot y_a + \mathfrak{S}_{z_b} \cdot z_a) + \\
 & + (\mathfrak{S}_{x_a} \cdot x_b + \mathfrak{S}_{y_a} \cdot y_b + \mathfrak{S}_{z_a} \cdot z_b) - \\
 & - (\varphi_a + \varphi_b) + D_{a,b} = 0;
 \end{aligned}$$

2) for the rod  $S_a S_{ref}$  of II type:

$$\begin{aligned}
 & \sum_{i=1}^{m-1} [(\delta_{i,a}^2 + (x_i - x_a) \cdot x_{ref} + \\
 & + (y_i - y_a) \cdot y_{ref} + (z_i - z_a) \cdot z_{ref}) \cdot \mathfrak{N}_{a,i}] + \\
 & + (\mathfrak{S}_{x_a} \cdot x_{ref} + \mathfrak{S}_{y_a} \cdot y_{ref} + \mathfrak{S}_{z_a} \cdot z_{ref}) + \\
 & + (R_{x_{ref}} \cdot x_a + R_{y_{ref}} \cdot y_a + R_{z_{ref}} \cdot z_a) + \\
 & + (R_{x_{ref}} \cdot x_{ref} + R_{y_{ref}} \cdot y_{ref} + R_{z_{ref}} \cdot z_{ref}) - \\
 & - \varphi_a + D_{a,ref} = 0.
 \end{aligned} \quad (13)$$

In the formulas (10) – (13):  $S_a$  and  $S_b$  – arbitrarily connected free  $a$ -th and  $b$ -th nodes,  $S_{ref}$  – some basic node of the model,  $\bar{R}_{ref}$  – the vector of support reaction in the reference node  $S_{ref}$ ,  $D_{a,b}$  и  $D_{a,ref}$  – the total integration constants.

The equations (10) – (13) have been obtained by differentiating the equations of the 1-st – 3-rd type from the system (9), as well as using algebraic operations on the equations of the 4-th type from the same system (9) [9, 10].

These equations have a several disadvantages. Thus, the identities (10) and (11) are bounded in the use of topological features of the rod system. With solving the system of equations (12) and (13) the matrix of coefficients always have zero diagonal. If the model has a large quantity of elements, then under certain its topological features the determinant the matrix of coefficients can tend to zero. In this case, the system of these equations will be degenerate.

The solution of the above-mentioned problems can be a replacement of diagonal elements or the non-zero. Since equations (10) and (11) have a simpler form of notation, it makes sense to modify exactly them.

To do this, we add to the equations (10) and (11) the following identities:

$$(\chi - 2) \cdot \delta_{a,b}^2 \cdot \mathfrak{N}_{a,b} - H_{a,b} = 0, \quad (14)$$

$$(\chi - 2) \cdot \delta_{a,ref}^2 \cdot \mathfrak{N}_{a,ref} - H_{a,ref} = 0, \quad (15)$$

where:  $\chi$  – some non-zero constant.

As a result, we obtain:

$$\begin{aligned}
 & \sum_{i=1}^{m-1} \delta_{a,i}^2 \cdot \mathfrak{N}_{a,i} + \chi \cdot \delta_{a,b}^2 \cdot \mathfrak{N}_{a,b} + \\
 & + \sum_{j=1}^{n-1} \delta_{b,j}^2 \cdot \mathfrak{N}_{b,j} - (\varphi_a + \varphi_b) + B_{a,b} = 0,
 \end{aligned} \quad (16)$$

$$\begin{aligned}
 & \sum_{i=1}^{m-1} \delta_{a,i}^2 \cdot \mathfrak{N}_{a,i} + \chi \cdot \delta_{a,ref}^2 \cdot \mathfrak{N}_{a,ref} - \varphi_a + \\
 & + (R_{x_{ref}} \cdot x_{ref} + R_{y_{ref}} \cdot y_{ref} + R_{z_{ref}} \cdot z_{ref}) + \\
 & + B_{a,ref} = 0,
 \end{aligned} \quad (17)$$

where:

$$B_{a,b} = D_{a,b} - H_{a,b}, \quad (18)$$

$$B_{a,ref} = D_{a,ref} - H_{a,ref}. \quad (19)$$

In (14), (15), (18) and (19):  $H_{a,b}$  and  $H_{a,ref}$  – constants, determined by the value of  $\chi$ .

The ability to perform such a procedure is explained as follows.

In the simplest case, the process of correcting the position of the model's nodes should be to replace the current values of node potentials to such that belong to a known isosurface of the scalar potential field  $\varphi$ . Form of these isosurfaces must take certain set of nodes and rods in the correcting of construction process. As a result should be selected optimal distribution of internal forces and the state parameters of the model. In the beginning of the selection we need to calculate the values of the integration constants  $B_{i,j}$  for all rods of the model, taking into account the initial internal forces  $R_{i,j}$ . After that, it becomes possible to solve the inverse problem of determining the internal forces taking into account the previous values of the constants of integration and the corrected (at the current stage of the iterative computation) values of the scalar potential  $\varphi$ .

Clearly that the inclusion of additional terms in the parametric equations at the pre-

vious stage of the calculation will only lead to a change in the value of the constants  $B_{i,j}$  in the next step of calculation, in no way affecting the character of the potential  $\varphi$ . This may change the rate of convergence of the iterative calculation. As a result, the zero diagonal elements of the matrix of coefficients will be replaced by  $\chi \cdot \delta_{i,j}$ .

### ALGORITHM OF THE ROD STRUCTURES SHAPE CONTROL

Recorded using the above equation, we formulate the order of adjustment of the shape of the rod structure [11]. The appropriate algorithm can be summarized to the serial repetition of iterative cycles, each of which is carried out before reaching the established calculation errors. In matrix form, this algorithm has the following form:

$$\begin{cases} [s^p] = [\mathbf{n}^{p-1}]^{-1} \cdot (-[g^{p-1}] - [\mathfrak{S}^p]), \\ \{\mathbf{n}^p\} = [(\delta^p)^2]^{-1} \cdot (\{\varphi^{p/p}\} - \{\varphi^p\} + \\ + [(\delta^p)^2] \cdot \{\mathbf{n}^{p-1}\}). \end{cases} \quad (20)$$

Here:  $[s]$  – matrix of coordinates (with dimension  $k \times 3$ , where  $k$  – the quantity of nodes of the model):

$$[s] = [X \quad Y \quad Z], \quad (21)$$

where:  $\{X\}$ ,  $\{Y\}$  and  $\{Z\}$  – the column vectors of coordinates of the nodes, which have the form:

$$\{X\}^T = [x_1 \quad x_2 \quad \dots \quad x_k], \quad (22)$$

$$\{Y\}^T = [y_1 \quad y_2 \quad \dots \quad y_k], \quad (23)$$

$$\{Z\}^T = [z_1 \quad z_2 \quad \dots \quad z_k], \quad (24)$$

where:  $[g]$  – matrix of the boundary conditions (with dimension  $k \times 3$ ):

$$[g] = [g_x \quad g_y \quad g_z], \quad (25)$$

where:  $\{g_x\}$ ,  $\{g_y\}$  и  $\{g_z\}$  – the column vec-

tors of the boundary conditions, which have the following form:

$$\{g_x\}^T = \begin{bmatrix} \sum_{i=1}^L x_i \cdot \mathbf{n}_{1,i} & \sum_{i=1}^M x_i \cdot \mathbf{n}_{2,i} & \dots \\ \dots & \sum_{i=1}^N x_i \cdot \mathbf{n}_{k,i} & \dots \end{bmatrix}, \quad (26)$$

$$\{g_y\}^T = \begin{bmatrix} \sum_{i=1}^L y_i \cdot \mathbf{n}_{1,i} & \sum_{i=1}^M y_i \cdot \mathbf{n}_{2,i} & \dots \\ \dots & \sum_{i=1}^N y_i \cdot \mathbf{n}_{k,i} & \dots \end{bmatrix}, \quad (27)$$

$$\{g_z\}^T = \begin{bmatrix} \sum_{i=1}^L z_i \cdot \mathbf{n}_{1,i} & \sum_{i=1}^M z_i \cdot \mathbf{n}_{2,i} & \dots \\ \dots & \sum_{i=1}^N z_i \cdot \mathbf{n}_{k,i} & \dots \end{bmatrix}, \quad (28)$$

where:  $[\mathfrak{S}]$  – matrix of external influences (with dimension  $k \times 3$ ):

$$[\mathfrak{S}] = [\mathfrak{S}_x \quad \mathfrak{S}_y \quad \mathfrak{S}_z], \quad (29)$$

where:  $\{\mathfrak{S}_x\}$ ,  $\{\mathfrak{S}_y\}$  and  $\{\mathfrak{S}_z\}$  – the column vectors of the components of external influences, which have the following form:

$$\{\mathfrak{S}_x\}^T = [\mathfrak{S}_{x_1} \quad \mathfrak{S}_{x_2} \quad \dots \quad \mathfrak{S}_{x_k}], \quad (30)$$

$$\{\mathfrak{S}_y\}^T = [\mathfrak{S}_{y_1} \quad \mathfrak{S}_{y_2} \quad \dots \quad \mathfrak{S}_{y_k}], \quad (31)$$

$$\{\mathfrak{S}_z\}^T = [\mathfrak{S}_{z_1} \quad \mathfrak{S}_{z_2} \quad \dots \quad \mathfrak{S}_{z_k}], \quad (32)$$

where:  $[\mathbf{n}]$  – matrix of stiffness parameters of rod structure (with dimension  $k \times k$ ), diagonal elements of this matrix contain the negative sums of stiffness parameters of the rods connecting to those nodes of the model, for which are made up the corresponding equations (according to the topology), the other elements contain stiffness parameters of bonds, that connect the corresponding to indexes nodes with the nodes, which corresponding to the diagonal elements in that row, or zeros (operation "or" will be denoted by « $\vee$ »), such a matrix has the following form:

$$[\mathbf{K}] = \begin{bmatrix} -\sum_{i=1}^P \mathbf{K}_{1,i} & \mathbf{K}_{1,2} \vee 0 & \cdots & \mathbf{K}_{1,k} \vee 0 \\ \mathbf{K}_{2,1} \vee 0 & -\sum_{i=1}^Q \mathbf{K}_{2,i} & \cdots & \mathbf{K}_{2,k} \vee 0 \\ \vdots & \vdots & \ddots & \vdots \\ \mathbf{K}_{k,1} \vee 0 & \mathbf{K}_{k,2} \vee 0 & \cdots & -\sum_{i=1}^R \mathbf{K}_{k,i} \end{bmatrix}, \quad (33)$$

where:  $\{\mathbf{K}\}$  – column vector of stiffness parameters of rod structure, which has the following form:

$$\{\mathbf{K}\}^T = [\mathbf{K}_{a,b_1} \quad \mathbf{K}_{a,b_2} \quad \cdots \quad \mathbf{K}_{a,b_h}], \quad (34)$$

where:  $h$  – the quantity of rods of the model;  $\{\varphi\}$  – column vector of nodal values of the scalar potential, which has the following form:

$$\{\varphi\}^T = \begin{bmatrix} \varphi_{a_1} + \varphi_{b_1} & \varphi_{a_2} + \varphi_{b_2} & \cdots \\ \cdots & \varphi_{a_h} + \varphi_{b_h} \end{bmatrix}, \quad (35)$$

$\{B\}$  – column vector of constants  $B_{a,b}$ , which has the following form:

$$\{B\}^T = [B_{a,b_1} \quad B_{a,b_2} \quad \cdots \quad B_{a,b_h}], \quad (36)$$

$[\delta^2]$  – matrix of geometric parameters of rod structure (with dimension  $h \times h$ ), the diagonal elements of which contain products of constants  $\chi$  and squares of the lengths of those bonds for which are made up the equations, corresponding to the specific row of the matrix; the other elements include squares lengths of bond, corresponding to the indices of the given cell of this matrix, or zeros; such a matrix has the following form:

$$[\delta^2] = \begin{bmatrix} \chi \cdot \delta_{a,b_{1,1}}^2 & \delta_{a,b_{1,2}}^2 \vee 0 & \cdots & \delta_{a,b_{1,h}}^2 \vee 0 \\ \delta_{a,b_{2,1}}^2 \vee 0 & \chi \cdot \delta_{a,b_{2,2}}^2 & \cdots & \delta_{a,b_{2,h}}^2 \vee 0 \\ \vdots & \vdots & \ddots & \vdots \\ \delta_{a,b_{h,1}}^2 \vee 0 & \delta_{a,b_{h,2}}^2 \vee 0 & \cdots & \chi \cdot \delta_{a,b_{h,h}}^2 \end{bmatrix}, \quad (37)$$

$\{\varphi'\}$  – column vector of expected nodal parameters of the scalar potential, which have the form of similar to  $\{\varphi\}$ ,  $p$  – index corre-

sponding to the current step of the iterative calculation.

The system (20) can be described by the following order of operations:

1. Constructing of a system of equilibrium equations of the rod construction nodes,

2. Calculation of current nodal coordinates of the rod construction per approximately given initial conditions (which include the initial values of external loads and stiffness parameters of rods),

3. Constructing of parametric equations of bonds of the rod construction,

4. Determination of the current value of the scalar potential field of external influences,

5. Determination of the constants  $B_{i,j}$  from the parametric equations of bonds with the current model coordinates and scalar potentials,

6. Solution of the system of parametric equations with respect to stiffness parameters with pre-replacement of values of the current potential on the potential values, which are desired, and taking into account the previously calculated values of the constants  $B_{i,j}$ ,

7. Substituting of founded stiffness parameters into the system of equilibrium of the rod construction nodes; solution of this system relative to coordinates of the nodes of the model,

8. Repeating of the steps 3 – 7 until a specified level of absolute or relative errors of calculation is reached.

It should be noted, that in modeling of rod architectural constructions the external loads can be invariable in all nodes of a model, irrespective of the coordinates nodes. At the same time, scalar potential field may not reflect the potential gravitational field of the Earth (as one might think). This is completely acceptable from a mathematical point of view, as in the continuum (theoretically) can exist any number of scalar fields. Some of them can be mutually neutralized. Therefore, if the construction has to take the form of iso-surface of one of a pair of these "mutually neutral" fields, the nodes of the model will not take the mechanical action of the gradient vector from not one of these fields.

That is why the offered algorithm for con-

trol of the rod construction parameters allows giving it almost any shape, admissible of its topology.

## CONCLUSIONS

On the basis of the generalized form of the static-geometric method of discrete geometry, was developed a new approach to solve the problems of shaping of rod spatial constructions. This approach allows not only to determine the preliminary shape of a designed construction by given conditions of external influence, but also, if necessary, to correct it by a system solution of parametric equations of rods of the model.

The proposed formulas allows determining the internal forces in the rods of the building structure. This makes it possible simultaneously to attribute this method to instruments of architectural forming and to instruments of numerical simulation.

## REFERENCES

1. **Kovalev S. 1986.** The formation of discrete surface models of spatial architectural structures. Dissertation of the Dr. Sci. Tech. Moscow, MAI, 348.
2. **Brebbia C. 1984.** Boundary Elements Techniques. Theory and Application in Engineering. Berlin – New York – Heidelberg – Tokyo, Springer-Verlag, 526.
3. **Fenner R. 1975.** Finite Element Method for Engineers. London, The Macmillan Press Ltd.
4. **Forrest A. 1972.** On Coons and Other Methods for the Representation of Curved Surfaces. New York, Comp. Graf. and Image Proc., 341-359.
5. **Holand I. 1969.** Finite Element Method in Stress Analysis. Trondheim, Tapir-Verlag.
6. **Richtmyer R. 1967.** Difference Methods for Initial-Value Problems. New York – London – Sydney, INTERCIENCE PUBLISHERS: a division of John Wiley & Sons, 419.
7. **Schutz B. 1979.** Geometrical methods of mathematical physics. Cambridge – London – New York – New Rochelle – Melborn – Sydney, Cambridge University Press, 303.
8. **Skochko V. 2013.** Special geometrical models of processes which develop in continuum. Dissertation of the Ph. D. Kyiv, KNUBA, 269.
9. **Skochko V., Skochko L. 2012/2013.** The differential laws between the geometrical and physical parameters of the meshes and the fields which balance them. Kyiv, Base and foundations, Nr 33, 85-95.
10. **Skochko V., Skochko L. 2013.** The equation of state and condition parameters of the mesh structure relationships. Kyiv, Base and foundations, Nr 34, 47-57.
11. **Ploskiy O., Skochko V. 2014.** Algorithm of meshwork's communications controlling based on adjustment of the scalar potential of external influences. Kyiv, Energy efficiency in the construction, Nr 6, 224-230.
12. **Ploskiy O., Skochko V. 2014.** The discrete cages of surfaces constructing using equations of state's parameters and conditions of the mesh structure's communications. Lutsk.

## ПРИНЦИПЫ ДИСКРЕТНОГО МОДЕЛИРОВАНИЯ СТЕРЖНЕВЫХ КОНСТРУКЦИЙ ОБЪЕКТОВ АРХИТЕКТУРЫ

**Аннотация.** В публикации раскрываются основные принципы моделирования стержневых пространственных строительных конструкций средствами дискретной геометрии. Приведены математические зависимости, составляющие основу данного подхода и представляющие собой дифференциальные закономерности между геометрическими и физическими параметрами моделируемых конструкций, а также параметрами внешних нагрузок, определяющих конечную форму модели.

**Ключевые слова:** геометрическое моделирование, дискретная модель, сетчатые структуры, стержневые конструкции, дифференциальные закономерности.

## Application of Generalized “Method of Lines”, for Solving Problems of Thermoelasticity of Thick Plates

*Valery Chybiryakov, Anatoly Stankevich, Dmitro Levkiuskiy,  
Volodymyr Melnychuk*

Kyiv National University of Construction and Architecture  
Povitroflotsky prosp., 31, Kyiv, Ukraine, 03680, e-mail: dmitriylev88@gmail.com

**Summary.** In this paper, a new combined method of reducing dimensions of spatial thermoelasticity problems was proposed; based on the “method of lines”, combined with Bubnov-Galerkin-Petrov’s projection method which significantly expands its capabilities. The generalized “method of lines” can be used for plates of variable thickness, in problems of dynamics and thermoelasticity. The basic idea is to reduce the dimension of the spatial coordinates using the projection method, with a system of basis functions. This article is the first part of the work. It shows the reduced differential equations and proposes a new way of modeling boundary conditions.

**Key words:** “method of lines”, method Bubnov–Galerkin–Petrov thermoelasticity, thick plates, structural mechanics.

### INTRODUCTION

One of the most effective methods of solving multidimensional problems of structural mechanics is the combination approach. In this approach a problem is solved in two stages:

- 1) decreasing the dimension of the input equations by one or two coordinates;
- 2) the reduced problem is solved analytically or numerically.

Traditionally in structural mechanics, lowering dimensionality of input equations is based on certain hypotheses. Accordingly, the first stage of the method was excluded in a separate research: theory of rods, plates and shells. Applied hypotheses were strong enough but less accurate. It led to creation of various theories of plates and shells.

Currently, lowering dimensionality is performed using mathematical methods (for example, the theory of shells I.N.Vekua [19]). With the next solution of reduced equations,

lowering the dimension creates a combined method for solving problems of mathematical physics. Such methods include Vlasov–Kantorovich’s method. These combined methods are alternative, compared to the general numerical methods such as finite element method, finite difference and variation–difference method.

Mathematical methods of lowering dimensionality are associated with the geometrical characteristics of the considered objects. It greatly restricts the geometry of the problems, for which it is possible to use the combined methods. However, limiting the complexity of the geometry allows the application of very efficient numerical methods. It increases the accuracy and stability of numerical calculation. It also significantly reduces computer time usage.

One of the known methods of lowering dimensionality input equations is the “method of lines”. In this method, the finite difference method is used for one of the two coordinates. This method will be effective, if

the input equations are systems of ordinary differential equations. In the case of constant coefficients in these equations, it is possible to use analytical solution of system of equations (Vinokurov [20], Shkelov L.T. [13]). In this regard, the “method of lines” is used for the solution of static problems for plates and shells of constant thickness.

The authors proposed a new version of lowering dimensionality in the application of the method of lines. It is greatly expanding the capabilities of “method of lines”.

### AIM OF WORK

To generalize the “method of lines” and its implementation in the solution of thermoelasticity problems, dynamics and transfer to three dimensional equations.

The proposed generalized “method of lines” may be used for calculating the plates of variable thickness, and also problems of dynamics. The basic idea of generalized “method of lines” is lowering the dimensionality of input equations per the spatial coordinate by projection method. The projection method includes the Bubnov–Galerkin method, generalized by Petrov [9].

In the case of thick plates with constant thickness for equations of plate deformations per thickness, locally basic restricted discrete linear functions are chosen (Fig. 1.).

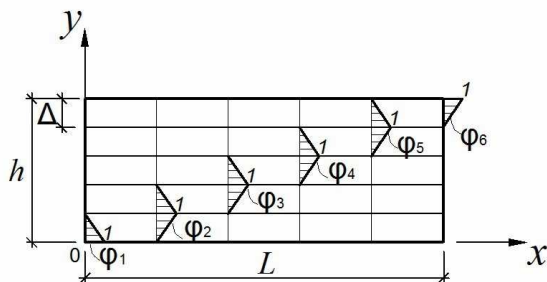


**Fig. 1.** Basis functions

As in the traditional version of the “method of lines”, a cross-section of the plate is divided into  $n$  lines (including two boundary lines) with an equal range  $\Delta$ . How-

ever, in order to reduce dimensionality, we do not use method of finite differences, but the generalized method of Bubnov–Galerkin–Petrov. By coordinate  $y$  the unknown functions  $f(x, y)$  is approximated in this manner:

$$f(x, y) \approx f^i(x)\varphi_i(y). \quad (1)$$

The constructed algorithm of lowering dimensionality formally resembles algebraic transformations of tensor calculus. In this connection, the generalized method of lines essentially tensor symbols and relevant rules are used. For example, by repeated indexes is assumed summation. Resolving equations according to Bubnov–Galerkin method, after substituting approximate ratios of the form (1) are scalar multiplied in Hilbert space for basic functions  $\varphi_i(y)$ .

It should be noted that in Bubnov–Galerkin method, basis functions must satisfy the homogeneous boundary conditions per coordinate  $y$ . These basis functions do not satisfy such conditions. However, according to the generalization of Petrov [9] it is enough that these functions satisfy natural boundary conditions. It should be noted that in the construction of reduced equations for intensive unknowns (displacement in the theory of elasticity) and extensive unknowns (stresses) transformation of corresponding components is performed differently. Here-with we get two basic matrices –  $G$  and  $B$ , which are recorded in an index form as:

$g_{ij} = (\varphi_i, \varphi_j)$ ,  $b_{ij} = (\varphi_i, \frac{d\varphi_j}{dy})$ . This is the scalar product of two functions:

$$(\varphi_i, \varphi_j) = \int_0^{h_y} \varphi_i(y)\varphi_j(y)dy. \quad (2)$$

Conversion of components with derivative  $y$  of the function  $n$  – type displacement and stresses–type functions is formed in different ways. This is the use of lowering the dimension of a plane problem using the theory of elasticity:

$$\left. \begin{aligned}
 & \left( \frac{\partial u(x, y)}{\partial y}, \varphi_i(y) \right) = \\
 & = \int_0^{h_y} \frac{\partial u(x, y)}{\partial y} \varphi_i(y) dy = \\
 & = \int_0^{h_y} \frac{\partial (u^j(x) \varphi_j(y))}{\partial y} \varphi_i(y) dy = \\
 & = u^j(x) \int_0^{h_y} \varphi_i(y) \varphi_j'(y) dy = b_{ij} u^j(x),
 \end{aligned} \right\} (3)$$

$$\left. \begin{aligned}
 & \left( \frac{\partial \sigma_x(x, y)}{\partial y}, \varphi_i(y) \right) = \\
 & = \int_0^{h_y} \frac{\partial \sigma_x(x, y)}{\partial y} \varphi_i(y) dy = \\
 & = \sigma_x(x, y) \varphi_i(y) \Big|_0^{h_y} - \int_0^{h_y} \sigma_x(x, y) \varphi_i'(y) dy = \\
 & = (\sigma_x(x, h_y) \varphi_n(h_y) - \sigma_x(x, 0) \varphi_1(0)) - \\
 & \quad - b_{ji} \sigma_x^j(x),
 \end{aligned} \right\} (4)$$

$\{b_{ji}\}$  is a transpose matrix of  $\{b_{ij}\}$ .

The peculiarity of this functional basis is that this basis is not orthogonal, and thus there exist two types of index values,  $f^i$  and  $f_i$ . These magnitudes are different by rules of conversion at transition on another basis. Contravariant magnitudes denoted by upper index and covariant magnitudes – lower index. Accordingly,  $\{g_{ij}\}$  – two indexes magnitude is twice covariant metric tensor and the inverse matrix  $\{g_{ij}\}^{-1} = \{g^{ij}\}$  is twice contravariant metric tensor. Metric tensor provides a transition from covariant to contravariant components and vice versa:

$$f_i = g_{ij} f^j, \quad f^i = g^{ij} f_j. \quad (5)$$

The scalar product in this case is the integral of multiplication of functional factors. Therefore in mathematics, covariant and contravariant function magnitudes have an identified name. Because the covariant magni-

tudes appear in the decomposition by basis (Fig. 1.), they are called coefficients. Covariant magnitudes appear as a scalar product of the basis elements:

$$f_i(x) = (f(x, y), \varphi_i(y)) = \int_0^{h_y} f(x, y) \varphi_i(y) dy,$$

they are called – moments.

Therefore, reduced equations can be written in four ways:

- in moments, if displacement and stresses in the moments,
- in coefficients, if all unknowns are written in coefficients,
- two versions of combined record: displacement in the moments, stresses in the coefficients or displacement in coefficient, stresses in the moments.

After formulating the construction equations, we need to formulate the reduced boundary value and initial – boundary value problem in index form.

The described technique can be applied to solve the problem of thermal stresses in a rod of rectangular cross-section (Fig. 2.), which occupies a three-dimensional region:  $[0 \leq x \leq l] \times [0 \leq y \leq h_y] \times [0 \leq z \leq h_z]$ .

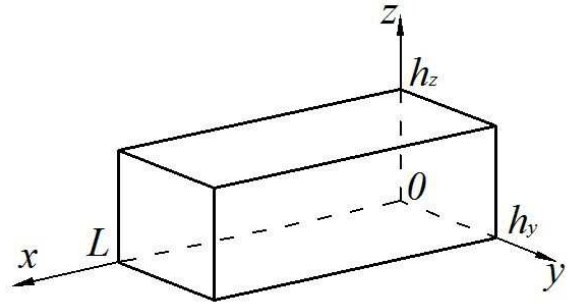


**Fig. 2.** Beam of rectangular cross section

The problem about thermal stresses is considered within limits of an important part of the theory of elasticity – thermoelasticity [6, 7]. In this problem we consider two physical fields – thermal and mechanical.

Thermal field in solids is described by the thermal conductivity equation. In the most

general form, thermal field depends not only on three spatial coordinates but also on time coordinates. The corresponding problem in determining the component of thermal field is described by the equations of non-stationary thermal conductivity. Components depend on the time coordinate. As a system of differential equations in partial derivatives of the first order in the spatial and time coordinates, these equations are written in the form:

$$\left\{ \begin{array}{l} \rho c \frac{\partial T}{\partial t} = \frac{\partial q_x}{\partial x} + \frac{\partial q_y}{\partial y} + \frac{\partial q_z}{\partial z} + Q \\ q_x = -\lambda_T \frac{\partial T}{\partial x} \\ q_y = -\lambda_T \frac{\partial T}{\partial y} \\ q_z = -\lambda_T \frac{\partial T}{\partial z} \end{array} \right. , \quad (6)$$

where:  $T = T(x, y, z)$  – temperature function,  $q_x, q_y, q_z$  – components of the heat flux  $\vec{q}(x, y, z)$ ,  $\rho$  – density of the material,  $c$  – specific heat,  $\lambda_T$  – coefficient of thermal conductivity,  $Q$  – the quantity of heat generated by internal heat sources.

To ensure unity of solution of the system (6) we need to specify the initial and boundary conditions. The initial conditions are in the form:

$$t = 0, \quad T(x, y, z) = T_0(x, y, z),$$

where:  $T_0(x, y, z)$  – temperature distribution throughout the volume of the body at the initial time.

The boundary conditions of the problem will be set as conditions of convective heat transfer.

When  $x = 0$ :

$$\left. \begin{array}{l} q_x(0, y, z, t) = \alpha_{xT}^0 (T_{xC}^0 - T_x^0) - \\ -q_{xC}(0, y, z, t), \end{array} \right\} \quad (7)$$

when  $x = l$ :

$$\left. \begin{array}{l} q_x(l, y, z, t) = \alpha_{xT}^l (T_x^l - T_{xC}^l) + \\ +q_{xC}(l, y, z, t). \end{array} \right\}$$

The temperatures and heat flows of external environment from the side of relevant part of boundary surface of beam are marked as “ $C$ ”:

when  $y = 0$ :

$$\left. \begin{array}{l} q_y(x, 0, z, t) = -\alpha_{yT}^0 (T_y(x, 0, z, t) - \\ -T_{yC}(x, 0, z, t)) - q_{yC}(x, 0, z, t), \end{array} \right\} \quad (8)$$

when  $y = h_y$ :

$$\left. \begin{array}{l} q_y(x, h_y, z, t) = \alpha_{yT}^{h_y} (T_y(x, h_y, z, t) - \\ -T_{yC}(x, h_y, z, t)) + q_{yC}(x, h_y, z, t), \end{array} \right\}$$

when  $z = 0$ :

$$\left. \begin{array}{l} q_z(x, y, 0, t) = -\alpha_{zT}^0 (T_z(x, y, 0, t) - \\ -T_{zC}(x, y, 0, t)) - q_{zC}(x, y, 0, t), \end{array} \right\} \quad (9)$$

when  $z = h_z$ :

$$\left. \begin{array}{l} q_z(x, y, h_z, t) = \alpha_{zT}^{h_z} (T_z(x, y, h_z, t) - \\ -T_{zC}(x, y, h_z, t)) + q_{zC}(x, y, h_z, t). \end{array} \right\}$$

In the next numerical calculations, such form of boundary conditions allows to take into account the relevant part of surface boundary conditions of first order  $\alpha_T \rightarrow \infty$  and second order  $\alpha_T \rightarrow 0$ .

Changing temperature of solid body in time practically does not cause dynamic effects. Therefore, mechanical fields (displacement, stress and strain fields) are stationary and are described by static equations.

These equations are written as equations in partial derivatives of first order:

$$\frac{\partial \sigma_x}{\partial x} = -\frac{\partial \tau_{xy}}{\partial y} - \frac{\partial \tau_{xz}}{\partial z} - X, \quad (10)$$

$$\frac{\partial \tau_{xy}}{\partial x} = -\frac{\partial \sigma_y}{\partial y} - \frac{\partial \tau_{yz}}{\partial z} - Y, \quad (11)$$

$$\frac{\partial \tau_{xz}}{\partial x} = -\frac{\partial \tau_{yz}}{\partial y} - \frac{\partial \sigma_z}{\partial z} - Z, \quad (12)$$

$$\left. \begin{aligned} \frac{\partial u^*}{\partial x} &= \frac{\mu}{(\lambda + 2\mu)} \sigma_x - \frac{\lambda}{(\lambda + 2\mu)} \frac{\partial v^*}{\partial y} - \\ & - \frac{\lambda}{(\lambda + 2\mu)} \frac{\partial w^*}{\partial z} + \frac{(3\lambda + 2\mu)}{(\lambda + 2\mu)} \alpha_T (T - T_0), \end{aligned} \right\} (13)$$

$$\frac{\partial v^*}{\partial x} = \tau_{xy} - \frac{\partial u^*}{\partial y}, \quad (14)$$

$$\frac{\partial w^*}{\partial x} = \tau_{xz} - \frac{\partial u^*}{\partial z}. \quad (15)$$

The equations can be separately considered:

$$\left. \begin{aligned} \sigma_y &= \frac{\lambda}{\mu} \frac{\partial u^*}{\partial x} + \frac{(\lambda + 2\mu)}{\mu} \frac{\partial v^*}{\partial y} + \\ & + \frac{\lambda}{\mu} \frac{\partial w^*}{\partial z} - \frac{(3\lambda + 2\mu)}{\mu} \alpha_T (T - T_0), \end{aligned} \right\} (16)$$

$$\left. \begin{aligned} \sigma_z &= \frac{\lambda}{\mu} \frac{\partial u^*}{\partial x} + \frac{\lambda}{\mu} \frac{\partial v^*}{\partial y} + \\ & + \frac{(\lambda + 2\mu)}{\mu} \frac{\partial w^*}{\partial z} - \frac{(3\lambda + 2\mu)}{\mu} \alpha_T (T - T_0) \end{aligned} \right\} (17)$$

$$\tau_{yz} = \left( \frac{\partial w^*}{\partial y} + \frac{\partial v^*}{\partial z} \right), \quad (18)$$

$$\left. \begin{aligned} \frac{1}{\sqrt{1 + (k_{xx}^0)^2}} \sigma_x^0 - \frac{k_{xx}^0}{\sqrt{1 + (k_{xx}^0)^2}} u^0 + \\ + \frac{1}{\sqrt{1 + (k_{xx}^0)^2}} q_{xx}^0 + \frac{k_{xx}^0}{\sqrt{1 + (k_{xx}^0)^2}} u_c^0 = 0, \end{aligned} \right\} (19)$$

$$\left. \begin{aligned} \frac{1}{\sqrt{1 + (k_{xy}^0)^2}} \tau_{xy}^0 - \frac{k_{xy}^0}{\sqrt{1 + (k_{xy}^0)^2}} v^0 + \\ + \frac{1}{\sqrt{1 + (k_{xy}^0)^2}} q_{xy}^0 + \frac{k_{xy}^0}{\sqrt{1 + (k_{xy}^0)^2}} v_c^0 = 0, \end{aligned} \right\} (20)$$

$$\left. \begin{aligned} \frac{1}{\sqrt{1 + (k_{xz}^0)^2}} \tau_{xz}^0 - \frac{k_{xz}^0}{\sqrt{1 + (k_{xz}^0)^2}} w^0 + \\ + \frac{1}{\sqrt{1 + (k_{xz}^0)^2}} q_{xz}^0 + \frac{k_{xz}^0}{\sqrt{1 + (k_{xz}^0)^2}} w_c^0 = 0. \end{aligned} \right\} (21)$$

When  $x = l$ :

$$\left. \begin{aligned} -\frac{1}{\sqrt{1 + (k_{xx}^l)^2}} \sigma_x^l - \frac{k_{xx}^l}{\sqrt{1 + (k_{xx}^l)^2}} u^l + \\ + \frac{1}{\sqrt{1 + (k_{xx}^l)^2}} q_{xx}^l + \frac{k_{xx}^l}{\sqrt{1 + (k_{xx}^l)^2}} u_c^l = 0, \end{aligned} \right\} (22)$$

$$\left. \begin{aligned} -\frac{1}{\sqrt{1 + (k_{xy}^l)^2}} \tau_{xy}^l - \frac{k_{xy}^l}{\sqrt{1 + (k_{xy}^l)^2}} v^l + \\ + \frac{1}{\sqrt{1 + (k_{xy}^l)^2}} q_{xy}^l + \frac{k_{xy}^l}{\sqrt{1 + (k_{xy}^l)^2}} v_c^l = 0, \end{aligned} \right\} (23)$$

$$\left. \begin{aligned} -\frac{1}{\sqrt{1 + (k_{xz}^l)^2}} \tau_{xz}^l - \frac{k_{xz}^l}{\sqrt{1 + (k_{xz}^l)^2}} w^l + \\ + \frac{1}{\sqrt{1 + (k_{xz}^l)^2}} q_{xz}^l + \frac{k_{xz}^l}{\sqrt{1 + (k_{xz}^l)^2}} w_c^l = 0, \end{aligned} \right\} (24)$$

where:  $f^* = \mu f$ .

Boundary conditions of stress-strain state in general are written by the analogy of work [16].

When  $x = 0$ :

where:  $f^0 = f(0, y, z)$ ,  $f^l = f(l, y, z)$ .

For construction of the boundary conditions (19) – (24) we write the sum of projections of all power factors that act on the boundary contour, on corresponding axis. In (Fig. 3.) on the plane  $xOy$ , the magnitudes which act on area  $x=0$  are shown.

The first index – signifies the number of the axis which is perpendicular to the area. The second index shows the direction of displacement or stress.

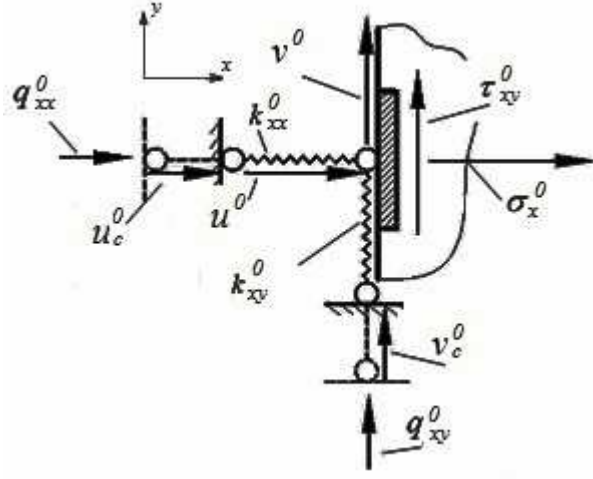


**Fig. 3.** Modeling of the boundary conditions:

$u_c, v_c$  – displacement of points of the external environment;  
 $u, v$  – horizontal and vertical displacement of points of object;  
 $q_{xx}, q_{xy}$  – external load on object;  
 $\sigma_x, \tau_{xy}$  – normal and tangential (shear) stresses along the contour inside the object;  
 $k_{xx}, k_{xy}$  – spring stiffness

By changing stiffness we can specify any standard conditions of interaction of the object with the external environment.

For Eq. (6) – (24) the procedure of lowering dimension is performed by coordinates  $y, z$ . At first – reduction by  $y$ . Basic functions are applied  $\{\varphi_i = \varphi_i(y)\}$ ,  $i = 1, \dots, n$ , where the following rules are taken into account:

$$f(x, y, z, t) = f^i(x, z, t)\varphi_i(y);$$

$$\left. \begin{aligned} (f(x, y, z, t), \varphi_i(y)) &= \int_0^{h_y} f(x, y, z, t)\varphi_i(y)dy = \\ &= f_i(x, z, t); \end{aligned} \right\}$$

$$\left. \begin{aligned} &\left( \frac{\partial f(x, y, z, t)}{\partial x}, \varphi_i(y) \right) = \\ &= \int_0^{h_y} \frac{\partial f(x, y, z, t)}{\partial x} \varphi_i(y)dy = \\ &= \frac{\partial}{\partial x} \int_0^{h_y} f(x, y, z, t)\varphi_i(y)dy = \frac{\partial}{\partial x} f_i(x, z, t). \end{aligned} \right\}$$

Where  $f$  is a factor of stress, then

$$\left. \begin{aligned} &\left( \frac{\partial f(x, y, z, t)}{\partial y}, \varphi_i(y) \right) = \\ &= \int_0^{h_y} \frac{\partial f(x, y, z, t)}{\partial y} \varphi_i(y)dy = f(x, y, z, t) \times \\ &\quad \times \varphi_i(y) \Big|_0^{h_y} - \int_0^{h_y} f(x, y, z, t)\varphi_i'(y)dy = \\ &= f(x, h_y, z, t)\varphi_i(h_y) - f(x, 0, z, t)\varphi_i(0) - \\ &\quad - \int_0^{h_y} f^j(x, z, t)\varphi_j(y)\varphi_i'(y)dy = \\ &= \delta_{ij}^n f^i(x, z, t) - \delta_{ij}^1 f^i(x, z, t) - \\ &\quad - b_{ji} g^{ju} f_u(x, z, t). \end{aligned} \right\}$$

When  $f$  is a factor of temperature and displacement ( $T, u, v, w$ ), then

$$\left. \begin{aligned} &\left( \frac{\partial f(x, y, z, t)}{\partial y}, \varphi_i(y) \right) = \int_0^{h_y} \frac{\partial f(x, y, z, t)}{\partial y} \times \\ &\quad \times \varphi_i(y)dy = \int_0^{h_y} \frac{\partial f^j(x, z, t)\varphi_j(y)}{\partial y} \varphi_i(y)dy = \\ &= \int_0^{h_y} \varphi_i(y)\varphi_j'(y)f^j(x, z, t)dy = \\ &= b_{ij} g^{ju} f_u(x, z, t). \end{aligned} \right\}$$

The first equation of system (6) is multiplied as a scalar by  $\{\varphi_i = \varphi_i(y)\}$ , where  $i = 1, \dots, n$ , and then integrated by coordinate  $y$ :

$$\left. \begin{aligned} & \left( \left( \frac{\partial q_x}{\partial x} + \frac{\partial q_y}{\partial y} + \frac{\partial q_z}{\partial z} - \rho c \frac{\partial T}{\partial t} + \right. \right. \\ & \left. \left. + Q(x, y, z, t) \right) = 0, \varphi_i(y) \right), \\ & \frac{\partial q_{xi}}{\partial x} + \delta_{\cdot i}^{n \cdot} q_{y \cdot}^i(x, z, t) - \delta_{\cdot i}^{1 \cdot} q_{y \cdot}^i(x, z, t) - \\ & - b_{ji} g^{ja} q_{ya}(x, z, t) + \frac{\partial q_{zi}}{\partial z} - \rho c \frac{\partial T_i}{\partial t} + \\ & + Q_i(x, z, t) = 0. \end{aligned} \right\} \quad (25)$$

In the next step – we perform the reduction by  $z$  of equation (25):

$$\left. \begin{aligned} & \left( \frac{\partial q_{xi}}{\partial x} + \delta_{\cdot i}^{n \cdot} q_{y \cdot}^i(x, z, t) - \delta_{\cdot i}^{1 \cdot} q_{y \cdot}^i(x, z, t) - \right. \\ & \left. - b_{ji} g^{ja} q_{ya}(x, z, t) + \frac{\partial q_{zi}}{\partial z} - \rho c \frac{\partial T_i}{\partial t} + \right. \\ & \left. + Q_i(x, z, t) = 0, \varphi_k(z) \right), \\ & \frac{\partial q_{xik}}{\partial x} + \left[ \delta_{\cdot i}^{n \cdot} q_{y \cdot}^i(x, t) - \delta_{\cdot i}^{1 \cdot} q_{y \cdot}^i(x, t) \right] - \\ & - b_{ji} g^{ja} q_{yak}(x, t) + \\ & + \left[ \delta_{\cdot k}^{m \cdot} q_{zi \cdot}^{\cdot k}(x, t) - \delta_{\cdot k}^{1 \cdot} q_{zi \cdot}^{\cdot k}(x, t) \right] - \\ & - b_{pk} g^{ps} q_{zis}(x, t) - \\ & - \rho c \frac{\partial T_{ik}}{\partial t} + Q_{ik}(x, t) = 0, \end{aligned} \right\} \quad (26)$$

here:

$$\begin{aligned} \left[ \delta_{\cdot i}^{n \cdot} q_{y \cdot}^i - \delta_{\cdot i}^{1 \cdot} q_{y \cdot}^i \right] &= \left[ -q_{y \cdot}^{1 \cdot} \quad 0 \quad \dots \quad 0 \quad q_{y \cdot}^{n \cdot} \right]^T \\ \left[ \delta_{\cdot k}^{m \cdot} q_{zi \cdot}^{\cdot k} - \delta_{\cdot k}^{1 \cdot} q_{zi \cdot}^{\cdot k} \right] &= \left[ -q_{zi \cdot}^{1 \cdot} \quad 0 \quad \dots \quad 0 \quad q_{zi \cdot}^{m \cdot} \right]^T \end{aligned}$$

$n$  – number of lines along the axis  $y$ ,  $m$  – number of lines along the axis  $z$ .

Indexes  $i, j, \alpha, \beta, \gamma$  – are related to reduction by coordinate  $y$ , indexes  $k, p, s, \xi, \varepsilon$  – reduction by coordinate  $z$ .

Taking into account the boundary conditions (8) – (9):

$$\left. \begin{aligned} & \left[ \delta_{\cdot i}^{n \cdot} q_{y \cdot}^i - \delta_{\cdot i}^{1 \cdot} q_{y \cdot}^i \right] = \\ & = \left[ \alpha_{yT}^0 T_{y \cdot}^{1 \cdot} \quad 0 \quad \dots \quad 0 \quad \alpha_{yT}^{h_y} T_{y \cdot}^{n \cdot} \right]^T - \\ & - \left[ \alpha_{yT}^0 T_{yC \cdot}^{1 \cdot} \quad 0 \quad \dots \quad 0 \quad \alpha_{yT}^{h_y} T_{yC \cdot}^{n \cdot} \right]^T + \\ & + \left[ q_{yC \cdot}^{1 \cdot} \quad 0 \quad \dots \quad 0 \quad -q_{yC \cdot}^{n \cdot} \right]^T \\ & \left[ \delta_{\cdot k}^{m \cdot} q_{zi \cdot}^{\cdot k} - \delta_{\cdot k}^{1 \cdot} q_{zi \cdot}^{\cdot k} \right] = \\ & = \left[ \alpha_{zT}^0 T_{zi \cdot}^{1 \cdot} \quad 0 \quad \dots \quad 0 \quad \alpha_{zT}^{h_z} T_{zi \cdot}^{m \cdot} \right]^T - \\ & - \left[ \alpha_{zT}^0 T_{zCi \cdot}^{1 \cdot} \quad 0 \quad \dots \quad 0 \quad \alpha_{zT}^{h_z} T_{zCi \cdot}^{m \cdot} \right]^T + \\ & + \left[ q_{zCi \cdot}^{1 \cdot} \quad 0 \quad \dots \quad 0 \quad -q_{zCi \cdot}^{m \cdot} \right]^T \end{aligned} \right\}$$

The substitution:

$$\left. \begin{aligned} & \left[ \alpha_{yT}^0 T_{y \cdot}^{1 \cdot} \quad 0 \quad \dots \quad 0 \quad \alpha_{yT}^{h_y} T_{y \cdot}^{n \cdot} \right]^T = \left. \begin{aligned} & = T \alpha_{y \cdot}^i, \end{aligned} \right\} \\ & \left[ \alpha_{yT}^0 T_{yC \cdot}^{1 \cdot} \quad 0 \quad \dots \quad 0 \quad \alpha_{yT}^{h_y} T_{yC \cdot}^{n \cdot} \right]^T = \left. \begin{aligned} & = T C_{y \cdot}^i, \end{aligned} \right\} \quad (27) \\ & \left[ q_{yC \cdot}^{1 \cdot} \quad 0 \quad \dots \quad 0 \quad -q_{yC \cdot}^{n \cdot} \right]^T = q_{yC \cdot}^i. \\ & \left[ \alpha_{zT}^0 T_{zi \cdot}^{1 \cdot} \quad 0 \quad \dots \quad 0 \quad \alpha_{zT}^{h_z} T_{zi \cdot}^{m \cdot} \right]^T = T \alpha_{zi \cdot}^{\cdot k}, \\ & \left[ \alpha_{zT}^0 T_{zCi \cdot}^{1 \cdot} \quad 0 \quad \dots \quad 0 \quad \alpha_{zT}^{h_z} T_{zCi \cdot}^{m \cdot} \right]^T = \left. \begin{aligned} & = T C_{zi \cdot}^{\cdot k}, \end{aligned} \right\} \quad (28) \\ & \left[ q_{zC \cdot}^{1 \cdot} \quad 0 \quad \dots \quad 0 \quad -q_{zC \cdot}^{n \cdot} \right]^T = q_{zCi \cdot}^{\cdot k}. \end{aligned}$$

Taking into account the boundary conditions (27), (28) in Eq. (26):

$$\left. \begin{aligned} & \frac{\partial q_{xik}}{\partial x} + \left[ g^{ia} T \alpha_{yak} - g_{ke} T C_y^{ie} + \right. \\ & \left. + g^{ia} q_{yCak} \right] - \\ & - b_{ji} g^{ja} q_{yak} + \left[ g^{ke} T \alpha_{z i \varepsilon} - g_{ia} T C_z^{ak} + \right. \\ & \left. + g^{ke} q_{zCi \varepsilon} \right] - \\ & - b_{pk} g^{ps} q_{zis} - \rho c \frac{\partial T_{ik}}{\partial t} + Q_{ik} = 0 \end{aligned} \right\} \quad (29)$$

Similarly, the reduction of remaining equations of system (6) is done:

$$q_{xik} = -\lambda_T \frac{\partial T_{ik}}{\partial x}, \quad (30)$$

$$q_{yik} = -\lambda_T b_{ij} g^{ja} T_{ak}(x, t), \quad (31)$$

$$q_{zik} = -\lambda_T b_{kp} g^{ps} T_{is}(x, t). \quad (32)$$

Substituting (30) – (32) in (29), Eq. (33) is formed:

$$\left. \begin{aligned} & -\lambda_T \frac{\partial^2 T_{ik}}{\partial x^2} + \left[ g^{ia} T \alpha_{y\alpha k} - g_{ke} T C_y^{ie} + \right. \\ & \quad \left. + g^{ia} q_{yCak} \right] + \\ & \quad + \lambda_T b_{ji} g^{ja} b_{\alpha\beta} g^{\beta\gamma} T_{\gamma k} + \\ & \quad + \left[ g^{ke} T \alpha_{zi\epsilon} - g_{ia} T C_z^{ak} + g^{ke} q_{zCie} \right] + \\ & \quad + \lambda_T b_{pk} g^{ps} b_{s\zeta} g^{\zeta\epsilon} T_{i\epsilon} - \rho c \frac{\partial T_{ik}}{\partial t} + Q_{ik} = 0 \end{aligned} \right\} \quad (33)$$

The reduced initial conditions will look like  $T_{ik}(x, 0) = T_{0ik}(x)$ .

The next step is the reduction of equations of system (10) – (15). In this system, the process of reduction expressions are substituted for  $\sigma_y, \sigma_z, \tau_{yz}$  (16) – (18), using the above mentioned operations:

$$\left. \begin{aligned} \frac{du_{ik}^*}{dx} &= \frac{\mu}{(\lambda + 2\mu)} \sigma_{xik} - \frac{\lambda}{(\lambda + 2\mu)} b_{ij} \times \\ & \times g^{ja} v_{ak}^* - \frac{\lambda}{(\lambda + 2\mu)} b_{kp} g^{ps} w_{is}^* + \\ & + \frac{(3\lambda + 2\mu)}{(\lambda + 2\mu)} \alpha_T (T_{ik} - T_{0ik}), \end{aligned} \right\} \quad (34)$$

$$\frac{dv_{ik}^*}{dx} = \tau_{xyik} - b_{ij} g^{ja} u_{ak}^*, \quad (35)$$

$$\frac{dw_{ik}^*}{dx} = \tau_{xzik} - b_{kp} g^{ps} u_{is}^*, \quad (36)$$

$$\left. \begin{aligned} \frac{d\sigma_{xik}}{dx} &= -b_{ji} g^{ja} \tau_{xyak} + b_{pk} g^{ps} \tau_{xzis} - \\ & - \left[ \delta_{\cdot i}^{n\cdot} \tau_{xy\cdot k}^{i\cdot} - \delta_{\cdot i}^{1\cdot} \tau_{xy\cdot k}^{i\cdot} \right] - \\ & - \left[ \delta_{\cdot k}^{m\cdot} \tau_{xyi\cdot}^{\cdot k} - \delta_{\cdot k}^{1\cdot} \tau_{xyi\cdot}^{\cdot k} \right] - X_{ik}, \end{aligned} \right\} \quad (37)$$

$$\left. \begin{aligned} \frac{d\tau_{xyik}}{dx} &= \frac{\lambda}{\lambda + 2\mu} b_{ji} g^{ja} \sigma_{xak} + \frac{4(\lambda + \mu)}{\lambda + 2\mu} \times \\ & \times b_{ji} g^{ja} b_{\alpha\beta} g^{\beta\gamma} v_{xyk}^* + \frac{2\lambda}{\lambda + 2\mu} \left[ b_{ji} g^{ja} \right] \times \\ & \times \left[ b_{kp} g^{ps} \right] w_{as}^* - \frac{2(3\lambda + 2\mu)}{\lambda + 2\mu} b_{ji} g^{ja} \alpha_T \times \\ & \times (T_{ak} - T_{0ak}) + b_{pk} g^{ps} b_{s\zeta} g^{\zeta\epsilon} v_{i\epsilon}^* + \\ & + \left[ b_{pk} g^{ps} \right] \times \left[ b_{ij} g^{ja} \right] w_{as}^* - \\ & - \left[ \delta_{\cdot i}^{n\cdot} \sigma_{y\cdot k}^{i\cdot} - \delta_{\cdot i}^{1\cdot} \sigma_{y\cdot k}^{i\cdot} \right] - \\ & \left[ \delta_{\cdot k}^{m\cdot} \tau_{xzi\cdot}^{\cdot k} - \delta_{\cdot k}^{1\cdot} \tau_{xzi\cdot}^{\cdot k} \right] - Y_{ik} \end{aligned} \right\} \quad (38)$$

$$\left. \begin{aligned} \frac{d\tau_{xzik}}{dx} &= \frac{\lambda}{\lambda + \mu} b_{pk} g^{ps} \sigma_{xis} + \frac{4(\lambda + \mu)}{\lambda + 2\mu} \times \\ & \times b_{pk} g^{ps} b_{s\zeta} g^{\zeta\epsilon} w_{xi\epsilon}^* + \frac{2\lambda}{\lambda + 2\mu} \left[ b_{pk} g^{ps} \right] \times \\ & \times \left[ b_{ij} g^{ja} \right] v_{as}^* - \frac{2(3\lambda + 2\mu)}{\lambda + 2\mu} \alpha_T b_{pk} g^{ps} \times \\ & \times (T_{is} - T_{0is}) + \left[ b_{ji} g^{ja} \right] \times \left[ b_{kp} g^{ps} \right] v_{as}^* + \\ & + b_{ji} g^{ja} b_{\alpha\beta} g^{\beta\gamma} w_{\gamma k}^* - \left[ \delta_{\cdot i}^{n\cdot} \tau_{yz\cdot k}^{i\cdot} - \delta_{\cdot i}^{1\cdot} \tau_{yz\cdot k}^{i\cdot} \right] - \\ & - \left[ \delta_{\cdot k}^{m\cdot} \sigma_{zi\cdot}^{\cdot k} - \delta_{\cdot k}^{1\cdot} \sigma_{zi\cdot}^{\cdot k} \right] - Z_{ik} \end{aligned} \right\} \quad (39)$$

The reduced boundary conditions of stress–strain state will look like:

$$\left. \begin{aligned} & \frac{\mu}{\sqrt{1 + (k_{xx}^0)^2}} \sigma_{xik}^0 - \frac{k_{xx}^0}{\sqrt{1 + (k_{xx}^0)^2}} u_{ik}^{*0} + \\ & + \frac{\mu}{\sqrt{1 + (k_{xx}^{*0})^2}} q_{xvik}^0 + \frac{k_{xx}^0}{\sqrt{1 + (k_{xx}^0)^2}} u_{cik}^{*0} = 0, \end{aligned} \right\} \quad (40)$$

$$\left. \begin{aligned}
 & \frac{\mu}{\sqrt{1+(k_{xy}^0)^2}} \tau_{xyik}^0 - \frac{k_{xy}^0}{\sqrt{1+(k_{xy}^0)^2}} v_{ik}^{*0} + \\
 & + \frac{\mu}{\sqrt{1+(k_{xy}^0)^2}} q_{xyik}^0 + \frac{k_{xy}^0}{\sqrt{1+(k_{xy}^0)^2}} v_{cik}^{*0} = 0, \\
 & \frac{\mu}{\sqrt{1+(k_{xz}^0)^2}} \tau_{xzik}^0 - \frac{k_{xz}^0}{\sqrt{1+(k_{xz}^0)^2}} w_{ik}^{*0} + \\
 & + \frac{\mu}{\sqrt{1+(k_{xz}^0)^2}} q_{xzik}^0 + \frac{k_{xz}^0}{\sqrt{1+(k_{xz}^0)^2}} w_{cik}^{*0} = 0, \\
 & - \frac{\mu}{\sqrt{1+(k_{xx}^l)^2}} \sigma_{xik}^l - \frac{k_{xx}^l}{\sqrt{1+(k_{xx}^l)^2}} u_{ik}^{*l} + \\
 & + \frac{\mu}{\sqrt{1+(k_{xx}^l)^2}} q_{xzik}^l + \frac{k_{xx}^l}{\sqrt{1+(k_{xx}^l)^2}} u_{cik}^{*l} = 0, \\
 & - \frac{\mu}{\sqrt{1+(k_{xy}^l)^2}} \tau_{xyik}^l - \frac{k_{xy}^l}{\sqrt{1+(k_{xy}^l)^2}} v_{ik}^{*l} + \\
 & + \frac{\mu}{\sqrt{1+(k_{xy}^l)^2}} q_{xyik}^l + \frac{k_{xy}^l}{\sqrt{1+(k_{xy}^l)^2}} v_{cik}^{*l} = 0, \\
 & - \frac{\mu}{\sqrt{1+(k_{xz}^l)^2}} \tau_{xzik}^l - \frac{k_{xz}^l}{\sqrt{1+(k_{xz}^l)^2}} w_{ik}^{*l} + \\
 & + \frac{\mu}{\sqrt{1+(k_{xz}^l)^2}} q_{xzik}^l + \frac{k_{xz}^l}{\sqrt{1+(k_{xz}^l)^2}} w_{cik}^{*l} = 0.
 \end{aligned} \right\}$$

The next step – the problem numerically is simulated using the method of discrete orthogonalization by S.K.Hodunov [4]. Differential equations in partial derivatives are solved using the method of Runge–Kutta–Merson. This problem is programmed by the Fortran programming language. Depending on the geometry and initial–boundary conditions; temperature, displacement and stress are determined at certain points of the construction, which will be described in the next sections of the work.

## CONCLUSIONS

1. The suggested modification of the method of lines significantly increases the accuracy of calculation.

2. The problem of setting boundary function is solved and this allows the solution of problem of dynamics and thermoelasticity.

## REFERENCES

1. **Ali, J.S.M., Bhaskar, K., Varadan, T.K. 1999.** A new theory for accurate thermal/mechanical flexural analysis of symmetric laminated plates. *Composite Structures*. Vol. 45, 227-232.
2. **Cho, K.N., Striz, A.G., Bert, C.W. 1989.** Thermal stress analysis of laminate using higher-order theory in each layer. *Journal of Thermal Stresses*. Vol. 12, 321-332.
3. **Deineka I., Riabchykov O. 2013.** Rational design modeling methods of complex surface workpiece creation. *Teka*, Vol. 13, Nr 4, 59-68.
4. **Godunov S.K. 1961.** On the numerical solution of boundary value problems for systems of linear ordinary differential equations. *Advances Mathematical Sciences*. Vol. 16, Nr 3, 171-174 (in Russian).
5. **Kharlamov Y., Kharlamov M. 2013.** Design concepts of gaseous detonation guns for thermal spraying. *Teka*, Vol. 13, Nr 4, 82-91.
6. **Kovalenko A.D. 1970.** Fundamentals of thermoelasticity. *Scientific thought*, 308 (in Russian).
7. **Kovalenko A.D. 1975.** Thermo-elasticity. Textbook. High School, 215. (in Russian).
8. **Lodwik D., Malesa W., Wiktorski Z. 2013.** Polyoptimalization of the construction of subatmospheric pressure press with implementation of the finite element method. *Teka*, Vol. 13, Nr 1, 103-108.
9. **Mikhlin S.M. 1957.** Variational methods in mathematical physics. *Science*. (Fizmatgiz), 476 (in Russian).
10. **Riabchykov M., Chelysheva S., Voloshina O., Mokshina O. 2013.** Thermomechanical polymer material molding technique. *Teka*, Vol. 13, Nr 4, 208-216.
11. **Savoia, M., Reddy, J.N. 1997.** Three-dimensional thermal analysis of laminated composite plates-closure. *International Journal of Solids and Structures*. Vol. 34, 4653-4654.
12. **Senthil S., Batra R.C. 2001.** Generalized plane strain thermoelastic deformation of laminated anisotropic thick plates. *International Journal of Solids and Structures*. Vol. 38, 1395-1414.

13. **Shkelöv L.T., Stankevich A.N., Poshivach D.V. 2004.** Application of the method of lines for the determination of the stress and strain states of the spatial and plate structural elements. Monograph. KNUCA, 136 (in Russian).
14. **Sklifus Y., Mohyla V. 2012.** The results of the experimental research of the heat transfer coefficient during steam condensation in the tubes of the diesel radiator sections. Teka, Vol. 12, Nr 4, 264-267.
15. **Starchenko V., Burjak V. 2012.** Thermoelastic contact problem for the elastic half-space. Teka, Vol. 12, Nr 3, 148-150.
16. **Stankevich A.M., Chibiriyakov V.K., Skele L.T. 2010.** The method of lines in space problem of elasticity theory. Scientific and technical collection. Strength of materials and theory of structures, Nr 87, 109-117 (in Ukrainian).
17. **Stavsky, Y. 1963.** Thermoelasticity of heterogeneous anisotropic plates. Journal of Engineering Mechanics Division, Proceedings of ASCE, Vol. 89, 89-105.
18. **Tauchert, T.R. 1980.** Thermoelastic analysis of laminated orthotropic slabs. Journal of Thermal Stresses, Vol. 3, 117-132.
19. **Vekua I.N. 1982.** Common methods of constructing different versions of the theory of shells. Science. Home Editorial physical and mathematical literature, 286 (in Russian).
20. **Vinokurov L.P. 1956.** Direct methods for solving spatial and contact problems for arrays and foundations. Vasyly Karazin Kharkiv National University, 279 (in Russian).

ПРИМЕНЕНИЕ ОБОБЩЕННОГО  
МЕТОДА ПРЯМЫХ К ЗАДАЧАМ  
ТЕРМОУПРУГОСТИ ТОЛСТЫХ ПЛИТ

**Аннотация.** В данной работе предложен новый комбинированный метод понижения размерности дифференциальных уравнений пространственной задачи термоупругости. В основе лежит метод прямых в сочетании с проекционным методом Бубнова–Галёркина–Петрова, что значительно расширяет его возможности. Обобщенный метод прямых может быть применен для плит переменной толщины, в задачах динамики, термоупругости. Основная идея заключается в снижении размерности по пространственной координате с помощью проекционного метода, используя систему базисных функций. Данная статья является первой частью работы. В ней приведены редуцированные дифференциальные уравнения и предложен новый способ моделирования граничных условий.

**Ключевые слова:** метод прямых, метод Бубнова–Галёркина–Петрова, термоупругость, толстые плиты, строительная механика.

## A Finite Element Technique and Results of Continual Fracture Process Modelling

*Victor Bazhenov, Sergii Pyskunov*

Kyiv National University of Construction and Architecture  
Povitroflotsky prosp., 31, Kyiv, Ukraine, 03680, e-mail: s\_piskunov@ua.fm

**Summary.** The techniques of modeling of continual fracture process for space circular and prismatic bodies under long-term static or cyclic force loading condition and some results of determination of responsible parts lifetime is presented in this paper. The scalar damage parameter is used to describe the material continual fracture process. A stress-strain problem solution made with semianalytic finite element method (SFEM). It's shown, that the value of residual lifetime could be differ significantly for different loading condition and object configuration.

**Key words:** long-term loading condition, creep, damage, continual fracture, lifetime, spatial problem, semianalytic finite element method (SFEM).

### INTRODUCTION

Structural elements of responsible objects function often under long-term static or cyclic force loading. The process of creep or fatigue, accompanied by the gradual accumulation of scattered damage, the formation and growth of macroscopic defects (fracture zones) are occurs under such a loading conditions. This problem, similarly as well as other aspects of reliability analysis [1, 4], is very important, for a reliable determination of long-term strength and lifetime.

A description of above mentioned processes, which took the name «continual fracture», may be fulfilled efficiently using phenomenological scalar damage parameter, proposed in the works of V.Bolotin, L.Kachanov and Yu. Rabotnov. This approach is developed and implemented for different loading conditions in the publication of M.Bobyry, V.Golub, G.Lvov, Yu.Shevchenko [5, 7, 8, 9, 12] and in publication of foreign scientists (Chen G., Hayhurst D., Lemaitre J., Murakami S.,

Otevrel I. etc.). However, as noted in [10], the most actual problem is the determining the residual lifetime – time of fracture zone growth after the local loss of the material bearing capacity. Solving of this problem in the spatial definition is not reflected enough in scientific publications. On the other hand, such as highlighted in [11], the residual lifetime value may be up to half of the total time of structure element operation. Thus, it should be taking into account for correct final definition of part's operating time.

### PURPOSE OF WORK

The purpose of this paper is to highlight the main provisions of the developed technique for modeling of continual fracture zone growth of spatial bodies and presentation of the results of residual lifetime determination of responsible structural elements under different loading conditions.

INITIAL EQUATION  
AND METHODS OF ANALYSIS

$$\frac{d\omega}{dt} = C \left[ \frac{\sigma_e}{1 - \omega^r} \right]^m \frac{1}{(1 - \omega)^q} \omega^\beta, \quad (3)$$

*Continuum fracture mechanics relations.*  
The damage accumulation process described with kinetic equations using phenomenological damage parameter (DP)  $\omega$ , which changed in time from  $\omega(t=0) = \omega_0 = 0$  to  $\omega(t^*) = 1$ , where:  $t^*$  – is the time of the local loss of material bearing capacity.

The next view of kinetic equation for DP calculation is most simply for the multi-cyclic force loading [13]:

$$\frac{d\omega}{dN} = A \left( \frac{\sigma}{\sigma_B (1 - \omega)} \right)^n, \quad (1)$$

where:  $A$  and  $n$  – experimentally determined material constants,  $\sigma_B$  – tensile strength of the material.

It is expected, that under multi-cyclic loading condition process of material deforms elastically and the loading process can be carried out with variable parameters of the cycle (mean middle stress and amplitude). Therefore, it is provided for construction of DP value determining algorithm, that load process must be divided into a number of steps - steps for problem solving -  $S^*$ . Within each stage  $s$  ( $s=1, 2, \dots, S^*-1, S^*$ ) load means constant stress  $\sigma_{0s}$  and constant amplitude  $\sigma_{as}$  during the some quantity of cycles  $N_s$ . Using this assumption, the DP value by previous load history (up  $N_s$  cycles,  $N_s = \sum_{s=1}^S N_s$ ) is determined by a formula which obtained in [13] as a closed form solution of equation (1):

$$\omega_S = 1 - (n+1) \sqrt[1 - \frac{A}{(n+1)\sigma_B^n \sum_{s=1}^S (\sigma_{as})^n N_s}]{1 - \frac{A}{(n+1)\sigma_B^n \sum_{s=1}^S (\sigma_{as})^n N_s}}. \quad (2)$$

A DP value description under long-term static loading condition (when a creep process presence) conducted using the follow expression [7]:

where:  $C$ ,  $m$ ,  $q$ ,  $r$ ,  $\beta$  – experimentally determined material constants, which are functions of temperature,  $\sigma_e$  – equivalent stresses calculated according to the chosen strength criterion.

*Semianalytic finite element method (SFEM).* The solution of evolutionary problems of spatial bodies deformation process requires significant computational expences and special algorithms for regarding of damaged accumulation process and fracture zones growth simulation. It is not always possible to solve these problems using modern powerful finite element software systems (ANSYS, ABAQUS, etc.), based on traditional three-dimensional finite element problem definition.

SFEM is an effective instrument for numerical modeling of stress-strain state and deformation process of canonical form spatial bodies – inhomogeneous circle and prismatic bodies. The term "inhomogeneous" is used in the sense of the variability of the physical, mechanical properties and geometrical dimensions of the body along the forming. Being based SFEM, a discrete calculation model suggests the finite element mesh in the cross section of the examined object, and one finite element (FE) to be used in the orthogonal towards the cross sectional plane (along the forming, i.e.  $z^3$  coordinates. Thus, the FE size in the  $z^3$  direction is the same as the body one (Fig. 1).

SFEM allows significantly reduce the computational expences for solving of spatial problem, particularly on the stages of stiffness matrix calculating and FEM linear equations systems solving. The efficiency and accuracy of the method is shown for a wide range of linear and nonlinear problems of mechanics [2-4], where readers can also find a more detailed description of the method features, its implementation and links to additional author's publications.

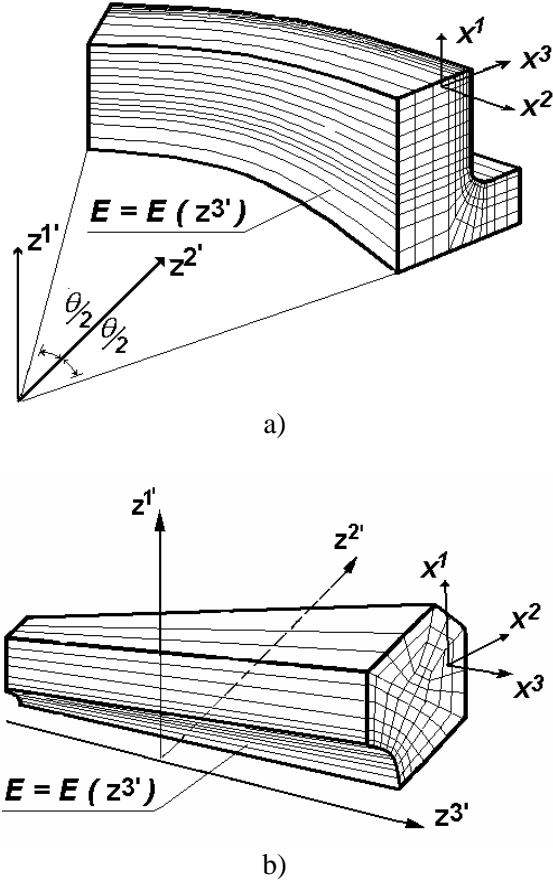


**Fig. 1.** Circle (a) and prismatic (b) inhomogeneous body

### FINITE ELEMENT ALGORITHMS FOR CONTINUAL FRACTURE PROBLEM SOLUTION

A problem of stress-strain state parameters determination under linear and nonlinear deformation process performed by the algorithm based on the use of the implicit integration over the time scheme with help of Newton-Kantorovich iterative procedure:

$$\{\Delta U_I\}_n^m = \{\Delta U_I\}_{n-1}^m + \beta [K_{II}]^{-1} (\{Q_I\}_n^m - \{R_I\}_n^m),$$

where: is  $1 \leq \beta < 2$  – relaxation parameter,

$\{Q\}_n^m$  – vector of full loads in nodes on step  $m$ ,  $[K_{II}]$  – FE stiffness matrix,  $\{R_I\}_n^m$  – vector of nodes reactions on iteration  $n$  of step  $m$ .

Creep problem solution considering damage accumulation is being executed by

means of step-by-step algorithm on the parameter of time. When starting each iteration  $n$  of a step  $m$ , stress values  $\sigma_{ij}$  are calculated considering creep deformation process by the formula:

$$(\sigma_{ij})_n^m = \frac{1}{3} \delta^{ij} (\overline{\sigma_{ij}})_n^m + (s^{ij})_n^m. \quad (4)$$

Components of stress tensor  $\overline{\sigma_{ij}}$  are defined in compliance with the Hook's law considering an increment of total deformation:

$$(\overline{\sigma_{ij}})_n^m = (\sigma_{ij})_{n-1}^m + (\Delta \overline{\sigma_{ij}})_n^m,$$

while the components of stress deviator  $(s^{ij})_n^m$  relate to an increment in creep deformation  $\Delta \varepsilon_{ij}^c$ :

$$(\Delta \varepsilon_{ij}^c)_n^m = (\xi_{ij}^c)_n^m \Delta t_m,$$

$$(s^{ij})_n^m = (\overline{s^{ij}})_n^m - G_1 (\Delta \varepsilon_{ij}^c)_n^m, \quad (5)$$

where:  $(\xi_{ij}^c)_n^m = \frac{3}{2} [\xi_i^c]_n^m \frac{(s^{ij})_n^m}{(\sigma_i)_n^m}$  – components

of creep deformation rate tensor,  $\xi_i^c = \frac{d\varepsilon}{dt}$ ,  $G_1 = E / (1 - 2\mu)$  – elastic constants,  $\Delta t_m$  – time interval value.

The DP values addition  $(\Delta \omega)_m$  and accumulated DP values  $\omega_m$  on a time interval  $m$  calculated with next relation:

$$\omega_m = \omega_{m-1} + (\Delta \omega)_m = \omega_{m-1} + \left( \frac{d\omega}{dt} \right)_m \Delta t_m. \quad (6)$$

The criterion of local loss of the material bearing capacity is  $\omega(t^*) > \omega^*$ , where  $\omega^* \approx 1$  – critical DP value. It's fulfillment in the some point of studied object  $K$  with coordinates  $(z^{i'})_K = z^{i'*} = \{z^{1*}, z^{2*}, z^{3*}\}$ ,

indicates the transition of the scattered damages accumulation process, which accounted integrally using DP, to occurrence of macroscopic defects – initial areas of continual fracture. This points in time determining the value of the estimated lifetime of studied object.

*Continual fracture zone growth modeling.* To simulate the initial macroscopic defects occurrence at the point  $K$  the area with volume  $V_0$  introduced there at the time point  $t = t^* + \Delta t$  (Fig. 2, a). The size of this area in plane  $z^1 - z^2$  is the same of FE size, in which condition  $\omega > \omega^*$  reached. The size  $\Delta z^3$  in the  $z^3$  direction defined as the sum of half the distance from the point  $K$  to neighboring integration points in FE (named as  $K-1$  and  $K+1$ ,  $\Delta z^3 = a_{k-1}/2 + a_k/2$ , Fig. 2, c). Values of stress and elastic modulus of the material taken as being equal to zero within a specified area:

$$\sigma_{ij}(t = t^* + \Delta t, z_i = z_i^*) = 0,$$

$$E(z_i = z_i^*) = 0. \quad (7)$$

Volume  $V_0$ , the value of which is caused by the discrete model parameters, defines the minimum increment of the characteristic size of the fracture zone in the course of its growth.

Implementation of (7) is carried out using special FE with adjusted values of physical and mechanical constants. The stress-strain state parameters and DP values determine by (3) - (6) during following point of time. This is accompanied by a gradual increase of fracture zone by acceding to it of a new volume  $V_m$  at time intervals  $t_m$  after fulfillment of condition  $\omega > \omega^*$  in appropriate points. The procedure of continual fracture zone growth modeling is performed to achieve a zone of critical size (volume)  $V^*$  (Fig.2, b). The appropriate time interval (number of cycles) determines the residual lifetime (vitality) of the object after the of fracture zones occurrence.

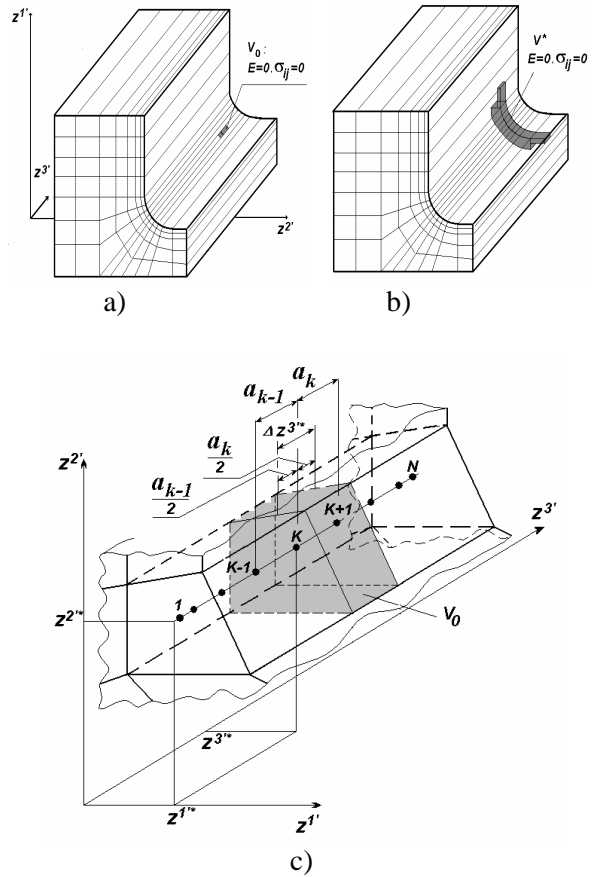


**Fig. 2.** Stages of continual fracture zone growth (a,b) and special finite element (c)

## RESULTS OF FINITE ELEMENT MODELING OF CONTINUAL FRACTURE ZONE GROWTH AND RESIDUAL LIFETIME DEFINITION

The allowed approaches being spent to solving of practical problems of residual lifetime definition of responsible structure element – the connecting union under multi-cyclic loading condition and the blade of a gas turbine under creep.

The connecting union (choke) of valve settings for high pressure polyethylene synthesis is a massive circle (cylindrical) body loaded with cyclic internal pressure. The initial defect is available on the inner surface of the choke - an weakened area of degraded material physical and mechanical properties. General view of the object and the FE discrete model, used for solving and

describing the defect presence, shown in Fig.3. The initial elastic stresses distribution in the absence of defect is uniform on choke's height ( $z^1$  axis).and variable along the it's radius.

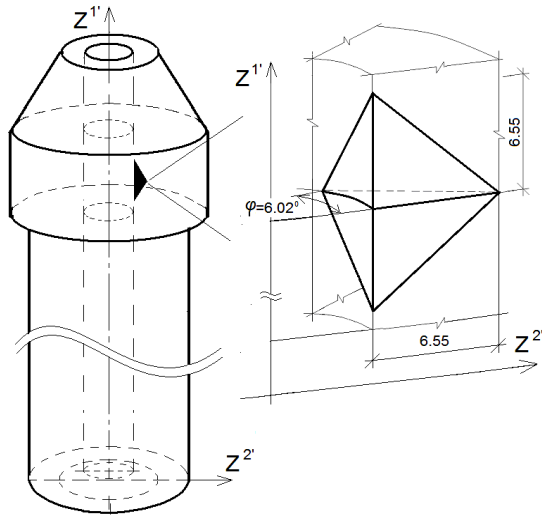


**Fig. 3.** The connecting union with initial defect

The description of the damage accumulation process performed with eq.(2) using  $\sigma_B = 1300$  MPa,  $A = 1.5495 \cdot 10^{-2}$  and  $n = 4,267$ . The degradation of material mechanical properties within the defect area performed with linearly change of  $n$  in the range 4,267-4,4 (increase of the value  $n$  indicates more intensive damage accumulation at the same level of stress). Estimated lifetime of the choke (until the local loss of the material bearing capacity) in the absence of the defect was  $4.9 \cdot 10^9$  cycles, and  $N^* = 3.89 \cdot 10^9$  for defect presence. The obtained DP values rapidly decreases at choke wall thickness with distance from the inner surface and at the distance of 3 mm from it DP value is less then 0,1. Thus, after the local loss of the material bearing capacity on the inner surface the wall remains virtually intact and the choke may be used stay in operation.

The simulation of fracture zone growth was conducted in axisimmetrical and spatial statement using FEM model, shown on Fig.4. It is shown, that time for zone growth in the radial direction (of the wall thickness) to

depth 1-5 mm, which obtained in axisymmetrical statement, is half less than one obtained in spatial statement. This difference gradually decreases: at a zone depth 12 mm (corresponding to half of the wall thickness) it is only near 5%. But in any case, the magnitude of the residual life after the fracture zone growth is almost an order greater than the time to zone occurred. Wherein, it should be noted, that during all of time of the fracture zone growth the detail keeps tight and relevant performance properties (Fig. 5).

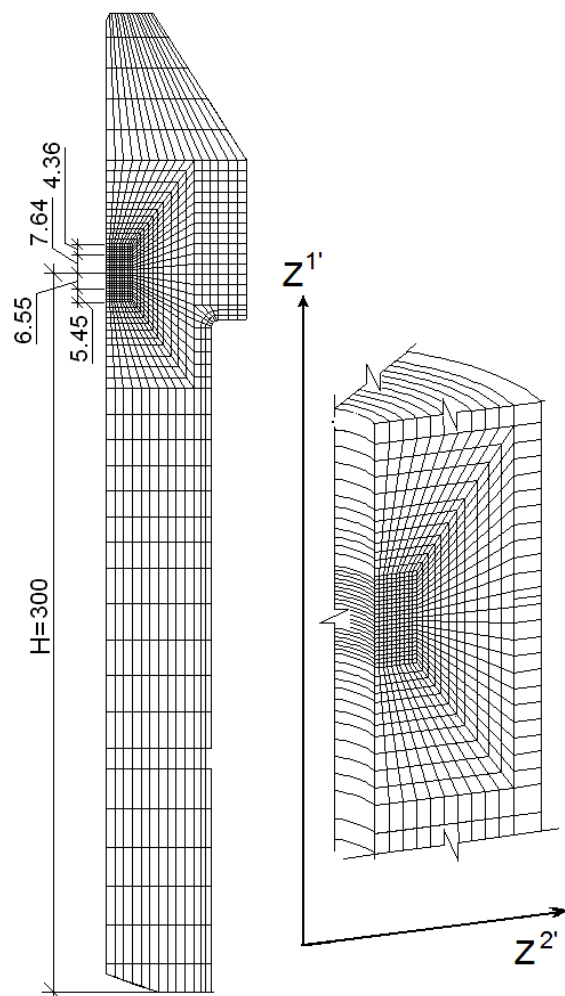


**Fig. 4.** SFEM discret model of connecting union pipe with defects

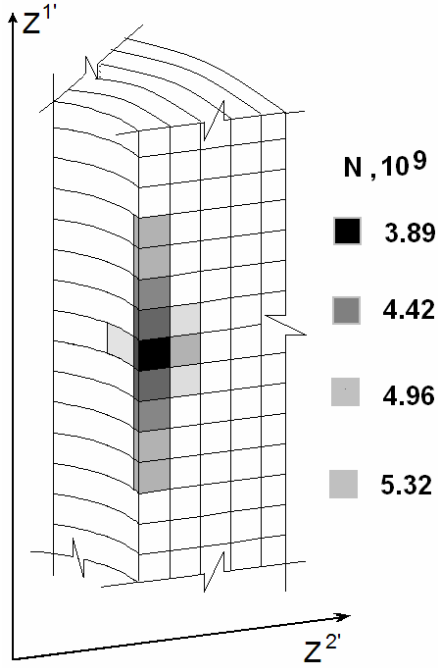


**Fig. 5.** Configuration of continual fracture zone after different number of cycles (b)

Stationary gas turbine blade is a spatial body of complicated shape. The blade is swirled at the vertical axis, has a variable at height cross-sectional area. It is influenced by centrifugal forces in a heterogeneous, both in height and in cross-section, temperature field (Fig.6, a). Based on results of elastic deformation modeling of blade, based on three-dimensional FEM, a dangerous cross section  $R_0$  was chosen. This section characterized with combination of average strain  $\sigma_0$  and average temperature  $T_0$ , which leads to the most intensive creep process and damage accumulation. Listed values ( $\sigma_0$  and  $T_0$ ) are used further to describe the design scheme and the results of the problem solving. Creep deformation process modeling is made for a blade fragment with size  $0,94 R_0 < R < 1,06 R_0$ . Fragment is loaded with its own centrifugal load  $p$ . The simulation of the upper part of blade in section  $R = 1,06 R_0$  implemented with unevenly distributed load  $q = q(z^1, z^2)$  that meets stress values, been applied in this cross-section (Fig. 6, b).

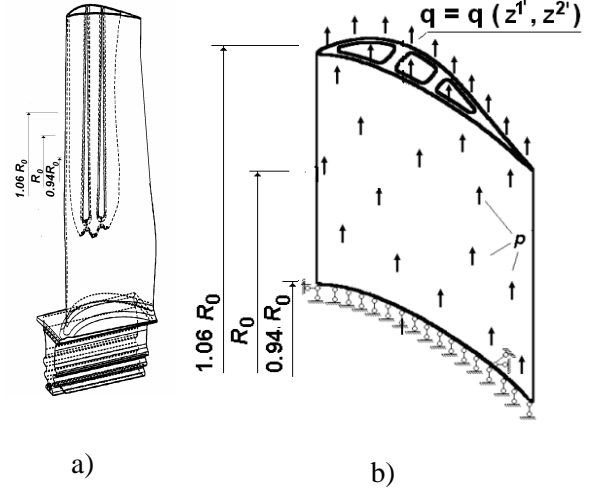


**Fig. 6.** Gas turbine blade: general view (a) and design scheme of blade fragment(b)

The description of creep and damage accumulation processes is carried out with the following equation:

$$\frac{d\epsilon_c}{dt} = \frac{B\sigma^n}{(1-\omega)^r}, \quad \frac{d\omega}{dt} = C \left( \frac{\sigma}{1-\omega} \right)^m \frac{1}{(1-\omega)^q}, \quad (8)$$

where:  $B = B(T)$ ,  $C = C(T)$ ,  $m = m(T)$ ,  $n = n(T)$ ,  $r = r(T)$ ,  $q = q(\sigma, T)$  – material constants,  $T$  – temperature.

The location of initial fracture zone within the fragment corresponding to the maximum value damage parameter was determined due to modeling of blade deformation under creep. Its location is aligned with the zone of maximum values of the DP at height of blade fragment (Fig. 7). It was required to use a finite element models with a significant number of nodes in a cross-section to determine of fracture zone's size and shape in the process of it's growth. The results fracture zone growth modeling up to complete loss of bearing capacity showed, that the proposed facility value of residual lifetime is low and is about 5% of the estimated lifetime. This suggests that the actual value of the blade lifetime is determined by local loss of bearing capacity in fact (Fig. 8).

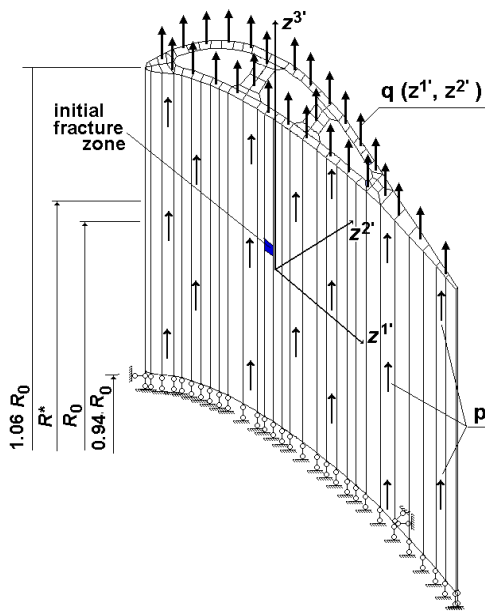


**Fig. 7.** Base SFEM discret model and initial fracture zone (c)

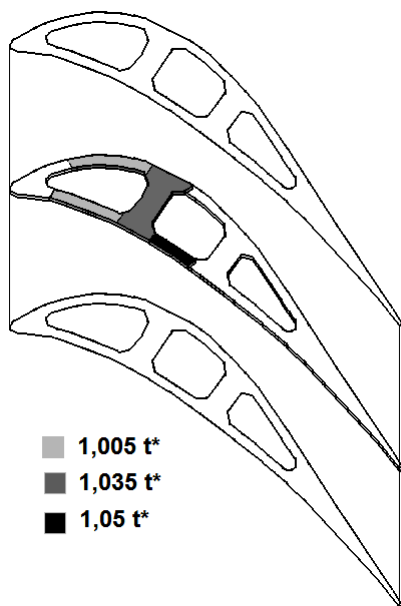


**Fig. 8.** Continual fracture zone configuration in blade fragment

### CONCLUSIONS

1. Developed in this paper methods for modeling of continual fracture process and fracture zone growth allows to determine of estimated and residual lifetime values for responsible structural elements that work under long-term static and high-cycle loading condition.

2. The values of residual lifetime may differ significantly for different objects and loading conditions. Thus, it's need to study a problem of extending of details operation time after local loss of bearing capacity in each individual case.

### REFERENCES

1. **Atamanyk I. 2012.** Polynomial stochastic algorithm of forecasting reliability of technical objects on the basis of the device of canonical decomposition. *Motrol*, Vol. 14, Nr 2, 67-73.
2. **Bazhenov V. 2011.** Linear and nonlinear fracture mechanic's problem solution using semianalytic finite element method: Part 1. Theoretical foundation and research of efficiency of finite element technique for fracture mechanic's problem solution. *Strengths of materials*, Nr 1, 24-33. Part 2. A technique for calculation of invariant of J-integral value in finite element model. *Strengths of materials*, Nr 2, 43-52.
3. **Bazhenov V. 2012.** Semianalytic finite element method in problems of continual fracture of spatial bodies. *Kyiv*, 248.
4. **Bazhenov V. 2014.** Semianalytic finite element method in problems of dynamic of spatial bodies. *Kyiv*, 336.
5. **Bobyry M. 2009.** Damage and fracture of structural elements. *Kyiv, Naukova dumka*, 392.
6. **Dumenko K. 2012.** Design of process of providing of reliability of combine harvesters. *Motrol*, Vol. 14, Nr 2, 51-56.
7. **Holub V. P. 2000.** Nonlinear continual damage mechanic and it's addition to creep and fatigue problem. *Int. Appl. Mech.*, Vol. 36, Nr 3, 31-66.
8. **L'vov H. 2008.** Creep and long-term strength of gas turbine structure parts regarding nonhomogenous temperature distribution. *Strengths of materials*, Nr 2, 37-44.
9. **Lelyukh Yu. 2006.** About finite-element solution of spatial termoviscoelasticity problem *Int. Appl. Mech*, Vol. 42, Nr 5, 16-25.
10. **Nikitenko A. 2007.** An evaluation of time of fracture front propagation of structural elements. *Strengths of materials*, Nr 6, 13-24.
11. **Nikitenko A. 2006.** A kinetic theory of creep and desing of structure elements for long-term strength. Part 3. The up and lower evaluation of start of fracture time for nonhomogeneous-heating structure elements. *Strengths of materials*, Nr 1, 32-40.

12. **Shevchenko Yu. 2011.** Specification of qualificatory equalizations of elasto-plastic deformation of transversal-izotropic material. Internatuional Apllied Mechanics, Vol. 47, Nr 6, 68-75.
13. **Sil'verstov Y. 2006.** Life-time determination and long-term strength using damage criterium. Problems of mashine-building and reliability of machines, Nr 6, 116-118.

**КОНЕЧНОЭЛЕМЕНТНАЯ МЕТОДИКА  
И РЕЗУЛЬТАТЫ МОДЕЛИРОВАНИЯ  
ПРОЦЕССОВ КОНТИНУАЛЬНОГО  
РАЗРУШЕНИЯ**

**Аннотация.** В статье представлена методика конечноэлементного моделирования процессов континуального разрушения

пространственных тел вращения и призматических тел под действием длительного статического и циклического нагружения. Для описания континуального разрушения использован скалярный параметр повреждаемости материала. Определение напряженно-деформированного состояния выполняется на основе полуаналитического метода конечных элементов. Показано, что относительная величина дополнительного ресурса существенно зависит от условий нагружения и конфигурации объекта.

**Ключевые слова:** длительное нагружение, ползучесть, повреждаемость, континуальное разрушение, ресурс, пространственная задача, полуаналитический метод конечных элементов (ПМКЭ).

## Modeling of Crack Growth Process in Spatial Bodies Under Cyclic Loading Condition

*Victor Bazhenov, Sergii Pyskunov, Oleksiy Shkryl*

Kyiv National University of Construction and Architecture  
Povitroflotskyy prosp., 31, Kyiv, Ukraine, 03680, e-mail: s\_piskunov@ua.fm

**Summary.** The algorithm for finite element modeling of fatigue cracks growth in the spatial bodies under cyclic loading using semianalytic finite element method (SFEM) is presented. The crack growth process is described by Paris' equation, stress intensity factor (SIF) is determined by the direct method. Testing of the algorithm is executed on the problem of the development of an elliptical crack in a prismatic body under the action of cyclic loading.

**Key words:** cyclic loading condition, crack, fracture mechanic, lifetime, spatial problem, semianalytic finite element method (SFEM).

### INTRODUCTION

The determination of bearing capacity of responsible structure elements of different industries of technique needs for the taking into account of initial cracks presence. At the static loading a crack growth and further swift destruction takes place at exceeding fracture mechanics parameters of their critical values. The other mechanism of destruction is a result of crack growth under cyclic loading condition. A value of fracture mechanics parameters (stress intensity factor, SIF, in particular), arrived under external loading can be substantially less than critical one in this case, but cyclic influence of loading causes the gradual increase of crack. The life-time of structure element with a crack is considered outspent when a crack sizes acquires critical values. Thus, it is of interest in this connection to model a crack growth process under cyclic loading condition and to determine the amount of loading cycles to the achievement of critical size a crack.

The most well-known results of research of deformation of spatial bodies with cracks are limited of fracture mechanics parameters

determination [1, 2, 6, 8, 10, 11] or with wide range experimental results of crack growth [12]. Moreover, there is some simplified and approximated methodologies for prediction of crack growth process: several results are known for plane (two-dimensional) problems [9, 13], three-dimensional problems has been considered using boundary elements method [7]. The more accurate results could be obtained using numerical techniques for stress-strain state analysis, in particular finite element method (FEM). Therefore the development of algorithms of crack growth process under the cyclic loading condition and it's realization using FEM is important problem.

### PURPOSE OF WORK

The purpose of this paper is to highlight the main feature semianalytic finite element method (SFEM), of the numerical techniques of crack growth process modeling for spatial prismatic bodies under cyclic loading condition, which has been developed using SFEM, and to show an

example of prognosis of shape and size changes of elliptical crack.

EQUATION AND METHODS OF ANALYSIS

*Fracture mechanics relations.* The crack growth process under the cyclic loading condition is characterized with the diagram of fatigue failure, that sets correlation between crack increment  $dl$  per number of loading cycle  $dN$  and change of SIF (or SIF increment  $\Delta K$ ). The most well-known approximation to this dependence is so-called Paris' relation [1, 12]:

$$\frac{dl}{dN} = C(\Delta K)^m, \quad (1)$$

where:  $C, m$  – constants, that is determined by material, temperature, environment and other loading factors.

Dependence (1) has some limitation concerned with terms of loading, sizes of details and other. Not looking on it, use of (1) allows to solve a wide range of practical problem about crack growth and life-time determination of responsible spatial structure elements [12].

*Semianalytic finite element method (SFEM).* The solution of spatial bodies deformation problems requires significant computational expences. The presence of crack increases it in times. Besides, a special algorithms for calculation of criteria fracture mechanic parameter (SIF in particular) and for crack growth process modeling are required. It is not always possible to solve these problems using modern powerful finite element software systems (ANSYS, ABAQUS, NASTRAN etc.), based on traditional three-dimensional finite element problem definition.

SFEM is an effective instrument for numerical modeling of stress-strain state and deformation process of canonical form spatial bodies - inhomogeneous circle and, in particular, prismatic bodies (Fig.1). The term "inhomogeneous" is used in the sense of the variability of the physical properties along

the forming. Being based SFEM, a discrete calculation model suggests the finite element mesh in the cross section of the examined object, and one finite element (FE) to be used in the orthogonal towards the cross sectional plane (along the forming, i.e.  $z^3$  coordinates). Thus, the FE size and configuration in the  $z^3$  direction is the same as the body one (Fig.2).

The main distinctive feature of SFEM is using of different approximation function in cross-section of the body (in plane  $z^1 - z^2$ ) and along  $z^3$  coordinates. Thus, the most universal representation of displacement using local FE coordinate system is:

$$u_{m'} = \sum_{S_1=\pm 1} \sum_{S_2=\pm 1} u_{m'(S_1 S_2)} \left( \frac{1}{2} S_1 x^1 + \frac{1}{2} S_2 x^2 + S_1 S_2 x^1 x^2 + \frac{1}{4} \right),$$

$$u_{s'} = \sum_{l=0}^L \bar{u}_{s'}^l \varphi^{(l)},$$

where:  $\varphi^{(l)}$  - is the coordination function systems, presented with Laugrange-Michlin polynoms.

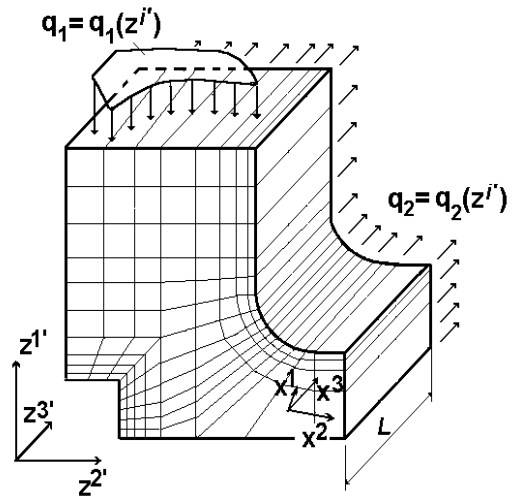
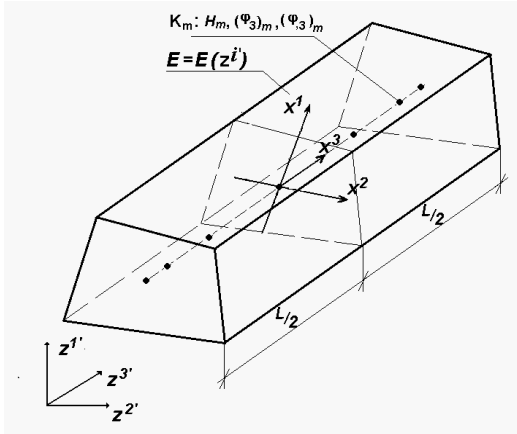


Fig. 1. Prismatic inhomogeneous body



**Fig. 2.** Prismatic inhomogeneous finite element

The stress-strained state parameters values are calculated in integration point  $K_m$  along  $z^3$  coordinates. The quantity of integration point depends of heterogeneity distribution of stress-strain parameters along  $z^3$  coordinates and determined on the basis of study of the convergence of obtained solution.

SFEM allows significantly reduce the computational expenses for solving of spatial problem, particularly on the stages of stiffness matrix calculating and FEM linear equations systems solving. The efficiency and accuracy of the method is shown for a wide range of linear and nonlinear problems of mechanics [3-5], where readers can also find a more detailed description of the method features, its implementation and links to additional author's publications.

### FINITE ELEMENT ALGORITHMS FOR FRACTURE MECHANIC'S PROBLEM SOLUTION

At the numerical decision of a crack growth problem under the cyclic loading condition the loading process presents with the sequence of steps after the cycles of application of the external loading. Corresponding discrete presentation of equation (1) for description of cracks growth has a next kind:

$$\frac{\Delta l}{\Delta N} = C(\Delta K)^m, \quad (2)$$

where:  $\Delta l$  – an increase of characteristic crack's sizes in the certain point of front for the amount of cycles of loading  $\Delta N$ .

At implementation of numeral integration of (2) provides calculation of follow values at each step:

- the SIF value  $K_I(l^i)$  in each point of crack front on the basis of results of the stress-strained state determination of body with a crack:
- the corresponding values of increase of characteristic sizes of crack after  $\Delta N$  cycles in every point of front  $i$  ( $i=1..k$ ):

$$\Delta l_m^i = C \left( K_I(l^i) \right)^b \Delta N_m. \quad (3)$$

- the characteristic sizes of crack  $l_m^i$  at every step  $m$  using sizes of crack on a previous step  $l_{m-1}^i$  taking into account their increases  $\Delta l_m^i$ :

$$l_m^i = l_{m-1}^i + \Delta l_m^i. \quad (4)$$

- the new coordinates of nodes of crack front are and of other nodes of FE model.

Consider the above procedure for the case of three-dimensional body.

In case of the spatial stress-strained state the curvilinear front of crack (shown on Fig.3 by a thick solid line) is approximated by the segments of polygon (shown on fig.1 by a stroke line), that consistently connect the nodes of discrete model, that located on the crack's front. Amount of this nodes is determined on the basis of convergence of numeral decision of problem about the stress-strained state of body with a crack and achievement of necessary exactness of determination of SIF distribution along front of crack.

In case of consideration of curvilinear cracks front, the SIF values and increases of characteristic sizes of crack, that is calculated on a formula (3), are variables along front. Accordingly, at every solution step the configuration of crack front changes.

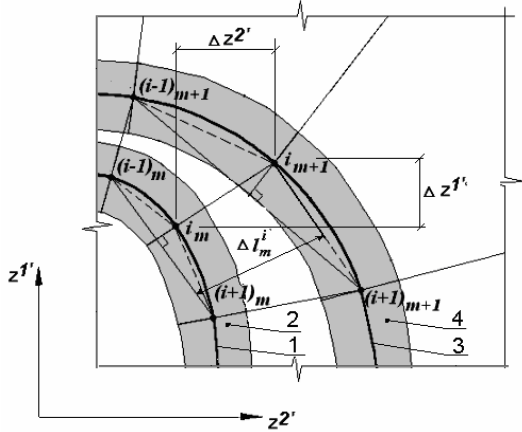


**Fig. 3.** The FE element discretization of the crack front and coordinates of front points: front of crack (1) and near-tip area (2) on the step of  $m$ ; front of crack (3) and near-tip area (4) on a step  $m+1$

A calculation of the SIF value  $K_I(l^i)$  executed by a direct method. It provides to use of obtained with finite element solution stress and displacement distribution near crack front (tip at two-dimensional case). The stress and displacement components, being oriented along the normal to the surface (front of crack) used in the most commonly sold type of fracture - normal separation crack, or crack of type I, Fig.4 [8].

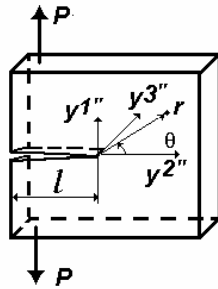


**Fig. 4.** Crack of type I (the normal separation crack)

SIF calculation executed separately from the values of stress  $K_I(\sigma)$  and displacement  $K_I(u)$  using well-known dependences :

$$K_I(\sigma) = \frac{\sigma^{1/2} \sqrt{2\pi r}}{\cos \frac{\theta}{2} \left( 1 + \sin \frac{\theta}{2} \sin \frac{3\theta}{2} \right)}$$

$$K_I(u) = \sqrt{\frac{2\pi}{r}} \frac{u_1 G}{\sin \frac{\theta}{2} \left( 2 - 2G - \cos^2 \frac{\theta}{2} \right)}, \quad (5)$$

where:  $r, \theta$  – point (nodes) coordinates (Fig.4).

SIF calculations executes within the limits of near-tip area of square form, with topological sizes of  $6 \times 6$  FE. The size of FE accepted as  $1/10$  of characteristic size of crack  $l_{cr}$ . The half of the marked near-tip area is examined for the case of the normal separation crack as a result of symmetry of distribution of stress-strain parameters in relation to the surface of crack. The description of crack location executed with boundary condition - absence of displacements in the nodes on plane of symmetry. Thus in prismatic bodies with transversal cracks (surface of crack is normal to  $z^3$  coordinates) the size of near-tip area in direction, normal to the surface of crack is equal to  $0,3 l_{mp}$  (Fig.5).

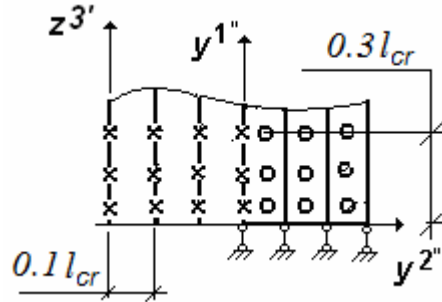


**Fig. 5.** The near-tip area for SIF calculation

SIF has been calculated after displacements ( $K_I(u)$ ) in part of area, that borders from a crack surface (in points, marked by crosses on Fig.5). SIF has been calculated after stresses ( $K_I(\sigma)$ ) in part of area, that that is located after front of crack (in points, marked by rounds on Fig.5).

Within the limits of each of the marked parts of near-tip area a mean SIF value after tensions  $K_{Iav}(\sigma)$  and after displacements  $K_{Iav}(u)$  are determined. Then this two values averaged in turn for determination resulting SIF value  $K_I$  :

$$K_I = \frac{K_{Iav}(\sigma) + K_{Iav}(u)}{2}. \quad (6)$$

At consideration of body with transversal crack SIF calculation is conducted in a certain amount of points along crack front. Their location coincides with nodes of FE model. Since SIF after displacements are calculated at the nodes (for example, crosssection 1-1, Fig.6), and SIF after stresses - in the center of finite element (crosssections 1'-1' i 2'-2', Fig.6), it is necessary to account for SIF after stresses in the two adjacent to FE nodes. This procedure is illustrated in Fig. 6 and with the following formulas:

$$[K_{I_{av}}(\sigma)]_1 = [K_{I_{av}}(\sigma)]_{1'} \quad (7)$$

$$[K_{I_{av}}(\sigma)]_2 = \frac{[K_{I_{av}}(\sigma)]_{1'} + [K_{I_{av}}(\sigma)]_{2'}}{2} \quad (8)$$

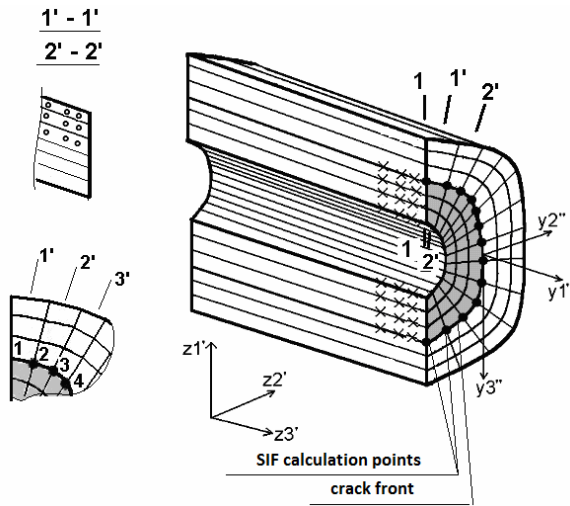


**Fig. 6.** Points of SIF calculation prismatic bodies

Calculation of coordinates  $(z^{k'})^i_m$  of node  $i$  of crack front on the step  $m$  executed after the values of increases of crack length  $\Delta l_m^i$  (3) in front points after next formulas (Fig.3):

$$\begin{aligned} (z^{k'})^i_{m+1} &= (z^{k'})^i_m + (\Delta z^{k'})^i_m, \\ (\Delta z^{k'})^i_m &= \Delta l_m^i \cos(\phi^{k'})^i_m, \end{aligned} \quad (9)$$

where:  $\phi^{k'}$  – a corner is between direction to the axis  $z^{k'}$  and by direction of movement of points of crack front:

$$\begin{aligned} \phi^{1'} &= \pi/2 - \alpha = \pi/2 - \text{arctg} \left( \frac{(z^{2'})_m^{i-1} - (z^{2'})_m^{i+1}}{(z^{1'})_m^{i+1} - (z^{1'})_m^{i-1}} \right) \\ \phi^{2'} &= \phi^{1'} - \pi/2. \end{aligned} \quad (10)$$

The change of all nodes of near-tip area executed on identical dimensions, calculated by after correlations (9), (10) along the line, that is normal to the front of crack. This line is passes through a point of front. It allows to save the characteristic sizes of FE of near-tip area during a crack increase.

The change of location of nodes, that lie outside of near-tip area on the same distance in the case of modeling of crack growth in the finite size bodies leads to the formation of degenerate FE at the boundary of the body, as illustrated in Fig.7,a. It was suggested to overcome this problem, to displace of nodes of a discrete model within near-tip area size on crack increment and to displace nodes outside of near-tip area to a distance that decreases linearly inverse-proportional to the distance from each node to the crack tip (Fig. 7,b). This method is more complex in terms of implementation, but it allows to get rid of the problem of the formation of degenerate FE.

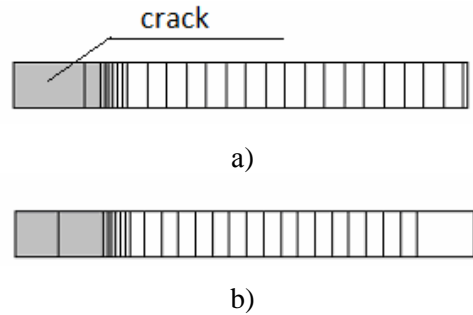


**Fig. 7.** Type of fragment of discrete model after crack growth: at the displace all the nodes on identical distances (a); at the displace the nodes on different distances with application of linearly inverse-proportional reduction (b)

## RESULTS OF FINITE ELEMENT MODELING OF FRACTURE DUE TO CRACK GROWTH

The approbation of algorithm of crack growth modelling in spatial bodies was con-

ducted on an example about growth of initial elliptic crack in an endless prismatic body under the action of the cyclic loading. (Fig.8,  $a=0.6$ ,  $b=0.4$  ).

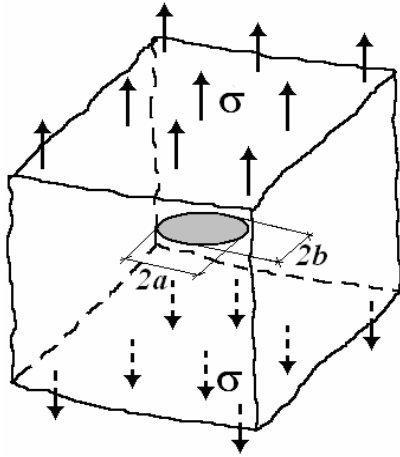


**Fig. 8.** An endless body is with an elliptic crack

As the examined object has three planes of symmetry, a discrete model is built for a 1/8 part of body (Fig.9).

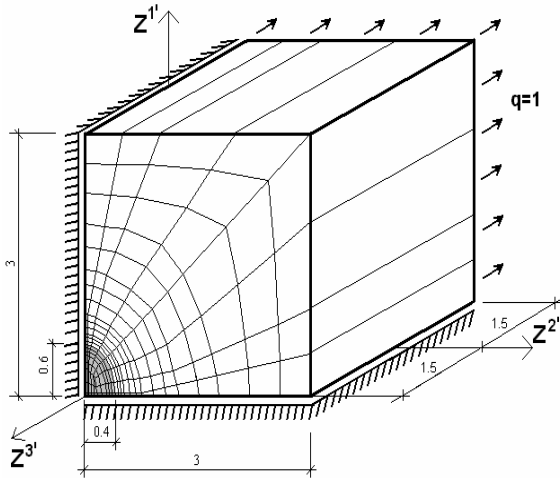


**Fig. 9.** A discrete model of SFEM for an endless body with an elliptic crack

The distribution of SIF along the front of initial crack, obtained with consideration of SFEM solution convergence on quantity of FE in cross-section mesh and on quality of polynoms  $\varphi^{(l)}$  in displacement distribution, is shown on Fig.7. It well comports with standard values of with well-known analytical decisions [6]. Thus, it could be expected, that further modeling of crack growth would be correct.

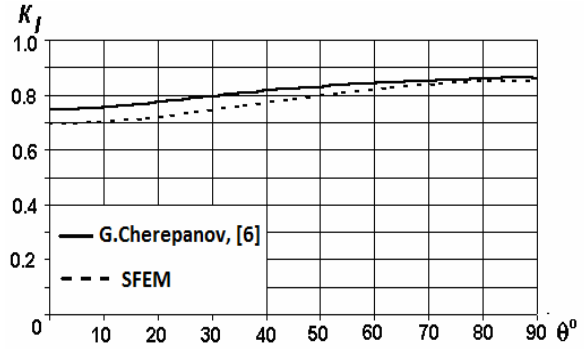


**Fig. 10.** Distribution of SIF along the initial front of crack

The values of constant of Paris' equation for crack growth description were accepted the next:  $b = 4$ ,  $C = 1.63 \times 10^{-10}$ , that corresponds to steel in normal temperature condition.

During realization of algorithm of crack growth modeling two alternate variants of changing of configuration of discrete model was studied. According the first one it is considered, that crack growth at every step takes place in orthogonal direction to current configuration of crack front. Realization of this supposition on a discrete model suggested, that the value of crack increases  $\Delta l_m^i$  is put aside along a line, which is orthogonal to the segment, that connects  $(i-1)_m$  and  $(i+1)_m$  points of front. According to the second variant crack growth at every step considered after a perpendicular to front of initial crack. In this case the value of crack increases  $\Delta l_m^i$  in points front is put aside along a line, orthogonal to the segment that connects points  $i-1$  and  $i+1$  of initial front of crack.

Verification of authenticity of application of foregoing suppositions was made on the basis of analysis of results convergence at successive reduction to the step after the some amount of loading cycles and on it coincidence of final result with the data given in [6].

Results testify that convergence of step-by-step algorithm of problem solution depending after the size of step  $\Delta N$  is more better at application of the first variant. The difference between the characteristic sizes of crack, calculated after 24 and 48 steps of problem solution, which corresponds

$30 \times 10^8$  cycles of loading is not significant and folds 2.6% for the first variant and 1.1% for second variant. However, the final characteristic sizes of crack after 48 steps differ on 14% for two variants. Dependence of error of length of crack calculation at  $M$  steps of problem solution in relation to the characteristic sizes of crack, certain at 48 steps for the front points, that is located on lines along axes  $z^1$  ( $\theta=0^\circ$ ),  $z^2$  ( $\theta=90^\circ$ ) for the first variant shown on a Fig 11. The general view of configuration of crack front and near-tip area after  $30 \times 10^8$  cycles by comparison to initial, shown on Fig.12.

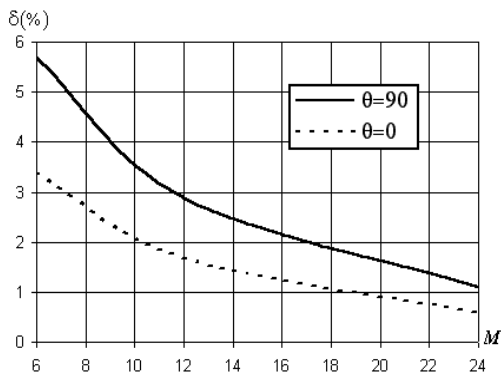
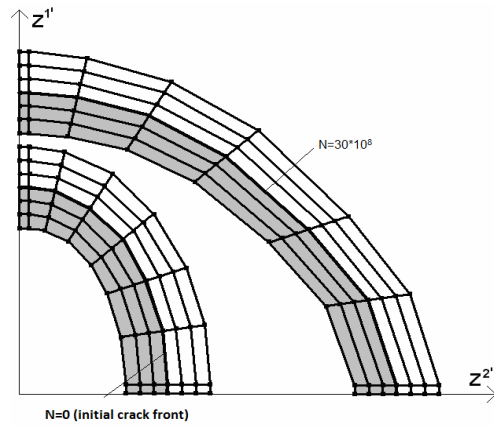
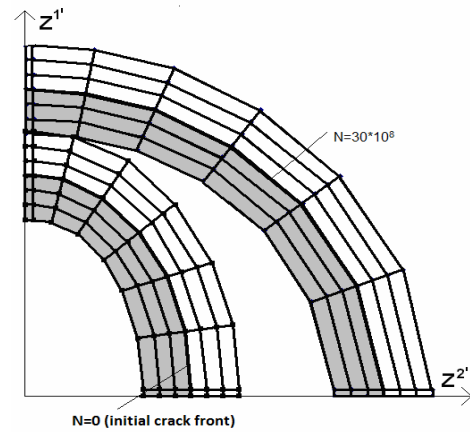


**Fig. 11.** A relative error of length of crack calculation

As as can be seen from Fig.12 the selection of algorithm significantly affects not only the quantitative growth of the crack (the number of cycles and the characteristic sizes) but also on the final configuration of the front. According to work [6] by conclusions, growth of initial elliptic crack will come true so that configuration of front will head for a circle. The marked reasoning is fully confirmed that the modeling of crack growth in every point should be in a direction orthogonal to current configuration of front (Fig.12, a). In another case, configuration of front crack takes shape of ellipse, prolonged in direction orthogonal to the initial location of front of crack (Fig.12, b).



a)



b)

**Fig. 12.** Configuration of crack front and near-tip area of discrete FE model at application of the first (a) and second (b) variants of algorithms

Further decision of problem has shown, that the crack front in future transformed to circle shape and the process of crack growth occurs rapidly (Fig. 13).

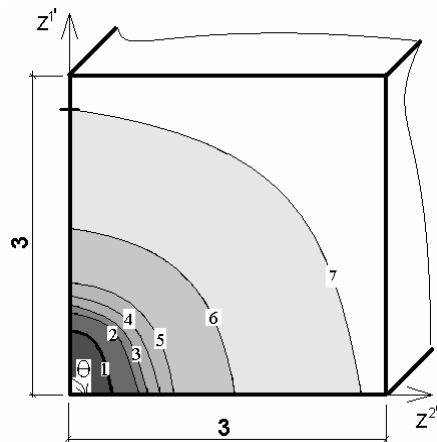


**Fig. 13.** Configuration of crack front after  $N$  of loading cycles: 1- initial crack ( $N=0$ ), 2 –  $N=16 \times 10^8$ ; 3–  $N=20 \times 10^8$ ; 4–  $N=24 \times 10^8$ ; 5–  $N=32 \times 10^8$ ; 6–  $N=48 \times 10^8$ ; 7–  $N=56 \times 10^8$

## CONCLUSIONS

1. The developed algorithm of restructuring of FEM discrete model provides the ability to reliably modeling crack growth. Numerical results of solving the test problem coincides with the calculated results of other authors.

2. Applied assumptions about the development of cracks in a direction orthogonal to its current configuration dozvolyayuye adequately simulate the process of crack growth in spatial bodies which are characterized by a curved crack front configuration and variability values SIF along the crack front.

## REFERENCES

1. **Anderson T.L. 2005.** Fracture mechanics: Fundamentals and Applications, Third Edition.-CRC Press, 640.
2. **Aturi S. 1986.** Computation Methods in the Mechanics of Fracture. North-Holland Publishing Co., Amsterdam, 430.
3. **Bazhenov V. 2011.** Linear and nonlinear fracture mechanic's problem solution using semianalytic finite element method: Part 1. Theoretical foundation and research of efficiency of finite element technique for fracture mechanic's problem solution. Strengths of materials, 2011, Nr 1, 24–33. Part 2. A technique for calculation of invariant of J-integral value in finite element model. Strengths of materials, 2011, Nr 2, 43–52.
4. **Bazhenov V. 2012.** Semianalytic finite element method in problems of continual fracture of spatial bodies. Kyiv, 2012, 248.
5. **Bazhenov V. 2014.** Semianalytic finite element method in problems of dynamic of spatial bodies. Kyiv, 2014, 336.
6. **Cherepanov G.P. 1974.** Mechanics of brittle fracture. – Moskow.: Nauka, 1974, 640.
7. **Cisilino A.P., Aliabadi M.H. 1999.** Three-dimensional boundary element analysis of fatigue crack growth in linear and non-linear fracture problems: Eng. Fract. Mech. 1999. 63, Nr 6, 713-733.
8. **Morozov E.M., Nikishkov G.P. 2002.** Finite element method in fracture mechanics. – Moskow.: "Librocom", 2010, 256.
9. **Plashinskaya A. 2002.** To the problem of fatigue failure modeling of the central cracked

- plates under single-axis loading condition. Tr. NGASU Proc., 2002, Nr 1, 22-31.
10. **Savruk M.P. 1988.** Fracture mechanics and strength of materials: Right. Manual, Vol.2: The stress intensity factors in bodies with cracks, Kiyv, Naukova Dumka, 1988, 620.
  11. **Sharan Shailendra K. 2000.** Elasto-plastic finite element analysis of a crack in an infinite plate: Int. J. Fract. 2000. 103, Nr 2, 163-176.
  12. **Troschenko V.T., Pokrovsky V.V., Prokopenko A.V. 1987.** Crack resistance of metals under cyclic loading condition. Kiyv, Naukova Dumka, 1987, 257.
  13. **Yonglin Xu. 1998.** Self-similar crack expansion method for two-dimensional cracks under mixed mode loading conditions: Eng. Fract. Mech., 1998, 59, Nr 2, 165-182.

МОДЕЛИРОВАНИЕ РАЗВИТИЯ ТРЕЩИН  
В ПРОСТРАНСТВЕННЫХ ТЕЛАХ ПРИ  
ЦИКЛИЧЕСКОЙ НАГРУЗКЕ

**Аннотация.** В статье представлен алгоритм конечноэлементного моделирования развития усталостных трещин в пространственных телах при циклическом нагружении. Механизм развития трещины описывается уравнением Пэриса. Коэффициенты интенсивности напряжений на каждом шаге задачи определяются прямым методом. Апробация алгоритма выполнена на задаче о развитии эллиптической трещины в призматическом теле под действием циклической нагрузки.

**Ключевые слова:** циклическая нагрузка б трещина, механика разрушения, ресурс, пространственная задача, ароуаналитический метод конечных элементов (ПМКЭ).

## Interaction Study of the Frame Building With Foundation Weakened by the Underground Mines Under the Seismic Load

*Volodymyr Sakharov, Veronika Zhuk, Liudmyla Skochko*

Kyiv National University of Construction and Architecture  
31, Povitroflotsky Avenue, Kyiv, Ukraine, 03680, e-mail: vlad@knuba.org.ua

**Summary.** These article describes the researching results of the underground man-triggered cavities' influence on the stress-strain state of the «soil base – foundation – structure» system elements under the seismic loads using the numerical simulation.

**Key words:** non-uniform deformation, frame, numerical modelling, mine, underworked area, seismic load, SFSI.

### INTRODUCTION

Today we need to increase the reliability and the safety of the buildings and the facilities usage (especially) in the seismic regions of Ukraine. It can be reached if we will do complex analysis with the numerical simulation with the usage of the seismic affection on the buildings components.

In the most cases there is the one special loading in force combinations is being considered at the designing [1]. At that time, as the other special loading can be added in practice, and this also can lead to the increased (total) impact. The proposal of the additional effects accounting was made at the new edition of the design standards [2], which can arise during the construction on the collapsible soils. There are a lot of the scientists agree with this point of view. The European design standards [3] give the designer opportunity to consider emergency combinations of the loading at his own discretion.

The one of such problem is the task of the accounting the underground cavities, which can affect on the behavior of the soil base. This article doesn't describe the common problems of the surface treatment at the coal

and other minerals underground extractions, because they are related to the specific man-triggered processes. The main question is the necessity of the accounting the mutual influence of the buildings and facilities on the built up areas with the anthropogenic or natural origin voids. All this can be concerned to the subway lines, underground transport tunnels, man-triggered premises, communications tunnels and cavities which historically formed in these areas (the catacombs, the underground passages and structures). The solution cavities have their own characteristics of the underground cavities forming.

This paper describes the problem of the influence of the man-triggered underground cavities on the stress-strain state of the buildings and soil base by the actions of the seismic loads.

### PURPOSE OF WORK

The purpose of the researching was the qualitative and quantitative estimation of the influence on the strain-stress state of the frame structures from the presence mines in the soil base and the consideration of their possible destruction.

## ANALYSIS METHODS OF EXTRACTION

The existing engineering calculation methods strongly limit the possibility of the excluding the impact of the mines on designed and operated building or structure. These tasks are difficult because of the necessity of the verifying the theoretical propositions; obtaining the detailed baseline data for the materials and loads as well as the time-consuming calculations. Such researches today are possible to carry out only by the numerical modeling.

### NUMERICAL MODELING CONCEPT

Modern development of the mechanic of massive medium relies on the phenomenological models for load and deformation determination in the soil base, oriented on opening of deformation processes in the massive medium. Algorithms of the mechanic of massive medium use mathematical set of theories of elasticity, plasticity and creep, based on the experimental parameters. To determine baseline data and choosing deformation models, soil base modeling is related to the problem of the iterative solving of high-order equation systems, which requires massive computer resources. As a result, in most cases, calculations on seismic impacts are limited to the use of simplified models and computational methods, which prevents consideration of the real properties of a soil base (e.g., the Winkler soil model and similar models).

Such approach requires the use of the numerical simulation methods of the processes of soil deformation on various stages of loading as a necessary condition for prognosis of stress-strain state of the soil base. The finite element method (FEM), boundary elements method (BEM) and others are used successfully for calculation of stress strain state (SSS) of the soil base. Also it is necessary to emphasize new problem of the identification of the functions defining change of parameters that correspond to the soil state depend-

ing on stress gradient in this zone and the character of loading (static or dynamic).

For discrete systems with many degrees of freedom for FEM we have system of ordinary differential equations:

$$[M] \frac{d^2}{dt^2} \{U\} + [C] \frac{d}{dt} \{U\} + [K] \{U\} = \{Q(t)\}, \quad (1)$$

where:  $[M]$  – mass matrix,  $[C]$  – dissipation matrix,  $[K]$  – rigidity matrix,  $\{U\}$  – vector displacement,  $\{Q(t)\}$  – loading vector represented as a time function.

To estimate the stress-strain state of the constructions under the seismic loads presented as three-component calculation accelerograms.

In the deformation of soil under the influence of dynamic oscillations, a significant role is played by the internal and external processes associated with energy dissipation. For structural constructions and bases, the main role is played by forces of internal resistance caused by the rheological characteristics of the material behavior.

To describe the decay processes should be used dependencies obtained from experimental data. However, given the complexity and high cost, and in some cases impossible to conduct experiments using different models of damping. In this work one of the commonly used Foight model, where dissipation  $[C]$  represented by the expression:

$$[C] = \beta [K], \quad (2)$$

where:  $\beta$  – damping coefficient with stiffness matrix.

To describe  $\beta$  damping the slide-decrement oscillations  $\delta$  used in standards [2]. To apply the parameter of the overall viscosity  $\xi$  should be determine due to decrement of oscillations  $\delta$ :

$$\xi = \frac{\delta}{\sqrt{4\pi^2 + \delta^2}} = \frac{\beta \cdot \omega_0}{2}, \quad (3)$$

where:  $\omega_0$  – natural frequencies.

Value  $\omega_0$  was adopted with first natural (eigen) frequency of the construction.

External factors for energy dissipation include the interaction of the system with elements of the environment in which the oscillations occur – the surrounding soil, air, special damping devices, seismic isolation systems, and so forth, designed for oscillation damping. These processes are not directly related to deformation of soil or of the construction's material, but affects the overall energy. In this paper we used one of the most common options for incorporating energy radiation into outer space – the limiting damping method proposed by Lismer [14] and based on the use of viscous damping of degrees of freedom on the boundary elements. The method provides absorption of energy approaching the border, and prevents the processes of wave reflection at the boundaries of the body corresponding with actual conditions.

To estimate the stress-strain state of the constructions under the seismic loads presented as three-component synthetic calculation accelerograms the method of the direct integration of incomplete spectrum of the own pares is used. Vector of full displacements can be factorized by forms of the eigen-oscillations and written through the amplitude and eigen forms as a sum:

$$\{U\} = \sum_{i=1}^N A^i \{X_i\}, \quad (4)$$

where:  $A^i$  – amplitude of the oscillations,  $\{X_i\}$  – vectors of the eigen oscillation forms,  $N$  – number of eigen oscillation forms.

Characteristics were defined through Duhamel integral for each component of the spectrum during the period of seismic oscillations validity. While the number of the own pares is increasing, their contribution to the displacement value is decreasing.

#### SOIL – FOUNDATION – STRUCTURE INTERACTION

Let us consider the research of the mutual influence on the system elements «soil base – foundation – structure» in the case of the real

object – the residential complex (Fig.1) the erection of which was planned on the potentially underworked area.

The multistoried residential complex with the underground parking is the complex of three 23-storey buildings, and the last two from those building are the three-section constructions, which have the expansion joints between the sections. The complex of the three buildings unites the solid two-storey underground parking under the entire area of the complex (Fig. 1). Each section of the residential buildings is the multistory construction: two underground floors of the parking, 23 aboveground floors and technical attic floor. The frame of buildings is designed in a monolithic form. The foundation of the residential complex is the pedestal footing with the jacked-in piles, the length of piles is 13m, cross-section of piles is 350×350mm. The height of the grillage for the altitudinal part of the building is 1.5 m, for parking – 1.0 m.



**Fig. 1.** A multi-storey residential complex with underground parking:

1 – adult zone, 2 – children's area, 3 – flowerbed, 4 – border of the parking

The geological structure of the site (Fig.2) is represented by the quaternary settlement, the Neogene soils are located below. The entire stratum of the surface is covered with the filled soils.

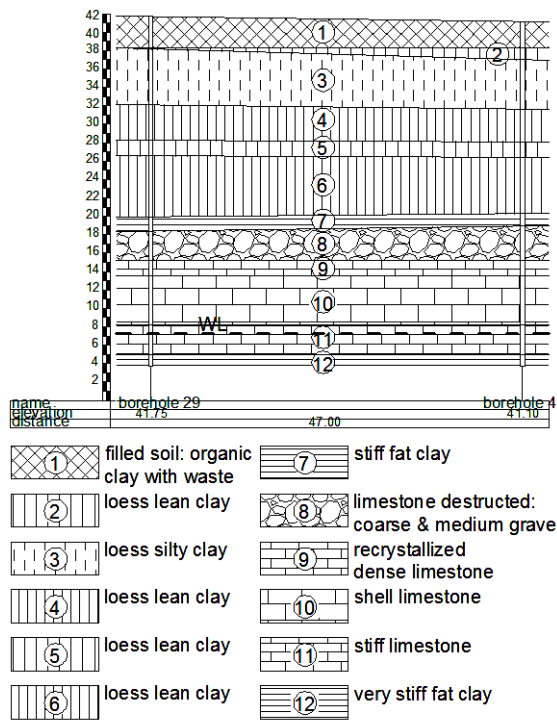


**Fig. 2.** The geological conditions of the site

The presence of the underground mines which eventually possible can cause the crash of the ceiling covering is fixed near to the excavation of the building in the shell limestone's layer (EGY – 10). The planning and vertical characteristics of the mine are shown in Fig. 3. This can cause the collapse deformation and surface dips at the larger destructions. Some reasons of the ceiling covering collapse are the pressure from the new buildings and the dynamic load (seismic intensity of territory is 7 balls). Therefore, the researches of the mutual influence of the building and the soil base with the mines were conducted with the considering emergencies.

Odessa mines are the underground quarries, where the stone buildings formerly dig. There was the widespread in the central part of Odessa region shell limestone layer extracted in that place for the building purposes. It was only durable and affordable building material in the steppe zone of southern Ukraine. At the present time the Pontian shell limestone cover all the central part of Odessa region. The average stratum of the limestone layer varies from 5 to 12 m near

Odessa area. The structure of the limestone strata is following: the lower part is represented by the uniformly cemented saw limestone, the top part is composed by the strongly recrystallized dense limestone - coarse gravel. The sawing limestones are the enough light formation (the volumetric weight is 1100...1500 kg/m<sup>3</sup>).

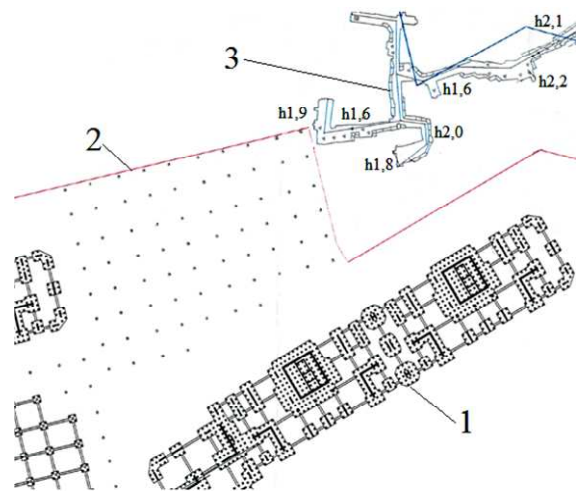


**Fig. 3.** Location of mines that were detected nearby the pit of the residential complex: 1 – altitudinal part of residential complex, 2 – border of the parking, 3 – underground cavities (mines)

The researches of the mine influence and the residential complex are conducted by using the numerical modeling of the teamwork of the system elements «soil base – foundation – structure», this model was made by the finite elements method based on the automated research system «VESNA» in the three-dimensional model. The soil base was considered as an elastic laminated soil according to the geological section (Fig. 2). The soil parameters are the following: the deformation modulus  $E$ , the specific gravity  $\gamma$ , the Poisson coefficient  $\nu$ , the specific cohesion  $c$ , the angle of the internal friction  $\varphi$ . The minimal value of the deformation modulus for the limestone layers  $E=50$  MPa has been accepted for the ensuring the reliability of the calculations. This value corresponds to the low compressibility soils (the uniaxial compression strength is  $R_c=0,8...1,0$  MPa according to the research).

The solution of the problems on the effect of the static and seismic loads were provided for the consideration of the interference between the construction of the residential complex and the parking in terms of the potentially underworked territory based on the emergency situations:

- the interaction between the building and the soil base does not taking into account the presence of underground mines,
- the interaction between the building and the soil base including the presence of underground mines,
- the interaction between the building and the soil base forced by the destruction of the catacombs,
- the interaction between the building with the soil base under the action of the seismic loads.

The part of the complex (Fig. 4), which is located closer to the underground mines considered for the evaluation of the collaborative framework and the soil, which has the underground cavities.

The results of the numerical modeling collaborative system «soil base – foundation – structure» do not taking into account the presence of the underground mines based on the following: the predicted settlement below the center of the gravity of the building is expected to be not more than 4.8 cm; the settlement of the last row of the piles – is not more than 1.57 cm. Wherein, the settlement of the soil base in the area of underground cavities is not more than 2...5 mm.

The comparison of the bearing structures' strains of the building and the soil bases elements showed that the presence of the underground mines near the excavation complex actually doesn't cause changes. The calculations were made for the soil base does not taking into the account the presence of the underground mines, and with taking into account their availability. In this case of the vertical stresses in the elements of ceiling coving of the underground mines (zone nearby parking's corner) are expected not more than 50 kPa by the results of the calculations. This is not more than the domestic pressure and is perceived easily by the layer of the li-

mestone, where the mine is made.

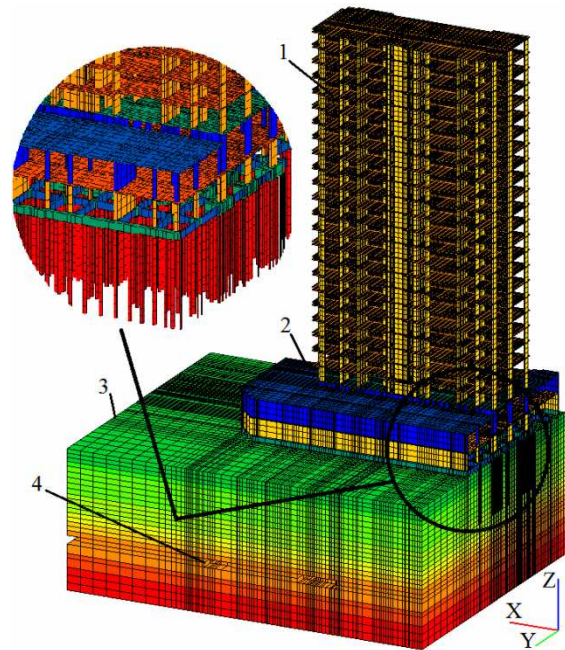


**Fig. 4.** Three-dimensional finite element model for solving the problem of teamwork structure with soil base by using «VESNA»:  
1 – altitudinal part of residential complex,  
2 – parking, 3 – laminated soil base,  
4 – underground cavities (mines)

The stress-strain state soil mass on the weight of the building with taking into account the presence of the workings in the vicinity of the pit complex was accepted for the assessing the relative subsidence of the residential complex, with the possible ceiling coving mines' collapse. At the same time the stress and strain of the previous stage were considered.

The numerical modeling of the disaster collapse of the catacombs ceiling coving was showed that the deformation of the soil base fragments are expected in the area which does not cover the foundation of the altitudinal part of the residential complex. At the same time, the predictable additional displacements of the parking foundation (Fig.5) that are causing the destruction by the emergency mines are not essential. The corner zone of parking received the additional settlement by 0.2 ... 0.8 mm. The settlement of the piles on the contour is expected maximum value 0.8 mm. In this case the predicted

relative difference of the settlements at grillage's corners (Fig.5) is  $\Delta S/L=0,00003$  (the maximum value by Code [4] is  $(\Delta S/L)_u=0,002$ ).

The numerical modeling for the system «soil base – foundation – structure» was made by the direct dynamic method in order to research the strain stress state of the bearing structures of the residential complex from the effect of the seismic loads. The Voigt model is used as the model for the energy dissipation for the soil and structures for solving this task. The own couples (for building structures with the soil base) were calculated to select the seismic loads and to determine the modes and the frequencies of the oscillations. These own couples were calculated in an amount which corresponds to a set of the modal mass in the directions  $X$ ,  $Y$ ,  $Z$  accordingly 85%, 85% and 75%.

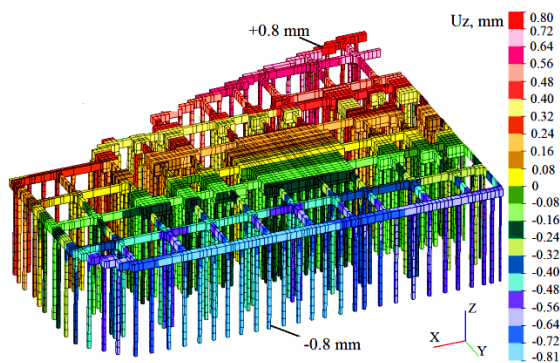


**Fig. 5.** The increase of settlement on the results of solving the problem of “soil-foundation-structure interaction” for the forced destruction of the catacombs

The damping parameter was adopted accordingly to the higher frequency oscillations of the system «soil base – foundation – structure», which amounted to  $\omega_0=2,67 \text{ s}^{-1}$  ( $n=0,425 \text{ Hz}$ ), that corresponds to the period of natural oscillations  $T_I=2,353071 \text{ s}$ . The logarithmic decrement of the oscillations was assumed such that corresponds to  $\xi=5\%$  of the critical damping of the oscillations ( $\delta=0,3145$ ). Thus damping parameter was  $\xi=0,037$ .

The calculations of the system «soil base – foundation – structure» on the action of the

seismic loads were performed using three-component calculation accelerograms.

Seismic load was modeled using special accelerograms designed especially for this site and derived from the actual earthquake records of Vrancea zone and local regions.

The oscillation amplitude for the designed earthquakes from the Vrancea zone is much more intense so the results using these accelerograms will be determined.

According to the results of the numerical simulation we got contour plots of the envelopes of the maximum and minimum pressure for the frame structures of parking in the directions  $X$ ,  $Y$ ,  $Z$ , which must be considered as the extra possible changes to the static stress state.

The analysis of the results showed that the additional vertical forces in the piles of the parking are expected to  $N=10\dots184 \text{ kN}$  (extreme values). The efforts in the cover plate parking from the seismic load can reach values  $M_x=5,2\dots9,3 \text{ kN}\cdot\text{m/m}$ ,  $M_y=5,2\dots11 \text{ kN}\cdot\text{m/m}$ . The increase efforts in the grillage of the parking lot is expected to  $M_x=33\dots112 \text{ kN}\cdot\text{m/m}$ ,  $M_y=52\dots148 \text{ kN}\cdot\text{m/m}$  (momentary extreme values). Expected gain of the vertical pressure under the action of the seismic loads (dynamic composes) does not exceed 100 kPa in the walls and the ceiling coving of the underground mines near the complexes excavation. In this case, the total value of the vertical pressures in these elements is expected not more than 200 kPa, which does not exceed  $R_c$ .

The tracking moving of the control points were provided in the calculations for the seismic loads. These points are: the grillage corners and the cover parking (Fig.6); the point on the ceiling coving of the underground mines, which situated near the building; the bottom and pile head which is located closest to the underground mines.

The analysis of the received results showed that the maximum expected deviation of the pile head is  $U_x=37,3 \text{ mm}$  (on 83 s),  $U_y=42,8 \text{ mm}$  (on 71s),  $U_z =7,8 \text{ mm}$  (on 68 s).

The maximum displacement of the grill-

lage with the soil projected by the amount of  $U_x=38,0$  mm,  $U_y=45,6$  mm,  $U_z =9,7$  mm. According to the results of the numerical simulation from the action of the seismic loads the slope roof slab parking is  $U_x=37,8$  mm,  $U_y=43,0$  mm,  $U_z =8,0$  mm. The control point on the ceiling coving of the underground mines get displacement  $U_x=37,6$  mm,  $U_y=44,1$  mm,  $U_z =7,8$  mm.

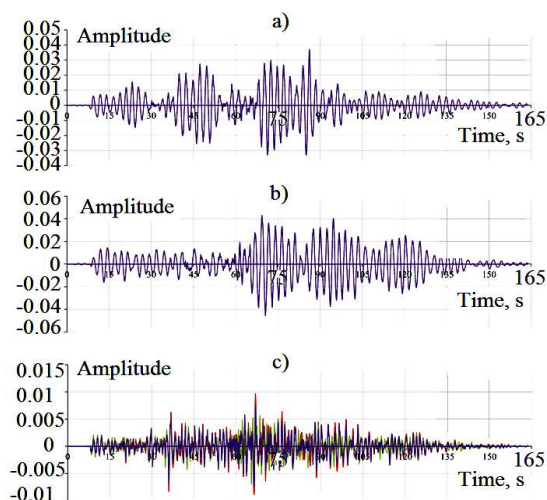


**Fig. 6.** Displacements of grillage corners on the results of calculations using the calculation accelerograms for the 7 – magnitude earthquake from Vrancea zone in directions: *a* – along *X*, *b* – along *Y*, *c* – along *Z*

Thus, the simulations were performed for the case of an emergency in order to be able to draw conclusions about the interaction of piles of soil base and the impact of their behavior catacombs.

## CONCLUSIONS

According to the results of the research by using the numerical simulation was found:

- The presence of the underground mines in the soil base near the apartment complex almost does not cause the stress-strain state changes of the building load-bearing elements and the soil base. At the same time vertical stresses in the soil (the ceiling coving and the walls of mines) do not exceed 100 kPa. This pressure is sensed by the layer of the limestone where the underground mines

are situated,

- The settlement of the mines' ceiling coving, related to the floor in the loads transmission from the building did not exceed 5mm and did not exceed the soil strength,

- The research of the emergency destruction of mine influence showed that the deformation occur within the radius 23 m and do not affect at the soil base of the altitudinal part of the building. However, due to the possible heterogeneity of the soils in such circumstances the usage of the pile foundations is justified,

- The influence of the mines destruction on the parking's foundation may lead to the additional settlement of the small amount of the piles, which situated near the mines due to low soil deformability. The usage of the grillage with cross straps enables the saving of the parking operating properties meet the requirements of standards [4],

- It is established that the seismic loads can lead to increase the pressure in the ceiling coving of mines up to 2 times, do not lead to exceed the strength of the soil and do not cause the destruction of the mine,

- We find that under the action of the seismic influence prevails rigid building foundation moving along with the soil. The maximum displacement of the grillage in the space was 50,4 mm at 71 s of load.

The numerical modeling results confirm the fact that the stress-strain state of the soil base and the load-bearing elements of the building significantly react to the impact of each element of the system: its own stiffness of the building, the components and the foundation stiffness, the characteristics of the soil base, the presence of the underground natural or man-made cavities, etc. All this confirms the necessity for a detailed study of the interference system «soil base – foundation – structure» in the designing for the reliable operation of the structures during the usage in the future by the numerical simulation considering the action of the seismic loads. This approach makes it possible to appreciate the character of the building interaction with the having cavities soil base: to as-

sess the impact of the building load of the building on the underground structures; to assess the impact from the presence of the cavities on the stress-strain state of the load-bearing elements of structure.

## REFERENCES

1. **DBN B.1.2-2:2006. 2006.** System reliability and safety of construction projects. Pressures and impacts. Design standards. Ministry of Construction of Ukraine, Kyiv, 75 (in Ukrainian).
2. **DBN B.1.1-12:2014. 2014.** Construction in seismic regions of Ukraine. Ministry of Regional Development, Construction and Housing and Communal Services of Ukraine. Kyiv, 117 (in Ukrainian).
3. **Eurocode 7: Geotechnical design - Part 2: Design assisted by laboratory testing, 2000.** EN 1997-2:2000. European Committee for Standardization. Brussels, 196.
4. **DBN B.2.1-10:2009. 2009.** Items of construction and industrial products for construction purposes. Bases and foundations of buildings and structures. The main provisions of the design. Ministry of Regional Development of Ukraine. Kyiv, 104 (in Ukrainian).
5. **Boyko I., Kornienko M., Sakharov V., Zhuk V. 2009.** Soil base deformation features of the pile foundations on loess and landsliding territories at static and dynamic loadings. Proceedings of the 17-th International conference on soil mechanics and geotechnical engineering, Egypt, Vol.2, 1271-1274.
6. **Sakharov V. 2014.** An investigation of system "soil base-foundation-structure" response to seismic forces with provision for nonlinear properties of materials. Materiały X Konferencji naukowej "Konstrukcje zespolone", Polska, Zielona Góra, 26-27 czerwca, Uniwersytet Zielonogórski, 407-426.
7. **Zhuk V. 2013.** Implementation of research methodology of nature of the interaction of frame buildings with uneven collapsible loess basis. Basis and i Foundations: Interdepartmental Scientific-Technical Collection – Kyiv: KNUCA, 2013, Vol. 33, 67-76. (in Ukrainian).
8. **Boiko I. 2013.** Behavior of the multi-story building under seismic loads with the account of the viscoplasticity of the soil base. Proceedings International Conference on Soil Mechanics and Geotechnical Engineering, Paris, 2013, 1443-1446.
9. **Tugaenko Yu. 2008** Investigation of the strength and deformation properties of shell limestone in the laboratory. Bulletin of the Odessa State Academy of Construction and Architecture. – Odesa, 2008, Vol. 29, 295-298. (in Russian).
10. **Yephoycehko G. 2009.** Experience of application of cellular concretes in seismic regions. MOTROL. Commission of Motorization and Energetics in Agriculture – Lublin, Vol. 11B, 140-151.
11. **Prusov D. 2011.** Effect of deep excavations with filler constructions on the groundwater filtration processes. MOTROL. Commission of Motorization and Energetics in Agriculture – Lublin, Vol. 13C, 43-50.
12. **Malesa W. 2011.** FEM application in the calculation of parameters for tire-soil interaction including contact stress. MOTROL. Commission of Motorization and Energetics in Agriculture – Lublin, Vol. 13, 227-235.
13. **Kovbasa V. 2011.** Physical equations of soil deformation with essential manifestations of viscoplastic properties. MOTROL. Commission of Motorization and Energetics in Agriculture – Lublin, Vol. 13B, 145-155.
14. **Prusov D. 2013.** Principles for municipal facilities reconstruction based stability assessment methodology. MOTROL. Commission of Motorization and Energetics in Agriculture – Lublin, Vol. 15(5), 31-34.

ИССЛЕДОВАНИЕ ВЗАИМОДЕЙСТВИЯ  
КАРКАСНОГО ЗДАНИЯ С ОСНОВАНИЕМ,  
ОСЛАБЛЕННЫМ ПОДЗЕМНЫМИ ВЫРА-  
БОТКАМИ, ПРИ ДЕЙСТВИИ СЕЙСМИЧЕ-  
СКИХ НАГРУЗОК

**Аннотация.** В статье приведены результаты исследования влияния подземных техногенных пустот на напряженно-деформированное состояние элементов системы «грунтовое основание – фундамент – здание» в условиях сейсмических нагрузок с использованием численного моделирования.

**Ключевые слова:** неравномерные деформации, каркас, численное моделирование, подземные техногенные пустоты, подрабатываемая территория, сейсмическая нагрузка.

## Calculation of Deflection of One- and Two-layer Slabs Supported on Four Sides

*Dmytro Smorkalov*

Kyiv National University of Construction and Architecture  
Povitroflotskyy prosp., 31, Kyiv, Ukraine, 03680, e-mail: smorkalov@i.ua

**Summary.** Presented method and results of experimental research of deflection of one-layer and two-layer slabs influenced by short-term lateral load. Proposed method of calculation based on the limit equilibrium method, calculation of slab deflections values by LIRA-CAD bundled software. The comparison of experimental and theoretical results of the calculation of deflections slabs.

**Key words:** slab, deflection, steel fiber concrete.

### INTRODUCTION

Layered constructions are increasingly applied in building recently. When appropriate composition of separate layers is selected, multi-layer constructions with perfect construction properties may be created [9]. Layers are mostly composed of heavy concrete and effective steel fiber concrete. Such constructive decisions have a widespread use in road and airfield pavements, logistics areas, heavy-weight industrial floors, etc. [13, 15, 16]. Among the most promising trends of reasonable usage of steel fiber concrete is its application in composite structures, as a rule, in combination with concrete or ferroconcrete, with distinct partition of functions of every material. In particular, the steel fiber concrete that is rather thriftily applied along the construction outline, in a thin layer, provides high crack resistance of constructions, as well as its high durability due to high indices of tensile strength, frost resistance, corrosion resistance, and high rates of other types of resistance of the steel fiber concrete [14]. At the same time, this solution provides necessary preconditions for signifi-

cant reduction of strength and value of the primary concrete and reduction of the number of reinforcement rod. Thus, there are preconditions for obtaining high indices created while their cost drops.

### PURPOSE OF WORK

The main purpose of proposed work is the comparison of proposed method of deflection calculation for layered slabs under lateral load with the results of experimental research.

### EXPERIMENTAL RESEARCH

According to the set purpose of research, slabs of 4 series were produced, two slabs for each series. The scope and outline of experimental studies is set in Table 1 [5].

The total size of single-layer slabs amounts to 800×800×60 mm; the thickness of each layer of reinforced concrete (concrete and steel fiber concrete) in two-layer slabs is 30 mm.

Series I (PF) represents a slab made of steel fiber concrete.

Series II (PZ) represents a single-layer reinforced concrete slab with single-layer reinforcement  $\text{Ø}4$  Bp-I laid at the bottom of the slab with protective concrete layer 10 mm thick with 75 mm pitch

Series III (PBF) represents a two-layer concrete slab, the top layer of which is made of unreinforced heavy concrete and the below one – of the steel fiber concrete.

Series IV (PZF) of studied samples represents slabs consisting of an upper layer of steel fiber concrete and a heavy concrete layer reinforced with metal reinforcement mesh  $\text{Ø}4$  Bp-I set with 75 mm pitch.

Slab concreting was carried out in two stages. Slabs of PZ grade and concrete layers of PZF and PBF slabs were concreted at the first stage. Siliceous sand and gaint gravel of 5...10 mm fraction; Portland cement of M400 grade was used as binding material; water-to-cement ratio amounted to  $W/C = 0,4$ . Plates of PZ and PZF grade were reinforced with binding wire mesh of Bp-I grade, 4 mm in diameter and 75 mm pitch in two directions. Concrete protective layer was 10 mm. The surface is bush-hammered while the concrete is immature.

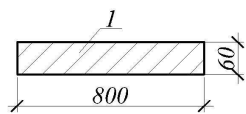
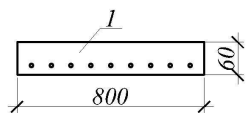
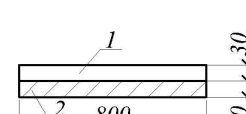
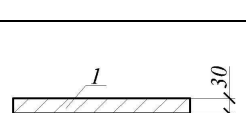
At the second stage, after 4 days, slabs of PF grade were concreted and steel fiber concrete layer slabs of PZF grade were additionally concreted.

Steel fiber concrete contained steel fiber with diameter  $d_f = 1.0$  mm and length  $l_f = 36$  mm; volume percent of reinforcement was  $\mu_f = 1\%$ . Fine concrete without coarse aggregate was used as a concrete matrix; water-to-cement ratio equaled to  $W/C = 0,4$ .

General appearance of testing bench is showed on Fig. 1.

The same calculation model was applied for both the one- and two-layer slabs exposed by lateral load: a slab is hinge-supported on four sides and influenced by evenly distributed load (Fig. 2)

**Table 1.** Scope of experimental studies

Series	Slab grade	Section	Composition
I	PF-1		1–steel fiber concrete
	PF-2		
II	PZ-1		1–reinforced concrete
	PZ-2		
III	PBF-1		1–concrete; 2–steel fiber concrete
	PBF-2		
IV	PZF-1		1–steel fiber concrete; 2–reinforced concrete
	PZF-2		

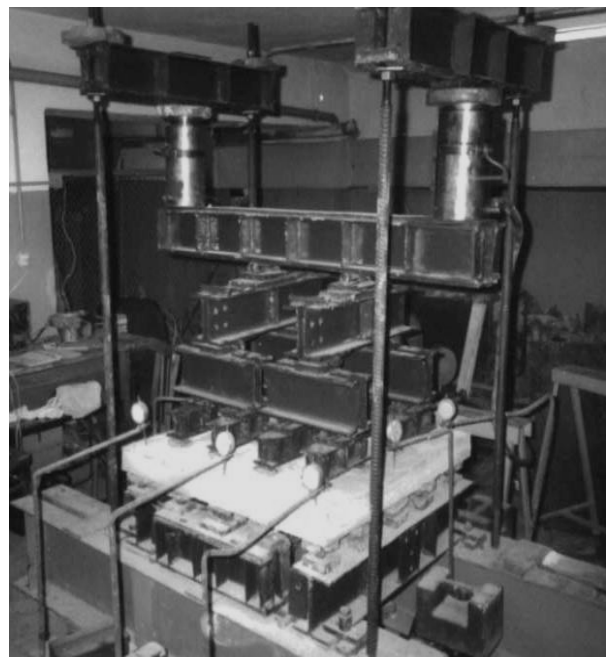


**Fig. 1.** General appearance of testing bench

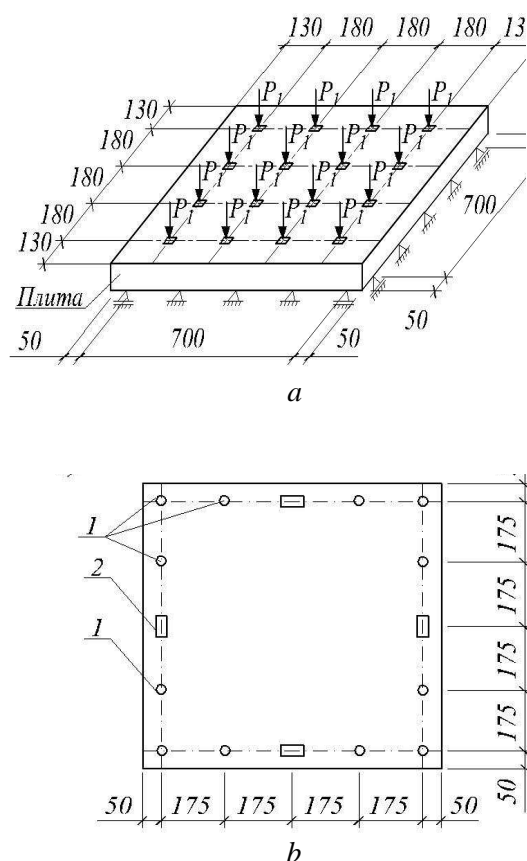


**Fig. 2.** Distribution of load (a), and support (b) upon slab:

1 – hinged support, 2 – cylinder support

It is suggested that 16 concentrated forces evenly allocated on the slabs surface show no significant difference during the operation, as compared to evenly distributed load, that is why in further theoretical study of strength, crack resistance, and deformation of studied slabs a design model was adopted for slabs supported by hinged bearings on four sides and influenced by evenly distributed load. The load was applied by degrees  $P_i=2,0$  kN with 15-minute timing at each stage to take readings from devices. The value of load was fixed by indices of model forcemeter of hydraulic pumping station. Before testing the hydraulic system consisting of a pumping station, jacks, and model forcemeter was calibrated using model forcemeter of Tokarev system.

During the application of load in the center of the slab deflections and deformations over supports were recorded using time indicators with 0.01 mm scale graduation value.

The load was applied by two hydraulic jacks of 250 kN united by common oil circuit connected to a common pump station.

Before testing the slabs, physical and mechanical properties of used materials were determined: those of heavy concrete, steel fiber concrete and reinforcement (Table 2).

**Table 2.** Physical and mechanical properties of concretes and reinforcement

Type of concrete or fitting	Strength, MPa		Tensile strength, MPa	Starting elasticity factor, MPa
	cube	prism		
concrete	16,3	11,9	1,5	22500
Steel fiber concrete	19,8	14,5	1,63	24600
Reinforcement Bp-1	–	–	393	192000

According to results of experimental studies with regard to nature of destruction [10], all slabs collapsed according to normal sections.

## CALCULATION OF DEFLECTION

The proposed method based on the limit equilibrium method, which may be represented – during the state of limit equilibrium – by the system of disks united along the lines of fracture with plastic hinges.

As proposed by A. A. Gvozdev [4], it is possible to make use of characteristic points 1 and 2 on the diagram (Fig. 3).

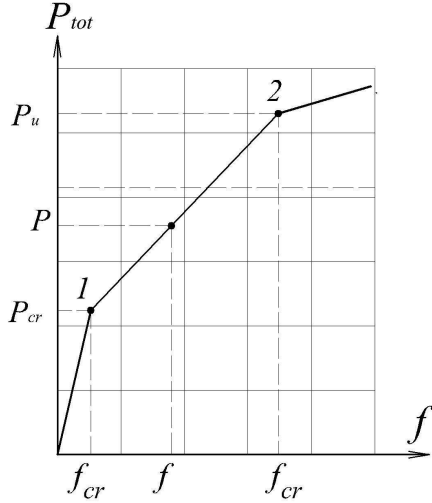


**Fig. 3.** Design diagram of slab deflection:  
1 – cracking, 2 – appearance of the plastic hinge

Deflection values in the areas between  $f_{cr}$  and  $f_u$  are determined by interpolation.

The general view of the formula  $f$  of slab deflection of slab supported on four sides and bearing a cracks, may be obtained from the following ratio:

$$\frac{q_u - q_{cr}}{q - q_{cr}} = \frac{f_u - f_{cr}}{f - f_{cr}}, \quad (1)$$

where:  $q_u$  and  $q_{cr}$  – load at destruction and crack formation,  
 $f_u$  and  $f_{cr}$  – slab deflection at the moment of destruction and crack formation correspondingly.

It should look as follows:

$$f = f_{cr} + \frac{q - q_{cr}}{q_u - q_{cr}} (f_u - f_{cr}). \quad (2)$$

The value  $f_{cr}$  is determined based on elastic system calculation according to load  $q_{cr}$ , which in turn may be obtained by bending factor, when first crack appeared in a slab area with the highest tension.

The deflections  $f$  at the moment of formation of plastic hinges may be determined as follows.

Until the conditional yield point of reinforcement achieved along all the lines of

fracture, cracks are formed and significantly increased on a slab. At the same time, areas with cracks will be especially distorted that will mostly determine the maximum value of slab deflection.

If insignificant curvature of slab areas neglected bearing no cracks, but rigidity is high, the slab calculation model may be represented as stiff disks connected by yielding bracing with width  $\Delta$ . Bending rigidity of all joints is calculated according to V.M. Murashov theory [7], though the coefficient  $\psi$  is taken as a one, as the reinforcements reaches instability the influence of stretched concrete between cracks disappears or becomes insignificant. This assumption substantially simplifies the calculation.

For further simplification the angle fracture between discs equal to  $\frac{\Delta}{r}$  is assumed as

if concentrated along the lines of fracture. The calculated deflection surface prior to exhaustion of the bearing capacity turns out to be similar to the surface used in calculating by limit equilibrium method for the calculation of works on possible movements. Though such likening is not accurate, it allows determining the maximum deflection at a rather decent level.

There is a calculation model of square slab presented on Fig. 3 and a diagram of angle rotation at slab center deflection that is equal to  $f_u$ . Owing to symmetry, the fracture diagram of value  $\Delta$  for all plastic hinges is the same.

Rigid discs of the slab will turn in relation to supports by angle:

$$\frac{\varphi}{2} = \frac{2f_u}{l}. \quad (3)$$

Mutual angle adjacent discs:

$$\varphi = \frac{2\sqrt{2}f_u}{l} = \Delta \frac{1}{r}, \quad (4)$$

where:

$$f_u = \frac{l\Delta f_{ym}}{2\sqrt{2}E_s(d-x)}, \quad (5)$$

where:  $\frac{1}{r}$  – curvature-multiplication of which by  $\Delta$  equals to reciprocal angle of rotation of adjacent discs:

$$\frac{1}{r} = \frac{f_{ym}}{E_s(d-x)}, \quad (6)$$

$\frac{1}{2\sqrt{2}}$  – factor derived from geometrical considerations, which is transition to the angle of rotation of the disk relative to the support,

For fiber reinforced structures (such as fiber concrete) the value  $f_y$  and  $E_s$  at the point of critical steel stress is replaced by the value  $f_{cf}$  and elastic modulus  $E_f$  suitable to the material. For two-layer slabs the given geometric, strength, deformation properties of two materials are used.

By the combination of Eq. (2)-(6) we can define a final ratio for the calculation of current deflection of the slab supported by four sides influenced by evenly distributed load:

$$f = f_{cr} + \frac{q - q_{cr}}{q_u - q_{cr}} \left( \frac{1}{r} \Delta - f_{cr} \right), \quad (7)$$

where:  $f_{cr}$  – slab deflection at the moment of formation of the first cracks in stretched area of the element,  
 $q_{cr}$  – load, when first cracks were created,  
 $q_u$  – load corresponding to the limit of the slab bearing capacity.

Thus, the calculated width of deformed area  $\Delta$  remains unknown in the Eq. (7); as a result it is not possible to calculate the value  $f$ .

In order to solve such problem the following method of finding the desired value of deflection  $f$  may be proposed. First of all, a boundary value of the slab deflection is set according to the standards for that class of structures  $f_u = [f]$  apply it in the Eq. (7)  $f = f_u = [f]$ . The Eq. (7) is settled with respect to value  $\Delta$  and then obtained result is applied to the Eq. (5), therefore obtaining the deflection at the time of formation of plastic hinges with regard to real-specified parameters. At the same time, the result of Eq. (7) shows the

value of current deflection by introducing the calculated value of width of deformed area  $\Delta$ .

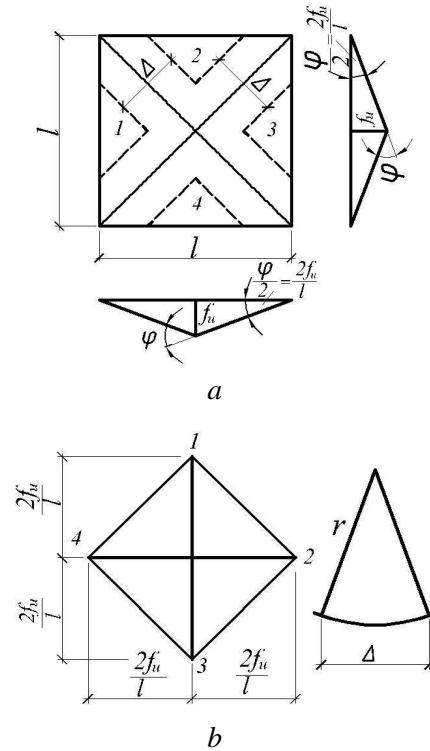


**Fig. 4.** Calculation diagram of square slab influenced by evenly distributed load: *a* – fracture diagram; *b* – diagram of disc rotation angle rate

The value of  $f_{cr}$  and  $q_{cr}$  can be calculated if the combine Eq. (7) with the formula B.H.Galerkina [2] for square plates, supported on four sides, the deflection at the center of slabs:

$$f = 0,04706 \frac{ql^4}{E_i h^3}. \quad (8)$$

To determine the width of the deformed zone  $\Delta$  slabs a series of isolated points on several research graphs deflections. Points are usually prescribed in the operational (working) load range: often – is 0,7...0,8 from destructive load. To find the value  $\Delta$  using Eq. (6) and (7), taking into account the specific slabs construction.

Results of calculation of one- and two-layer slabs by the limit equilibrium method are shown on Fig. 7, 8.

Considering complexity of mathematical calculations for slab deflection due to analytical methods [6] and unsatisfactory precision of results, a decision was made to do calculations on computing machine with a help of LIRA-CAD bundled software [3, 8].

The basis of LIRA-CAD is represented by the calculation of components and structures by finite element method [3].

The calculation model of a slab (Fig. 5) is built out of tridimensional finite elements (type CE-36). The slab is separated into 1444 finite elements according to plan. The sectional area of the slab is composed of 12 layers 5 mm each. The load is applied in the form of 16 concentrated forces. The distribution of load and supports is accepted as per Fig. 2.

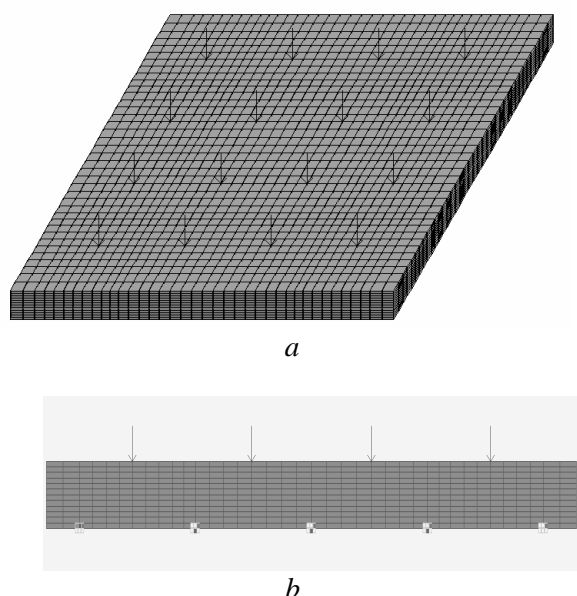


**Fig. 5.** Calculation model of slab in LIRA-CAD: *a* – general view, *b* – side view

The CE-36 finite element is a universal tridimensional eight-node isoparametric finite element, designed for the calculation of tridimensional constructions. There is a diagram represented on Fig. 4. Each of finite element nodes has three degrees of variance  $U$ ,  $V$ ,  $W$  defined with regard to global coordinates  $X$ ,  $Y$ ,  $Z$  and are linear displacements according to axis, whose positive direction coincides with the direction of coordinate axis. As a result of modeling, there are 19,773 nodes and 17,328 elements.

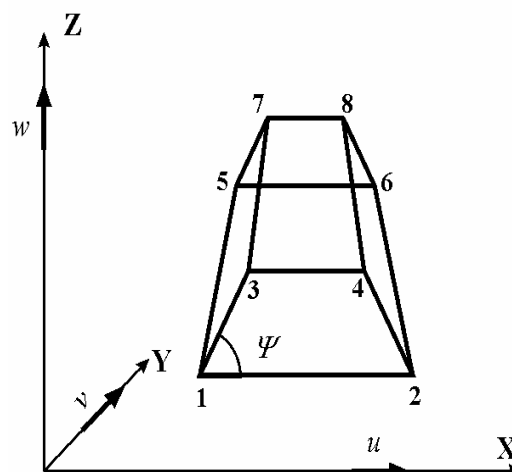


**Fig. 6.** Diagram of CE-36 finite element

The assumed calculation model makes it possible to change the rigidity of materials for both one-layer and two-layer slabs.

The slab calculation was performed in linear position for loads corresponded to loading pitches at testing. Non-linear physical-mechanical properties were taken into consideration by means of changing the elasticity modulus.

Initial values of elasticity modulus for concrete and steel fiber concrete were assumed according to [1], that is  $E_c = 22,5 \cdot 10^3$  MPa,  $E_{cf} = 23,8 \cdot 10^3$  MPa.

In accordance with recommendations [11] the nonlinear behavior of construction is recommended to consider by means of introducing decreasing coefficients: 0,2 – in case of any cracks, or 0,3 – in case no cracks revealed.

That is why during the calculations the decreasing coefficient was 0,3 before appearance of any cracks and 0,2 – after the first cracks appeared. Reduction of slab rigidity as a result of crack was also considered by means of introducing zero rigidity elements in the tensile area within height of the crack. The rigidity of slab supports was not reduced to avoid forcing through the slab thickness

As a result of calculation of one-layer slabs in LIRA bundled software, diagrams of deflection of the slab center  $f$  of the total pressure  $P_{tot} = 16P_i$  were obtained, which are presented on Fig. 7.

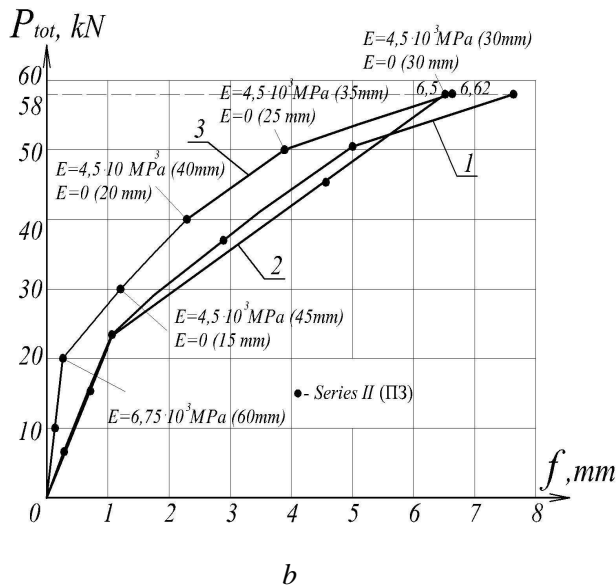
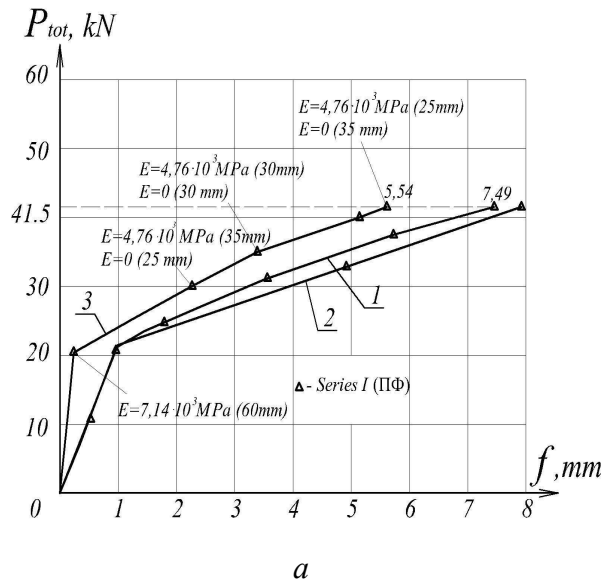


**Fig. 7.** Calculation results for deflection of one-layer slabs of series I grade ПФ (a) and slabs of series II grade ПЗ (b):  
 1 – experimental; 2 – calculation by the limit equilibrium method; 3 – calculated in LIRA bundled software

When calculating the two-layer slabs, relevant elasticity modulus of material was applied for each slab layer. The value of decreasing coefficients and zero elasticity elements were applied similar to the calculation of one-layer slabs.

As a result of calculation of two-layer slabs by means of LIRA bundled software, diagrams of deflection of the slab center  $f$  of

the total pressure  $P_{tot}=16P_i$  were obtained, which are presented on Fig. 8.

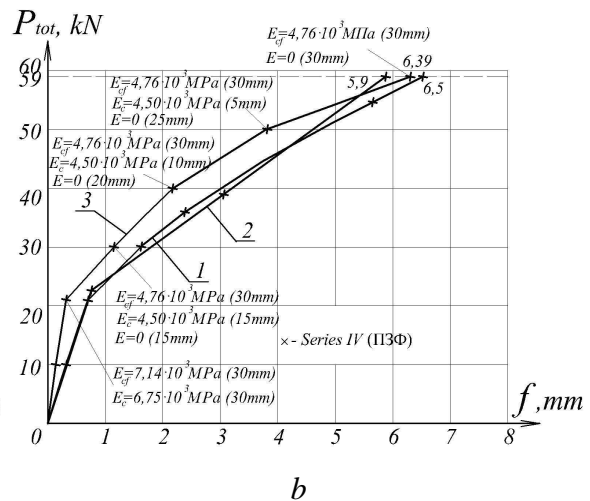
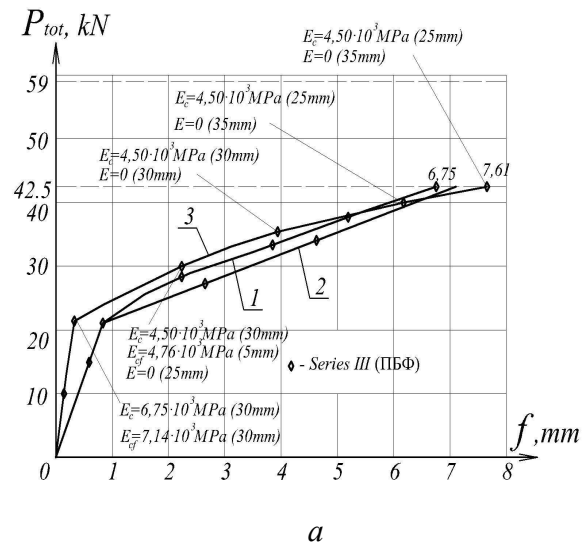


**Fig. 8.** Calculation results for deflection of two-layer slabs of series III grade ПБФ (a) and slabs of series IV grade ПЗФ (b):  
 1 – experimental; 2 – calculation by the limit equilibrium method; 3 – calculated in LIRA bundled software

## CONCLUSIONS

1. Given that today's construction industry is represented by the vigorous process of increasing the strength of construction materials, particularly concrete and reinforcement, due to achievements in chemistry, there is a strengthening of quality indicators of buildings and constructions, in particular bearing construction arrangements. Thus, systems

making it possible to work in a multi-axial load state (shell structures, slabs, wall-beams, etc.) are getting more popular. There is an opportunity to significantly reduce the cost by reduction of cross-section operational overcuts at the expense of increased strength of materials. The new technologies make it possible to perform the most complex design elements made of any materials. Considering the current trends, it should be noted that the issue of performance reliability for buildings and structures is not about the strength requirements, but the rigidity of elements and buildings in general. Therefore, the study of rigidity (most commonly the deflections) of examined slabs seems to be a topical issue.

2. Another question this work bears an answer to is the feasibility of using multi-layer slabs. From the point of view of rigidity (bending) of slabs, the two-layer slabs have an advantage: they show 10% less deflections, than the one-layer ones. Considering the higher level of crack resistance of two-layer slabs, the use of two-layer slabs is absolutely justified.

3. Calculation on computer using LIRA bundled software provides wide opportunities to determine rigidity (deflection) for both single-layer and multi-layer slabs owing to computing technologies. However, the calculation results obtained indicate deficiency in accuracy compared with the experimental data. The fact is that compliance with regulatory guidelines, implemented to consider nonlinear structure operation by introduction of decreasing coefficients, sometimes does not match the actual conditions of slab deformation. Furthermore, there are some doubts as to the correctness of defining the depth crack distribution along the slab height, which determines its actual rigidity.

4. The comparative analysis of experimental and theoretical diagrams of slab deflection evidences good matching of results. Deviations at maximum loads were as follows: for one-layer slabs of series I (PF) – 26%, for slabs of series II (PZ) – 13%; for two-layer slabs of series III (PBF) – 11%, for slabs of series IV (PZF) – 2%. Such deviation in calculations may be explained by complexity of defining the real rigidity of slabs, i.e. the

definition of deformation modulus and the height of crack creation to set the zero rigidity elements.

## REFERENCES

1. **Barashykov A.Ya., Smorkalov D.V. 2014.** Calculation of solidity of one-layer and two-layer reinforced concrete slabs supported on four sides. Resource efficient materials, structures, buildings, and constructions: Collected studies. Rivne, 2014, Issue 28, 127-134 (in Ukraine).
2. **Galerkin B.G. 1933.** The resilient thin plate. M, Gosstroizdat, 1933, 458 (in Russian).
3. **Gorodetsky A.S., Schmukler V.S., Bondarev A.V. 2003.** Information Technology of calculation and design of building konstruktсий: Proc. Manual. Kharkiv, NTU "KPI", 2003, 889 (in Russian).
4. **Gvozdev A.A. 1949.** Calculation of bearing capacity by limit equilibrium method. Moscow, Stroyizdat, 1949, 280 (in Russian).
5. **Zhuravskiy O.D., Smorkalov D.V. 2002.** Methodology and results of experimental studies of two-layer slabs. Steel reinforcement concrete constructions. Research, design, construction, operation: Collected research papers, Issue 5, Kryvyi Rig, KTU, 2002 (in Ukraine).
6. **Korolyov A.N.** Calculation methods for slab deflections supported on four sides at short-term load. Concrete and reinforced concrete Vol. 3, 1960, 9-11 (in Russian).
7. **Murashev V.I. 1950.** Crack resistance, stiffness and strength of concrete. M, Mashstroyizdat, 1950, 230 (in Russian).
8. **LIRA-CAD. 2011.** Tutorial: Electronic Edition, 2011, 396 (in Russian).
9. **Rudenko N. 2010.** The development of conception of new generation concretes. TEKA: Kom. Mot. Energ. Roln, 2014, Vol. XB, 128-133.
10. **Smorkalov D.V. 2003.** Crack resistance and fracture modes for two-layer slabs. Resource efficient materials, structures, buildings, and constructions: Collected research papers. Rivne, 2003, Issue 9, 323-330 (in Ukraine).
11. **Snyder M. 1972.** Factors affecting the flexural strength of steel fibrous concrete. ACI Journal, 1972, Vol. 69, No. 2, 96-100.
12. **SP 52-103-2007. 2007.** Code of practice on design and construction. Reinforced concrete cast-in-place constructions of buildings. Moscow, 2007 (in Russian).

13. **Stages A. 1981.** Ring fiber reinforced concrete. ACI Journal. 1981, Vol. 78, No. 5, 369-373.
14. **ACI Journal. 1973.** State-of-the-art report on fiber reinforced concrete, 1973, Vol. 70, 729-744.
15. **Tarasov V.P. 1974.** The use of fiber-reinforced concrete in construction. Industrial construction. 1974, Vol. 7, 44-45 (in Russian).
16. **Tattersall G.H. 1974.** Bond strength in steel-fibre-reinforced concrete. Journal of Concrete Research. 1974, Vol. 26, No. 87, 105-113.

РАСЧЕТ ПРОГИБОВ  
ОДНО- И ДВУХСЛОЙНЫХ ПЛИТ,  
ОПЕРТЫХ ПО КОНТУРУ

**Аннотация.** Приведены методика и результаты экспериментальных исследований прогибов однослойных и двухслойных плит под действием поперечного кратковременного нагрузки. Рассчитаны прогибы плит способом, основанном на методе предельного равновесия, и методом конечных элементов, с помощью программного комплекса ЛИРА. Выполнены сравнения экспериментальных и теоретических результатов расчета прогибов плит.

**Ключевые слова:** плита, прогиб, стале-фибробетон



## Progress in Cement Science - Why Alkaline Activation?

*Pavel Krivenko*

V. D. Glukhovskiy Scientific Research Institute for Binders and Materials,  
Kiev National University of Construction and Architecture,  
Povitroflotskyy prosp., 31 Kiev, Ukraine, 03680, e-mail: pavlo.krivenko@gmail.com

**Summary.** Fifty years ago just an idea of the presence of free alkalis in a cement matrix was considered by the ordinary portland cement (OPC) people as an absurd one and this was a basic postulate accepted in the chemistry of cements. In 1957 a scientist from Ukraine (USSR) Victor Glukhovskiy put forward an assumption which was taken as a base for development and bringing into practice of construction a principally new class of cementitious materials which first appeared in the art under a name of “alkaline cements” (now also known under a general name of “alkali-activated cements (AAC)”). A validity of these ideas is confirmed by more than 50 years of evolutionary development and vast experience collected from practical use of new materials in a variety of large-scale applications. A present review covers theoretical views on role played by alkali in cement stone structure formation. Examples of compositional build-up of the alkali- activated cementitious materials as a function of quantity of alkali and type of aluminosilicate component are reported as well as the results of inspection taken over the AAC concrete structures made with these cements.

**Key words:** alkali- activated, aluminosilicate, cements, durability, hydration products.

### INTRODUCTION

The alkali metal compounds were excluded from traditional hydraulic cement constituents due to their high solubility. At the same time, the studies held in order to reveal the reasons for excellent durability of ancient cements together with the data collected on stability and composition of natural mineral formations testified that this postulate was not correct.

According to the data reported in [1-7], excellent durability of the ancient structures is attributed to considerably greater quantities of the alkali metal compounds contained in the ancient cements compared to contemporary portland cements. This was found to result in the formation of alkaline hydroaluminosilicate compounds- analogous to natural zeolites in a cement stone structure along with the calcium hydrosilicates.

A strategy of sustainable development predetermines actions to be taken by the industry of building materials and, in particular, by cement industry.

The OPC-based cements are not able to meet today’s requirements due to:

- not high enough physico- mechanical properties and required durability resulted from low- effective strength of the OPC stone:
- metastability of the hydration products resulted from transformation of  $C_2SH$  into  $CSH(B)$ ,
- relatively high solubility of the phases,
- low corrosion resistance in the presence of  $Ca(OH)_2$  and  $3CaO \cdot Al_2O_3 \cdot 3CaSO_4 \cdot 31H_2O$ ,
- high consumption of energy (7500 J/1t),
- high carbon dioxide emissions (0.5 metric t  $CO_2$ /1t OPC),
- depletion of natural resources.

That’s why the cement science should evolve in the direction of the cements alter-

native to OPC. One of such cement that appeared in the art 50 years ago is an alkaline cement with a number of building products made from it. This paper covers theoretical principles laid down in the creation of these cements, history and experience collected from large-scale application.

## HISTORICAL ASPECTS AND OVERVIEW

First attempts to use an alkali in cementitious materials goes back to 1930s, when H.Kühl reported [8] about his studies on setting behaviour of the mixtures of ground slag and solution of caustic potash. R.Feret [10] reported on necessity of study to be taken on slags as cement constituent. In 1940, A.O. Purdon [19] reported on the results of first extensive laboratory study on the cements without OPC clinker consisting of the slag and caustic soda and the slag and caustic alkalis produced by a base and an alkaline salt. Important historic developments of the alkali-activated cements (AAC) are summarized in Table 1.

Later, in 1957 Victor Glukhovsky [12] was the first who discovered the possibility of making binding materials using low basic calcium or calcium-free aluminosilicate (clays) and solutions of alkali metals. He called these binders “soil cements” and the corresponding concretes “soil silicates”. Depending on the composition of starting materials, the binders can be divided into two groups: alkaline binding system  $\text{Me}_2\text{O}-\text{Me}_2\text{O}_3-\text{SiO}_2-\text{H}_2\text{O}$  and alkaline-earth alkali binding system  $\text{Me}_2\text{O}-\text{MeO}-\text{Me}_2\text{O}_3-\text{SiO}_2-\text{H}_2\text{O}$ . Also, a variety of the alkaline binders which used other metallurgical slags, clays, aluminosilicate rocks, fuel ashes and other constituents have been proposed. Extensive researches and developments on alkali-activated cements (AAC) and AAC-based concrete started since then. Trief cements and F-cements from the Scandinavian countries (Forss 1983a, 1983b) and alkali-activated blended cements are more recent examples (Davidovits, 1988, Roy and Silsbee, 1992).

In 1981 Josef Davidovits [13] from France published his results on making binders by mixing alkalis with burnt mixture of kaolinite, limestone and dolomite. He called these binders “geopolymer” for their polymeric structure. He also registered several trademarks such as Pyrament, Geopolycem and Geopolymite. These materials belong to the alkaline binding system  $\text{Me}_2\text{O}-\text{Me}_2\text{O}_3-\text{SiO}_2-\text{H}_2\text{O}$ , as was discovered by Victor Glukhovsky.

In 1986 Pavel Krivenko published the results of his research on principles of regulation of technological and physico-mechanical properties of the AAC and ACC concretes in order to achieve the required properties [14].

Malek and Roy at al. [15] identified alkali-activated cement type materials as the matrix formed in the solidification of certain radioactive wastes, while Roy and Langton [16] showed some analogies of such materials with ancient concretes.

**Table 1.** Important historic developments of the AAC

Year	Name	Country	Work/impact
1930	Kühl	Germany	Investigated setting behaviour of slags in the presence of caustic potash
1937	Chassevent	unknown	Measured reactivity of slags using caustic potash and soda solution.
1940	Purdon	Belgium	Investigated clinker-free cements consisting of slag and caustic soda or slag and caustic alkalis produced by a base and an alkaline salt.
1957	Glukhovsky	USSR	Synthesized binders using hydrous and anhydrous aluminosilicates (glassy rocks, clays, metallurgical slags, etc.) and alkalis, proposed $\text{Me}_2\text{O}-\text{MeO}-\text{Me}_2\text{O}_3-\text{SiO}_2-\text{H}_2\text{O}$ cementitious system, and called the binder “soil cement”.
1981	Davidovich	France	Mixed alkalis with a burnt mixture of kaolinite, limestone and dolomite, and used several trademarks such as Geopolymer, Pyrament, Geopolycem, Geopolymite.
1986	Krivenko	USSR	Developed principles of regulation of properties of the system $\text{Me}_2\text{O}-\text{MeO}-\text{Me}_2\text{O}_3-\text{SiO}_2-\text{Al}_2\text{O}_3$ Proposed name “alkaline cements” and its particular case- “geocement”

Pavel Krivenko [17] further showed that alkalis and alkali metal salts similar to silicates, aluminates, and aluminosilicates enter

into reaction in the alkaline aqueous medium under condition that alkali concentration is sufficient. Such interaction takes place with clay minerals, aluminosilicate glasses of natural and artificial origin, in which calcium is absent, as well as with calcium-based cementitious systems under natural condition with the formation of water-resistant alkali or alkali-alkaline-earth hydroaluminosilicates, which are analogous to natural zeolites and micas.

Kiev National University of Civil Engineering and Architecture organized two international conferences on alkali-activated cements and concretes in 1994 and 1999 in Kiev, Ukraine [Krivenko, 1994, 1999] and the third conference was held in 2007 in Prague, Czech Republic (sponsored by the EU, Government of the Czech Republic and the City Government of Prague). Professor Josef Davidovits from France organized three international conferences on geopolymer in 1988, 1999 and 2007. Professor Jannie van Deventer from the University of Melbourne, Australia, organized the conference on geopolymer in 2002. The fourth international conference and a workshop on geopolymer were held in France and Australia, respectively, in 2005.

### WHY ALKALI ACTIVATION?

The alkalis are known to play an important role in the processes of artificial stone synthesis which take place in nature, are found in the concrete of ancient structures and are contained in contemporary cements.

Less than a century ago just an idea of presence of free alkali in a cement composition was considered by cement people as absurd one and this was a basic postulate of fundamentals of exhibiting hydraulic properties by mineral systems. The alkali metal compounds were excluded from traditional hydraulic cements because of their high solubility.

At the same time, the studies held to reveal the reasons explaining excellent durability of the ancient concretes in combination with the data collected on stability and com-

position of natural mineral formations testified that this postulate was not correct.

Professor Glukhovsky has made a discovery that compounds of alkali metals (Li, Na, K, Rb, Cs) - the elements of the first group of the Periodic Table- exhibit hydraulic binding properties similar to those of the alkali earth metals (Mg, Ca, Sr, Ba)- the elements of the second group.

The idea itself of using these systems as cementitious ones was based, first of all, on collected geological data that sodium- potassium- calcium aluminosilicate compounds, which are known to have the higher stability and resistance to atmospheric reagents, are present in the Earth crust. Secondly, this idea was based on the results of experimental studies which proved that alkali hydroxides and salts of alkali metals entered into interaction with clay minerals, aluminosilicate glasses and crystalline substances of natural and artificial origin with the formation of water resistant alkaline and alkaline-alkali-earth aluminosilicate hydration products that were analogous to natural minerals of the zeolite and mica types.

### *ALKALIS IN NATURE*

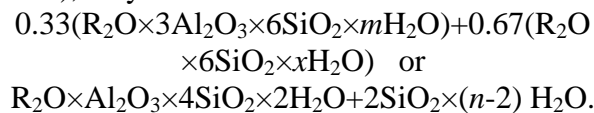
Geological data on conditions under which sedimentary and metamorphic silicate rocks occur and on constituent composition of basic rock-forming minerals along with the above reported data can serve as a theoretical substantiation of a possibility to produce and use in practice of construction of the concretes made using alkali metal compounds along with those made using only calcium compounds.

Some of the processes of formation of the sedimentary stone-like rocks take place under temperatures and pressures close to those which take place in production of materials of hydraulic hardening and, hence, can be simulated in the building materials industry. For example, zeolites of sedimentary origin, such as analcime  $\text{Na}[\text{AlSi}_2\text{O}_6] \cdot \text{H}_2\text{O}$ , phillipsite ( $\text{K}_2, \text{Ca}$ )  $[\text{Al}_2\text{Si}_9\text{O}_{22}] \times 4.5\text{H}_2\text{O}$ , mordenite ( $\text{Ca}, \text{Na}_2, \text{K}_2$ )  $[\text{Al}_2\text{Si}_9\text{O}_{22}] \times 6\text{H}_2\text{O}$ , natrolite  $\text{Na}_2$   $[\text{Al}_2\text{Si}_3\text{O}_{10}] \times 2\text{H}_2\text{O}$  scolecite  $\text{Ca}$   $[\text{Al}_2\text{Si}_3\text{O}_{10}] \times 2\text{H}_2\text{O}$  and other occur in the residual soil as a result of low-temperature

hydrothermal reactions. So, analcime is formed on the bottom of sea basins at a temperature lower than 30 C as a result of interaction between volcanic ash which decomposes into a silicic acid and alumina and alkali metal salt dissolved in water. An occurrence of this or other type of zeolites depends upon chemical composition of the hydrothermal solutions. For example, in the rich-calcium solutions mainly calcium varieties are known to occur and with increase in concentration of the alkalis the alkali- earth cations are partially or completely replaced with sodium or potassium resulting in the formation of zeolites of alkaline and alkaline-alkali-earth composition.

Analysis of the data on sedimentation processes indicates that chemical decomposition of the rocks under action of alkaline solutions is a reason of their chemical and constituent compositions. Hydroaluminosilicates: muscovite, sericite, zeolites, etc. are the products of chemical decomposition of the widely spread rocks of alkaline and alkaline- alkali- earth aluminosilicate compositions such as plagioclases and sodium- potassium feldspars/ The most characteristic process of decomposition of the plagioclases (alkaline- alkali-earth hydration products) is a process of sericitization- a replacement of plagioclases with muscovite, that is a conversion of anhydrous aluminosilicates containing anorthite into hydrous alkaline aluminosilicates.

Finally, as a result of interaction of the feldspar  $R_2O \cdot Al_2O_3 \cdot 6SiO_2 \cdot nH_2O$  with water two reactions may take place which can be schematically represented (with approximation), they are:



Their essence can be explained as hydration of the anhydrous alkaline aluminosilicate and formation of a system of hydrates, including an aluminosilicate of the muscovite or analcime type. In its essence this process is similar to the process of portland clinker minerals hydration and an assumption can be put forward that it may take place and under

hardening of the alkaline and alkaline- alkali- earth cementitious systems [18].

According to their flowability in the zone of weathering the alkaline elements can be arranged as the following: calcium (with the highest flowability), sodium and magnesium and at last potassium. For example, potassium feldspars tend to decompose slower than the calcium and sodium ones, out of which an albite was found to be the most stable mineral. For plagioclases, an inverse relationship of resistance of the minerals upon quantity of the anorthite component: the calcium plagioclases decompose with a greater rate.

The alkaline hydrates such as muscovite and paragonite feature the increased resistance to weathering compared to the calcium ones.

These data provide evidence of durability of the AAC hydration products containing sodium and potassium hydroaluminosilicates. A tend to reduce a basicity of the hydration products compared to initial anhydrous minerals in cements used in construction also is a proof of analogy between the processes taking place in natural and man-made substances of alkaline and alkaline- alkali-earth aluminosilicate compositions. In general case these processes have such basic stages connected with changes in an alkalinity of the environment: hydration of the alkali metal and alkali-earth metals, partial replacement of the alkalis and alkali- earth metals. With the ions of hydrogen or hydroxon, the occurrence of the less alkaline almost not dissoluble hydroaluminosilicates of the  $R_2O \times (1 - 3) Al_2O_3 \times (2 - 6) \times nH_2O$  type and low basic alkali-earth hydrosilicates of the  $RO \times SiO_2 \times nH_2O$  type as well as soluble hydrates of the  $R(OH)_2$ ;  $ROH$ ;  $R_2O \times SiO_2 \times nH_2O \times Al_2O_3 \times nH_2O$  type in amorphous or submicrocrystalline state.

Under conditions of low temperature hydrothermal metamorphism which occurs in the Earth crust at relatively low temperatures and pressures, the processes of transformation of the rocks are accompanied also by hydration of the feldspar minerals and formation of water resistant and not water resistant alkaline hydration products. In their essence

and orientation they are similar to the processes taking place in the zone of accumulation of the sediments and to the hydration processes of building cements. Side by side with this the aqueous non-alkaline or low in alkali substances convert into more basic ones, for example, clay minerals- into zeolites, hydromicas- into micas, etc., similar to that taking place under conditions of autoclave treatment- a low basic hydrosilicate is formed from lime-siliceous mixtures and tricalcium hydrosilicate- from a mixture of  $\beta$ - $C_2S$  and lime. In both cases the natural processes of metamorphism lead to changes in the mineral hydration products as a result of bringing or loss/removal of the alkaline substances by circulating overheated aqueous solutions. They are reflected in removal or binding of the alkalis, crystallization of the zeolites, hydromicas, micas, which under conditions of thermal metamorphism later recrystallize in albite, orthoclase, feldspathoids, etc.

Worthy mentioning is the fact that a specific feature of the metamorphism stage is more higher pressures compared to those used in the building materials production that is why simulation of this process is complicated. However, the works of the scientists of the Scientific Research Institute of Binders and Materials (Kiev, Ukraine) suggested to establish that by using the aluminosilicate substances of metastable structure and active alkali metal non-silicate or silicate compounds in quantities required for synthesis of the alkaline hydroaluminosilicates, similar processes might be simulated in the larger volumes and under curing regimes (temperatures and humidity) used in the production of traditional concretes.

By summarizing the above a conclusion may be drawn that in the Earth crust and on its surface the continuous stage-by-stage condensation and dispergation processes of the silicate substances accompanied by mutual transformations of hydrous and anhydrous mineral systems, take place and they flow mainly with participation of the alkaline and alkali-earth oxides resulting, similar to processes of hydration and hardening of the building cements, in synthesis of stone-like

hydration products. These data serve as a prerequisite for the synthesis of analogs to natural aqueous sodium- potassium-calcium minerals through hydration of alkaline- alkali-earth systems, they are: alkaline- alkali-earth cement concretes which contain in general case: slags, intrusive and effusive rocks, clay minerals, silica, etc. In the process of interaction of these substances with alkali hydroxides, the processes of formation of the minerals of the Earth crust and stone-like rocks.

**MODELLING OF ROCK- MINERAL FORMATION PROCESSES**

Taken as a base for modeling was a scheme of formation of sedimentary rocks based on rock weathering products [18].

It was established that alkali hydroxides and salts of alkali metals producing in a aqueous medium an alkaline reaction, under condition of their high concentration, come into interaction with the clay minerals (Fig. 1, 2), aluminosilicate glasses (Fig. 3, 4) with the formation of water resistant alkaline and alkaline-alkali-earth aluminosilicate new hydration products like minerals of zeolite and mica types.

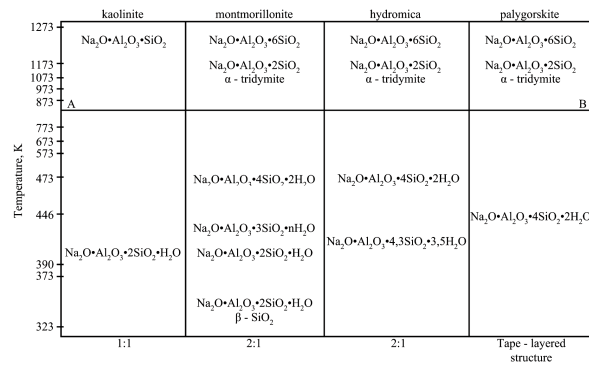


**Fig. 1.** Conditions of formation of various zeolites based on clays and sodium carbonate

The study results suggested concluding that basic composition of the cement stone hydration products depended upon type of the alkaline activator/admixture/used:

- I – (addition –  $H_2O$ ) –  $RO-SiO_2-H_2O$ ,
- II – (addition – hydroxides of alkali metal) –  $RO-SiO_2-H_2O, R_2O-Al_2O_3-SiO_2-H_2O, R_2O-RO-Al_2O_3-SiO_2-H_2O$ ,

III – (addition – hydroxides of alkali earth metal) – RO-SiO<sub>2</sub>-H<sub>2</sub>O,  
 IV – (addition – carbonates of alkali metal) – RO-SiO<sub>2</sub>-H<sub>2</sub>O, R<sub>2</sub>O-Al<sub>2</sub>O<sub>3</sub>-SiO<sub>2</sub>-H<sub>2</sub>O, R<sub>2</sub>O-RO-Al<sub>2</sub>O<sub>3</sub>-SiO<sub>2</sub>-H<sub>2</sub>O,  
 V – (addition – carbonates of alkali earth metal) – RO-SiO<sub>2</sub>-H<sub>2</sub>O,  
 where: RO – CaO, SrO, BaO, MgO; R<sub>2</sub>O – K<sub>2</sub>O, Na<sub>2</sub>O, Li<sub>2</sub>O.

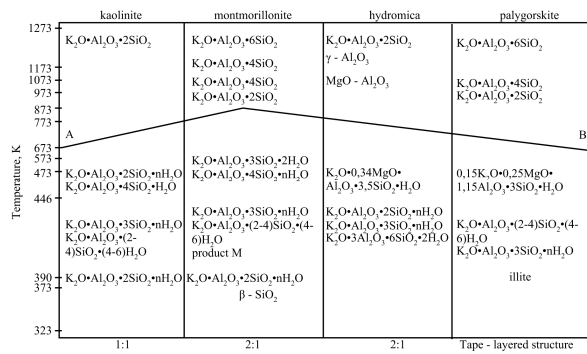


**Fig. 2.** Conditions of formation of various zeolites based on clays and potassium carbonate

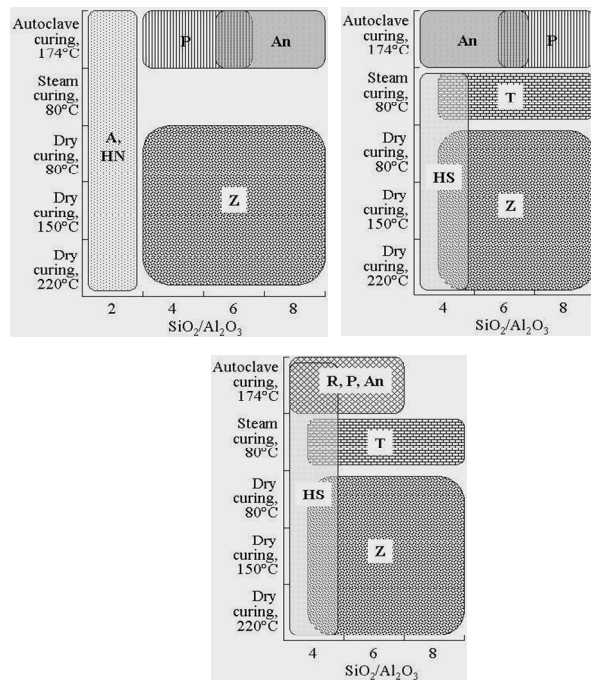


**Fig. 3.** Geocement composition (source of aluminosilicate):  
 a – metakaolin, b - fly ash 1, c- fly ash 2 vs curing conditions and hydration products. An – analcime, A – zeolite Na-A, P – zeolite P, R – zeolite R, HN – nepheline hydrate, HS – hydroxysodalite, Z – trona, T – sodium carbonate hydrate

The studies held allowed to draw the following conclusions:

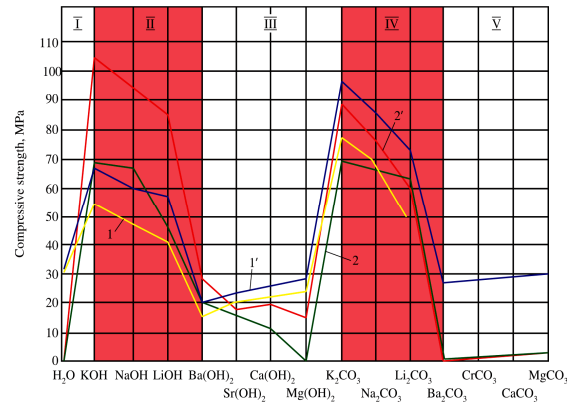


**Fig. 4.** Compressive strength of the AAC compositions vs type of alkaline activator and composition of hydration products:

1 and 1\* – slag with Mb=1.13 (Al<sub>2</sub>O<sub>3</sub>=6.75%), 2 and 2\* – slag with Mb=0.85 (Al<sub>2</sub>O<sub>3</sub>=15.85%), 1 and 2 – steam-cured specimens (T= 90±5°C, 3+7+2 hrs.), 1\* and 2\* – specimens cured in autoclave (T=173°C; 3+7+2 hrs)

- physico- chemical processes taking place during hardening of the conventional building calcium-based cementitious materials are similar to those of chemical weathering of rocks and formation of structure of the stone-like substances of sedimentary and metamorphous origin,
- being similar in essence, these processes take place at different rate, since starting materials vary in basicity and physical state,
- hydration processes in the calcium-based cements due to a higher basicity and metastability of the constituent minerals take place more actively compared to those of the alkaline rocks of stable structure; their hydration products are water resistant hydrosilicates and aluminates as well as soluble hydroxide of calcium,
- acceleration of these processes both in natural rocks and artificial alkaline and alkaline- alkali-earth aluminosilicates which are similar in composition up to the limits, under which they can be used in a form of hydraulic cementitious materials can be done through conversion of a substance from a stable crystalline state into more active metastable one, including

a glassy one, and, when necessary, by introduction of the alkaline oxides or hydroxides from outside. As a result, the hydration processes of high-basic alkaline substances will be similar in their character to natural processes of formation of the stone-like sediments of feldspar and nepheline rocks, and in activity – to portland cements. The hydration processes of low-basic or alkali-free substances in their character will be similar to natural processes of step-by-step conversion of pozzolana, lime-clay, lime- slag and slag (portland) cements,

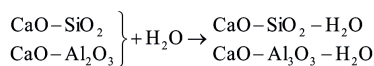
hydration products of high- basic and low-basic substances are similar to natural mineral formations are water- resistant hydroaluminosilicates- micas, zeolites and low-basic calcium hydrosilicates, as well as soluble hydroxides or silicates of sodium and potassium.

### ALKALI- ACTIVATED CEMENTS

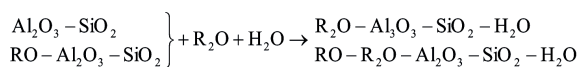
Simulation of the naturally occurring processes of transformation of the hydrous aluminosilicates into anhydrous ones allowed to develop systems of binding materials, the hydration products of which are capable to change their chemical composition and crystal lattice from hydrous to anhydrous one depending upon temperature curing conditions under which the concretes will be in service.

As a result, an idea of creation of cementitious materials was transformed as the following:

“OLD” scheme (OPC), high-alumina cement)



“NEW” scheme (alkali- activated cement)(AAC)



where R- Na, K, Li, Rb, Cs.

### PRINCIPLES OF COMPOSITIONAL BUILD-UP OF THE ALKALI-ACTIVATED CEMENTS

The following postulates have been laid down in their creation:

- alkalis act not only as activators but as structure- forming elements included into the formed phases as well,
- the formed hydration products phases are characteristic of the presence of new formations of the  $\text{R}_2\text{O}-\text{Al}_2\text{O}_3-\text{SiO}_2-\text{H}_2\text{O}$  and  $\text{R}_2\text{O}-\text{CaO}-\text{Al}_2\text{O}_3-\text{SiO}_2-\text{H}_2\text{O}$  types;
- quantities of alkalis to be introduced are caused by a necessity to meet a stoichiometric composition/ stoichiometry requirement/ of the alkaline and alkaline-alkali-earth hydroaluminosilicates analogous to natural zeolites.

In compliance with these principles the alkali content of the cement will be determined by an  $\text{Al}_2\text{O}_3$  content of the aluminosilicate component (Fig. 5).

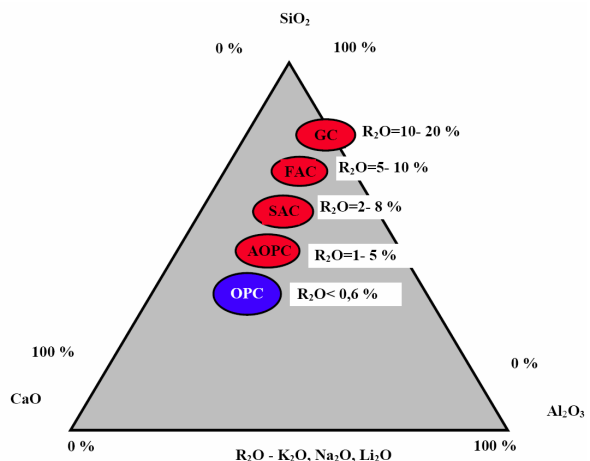


**Fig. 5.** Comparative chemical analysis of different types of OPC and AAC.

Abbreviations: **OPC**- ordinary Portland cement, **AOPC** – alkali- activated ordinary Portland cement, **SAC** – slag alkali- activated cement, **FAC** – ash alkali- activated cement, **GC** – geocement

The introduction into a cement composition of the alkali metal compounds in much larger quantities than was allowed in compliance with the principles of compositional build-up of the traditional cements based on

calcium and magnesium compounds suggested to consider that the alkali metal compounds acted not only as activators of hardening but as self-functioning components of the binding system  $\text{Me}_2\text{O}-\text{MeO}-\text{Me}_2\text{O}_3-\text{SiO}_2-\text{H}_2\text{O}$ , the main structure-forming products of which were low-basic calcium hydrosilicates and zeolite-like products. A low basicity of the hydration products is attributed to specific features of the structure-forming processes taking place in case of the slag alkali-activated cements, namely: a hydrolytic destruction of the solid phase of the low-basic phases is caused, first of all, by the break of the covalent bonds  $\text{Si}-\text{O}-\text{Si}$ ,  $\text{Me}^{3+}-\text{O}-\text{Me}^{3+}$ ,  $\text{Si}-\text{O}-\text{Me}^{3+}$  according to a scheme  $\equiv\text{Si}-\text{O}-\text{Si}\equiv \leftrightarrow [\equiv\text{Si}-\text{O}-\text{Si}\equiv]^- \leftrightarrow \equiv\text{Si}-\text{OH} + \equiv\text{Si}-\text{O}^-$  with protonization of the ion  $\text{Me}^{2+}-\text{O}$  bonds taking place in parallel, as it is known to happen in the high-basic systems [14].

An alkaline cation promoting flow of hydrolytic destruction of the low-active low-basic phases acts at early stages of structure formation as a catalyst of destruction. Later, as far as the condensation processes evolve, it takes an active part as a co-partner of  $\text{Ca}^{2+}$  and  $\text{Mg}^{2+}$  in the structure formation processes, thus facilitating its modification due to formation of the alkaline and alkaline-alkali-earth hydroaluminosilicates that are morphologically homogeneous with the low-basic calcium- magnesium hydrosilicate phases.

At early stages of hydration and hardening (for example, of the slag alkali-activated cements), the structure formation is caused, mainly, by the formation and crystallization of the low- basic hydrosilicates and hydrogarnets. The alkaline and alkali- earth hydroaluminosilicates, as a result of their slower crystallization, occur at the later stages. Being formed, mainly, in the pore space, they fill it and promote strong crystallization contacts with the primary phases to occur, as well as initiate the formation of more homogeneous and dense structure.

Besides, high pH-values of the medium at which the hydration process takes place tend to block a transfer of the Ca-ions into solution, thus explaining the absence of  $\text{Ca}(\text{OH})_2$  and the fact that the resulted calcium hy-

drosilicate has, as a rule, a basicity exceeding 1.

**CLASSIFICATION**

A classification proposed in [19] is based on the characteristic features of the products of hydration and hardening of the alkali-activated cements, the “edge” variants of which may be represented by the compounds of two types: alkaline hydroaluminosilicates of the system  $\text{R}_2\text{O}-\text{Al}_2\text{O}_3-\text{SiO}_2-\text{H}_2\text{O}$  and earth metal hydrosilicates.

A variety of blended alkaline- alkali- earth hydroaluminosilicates may fall within these ranges. A phase composition of the hydration products of a cement stone is determined by a kind of starting raw material (Table 2). Depending upon these starting materials the best application of the alkali- activated cements is to be chosen (Fig. 6).

**Table 2.** Mineralogical composition of the cement hydration products vs type of starting aluminosilicate component

Cement type	Initial solid phase	Alkali content, $\text{R}_2\text{O}$ , %	Hydration product
OPC	OPC clinker	< 0.6	0% 100%
Alkaline OPC	OPC clinker+ $\text{R}_2\text{O}$	1-5	
Blended alkaline OPC	OPC clinker+ additive (slag, ash, basalt)+ $\text{Me}_2\text{O}$	2-5	
Slag alkali-activated cement	Metallurgical slag+ $\text{R}_2\text{O}$	4-8	
Ash alkali-activated cement	Ash - product of coal combustion	5-10	
Geocement	Clay+ $\text{R}_2\text{O}$	10-20	

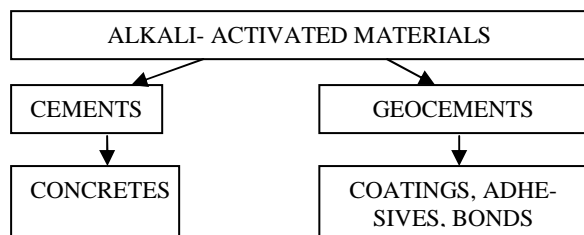


**Fig. 6.** Fields of application of the alkali-activated cementitious materials

### INDUSTRIAL USES

The experience from the small- and large scale industrial uses of the alkali- activated cements gained starting the 1960s in construction (hydropower engineering, road, agricultural, industrial, civil engineering, mining, etc.) gave proofs to high performance properties of the concretes on them. The use of the alkali- activated cement- based materials was found to be especially effective one for specially intended use in many fields besides construction [20].

Below are given some fields of the manufacture and use of the alkali- activated aluminosilicates.

### EFFICIENCY

More than 50 years passed since the alkali- activated cements appeared in the field and their efficiency and potential have been proved by extensive researches held not only in the Soviet Union but in many countries over the world: Poland, Finland, The Netherlands, Germany, Czech Republic, Romania, Slovak Republic, Bulgaria, Japan, China, USA, Canada, India, Brazil, Spain, the UK. The experience collected for this period of commercial- scale manufacture and use of structures and articles made from the slag alkali- activated cement concretes in various fields of construction testifies to their higher service properties as compared with those of Portland cement concretes (Table 3).

These materials were found to be the most highly effective ones when used in extremely severe conditions as well as in non- civil engineering fields (Fig. 7). Moreover, compared to traditional cements, the AAC possess polyfunctional properties and can be successfully used as high strength, quick

hardening, corrosion resistant, frost resistant, heat- and fire resistant and low exothermal cements [21].

**Table 3.** Properties of different cements

Cement type	Early strength	Durability	Chemical resistance
Portland cement	++	++	+
Blended cement	+	+++	++
High alumina cement	+++	+	+++
High sulphate cement	+	++	+++
Alkali-activated cement	+++	+++	+++
Sulphoaluminate cement	+++	++	+++

### TECHNOLOGY

More than 50 years practical experience of the Kiev school is connected with a manufacturing technology under which the alkaline activator was introduced into a concrete in a form of aqueous solution- so-called CONCRETE technology. Now there are two technologies, they are:

So-called “concrete” technology– under which all raw materials, they are: aluminosilicate component, alkaline activator and modifying additives/admixtures are introduced in a dry form or in a form of solution during mixing concrete ingredients similar to conventional concrete technology [22].

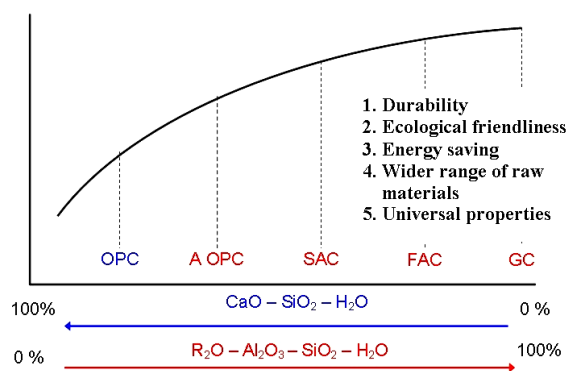


**Fig. 7.** Benefits of the AAC as compared to OPC-based cements

So-called “cement” (all-in-one) technology– under which all raw materials: aluminosilicate component, alkaline activator and modifying additives/admixtures are ground together and packed in bags for further use similar to other know-in-the-art cements for

the use in concrete under traditional OPC-based concrete technology (Fig. 8). This scheme in general features is given below. As to required equipment- *the best available techniques* (BET) can be successfully explored in it.

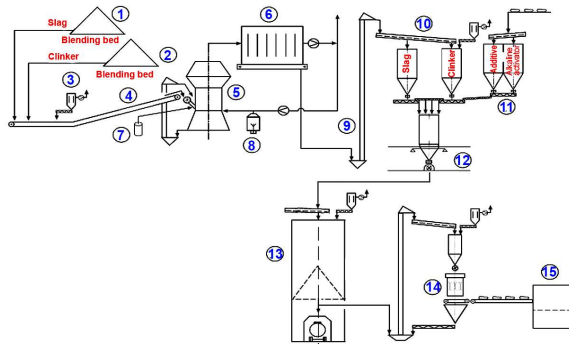


**Fig. 8.** “Cement” technology for the ACC manufacture. 1 – blending bed for slag, 2 – blending bed for clinker, 3 – dust collector, 4 – belt conveyor, 5 – vertical roller mill, 6 – fabric filter, 7 – metering equipment for water repellent, 8 – heat generator for drying, 9 – elevator, 10 – silos for cement constituents, 11 – bunker for additives/admixtures and alkaline activator, 12 – mixer for dry cement constituents, 13 – ready product storage silo, 14 – packer for bags, 15 – palletizer

### STANDARDISATION AND TEST PROCEDURES

In order to bring a newly developed product into a commercial-scale production it should pass all standardisation procedure according to national rules. In the former USSR, the commercialization of the ACCs was possible through its full-scale standardisation: a variety of national and industry standards have been issued [23]. As a result, the AACs were officially approved by the governmental bodies of the USSR for the use in construction for all structures along with OPC (Fig.9).

The latest achievement in standardisation of the ACCs is a newly issued national standard of Ukraine covering some ACC types [24]. Similar to the EN-196, the standard specifies only strength classes and compressive strength after 2, 7 and 28 days. In composition and strength at an age of 28 days the ACCs are classified as the following:



**Fig. 9.** The first residential house made without nay OPC from alkali- activated cement concrete (Lipetsk, Russian Federation)

slag alkaline cement, alkaline Portland cement, alkaline pozzolana cement, alkaline slag Portland cement, alkaline composite cement, which differ in combination of such aluminosilicate component as granulated blast furnace slag, OPC clinker, ashes from coal combustion, and basalt taken in combination with the alkaline activator (Table 4). Compressive strength classes under the standard are: 300, 400, 400R, 500, 500R, 600, 600R, 700, 800, 900, 1000. The standard is applicable to making concretes for common application.

Determination of mechanical and physical properties of the AACs is carried out in compliance with Ukrainian standard DSTU B V 2.7-24-95 and US standard ASTM C 109/C 109M. According to these standards, a water to cement ratio (W/C) is to be chosen to provide a flow value (measured on cone) =106 – 115 mm. In case of using these test methods according to EN standards (EN 196-1, 196-3, and 196-6, under which the W/C is restricted to a value of 0.5), the following amendments should be introduced: in determination of flowability of the cement/sand mortar the alkaline solution/ solid constituents or water/ solid constituents ratio should be chosen ex-

**Table 4.** Cement types according to National Standard of Ukraine DSTU B V.2.7-181:2009 “Alkaline Cements”

Cement type		Designation	Content, % by mass				
			Aluminosilicate constituent				Alkali metal compounds (sodium or potassium)
			Granulated blast-furnace slag	OPC clinker	Fly ash	Basalt	
ACEM I	Slag alkaline cement	ACEM I	90-100	0-10	-	-	1.5-12
	Slag alkaline cement with additive of fly ash	ACEM I -3	55-90	0-10	10-35	-	1.5-12
ACEM II	Alkaline portland cement	ACEM II	-	100	-	-	1.5-12
ACEM III	Alkaline pozzolana cement	ACEM III-3	←-----→		36-80	-	1.5-12
		ACEM III-B			-	36-80	
ACEM IV	Alkaline slag portland cement	ACEM IV	36-89	11-64	-	-	1.5-12
ACEM V	Alkaline composite cement	ACEM V	30-50	5-10	40-65	-	1.5-12

perimentally in such a way that to provide the flow values between 160-180 mm.

### CONCLUSIONS

Now Ukraine has all normative documentation required for a large-scale application of the alkali-activated cementitious materials into practice of construction.

In order to bring this technology into a large-scale world-wide application, the RILEM Technical Committee “Alkali Activated Materials” was organized in 2007 (www.rilem.net). Its tasks are: to collect and summarize the experience on raw materials; cements; concretes; structures; production; test procedures; durability; intended use and to develop basic recommendations on preparation of performance-based specification for cast-in-place alkali-activated cements and concretes.

The results of this work are expected to allow to develop and approve national and international standards for the alkali-activated materials.

### REFERENCES

1. **Malinowski R. 1982.** Ancient mortars and concretes: aspect of their durability. History of Technology, Nr 7, 9-101.
2. **Malinowski R., Stalkine A., Ben Yair M. 1961.** Durability of Roman mortars and concretes for hydraulic structures at Caesarea and Tiberias. Proceed. Int. Symp. On Durability of Concrete, Prague, 1-14.

3. **Malinowski R. 1979.** Concrete and mortars in ancient aqueducts, Concrete International, Nr 1, 66-67.
4. **Malinowski R. 1979.** Betontechnische Problemlösung bei antiken Wasserbauten. Leichtweiss Institut, Braunschweig, Germany, Mitteilungeng, Nr 64, 7-12.
5. **Langdon C. A., Roy D. M. 1984.** Longevity of borehole and shaft sealing materials: characterization of ancient cement-based building materials. Materials Research Society Symposium Proceedings, Nr 26, 546-549.
6. **Davidovich J. 1988.** Ancient and modern concretes: what is the real difference? Concrete International, Nr 9, 23-29.
7. **Glukhovsky V. D. 1989.** Ancient, Modern and Future Concretes, Proceed. 2nd International Seminar, Gothenburg, Sweden, 53-62.
8. **Kühl H. 1930.** Zementchemie, Berlin, Germany: Verlag Technik, Band III; 1958 or Zement 19.
9. **Chasserent L. 1937.** 17 me Congr. De Chim.
10. **Feret R. 1939.** Slags for the manufacture of cement. Rev. Mater. Constr. Tr. Publications, 1-145.
11. **Purdon A. 1940.** The action of alkalis on blast furnace slag. Journal of the Society of Chemical Industry, Nr 59, 191-202.
12. **Glukhovsky V.D. 1957.** Soil silicate-based products and structures. Kiev, USSR: Gosstroizdat Publish.
13. **Davidovich J.** Synthetic mineral polymer compound of the silicoaluminates family and preparation progress, US Patent, 4, 472,199.
14. **Krivenko P. 1986.** Synthesis of cementitious materials of the Me<sub>2</sub>O-MeO-Me<sub>2</sub>O<sub>3</sub>-SiO<sub>2</sub>-H<sub>2</sub>O system with required properties, DSc(Eng) Degree Thesis, Kiev, USSR: KISI Publish.
15. **Malek R.I., Licastro P.H., Roy D.M., Langton C.A. 1986.** Slag cement-low level radioactive waste forms at Savannah River Plant. Ceramic Bulletin; Nr 65, 1578-1583.

16. **Langton C.A., Roy D.M. 1984.** Longevity of bore hole and shaft sealing materials, characterization of ancient cement-blast building materials. Scientific Basis of Nuclear Waste Management, Nr 26, 543-549.
17. **Krivenko P.V. 1995.** Special slag alkaline cements. Kiev, USSR: Budivel`nyk Publisher.
18. **Ginzburg I.J., Rukavishikova I.A. 1951.** Minerals of the ancient zone of weathering of the Ural Mountains, Moscow, USSR.
19. **Krivenko P.V. 1997.** Alkaline cements: terminology, classification, aspects of durability. Proceed 10th Congress on the Chemistry of Cements, Sweden, 4 iv 046.
20. **Efremov A.N., Krivenko P.V. 2008.** Fire-resistant concretes from alkaline cements with the higher thermo- mechanical properties. Makeevka, Ukraine, DonNASA Publish.
21. **Krivenko P.V., Pushkaryeva E.K. 1993.** Durability of slag alkaline cement concretes. Kiev, Ukraine, Budivel`nyk Publish.
22. **Glukhovsky V. D., Krivenko P.V. at al. 1988.** Manufacture of concretes and structures from slag alkaline binders. Kiev, Ukraine, Budivel`nyk Publish.
23. **Shi C., Krivenko P., Roy D. 2006.** Alkali-activated cements and concretes. London: Taylor and Francis.
24. **National Standard of Ukraine DSTU B V.2.7-181:2009. 2009.** "Alkaline Cements".

## СПИРАЛЬНЫЙ СПОСОБ ДОБЫЧИ КОНКРЕЦИЙ СО ДНА АКВАТОРИЙ

**Аннотация.** В связи с имеющими место в настоящее время энергетическими, экономическими и экологическими проблемами прогресс в науке о цементе приобретает актуальное значение.

С 1957 года Киевская научная школа развивает новое направление в цементоведении, основанное на установленных профессором В.Д. Глуховским закономерностях проявления вяжущих свойств соединениями I-й группы периодической системы элементов. Результатом этой работы явилось создание принципиально новых цементов, в которых соединения щелочных металлов выступают не в роли активаторов, как их использовали ранее, а в роли структурообразующих элементов, формируя фазовый состав цементного камня новообразованиями типа щелочных и смешанных щелочно-щелочноземельных гидроалюмосиликатов, которые являются аналогами природных цеолитов.

Эффективность таких цементов подтверждена более чем 50-летним опытом их изучения, производства и применения.

**Ключевые слова:** щелочеактивированные, алюмосиликаты, цементы, долговечность, продукты гидратации.

## Penetrability Waterproofing Mortar Based on Slag-contain Compositions, Modified by Zeolites

*Kateryna Pushkarova, Maryna Sukhanevych, Kateryna Bondar*

Kyiv National University of Construction and Architecture  
Povitroflotskyi prosp., 31, Kyiv, Ukraine, 03680, e-mail: m.suhanevich@ukr.net

**Summary.** Investigated waterproofing penetrability mortars inflicted on concrete structures to improve their water resistance, durability, frost resistance. Optimized binder composition. Investigated performance of the mortars was confirmed increased water resistance of coatings after 1.5 years of operation.

**Key words:** waterproofing mortar, coatings of penetrating action, slag-contain cement, natural zeolite, salts-electrolytes.

### INTRODUCTION

It is known that the problem of protection for massive designs is solved with the use of thin layer coverings which are put on available places of a construction and create a strong layer, impenetrable for water and aggressive environment [1]. Cementations materials which are put on a surface in the different ways: plaster, smear, injection are widely use. To the smear coverings which were widely adopted recently in construction, drawing coverings of water proofing of penetration action [2]. The principle of work consists in ability of active chemical components of a covering to get into a pore and emptiness of concrete, to enter interaction with free hydroxide of calcium and to form needle-shaped water insoluble new formations which fill free space in concrete and condense structure, without allowing water to pass through an artificial stone.

Materials of penetrating action irrespective of manufacturing firm have similar composition: Portland cement, quartz sand of certain fractions and active chemicals components. These active additives which are

know-how of the company, also define the main difference between compositions the waterproofing materials. However, the durability and reliability of coverings of penetrating action cause certain questions and not always satisfy the consumer [3].

Besides, the maintenance of a large number of penetrating chemical additives is accompanied by salting-out, formation of cracks, flaking of coverings that leads to repeated destruction of a design and demands the increasing costs of its restoration [4].

It is known that replacement of part Portland cement with the blast-furnace granulated slag promotes full binding of free  $\text{Ca}(\text{OH})_2$  in the low-main hydrosilicates of calcium. It's provided that the slag-content cements have high water resistance in the fresh and mineralized water [5]. Besides, the artificial stone on the basis of such cement is characterized by high water resistance, frost resistance, sulfate resistance [6].

Application as modifying additives in cements of natural zeolites justified itself from the point of view of possibility to change the structure of new formations towards creation the zeolite-likes combinations of the increased durability and water tightness and

ability to occlude the anions which are present in aggressive environment, in difficult inorganic complexes [7].

## PURPOSE OF WORK

The purpose of work is development of durable waterproofing coverings of penetrate action with the increased operational properties on the basis the slag-contain cement modified by additives of natural zeolites and a complex additive of salts-electrolytes. The last will allow to synthesize ettringite like combinations which will serve as the crystallization centers for the low-main hydrosilicates of calcium.

## MATERIALS AND METHOD OF TESTING

Experimental researches were conducted on the basis of cementitious composition which consisted of Portland cement M 500, the blast-furnace granulated slag of Krivorozhsky plant (Ukraine) and natural zeolite-clinoptilolite (Ukraine).

As components of chemically active complex action salts of alkaline metals were accepted: sodium nitrates, sodium carbonates and sodium sulfates.

Mixture for receiving a waterproofing covering consisted of mineral binding and quarts sand with size less than 0,63 mm. The ratio a cement:sand made 1:1,5. The amount of water selected resulted from need of ensuring sufficient mobility and spreadability of mix. Taking into account these requirements the water:cement ratio was within  $W/C=0,45-0,5$  and flow table test with using of Vick's ring reached 200-210 mm.

As compositions of comparison widely known waterproofing materials of penetrating action (the Penetron and Kalmatron, production of Russia) were chosen. Physico-mechanical researches were made according to standards on dry construction mixes DSTU B.V.126:2011. Durability of the coverings put on a concrete basis, was defined

with the help of non-destructive measurement of compressive strength by sclerometer, and water tightness - by Karsten's tube. Composition of products hydration was identified, using physical and chemical methods of researches: X-ray phase, differential and thermal methods of the analysis and electronic microscopy.

## RESULTS AND DISCUSSION

Researches on optimization of composition of slag-contain materials with an additive of natural zeolite was made with use of a mathematical method of planning experiment. As varied factors were accepted by  $X_1$ -amount of slag: 20; 30; 40% of weight binding and  $X_2$ -amount of natural zeolite 5; 10; 15%. As functions of a response chose compressive strength ( $R_{st}$ ) of samples in different terms of curing of 3, 7, 28 days and capillary water absorption of the covering with putting on a glass plate and 24 hours sustained in water. Results of researches are presented in Fig. 1.

The analysis of the received isoparametrical diagrams of change functions of a response from factors of a variation allowed to establish the optimum content of slag and natural zeolite in binding system which provides at the same time high compressive strength and low water absorption of waterproofing coverings.

The obtained data show that the optimum content of natural zeolite is in limits of 5,5-7,5% at the content of slag as a part of a Portland cement about 22-25% for ensuring the maximum strength of samples (for 3 days - 7,5 MPa, for the 7th days - 17,0 MPa; for the 28th days - 34,8 MPa). Water absorption of optimum composition makes 0,11-0,12 kg/sq.m.

Thus, it is established that the optimum ratio of slag as a part of cementitious composition makes 22-25 % and natural zeolite of 5,0-7,5 %.

The received binding composition is accepted as basic for its further modification by a complex additive of alkaline metals salts

[8]. The last raises a concrete waterproofing to create additional amount of crystalline hydrates new formations of the needle-type filling a pore, capillaries and cracks of a concrete stone, and creating dense, inaccessible to a water filtration structure.

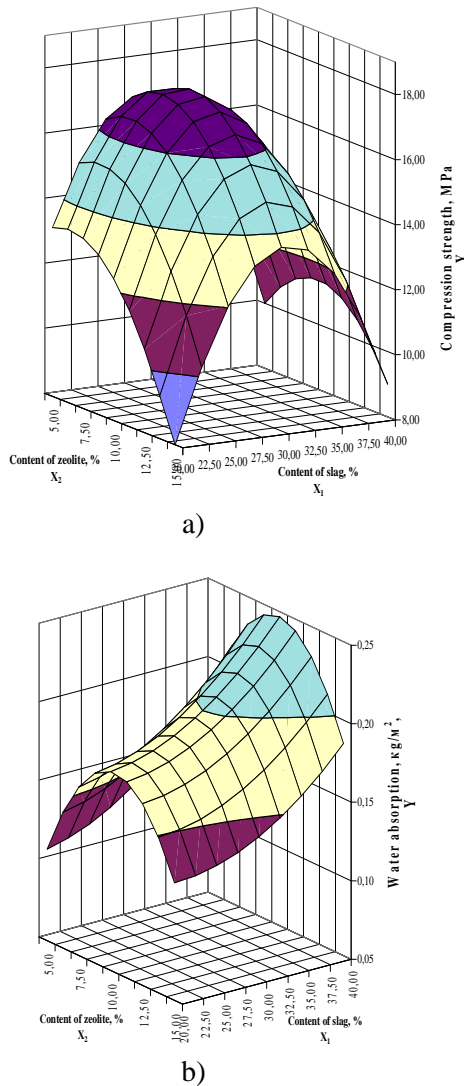


**Fig. 1.** Isoparametrical diagrams change of compressive strength of cementitious composition after hardening of 7 days (a) and water absorption changes in 24 hours (b) depending on a ratio of components:  $X_1$  – the content of slag;  $X_2$  – the content of natural zeolite

The maintenance of a complex penetrating additive makes 10% of the mass of the binding. The chosen salts of sodium ( $Na_2CO_3$ ,  $Na_2SO_4$ ,  $NaNO_3$ ) used in various ratios, and their necessary contents were determined by criterion of the smallest capillary water ab-

sorption of a covering (with application of a Karsten’s tube) and by the greatest strength (about application sclerometer). Ratio between salts of sodium changed within 2,4,6,8,10 parts from total quantity of entered salts-electrolytes.

Tests by determination of strength and water absorption of coverings were carried out in 7 days after drawing. Coverings were maintained at first 3 days in water, and then 3 days in dry conditions.

Water absorption was defined in 24 hours after filling of a Karsten’s tube with a way of fixing the amount of water (in ml) which was absorbed by a covering at a definite time. Also for the purpose to check the ability of materials to carry out hydroprotection functions throughout a long time strength and water absorption of studied coverings and comparison compositions in 365 days were studied. Results of researches are given in Fig. 2.

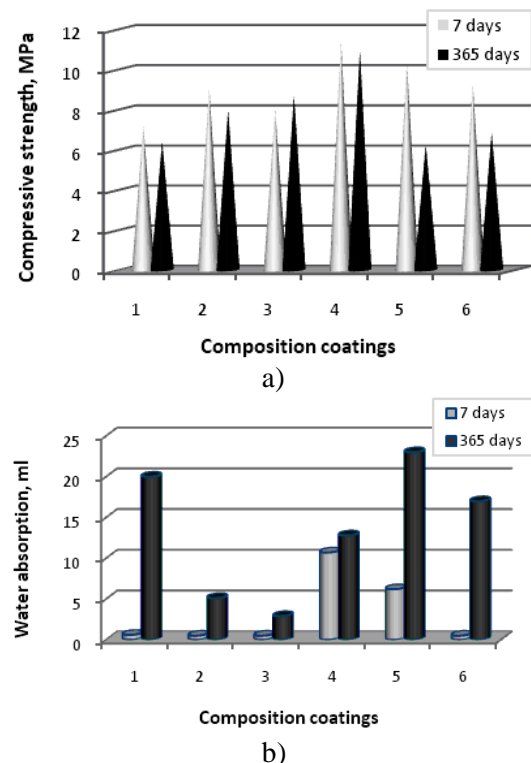


**Fig. 2.** The compressive strength (a) and water absorption (b) coverings on the basis of slag contain cement with an additive of natural zeolite (composition 4) and with additives of sodium salts (carbonates, sulfates, nitrates), taken in various ratios (composition 1,2,3); comparison compositions of Penetron and Kalmatron (5, 6) respectively

Comparison of the above-stated data shows that introduction of salts- electrolytes significantly doesn't influence the strength of binding systems (when curing within 7 days) which makes 8,17 MPa and concedes to comparison composition – the brand Kalmatron, the brand Penetron and the composition without salts.

The analysis of results shows that the compressive strength of coverings decrease after 365th days hardening, except composition 3. The greatest loss of strength have analogs of compositions (the brand Kalmatron and the brand Penetron) after 1 year of hardening. Their strength decreased approximately about 1,3 - 1,6 times.

Thus, impregnation of cement-sand samples by waterproofing solutions on the basis of slag contain mineral binding with an additive of natural zeolite and an optimum complex chemical additive, allows to reduce the volume of water absorption by 17,7-21,4 times (after 7 days of curing) and by 2,5-4,4 times (after 365 days of hardening). Generalization of the received dependencies shows that the smallest size of water absorption as for the 7th days (0,5 ml), and for the 365th days (2,9 ml), at strength preservation, characterizes coverings of composition 3. And it is visible that low water absorption remains for this composition after 365 days of hardening while other structures show bigger water absorption, not to mention the comparison compositions which waterproofing properties after 1 year decreased almost by 10 times, and permeability of the bases covered with them increased in comparison with the unprotected surface of concrete (composition 4).

The developed coverings are characterized by much higher reliability in comparison with traditionally applied materials of the similar mechanism of action and appointment, and their ability to a waterproofing of concrete doesn't decrease even after 1 year of operation as it was recorded for analogs of comparison [9].

The obtained data of physico-mechanical tests are confirmed by results X-ray phase

(Fig. 3) and given to electronic microscopy (Fig. 4).

At identification of products hydration of an artificial stone in 365 days of hardening it is established that at long hardening of binding composition (Fig. 3, the curve 1) are presented by hillebrandite ( $d=0,301; 0,275; 0,237; 0,205; 0,196; 0,192; 0,181; 0,174$  nm) and ettringite ( $d= 0,301; 0,256; 0,234; 0,220; 0,215; 0,206; 0,197; 0,175; 0,166; 0,162; 0,157$  nm).

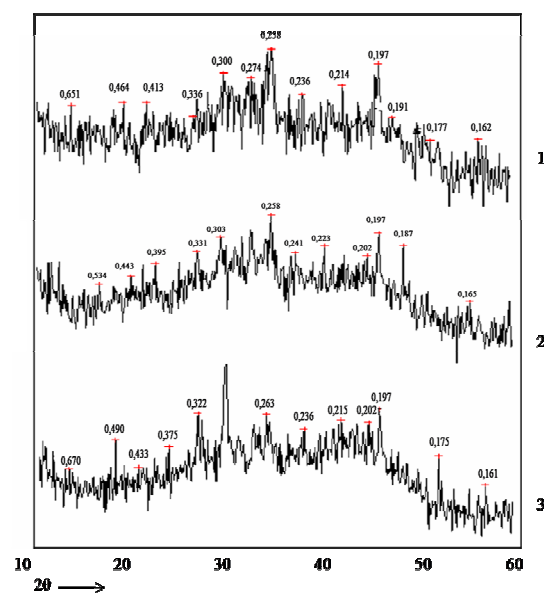


**Fig. 3.** X-ray diffractograms products of hydration of the artificial stone received after 1 year of curing on the basis of binding compositions: "portland cement+slag+water" (1), "portland cement +slag+zeolite+water" (2), "portland cement+slag+zeolite+complex of salts + water" (3)

In the course of composition modification by natural zeolite there is its decomposition, and then – in late terms synthesis analcime ( $d=0,241; 0,221; 0,190; 0,185; 0,178; 0,168; 0,165; 0,160$  nm) and gmelinete ( $d=0,455; 0,332; 0,259; 0,207; 0,195; 0,187; 0,178; 0,168; 0,166$  nm) - analogs of natural zeolites are observed [4]. Also as a part of hydration products after 1 year of hardening (Fig. 3, line 2), are present ettringite ( $d=0,240; 0,223; 0,212; 0,197; 0,166; 0,162$  nm) and hillebrandite ( $d=0,301; 0,275; 0,224; 0,196; 0,192; 0,186$  nm).

At introduction of salts in binding composition (Fig. 3, line 3), in addition to the

above-established substances as a part of new formations are recorded: low-sulphatic form hydrosulphoaluminate calcium  $3\text{CaO}\cdot\text{Al}_2\text{O}_3\cdot 3\text{CaSO}_4\cdot 12\text{H}_2\text{O}$  ( $d=0,287; 0,260; 0,235; 0,206; 0,190; 0,187; 0,166; 0,155$  nm), four-calcium monocarbonate hydro-aluminate  $3\text{CaO}\cdot\text{Al}_2\text{O}_3\cdot\text{CaSO}_3\cdot 12\text{H}_2\text{O}$  ( $d=0,346; 0,330; 0,286; 0,217; 0,201; 0,186; 0,166; 0,160; 0,155$  nm), calcium hydro-nitroaluminate  $\text{CaO}\cdot\text{Al}_2\text{O}_3\cdot\text{Ca}(\text{NO}_3)_2\cdot 10\text{H}_2\text{O}$  ( $d=0,187$  nm).

Thus, the analysis of results of RFA confirms existence as a part of hydration products of an artificial stone of a large number hydrosulphoaluminate type of ettringite structure (AFt that Afm), the occlude his pore space both reducing water absorption and water penetration in time.

The microstructure of the artificial stone hardening throughout 1 year is presented (Fig. 4).

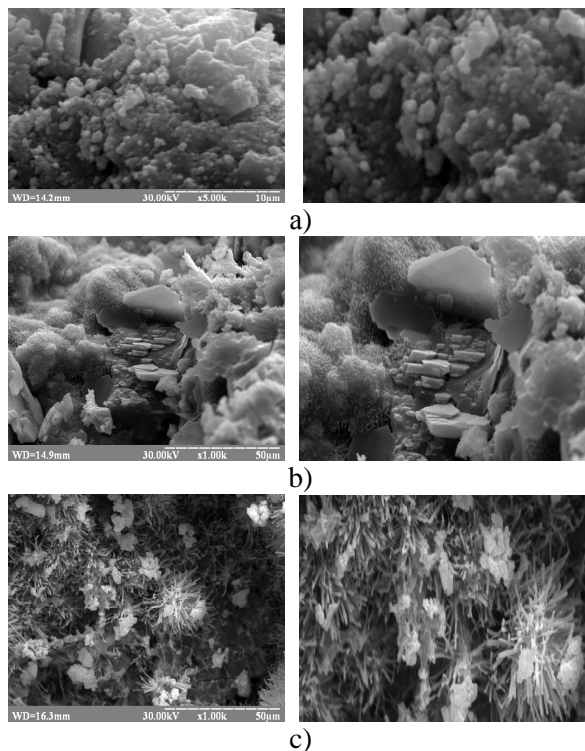


**Fig. 4.** SEM micrograph of sample, hardening for 1 year, on the basis of binding compositions: "portland cement + slag" (a), "portland cement + slag + zeolite" (b), "portland cement + slag + zeolite + complex of salts" (c) at increase: x1000, x3000. The presented microphotos of an artificial stone on the basis of slag contain cement with an additive of natural zeolite testify to formation of a large amount of the modified hydrosilicates of calcium and analcime (Fig. 4, b)

While microphotos of this composition modified by a complex additive of salts (Fig. 4,c) show formation of solid solutions ettringite and the modified hydrosilicates and calcium hydroaluminates.

In microphotos it is visible that crystals are presented by long thin prismatic needles (20-30 nm). Ettringite takes place in all volume of a cement stone, especially in a pore and has an appearance of rather evenly distributed grid in which crystals of hydrosilicates of calcium are chaotically located.

It is experimentally established that when drawing a covering up to 2 mm thick, depth of penetration of a waterproofing material in structure of concrete makes some tens of centimeters, and introduction of a zeolitic additive in structure cementations compositions are provided by binding of free alkaline connections in insoluble hydroaluminosilicate connections, the amount of the salts-electrolytes getting to structure of protected concrete, doesn't exceed 0,04% for  $1\text{ m}^3$ .

Thus, introduction of salts-electrolytes accelerates crystal hydrate of connections crystallization, but also initiates the directed crystallization of the low-main hydrosilicates of calcium. There is a reduction of a macrotime to simultaneous increase in the micropores, caused by formation of more uniform dense structure of a cement stone. Replacement of Portland cement part with the blast-furnace granulated slag promotes full binding of  $\text{Ca}(\text{OH})_2$  in hydrosilicate substances which are more durable and resistant to the influence of aggressive environment. At the same time, introduction in slag-content systems of natural zeolites gives the chance to connect excess alkalis ( $\text{Na}^+$ ,  $\text{K}^+$ ) in insoluble hydroaluminosilicates and to occlude anions ( $\text{SO}_3^{2-}$ ,  $\text{SO}_4^{2-}$ ,  $\text{NO}_3^-$ ) as a part of inorganic complexes.

The established features of modification the slag contain cements by natural zeolites and a complex of salts allow to receive waterproofing coverings of penetrating action with rather high physico-mechanical properties which don't concede to domestic and foreign analogs, but differ from them during the increased term of exploitation.

## CONCLUSIONS

1. Structures of waterproofing coverings of penetrating action on the basis the slag-contain cement compositions modified by natural zeolites and a complex of salts which differ high operational characteristics and stability of properties in time are developed.

2. Introduction of natural zeolites in Portland cement and slag system allows to connect free alkali (Na, K) in insoluble hydroaluminosilicates and to occlude anions ( $\text{SO}_3^-$ ,  $\text{SO}_4^{2-}$ ,  $\text{NO}_3^-$ ) in difficult inorganic complexes that in turn serves as a guarantee of durability of a waterproofing covering in time.

3. The offered structures of waterproofing materials provide a durable covering with high operational characteristics (in 1 year hardening a compressive strength makes more than 8 MPa, and water absorption – less than 3 ml) which aren't inferior to characteristics of analogs of comparison of domestic and foreign production.

## REFERENCES

1. **Soloviev V., Sychev A., Korobov N. 2009.** Increase of operational properties of concrete thin-cement compositions superficialis and penetrating. Concrete and reinforced concrete, Nr 3, 16–19.
2. **Kotsenko A. 2002.** Some aspects of the use of penetrating waterproofing. Building Materials, Nr 12, 44–45.
3. **Balakin D. 2007.** Difference capillary penetrating waterproofing concrete waterproofing materials from cement binder. Dry mixes, Nr 1, 10–3.
4. **Brovkina N., Ovcharenko V., Bulls V., Izosimov M. 2010.** Role of salts in the compositions of penetrating waterproofing for concrete. Proceedings of the universities. Building, Nr 8, 28–34.
5. **Kravchenko K. 2011.** "Kalmatron" - a necessary and sufficient protection for concrete constructions. Building materials, equipment, technologies of XXI century, Nr 4, 9–10.
6. **Sanitskiy M, Shevchuk G., Khaba P. 1997.** Structure formation of composite Portland cement with chemical applications. Chemistry, Technology and Applications substances, Lviv, Nr 316, 195–197.
7. **Pushkarova K., Sukhanevych M., Bondar K., Martsih A. 2010.** Slag-content cement modify zeolite as basis for waterproofing solutions. News DonDABA. Modern building materials, design and innovative technology of buildings, Vol. I, 5 (85), 102–108.
8. **Pushkarova K., Sukhanevych M., Bondar K. 2010.** Optimization of composite materials for waterproofing coatings of concrete structures. News of ODABA, Odesa, 39 (2), 181–187.
9. **Pushkarova K., Sukhanevych M., Bondar K. 2011.** Waterproofing coating penetrating action with improved performance properties. Resource-efficient materials, structures, buildings and constructures, Rivne, Nr 22, 125–131.

ГИДРОИЗОЛЯЦИОННЫЕ РАСТВОРЫ  
ПРОНИКАЮЩЕГО ДЕЙСТВИЯ  
НА ОСНОВЕ ШЛАКОСОДЕРЖАЩИХ  
КОМПОЗИЦИЙ, МОДИФИЦИРОВАННЫХ  
ЦЕОЛИТАМИ

**Аннотация.** Исследованы гидроизоляционные растворы проникающего действия, наносимые на бетонные конструкции для повышения их водонепроницаемости, прочности, морозостойкости. Оптимизирован состав вяжущего, исследованы эксплуатационные свойства растворов, подтверждена повышенная водонепроницаемость покрытий после 1,5 лет эксплуатации.

**Ключевые слова:** гидроизоляционные растворы, покрытия проникающего действия, шлакосодержащий цемент, природный цеолит, соли электролитов.

## Analysis of Space Planning and Design Decisions Modern Cottage

*Maksym Klys*

Kyiv National University of Construction and Architecture  
Povitroflotskyi prosp. 31, Kyiv, Ukraine, 03680, e-mail: maxdbc@ukr.net

**Summary.** This article reports analysis of the major space planning and design solutions to contemporary cottages. Also considered the land on which built or being built these cottages. Realized statistical processing of the results. Definitely, a line of research of technical parameters of the device bearing structures cottages. Inspected the 68 modern houses and land plots for them in Kiev and Kiev region. Based on these data the histogram parameters most significantly influence the choice of process parameters erection. The results of analysis are a set of body-planning and design parameters that significantly affect the technological solutions.

**Key words:** cottage, parameters, technological solutions, mechanization, statistics.

### INTRODUCTION

Improving the efficiency of the construction of modern cottages is not possible without the constant improvement of technological processes on the device support structures. Analysis, evaluation and synthesis of the features of space-planning and design decisions that have a significant impact on the change in the parameters of technology of construction of buildings allows for more detailed study of the relationship between design decisions and process parameters.

### ANALYSIS OF PUBLICATION, MATERIALS AND METHODS

Features space planning and design solutions cottages disclosed in Getun G., Velikovsky L. and other [3, 15]. However, were not present statistical analyzes to address issues of mechanization and organization building processes that relate to modern cottages [8, 11, 18].

### PURPOSE AND STATEMENT OF THE PROBLEM RESEARCH

To conduct the analysis, evaluation and synthesis of space planning and design parameters of modern houses and land plots for them, which act as a factor in determining the organizational and technological parameters of the device monolithic structures [2].

### MAIN SECTION. RESULTS AND THEIR ANALYSIS

To date, in a residential building, there is similarity space planning and design solutions while maintaining and, if necessary, an individual approach to specific conditions and construction requirements [6]. For this, we used the methodology of statistical research presented in the works of Wentzel E [16] Gmurmana V. [4] and other [7, 9, 17].

To accomplish this, inspected the 68 modern houses and land plots for them in Kiev and Kiev region. Based on these data the histogram parameters most significantly influ-

ence the choice of process parameters erection [5]. According to the analysis identifies the main space planning and design characteristics (geometry, weight, quantity) of buildings [1, 10, 12]. The characteristics selected for analysis shown in Table 1.

**Table 1.** Characteristics that the affect the parameters of technological process

Classification of characteristics		Formalizing
Groups	Subgroups	
Space planning performance of buildings	Built area under the cottage	$S_1$
	Quantity of floors	$n$
	Length of the building	$L$
	Width of the building	$B$
Constructional features of the buildings	Floor height	$H$
	Span length	$l$
Geometric parameters of structures	The thickness of the supporting structure	$t$
	Plinth height	$h$
Geometric parameters of the land plot	Distance from the boundary of the building to the property line	$b$
	Land plot area	$S_2$

The histogram shows that the investigated houses with area up to 200 m<sup>2</sup>, from 200 m<sup>2</sup> to 300 m<sup>2</sup> and over 300 m<sup>2</sup> are in the same range with a standard deviation 63.05 (Fig. 1, a).

The number of floor buildings, most in the range one and two floors, is rarely possible to find 3-storey cottages. A substantial share ( $\mu=55\%$ ) are the building height of two floors (Fig. 1, b). Reducing the frequency of buildings for more than two floors due to lack of demand for such buildings [13, 14].

To date, the Ukrainian family, on average, consists of no more than five people. In addition, for this family enough to the house was a 2-storey.

The length of the vast number of buildings ( $\mu=86\%$ ) of 11 m to 20 m (Fig. 1, c). Width – from 9 m to 16,5 m (82%) (Fig. 1, d).

The most common buildings with floor height within 2,7...3 m, constituting the bulk of the population (86%), less common is a group of buildings with a floor height within 3,1...3,5 m (Fig. 2, a).

The values of the span of the building are within 4,0...10,5 m with an average of – 6,2 m (Fig. 2, b).

As seen in the histogram, the height of the cap ranges from 0,05 m to 2,0 m with an average value of 0,5 m and depends not only on the architecture of the building (Fig. 3, a).

In Kiev and region, thickness of the snow cover is 0,84 m. This is one reason why Most of the buildings, namely 87%, has a height of 1,2 m to the cap.

The distribution of the thicknesses of the bearing members has an average value of 380 mm at a low level of variation indicates the relative homogeneity of this factor. (Fig. 3, b).

The histogram, you can see that the land in Kiev and Kiev region, with an area of up to 8 acres is 41%, from eight to twelve acres –  $\mu=45\%$  and more than 12 acres only 14%. House with a large plot of land can be found in extremely rare because of the high cost of land (Fig. 4, a).

The second reason for the popularity of small and medium-sized sections depends on the unwillingness to live in extended families with relatives in the big houses.

Respectively, due to not large areas of land, distance from the boundary of the building to the property line, in most cases (83%), limited to 10 m. More than 10 meters in just 17% of all study sites (Fig. 4, b).

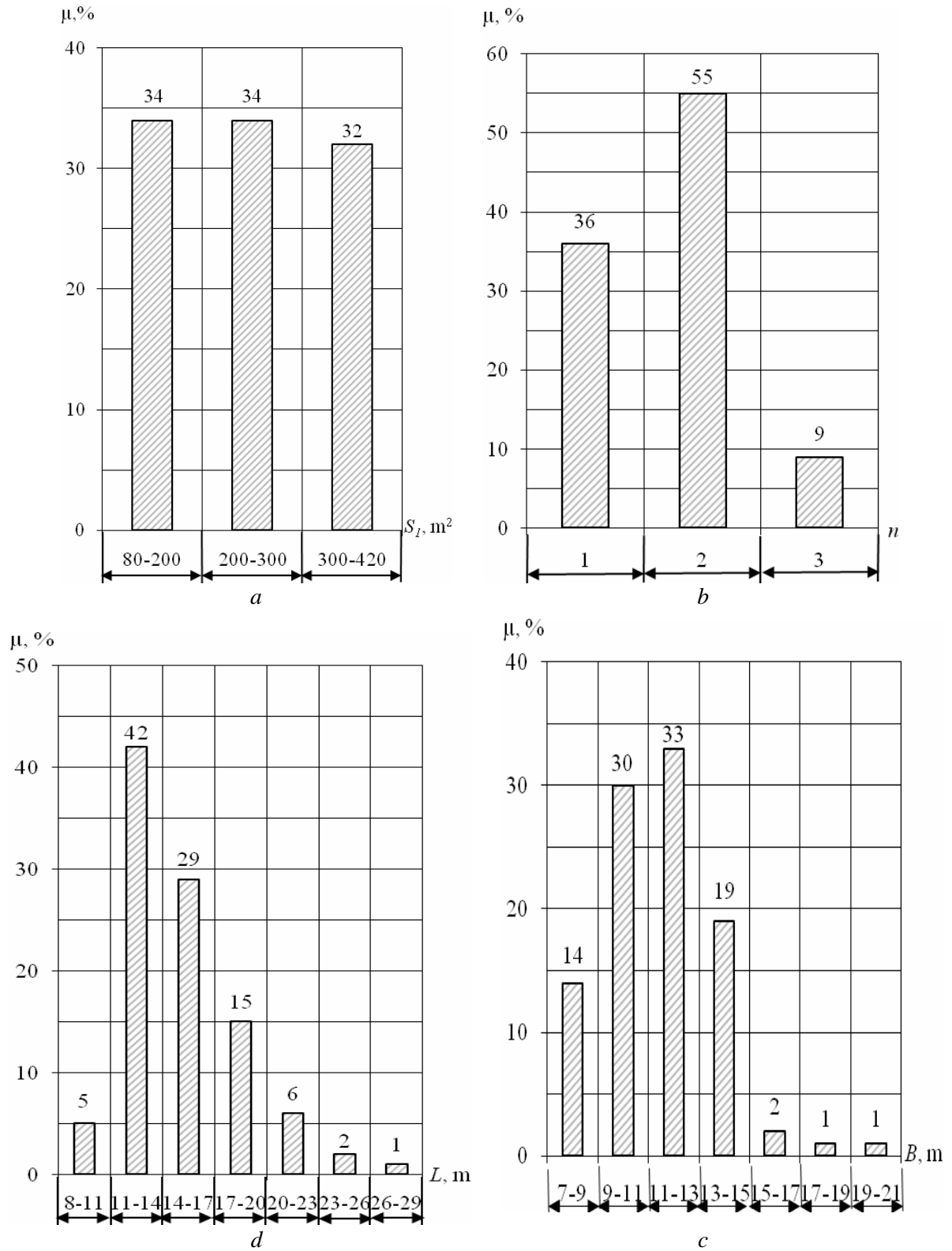


**Fig. 1.** The distribution of space-planning features:  
*a* – built area under the cottage, *b* – number of storeys, *c* – length of buildings, *m*, *d* – width of buildings, *m*

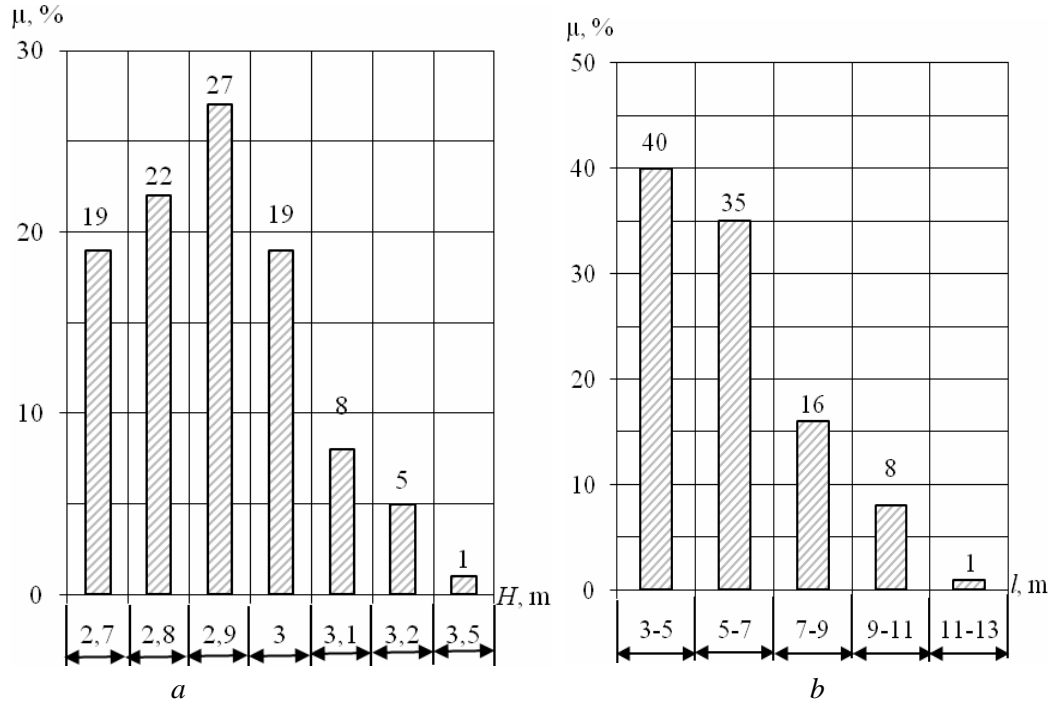


**Fig. 2.** The distribution of design characteristics:  
*a* – floor-to-floor height, m, *b* – span length, m

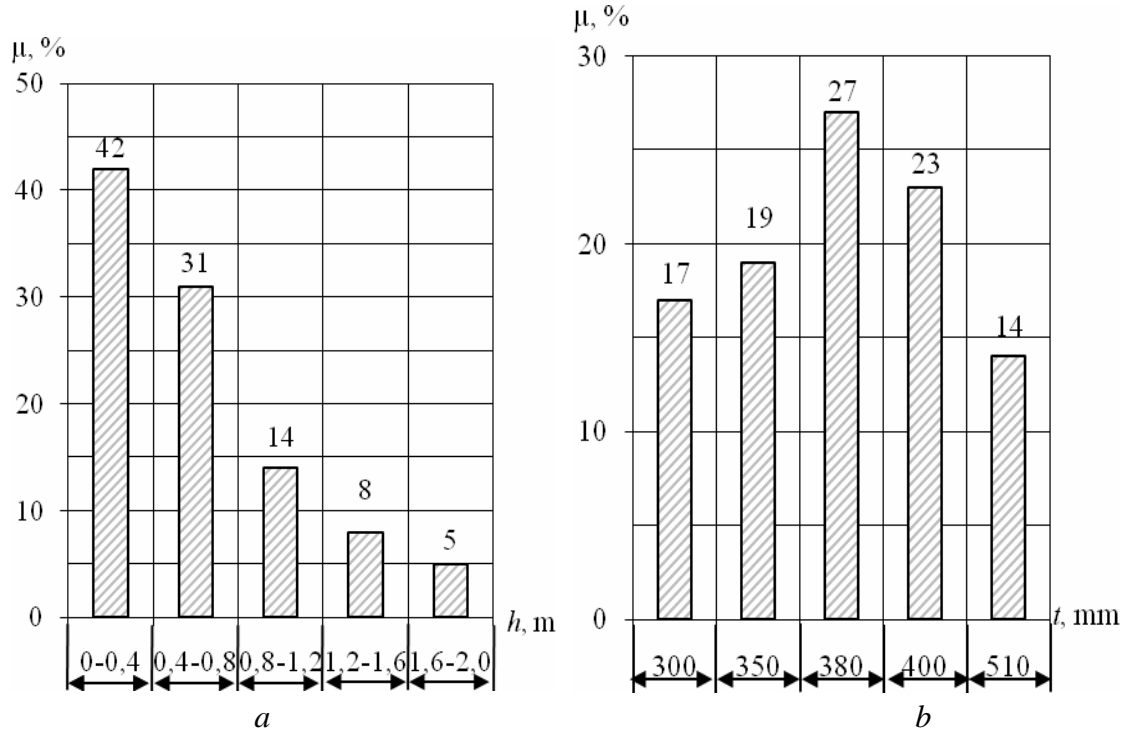


**Fig. 3.** The distribution of geometrical parameters:  
*a* – plinth height, m, *b* - thickness of the load-bearing elements, mm

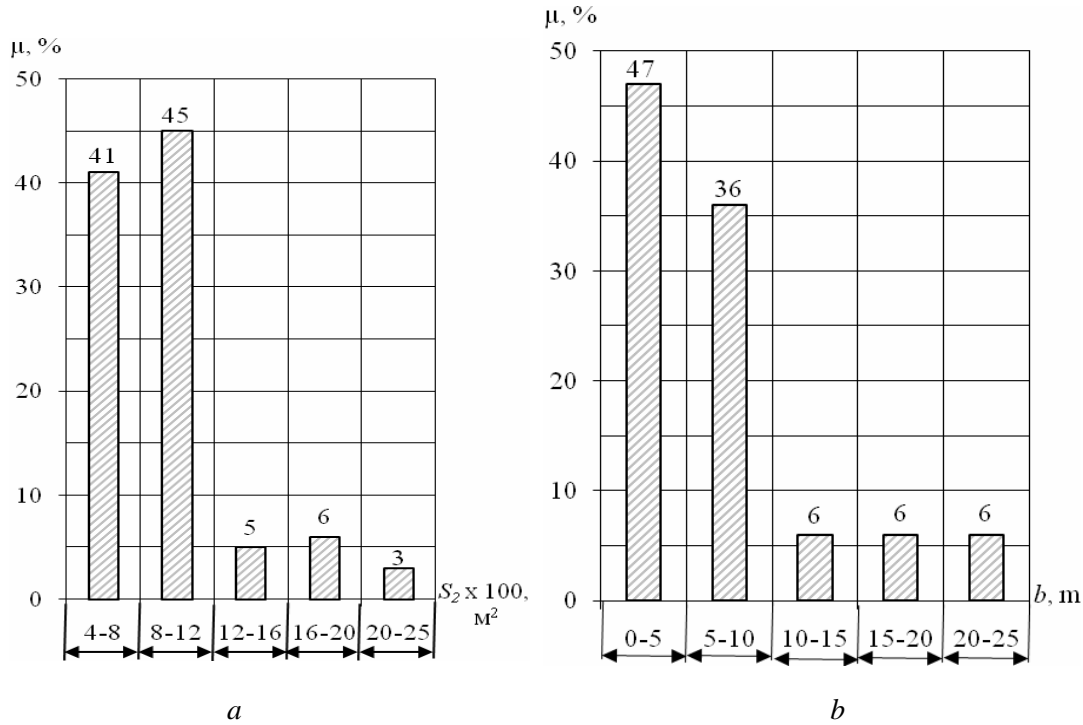


**Fig. 4.** The distribution of geometrical parameters of land: *a* – land area, m<sup>2</sup>, *b* – free place, m

Due to the fact that 47 % of the sites has a distance between the building and the boundary portion to 5 m, such that during construction of the house is very difficult to use a crane. Therefore, it is necessary to choose the larger capacity crane and boom to could work outside the station on the road or neighboring property, which not always permitted, especially in those areas where people living.

In such areas, you need to move away from the use of a crane. It will be safer, solves the problem of transport, transportation, loading and unloading.

Using the methods of probability theory and mathematical statistics performed analysis and evaluation of the data (Table 2). For describing these variables, the following characteristics:

- $m^*$  (the arithmetic mean of the sample) - evaluation of the expectation, the most important exponent of the random variable,
- $\Delta_x$  (margin of error) - the range of feasible values for the error level is 95 %,

Me (median) - the value of a random variable, separating variation series into two parts of equal number of values,

$\sigma$  (standard deviation) - evaluation of the scattering has the dimension of the random variable,

$v$  (variation coefficient) - a dimensionless quantity that is used to compare scattering variational series, the values of which have different dimensions,

$Q_1$  (lower quartile) - separates the 25 % of the population with the lowest values,

$Q_3$  (upper quartile) - separates the 25 % of the population with the highest value.

The variation in economic statistics is rarely used as an independent measure of the deviation. It is part of the expression of the variance and standard deviation. The deviation is used in some sections of statistical physics, in particular in the evaluation of the fluctuations of random thermal motion of the particles as an independent measure of variation.

Result: it computes the average linear deviation of a data set.

The average sampling error gives some representation of the error, i. e. the error with which the sample mean is the actual value of the general average. That it shows what will be the error on the average, if one makes many samples of the same volume out of one and the same population. However, in each actual sample, the error may differ significantly from the average error, i. e. there is no guarantee that the error that really was made in the particular sample study does not exceed the average error.

Therefore, it would be much more useful to know the boundaries within which the actual error in this particular sample is "almost certainly". These boundaries (limits) are specified by limit sampling error (denoted by  $\delta_x$ ). Limiting accuracy of the sample indicates that limit, which the actual error is almost certainly will not exceed. In other words, the maximum error  $\Delta$  shows really committed error in abundance, with excess (possibly very high) and thus ensures that the actual error is less than  $\delta_x$ .

Therefore, the required sample size increases as the square of the desired accuracy, which follows directly from the formula. As the squares of the numbers with increasing numbers themselves increase very rapidly, then increasing accuracy requirements can lead to immoderate increase of the sample

size. Therefore, it is important that the requirements to accuracy of sampling is always dictated by the objectives and content of the study. In this example, such goal was to justify the meaningful scientific hypothesis.

Median function computes the value of the sample coming into the middle of the ordered sample. If the sample has an even number of the elements, then the value of the function is equal to the average of the two values that are in the middle of the ordered sample.

The median is used instead of the arithmetic mean, when extreme variants of the ranked series (the smallest and the largest variants) compared with the rest are too big or too small [17].

The deviation of the mean square in probability theory and statistics is the most common measure of dispersion of values of a random variable with respect to its mathematical expectation. With limited sample arrays, the arithmetic mean of aggregate samples is used instead of the expectation value.

The standard deviation is measured in units of the random variable and is used in calculation of the standard error of the arithmetic mean, in the construction of confidence intervals, in statistical hypothesis testing, in the measurement of the linear relationship between random variables. It is defined as

**Table 2.** Factors analysis results

	$S_1, m^2$	$L, m$	$B, m$	$n$	$H, m$	$l, m$	$t, m$	$h, m$	$b, m$	$S_2, m^2$
$m^*$	250,64	15,25	12,11	1,73	2,90	6,19	383,26	660,00	7,02	927,91
$\Delta_x$	$\pm 13,52$	$\pm 0,77$	$\pm 0,63$	$\pm 0,13$	$\pm 0,03$	$\pm 0,34$	$\pm 13,16$	$\pm 99,09$	$\pm 1,19$	$\pm 91,28$
$Me$	247,50	14,67	11,95	2,00	2,90	6,00	380,00	500,00	5,20	800,00
$\sigma$	63,05	3,61	2,94	0,62	0,15	1,58	61,38	462,23	5,57	425,83
$\nu$	0,25%	0,24%	0,24%	0,36%	0,05%	0,25%	0,16%	0,70%	0,79%	0,46%
$Q_1$	191,25	12,76	9,92	1,00	2,80	5,00	350,00	350,00	3,25	650,00
$Q_3$	316,00	16,59	13,85	2,00	3,00	7,08	400,00	1000,00	7,60	1050,00

the square root of variance of the random variable.

Variation coefficient is the relative value that is used to characterize the fluctuations (variability) of the sign. It is the ratio of standard deviation to arithmetic mean and is expressed as in percentage.

The coefficient of variation is used when it is necessary to evaluate the variability of object attributes that are expressed in different units.

The variation is considered weak if  $v < 10\%$  if  $v$  varies from 11-25%, the average and significant when  $v > 25\%$ .

To calculate the quartiles one must divide variation series by into two equal parts, then find the median in each of them. For example, if a sample consists of 6 elements, then the initial point of a sample is the second element and the bottom quartile is the fifth element.

## CONCLUSIONS

1. The results of analysis are a set of body-planning and design parameters that significantly affect the technological solutions.
2. To further investigate the parameters are defined as the main factors.
3. Realized statistical processing of the results. Definitely, a line of research of technical parameters of the device bearing structures cottages.

## REFERENCES

1. **Boyko A, Dumenko K. 2011.** Research on reliability of subsystems of grain harvesting combine. TEKA: kom. Mot. Energ. Roln., OL PAN, vol. XIC, 5-11.
2. **Drosio A., Klimkiewicz M., Mruk R. 2011.** Energetic and Technological analysis of the process of oil pressing from winter rape. TEKA: kom. Mot. Energ. Roln., OL PAN, vol. XIC, 25-37.
3. **Getun V. 2010.** Architecture of buildings and constructions. Part 1. Principles of design. Kyiv, Kondor, 378 (in Ukraine).
4. **Gmurman V. 2003.** Probability theory and mathematical statistics. Moscow, Vysshaya shkola, 479 (in Russian).
5. **Hubka V. 1987.** Theory of Technical Systems. Moscow, Mir, 208 (in Russian).
6. **Lisician M., Pashkovskiy V., Petunina Z. 2006.** Architectural design of residential buildings. Moscow, Architektura, 488 (in Russian).
7. **Makarov N., Trofimec V. 2002.** Statistics in Excel. Moscow, Finance and Statistics, 368 (in Russian).
8. **Malkov I., Sirovoy G., Nepran I. 2013.** Stress- strain analysis of metal butt connection with composite propeller blade. TEKA: kom. Mot. Energ. Roln., OL PAN, vol. XIII (4), 143-148.
9. **Mihels V, Berkuta A, Goyko A., Bondar V., Vahovych I., Grycenko Y. 2010.** Economic-mathematical models and methods in construction. Kyiv, Milenium, 464 (in Russian).
10. **Nekipovenko V.I. 1977.** Structural Analysis of systems. Moscow, Sovetskoe radio, 214 (in Russian).
11. **Slobodyanyuk M., Tararychkin I., Nechaev G. 2013.** Structural analysis of an interregional transport network and assessment of capability for its multi-level optimization. TEKA: kom. Mot. Energ. Roln., OL PAN, vol. XIII (4), 250-257.
12. **Smith L. April 2009.** Tilt – Up Engineering. USA, Structure magazine, 12-15.
13. **State building codes of Ukraine B.1.1-7-2002.** Fire safety of construction. Kyiv, Derjbud Ukrayny, 42 (in Ukraine).
14. **State building codes of Ukraine B.2.2-15-2005.** Residential buildings. The main provisions. Kyiv, Derjbud Ukrayny, 36 (in Ukraine).
15. **Velikovskiy L., Ilyashev A., Maklakova T. 1983.** Architecture of civil and industrial buildings. Moscow, stroyizdat (in Russian).
16. **Ventsel E. 1998.** Probability theory. Moscow, Vysshaya shkola, 576 (in Russian).
17. **Voskoboynikov Y.E., Timoshenko E.I. 2006.** Mathematical Statistics (with examples in Excel). Novosibirsk, Novosibirsk State Architectural – Construction University (Sibstrin) second edition, 152 (in Russian).
18. **Zharikov E. 2013.** Analysis of the theoretical and applied aspects of modern it infrastructure. TEKA: kom. Mot. Energ. Roln., OL PAN, vol. XIII (4), 297-306.

## АНАЛИЗ ОБЪЕМНО-ПЛАНИРОВОЧНЫХ И КОНСТРУКТИВНЫХ РЕШЕНИЙ СОВРЕМЕННЫХ КОТТЕДЖЕЙ

**Аннотация.** В статье представлен анализ основных объемно-планировочных и конструктивных решений современных коттеджей, а также рассмотрены земельные участки, на которых построены или достраиваются эти коттеджи. Проведена статистическая обработка результатов. Определено направление исследования технических параметров устройства несущих конструкций коттеджей.

В результате выполненных объектов представителей 68-ми современных коттеджей и земельных участков под них в Киеве и Киевской области, и на основании полученных данных построены гистограммы

распределения параметров, наиболее существенно влияющих на выбор параметров технологического процесса возведения. По результатам анализа определены основные объемно-планировочные и конструктивные характеристики (геометрические, весовые, количественные) зданий.

Используя методы теории вероятностей и математической статистики выполнены анализ и оценка полученных данных.

Результаты анализа стали совокупность объемно-планировочных и конструктивных параметров, которые существенно влияют на технологические решения.

**Ключевые слова:** коттедж, параметры, технологические решения, механизация, статистика.

## Statistical Research of Retaining Walls Displacement on the Results of Geodetic Measurements by Analysis of Variance

*Roman Schultz<sup>1</sup>, Andriy Annenkou<sup>2</sup>, Andriy Khailak<sup>1</sup>, Valentyna Strilec<sup>1</sup>*

<sup>1</sup>Kyiv National University of Construction and Architecture  
Povitroflotskyi prosp., 31, Kyiv, Ukraine, 03680, e-mail: r-schultz@mail.ru

<sup>2</sup>Donbass National Academy of Construction and Architecture  
Derzhavin str., 2, Donetsk region, Makiyivka, Ukraine, 86123, e-mail: geodez@mail.ru

**Summary.** The analysis of geodetic measurements of retaining walls displacements in the residential quarter of the city of Kyiv is executed. For processing the observations, it was suggested to use a method of analysis of variance (ANOVA). The influence of changes displacement depending on the cycles of observations by one-factor analysis of variance is investigational. Method of one-factor ANOVA allowed also defining that for different retaining walls, a deformation process has a different dynamics. The relationship between cycles and retaining walls placement was determined using two-factor ANOVA. Method three-factor analysis of variance allowed additionally defining influence of location of deformation marks on the value of displacement. It was confirmed that the variance analysis method has great potential for the analysis of geodetic measurements, especially at the large volumes of observations.

**Key words:** ANOVA, displacement, dispersion relation, the level of significance, retaining wall, landslide, deformation prediction.

### INTRODUCTION

At observing the displacements always arises the problem of correct interpretation of measurement results. After many years, many mathematical models for approximation and prediction of engineering structures displacements were developed. However, for modern engineering buildings often impossible to find a single model that will fully describe the deformation process. Actual such problem is for observations on landslides, which have a difficult multisectional structure and hold out different retaining walls [7]. Observations of the retaining walls on the landslides are complex [1, 6]. The nature of displacements on landslide and retaining walls caused by many factors, which is confirmed in researches [1, 6]. In such circumstances, the construction of a predictive model is a very difficult task. Way out of this

situation is the use of statistical research methods such as regression analysis [2, 13]. In the geodetic practice have spread prediction models based on polynomial and exponential functions [10], Kalman filtering [5] and fuzzy systems modeling [3]. However, for landslide and retaining walls it is necessary at first determine the nature of the displacement distribution. Get single models predicting a deformation of retaining walls is impossible. In such case, it is necessary to divide the landslide or landslide structures on individual blocks within which to perform the construction of appropriate models of deformation [8]. This problem is quite complex. Even for landslide structures, which are structurally divided into separate blocks deformation process can have the same nature for several blocks or changed within one block. Application of multivariate analysis of variance methods gives the opportunity to

explore the distribution and nature of displacements and highlight landslide areas or landslide structures within which can be used a single model of deformations predicting.

### PURPOSE OF WORK

The task of work is research of one-factor and multivariable analysis of variance possibilities at determination of various factors influence on the nature and distributing of displacements during observations retaining walls on the example of the observations results of the retaining walls in the residential quarter of the city of Kyiv.

### DESCRIPTION THE OBJECT OF RESEARCH

Analysis of variance as a method of research data is known for a long time [4, 11]. In geodesy this method is used recently at research of GNSS measurements and solving navigation tasks [8, 12]. We will apply the

analysis of variance for research of nature and connection of retaining walls displacements that hold the landslide slope. A general view and placement of retaining walls are shown on a Fig. 1.

Landslide slope has a height of 30 meters and a width of 20 meters. Landslide is held by four retaining walls (PS-1, PS-2, PS-3, PS-4). The height of retaining walls is in the range of from 8 to 14 meters. Location plan of retaining walls is presented in figure 2.

All retaining walls have a pile foundation with piles at depth of 20 meters.

### RESULTS OF MEASUREMENTS

To measure the displacements a spatial geodetic network was built. The network consists of 5 points from which executed minimum twice coordinating deformation marks on retaining walls. According to the results of adjustment, the root mean square error along the coordinate axes were: for reference points  $m_x = 1,5$  mm,  $m_y = 3$  mm,



**Fig. 1.** A general view of retaining walls placement

$m_z = 4$  mm. The main requirement was to determine with the accuracy of 3 mm displacements in the direction of the  $X$  axis. For the rest coordinate axes the displacements are not critical and does not affect the stability of retaining walls. The measurements were performed weekly in the flow of six months. The total number of cycles is 27. Fig. 3 shows the measured displacement in the  $X$  axes direction for all marks on the four retaining walls in 27 cycles.

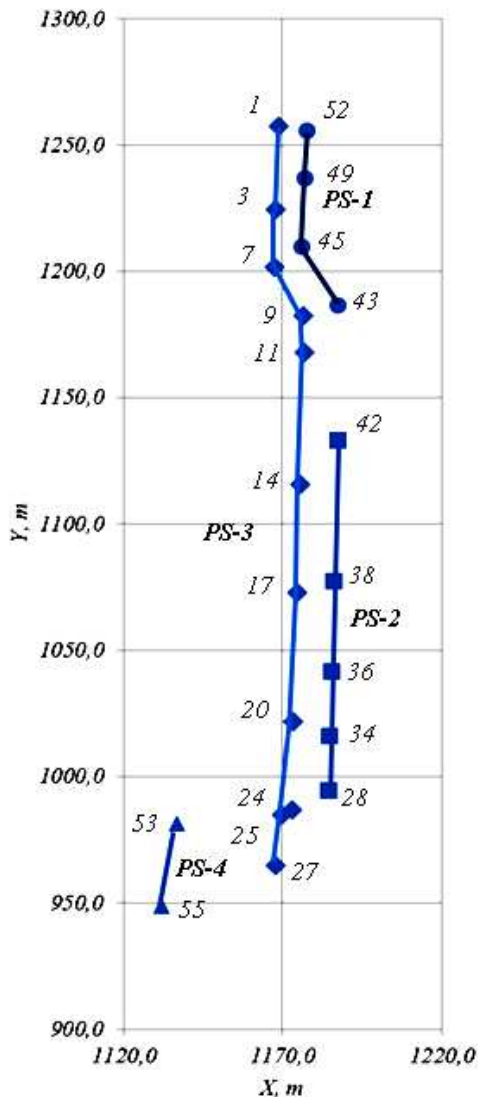


**Fig. 2.** Location plan of retaining walls and deformation marks numbers

In the direction of the coordinate axes  $Y$  and  $Z$  the maximum displacement were recorded at 10 mm. Such displacements are not critical and therefore we perform analysis of

displacements only along the  $X$  axis, which are shown in Fig. 3.

### STATISTICAL RESEARCH OF DISPLACEMENTS

The first necessary step of geodetic measurements analysis is to check the form of the distribution law. We used three nonparametric tests: Kolmogorov-Smirnov, Anderson-Darling,  $\chi^2$  [4]. The results of testing the hypothesis of normal distribution of the results of measurements are shown in Table 1.

**Table 1.** Testing the hypothesis of a normal distribution

Kolmogorov-Smirnov			
Sample Size	1188		
Statistic	0,0982		
$q$	0,05	0,02	0,01
Critical Value	0,039	0,044	0,047
Reject	<u>Yes</u>	<u>Yes</u>	<u>Yes</u>
Anderson-Darling			
Sample Size	1188		
Statistic	24,874		
$q$	0,05	0,02	0,01
Critical Value	2,502	3,289	3,907
Reject	<u>Yes</u>	<u>Yes</u>	<u>Yes</u>
$\chi^2$			
Deg. of freedom	10		
Statistic	186,670		
$q$	0,05	0,02	0,01
Critical Value	18,307	21,161	23,209
Reject	<u>Yes</u>	<u>Yes</u>	<u>Yes</u>

Hypothesis testing showed that the data did not submit the normal distribution law. This is not a hindrance to the analysis of variance, but confirms the necessity for statistical check. Deviation of the distribution law of the measured displacements from normal indicates the presence of systematic factors and confirms that all the measured displacement cannot be considered as a whole. The displacements for different retaining walls are different and need to analyze them separately. For clarity, we present

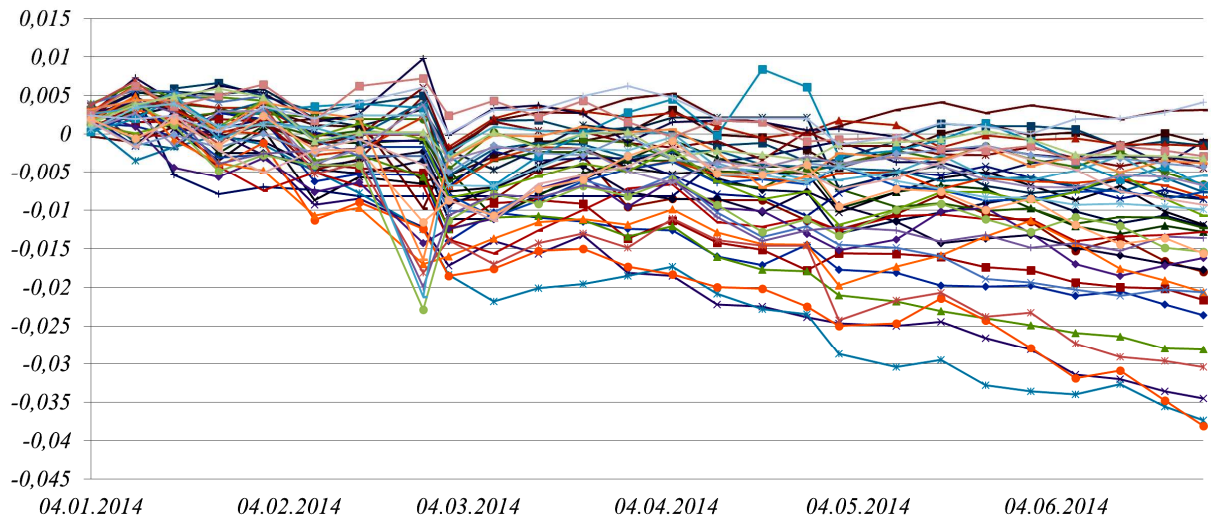


**Fig. 3.** The results of measurements along  $X$  axes for all retaining walls. Each chart is presented by the separate displacement of deformation mark

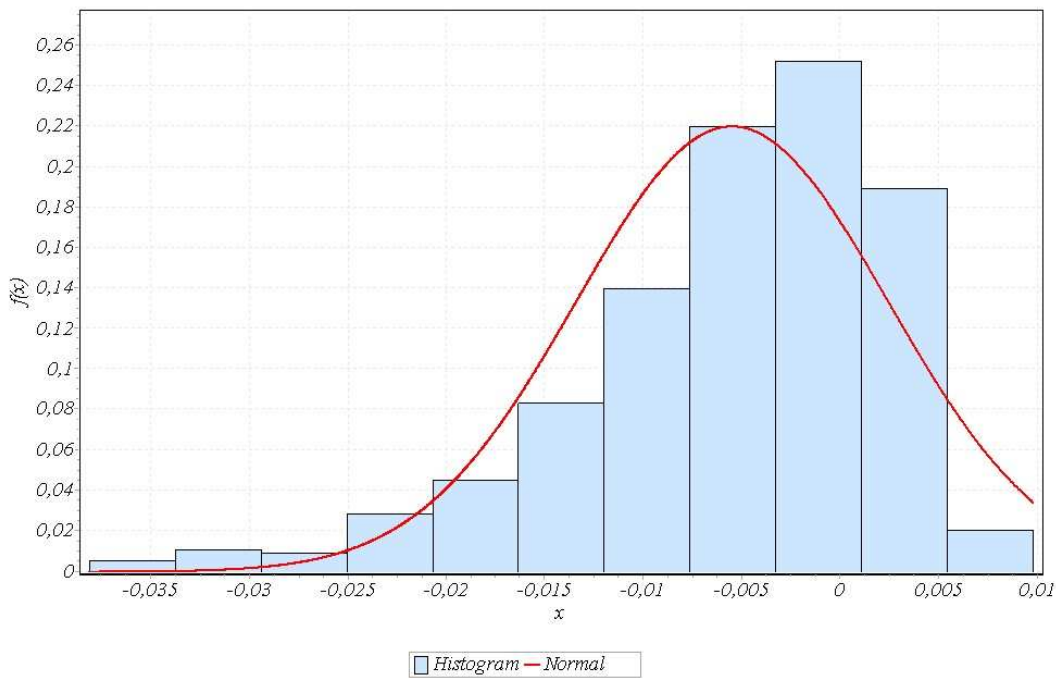


**Fig. 4.** Histogram and normal probably density function

the histogram and the probability density function of the statistical analysis results.

For establishment of factors, which influence on the nature of the displacement distribution perform analysis of variance of measurements results.

#### ONE-FACTOR ANOVA

Analyzing the charts in Fig. 3 it is difficult to establish whether the displacement marks

vary between cycles of measurements. To determine whether the actual deformation process occurs perform one-factor ANOVA.

The first stage of analysis of variance is to calculate basic statistical characteristics.

If there are  $k$  cycles of measurements of displacements  $x_i, i = 1, \dots, k$ . According to the results of measurements adjustment known that all measurements have the same variance and distribution centers are differ-

ent. In each cycle performed observing  $n$  deformation marks. In the  $i$ -th cycle, we have:

$$\Delta x_{i1}, \Delta x_{i2}, \dots, \Delta x_{in}.$$

Total number of observations:

$$N = \sum_{i=1}^k n_i. \quad (1)$$

If we assume that factor  $\alpha$  is the presence of displacements between the cycles, then in the absence of this displacement the most probable value of the measured value is the arithmetic mean of displacements:

**Table 2.** Statistical characteristics of displacement measurement

Cycle	Mean	RMS	95% interval for the mean		Max	Min
			Lower limit	Upper limit		
1	0,000	0,000	0,000	0,000	0,000	0,000
2	0,002	0,000	0,002	0,002	-0,000	0,004
3	0,003	0,000	0,002	0,004	-0,004	0,007
4	0,002	0,000	0,001	0,003	-0,005	0,006
5	0,000	0,000	-0,001	0,001	-0,008	0,007
6	0,001	0,000	-0,000	0,002	-0,008	0,006
7	-0,002	0,001	-0,004	-0,001	-0,011	0,004
8	-0,002	0,001	-0,003	-0,001	-0,010	0,006
9	-0,004	0,001	-0,007	-0,002	-0,023	0,010
10	-0,008	0,001	-0,009	-0,006	-0,018	0,002
11	-0,006	0,001	-0,008	-0,004	-0,022	0,004
12	-0,005	0,001	-0,007	-0,003	-0,020	0,004
13	-0,004	0,001	-0,006	-0,003	-0,020	0,005
14	-0,005	0,001	-0,007	-0,003	-0,018	0,006
15	-0,004	0,001	-0,006	-0,003	-0,018	0,005
16	-0,006	0,001	-0,008	-0,005	-0,022	0,002
17	-0,007	0,001	-0,009	-0,005	-0,023	0,008
18	-0,007	0,001	-0,010	-0,005	-0,024	0,006
19	-0,009	0,001	-0,012	-0,007	-0,029	0,002
20	-0,009	0,001	-0,011	-0,006	-0,030	0,003
21	-0,008	0,001	-0,011	-0,006	-0,030	0,004
22	-0,009	0,001	-0,011	-0,006	-0,033	0,003
23	-0,009	0,001	-0,012	-0,007	-0,034	0,004
24	-0,010	0,001	-0,013	-0,008	-0,034	0,003
25	-0,011	0,001	-0,014	-0,008	-0,033	0,002
26	-0,011	0,002	-0,014	-0,008	-0,036	0,003
27	-0,012	0,002	-0,015	-0,009	-0,038	0,004
Total	-0,005	0,000	-0,006	-0,005	-0,038	0,010

$$\text{mean}\Delta x = \frac{1}{N} \sum_{i=1}^k \sum_{j=1}^{n_i} \Delta x_{ij} . \quad (2)$$

If the values of displacements is significant, then the mean values:

$$\text{mean}\Delta x_i = \frac{1}{n_i} \sum_{j=1}^{n_i} \Delta x_{ij} , \quad (3)$$

differ considerably from the overall average (2).

For analysis, calculate deviation using expressions (2) – (3):

$$Q = \frac{1}{N} \sum_{i=1}^k \sum_{j=1}^{n_i} (\Delta x_{ij} - \text{mean}\Delta x)^2 , \quad (4)$$

$$Q_{\alpha} = \sum_{i=1}^k n_i (\text{mean}\Delta x_i - \text{mean}\Delta x)^2 , \quad (5)$$

$$Q_r = \sum_{i=1}^k \sum_{j=1}^{n_i} (\Delta x_{ij} - \text{mean}\Delta x_i)^2 . \quad (6)$$

Dispersions according to expressions (4-6) will be:

$$m^2 = \frac{Q}{N-1}, \quad m_{\alpha}^2 = \frac{Q_{\alpha}}{k-1}, \quad m_r^2 = \frac{Q_r}{N-k} . \quad (7)$$

The critical region is defined as the dispersion relations:

$$F \geq F_q, \text{ where: } F = \frac{m_{\alpha}^2}{m_r^2} . \quad (8)$$

A value  $F_q$  selected on the basis of the accepted significance level  $q$  and the number of degrees of freedom (DoF):  $k_{\alpha} = k - 1$ ,  $k_r = N - k$ .

Perform ANOVA in which we establish the dependence of the displacement from measurement cycle. The results are shown in Table 3.

By the criterion to confirm the hypothesis about the change displacements between cycles is the level of significance. At confidence probability 95% level of significance should not exceed 0,05. Thus, the fact of displacements between cycles can be regarded as established. Figure 5 shows a graph of the average displacement the whole complex of retaining walls.

To check the influence factor numbers retaining wall on the displacement values performed one-factor ANOVA. A hypothesis was tested that displacement of deformation mark depends on what retaining wall it is located.

The analysis found that the magnitude of the displacements depend on the retaining wall which is deformation mark is located on. The construction of deformation models process must be carry out for every retaining wall separately.

The results of analysis push on an idea about dependence of displacement size simultaneously on that in what cycle and what retaining wall, displacement was fixed on. For verification of such hypothesis the two-factor ANOVA was applied.

**Table 3.** One-factor ANOVA (Displacement - Cycle)

Feature	Sum of squares	DoF	The mean square	F	Significance level
Between groups	0,023	26	0,001	20,010	0,000
Within groups	0,050	1161	0,000		
Total	0,073	1187			

STATISTICAL RESEARCH OF RETAINING WALLS DISPLACEMENT ON THE RESULTS OF GEODETIC MEASUREMENTS BY ANALYSIS OF VARIANCE

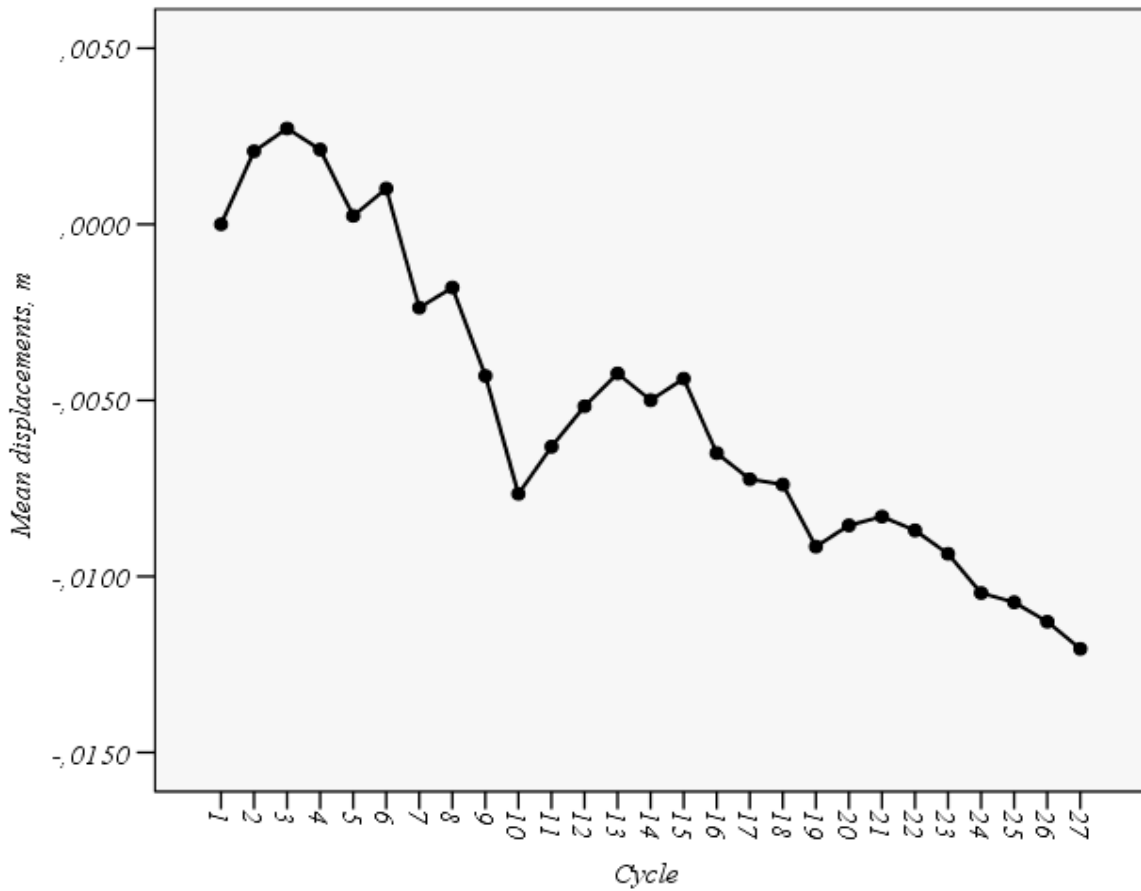


**Fig. 5.** Mean displacement on X axis

**Table 4.** Statistical characteristics of displacement for retaining walls

Wall	N	Mean	RMS	95% interval for the mean		Min	Max
				Lower limit	Upper limit		
1	594	-0,003	0,000	-0,004	-0,003	-0,018	0,010
2	270	-0,011	0,001	-0,012	-0,009	-0,038	0,006
3	216	-0,007	0,001	-0,008	-0,006	-0,030	0,008
4	108	-0,001	0,000	-0,002	-0,000	-0,007	0,007
Total	1188	-0,005	0,000	-0,006	-0,005	-0,038	0,010

**Table 5.** One-factor ANOVA (Displacement - Retaining wall)

Feature	Sum of squares	DoF	The mean square	F	Significance level
Between groups	0,013	3	0,004	86,672	0,000
Within groups	0,060	1184	0,000		
Total	0,073	1187			

## TWO-FACTOR ANOVA

Under the hypothesis of the presence of several influencing factors used multivariate analysis of variance. We investigate the influence of the factors  $\alpha$  (cycle observations) and  $\beta$  (number of retaining wall) on the measurement results. Measurement series can be represented as:

$$\begin{aligned}
 &\alpha_1\beta_1 \Delta x_{111}, \Delta x_{112}, \dots, \Delta x_{11k}, \dots, \Delta x_{11s_{11}} \\
 &\alpha_1\beta_2 \Delta x_{121}, \Delta x_{122}, \dots, \Delta x_{12k}, \dots, \Delta x_{12s_{12}} \\
 &\quad \dots \\
 &\alpha_1\beta_l \Delta x_{1l1}, \Delta x_{1l2}, \dots, \Delta x_{1lk}, \dots, \Delta x_{1ls_{1l}} \\
 &\alpha_2\beta_1 \Delta x_{211}, \Delta x_{212}, \dots, \Delta x_{21k}, \dots, \Delta x_{21s_{21}} \\
 &\alpha_2\beta_2 \Delta x_{221}, \Delta x_{222}, \dots, \Delta x_{22k}, \dots, \Delta x_{22s_{21}} \\
 &\quad \dots \\
 &\alpha_2\beta_l \Delta x_{2l1}, \Delta x_{2l2}, \dots, \Delta x_{2lk}, \dots, \Delta x_{2ls_{21}} \\
 &\quad \dots \\
 &\alpha_n\beta_1 \Delta x_{n11}, \Delta x_{n12}, \dots, \Delta x_{n1k}, \dots, \Delta x_{n1s_{n1}} \\
 &\alpha_n\beta_2 \Delta x_{n21}, \Delta x_{n22}, \dots, \Delta x_{n2k}, \dots, \Delta x_{n2s_{n2}} \\
 &\quad \dots \\
 &\alpha_n\beta_l \Delta x_{nl1}, \Delta x_{nl2}, \dots, \Delta x_{nlk}, \dots, \Delta x_{nls_{nl}}
 \end{aligned}$$

Total number of measurements will be:

$$N = \sum_{i=1}^n \sum_{j=1}^l s_{ij}. \quad (9)$$

Overall arithmetic mean would be:

$$\text{mean}\Delta x = \frac{1}{N} \sum_{i=1}^n \sum_{j=1}^l \sum_{k=1}^{s_{ij}} \Delta x_{ijk}. \quad (10)$$

Particular arithmetic means by the series of measurements calculating:

$$\text{mean}\Delta x_{ij} = \frac{1}{s_{ij}} \sum_{k=1}^{s_{ij}} \Delta x_{ijk}. \quad (11)$$

Determine the arithmetic mean on the factors for considering factor  $\alpha_i$  with (12):

$$\text{mean}\Delta x_{i0} = \frac{1}{N_{i0}} \sum_{j=1}^l s_{ij} \text{mean}\Delta x_{ij}, \quad (12)$$

where:

$$N_{i0} = \sum_{j=1}^l s_{ij}.$$

for factor  $\beta_j$ :

$$\text{mean}\Delta x_{0j} = \frac{1}{N_{0j}} \sum_{i=1}^n s_{ij} \text{mean}\Delta x_{ij}, \quad (13)$$

where:

$$N_{0j} = \sum_{i=1}^n s_{ij}.$$

To determine the general empirical dispersion found fluctuations:

$$\text{empirical}\delta_{ijk} = \Delta x_{ijk} - \text{mean}\Delta x. \quad (14)$$

General deviation using (14) is calculated:

$$Q = \sum_{i=1}^n \sum_{j=1}^l \sum_{k=1}^{s_{ij}} \text{empirical}\delta_{ijk}^2, \quad (15)$$

and proper dispersion:  $m^2 = \frac{Q}{N-1}$ .

Fluctuations of factors  $\alpha$  and  $\beta$  are calculated using formulas (10), (12), (13):

$$\left. \begin{aligned}
 \delta_{i0} &= \text{mean}\Delta x_{i0} - \text{mean}\Delta x, \\
 \delta_{0j} &= \text{mean}\Delta x_{0j} - \text{mean}\Delta x, \\
 \delta_{ij} &= \text{mean}\Delta x_{ij} - \text{mean}\Delta x, \\
 \text{empirical}\delta_{ij} &= \Delta x_{ij} - (\delta_{i0} - \delta_{0j})
 \end{aligned} \right\} \quad (16)$$

Deviation of factors calculated by the fluctuations (16):

$$\begin{aligned}
 Q_\alpha &= \sum_{i=1}^n N_{i0} \delta_{i0}^2, \quad Q_\beta = \sum_{j=1}^l N_{0j} \delta_{0j}^2, \\
 Q_{\alpha\beta} &= \sum_{i=1}^n \sum_{j=1}^l s_{ij} \text{empirical}\delta_{ij}^2.
 \end{aligned} \quad (17)$$

Dispersions of factors using deviation (17)  
 will be:

$$m_{\alpha}^2 = \frac{Q_{\alpha}}{n-1}, \quad m_{\beta}^2 = \frac{Q_{\beta}}{l-1}, \quad (18)$$

$$m_{\alpha\beta}^2 = \frac{Q_{\alpha\beta}}{(n-1)(l-1)}.$$

Next, calculate the residual fluctuations:

$$\delta_{ijk} = \Delta x_{ijk} - \text{mean} \Delta x_{ij}, \quad (19)$$

and deviation:

$$Q_r = \sum_{i=1}^n \sum_{j=1}^l \sum_{k=1}^{s_{ij}} \delta_{ijk}^2. \quad (20)$$

Suitable dispersion is:

$$m_r^2 = \frac{Q_r}{N - nl}. \quad (21)$$

Thus, we obtain the total contribution of each factor to the total variance:

$$Q = Q_{\alpha} + Q_{\beta} + Q_{\alpha\beta} + Q_r,$$

$$(N - 1)m^2 = (n - 1)m_{\alpha}^2 + (l - 1)m_{\beta}^2 +$$

$$+ (n - 1)(l - 1)m_{\alpha\beta}^2 + (N - nl)m_r^2.$$

Influence of factors  $\alpha$  and  $\beta$  is determined from the dispersion relations:

$$F_{\alpha} = \frac{m_{\alpha}^2}{m_r^2}, \quad F_{\beta} = \frac{m_{\beta}^2}{m_r^2}. \quad (22)$$

Critical areas are defined as before on the basis of accepted significance level  $q$  and the number of degrees of freedom:  $k_{\alpha} = n - 1$ ,  $k_{\beta} = l - 1$ ,  $k_r = N - nl$ .

Perform two-factor ANOVA to test the hypothesis according to the value of displacement at the same time from the cycle of observations and numbers of the retaining wall.

Two-factor analysis confirms a hypothesis about dependence of displacements size simultaneously on the cycle of observations and number of retaining wall. The value  $\eta^2$  in the table shows the percentage contribution of each factor in the total dispersion. The stake of joint influence of observations cycle and number of retaining wall is equal to 17%.

Such index indicates the presence of systematic factors, the nature of which must be found by further analysis of the results of measurements and observations of the slope, retaining walls and atmospheric parameters (air temperature, soil temperature and humidity, amount of precipitation).

Fig. 6 shows the values for each displacement on every retaining wall, and in Fig. 7 the average displacement values for retaining walls.

**Table 6.** Two-factor ANOVA (Displacement-Cycle-Number of retaining wall)

Feature	DoF	The mean square	F	Significance level	$\eta^2$
$\alpha$	26	0,001	22,494	0,000	0,351
$\beta$	3	0,004	152,875	0,000	0,298
$\alpha * \beta$	78	8,1E-5	2,823	0,000	0,169
Error	1080	2,9E-5			
Total	1188				

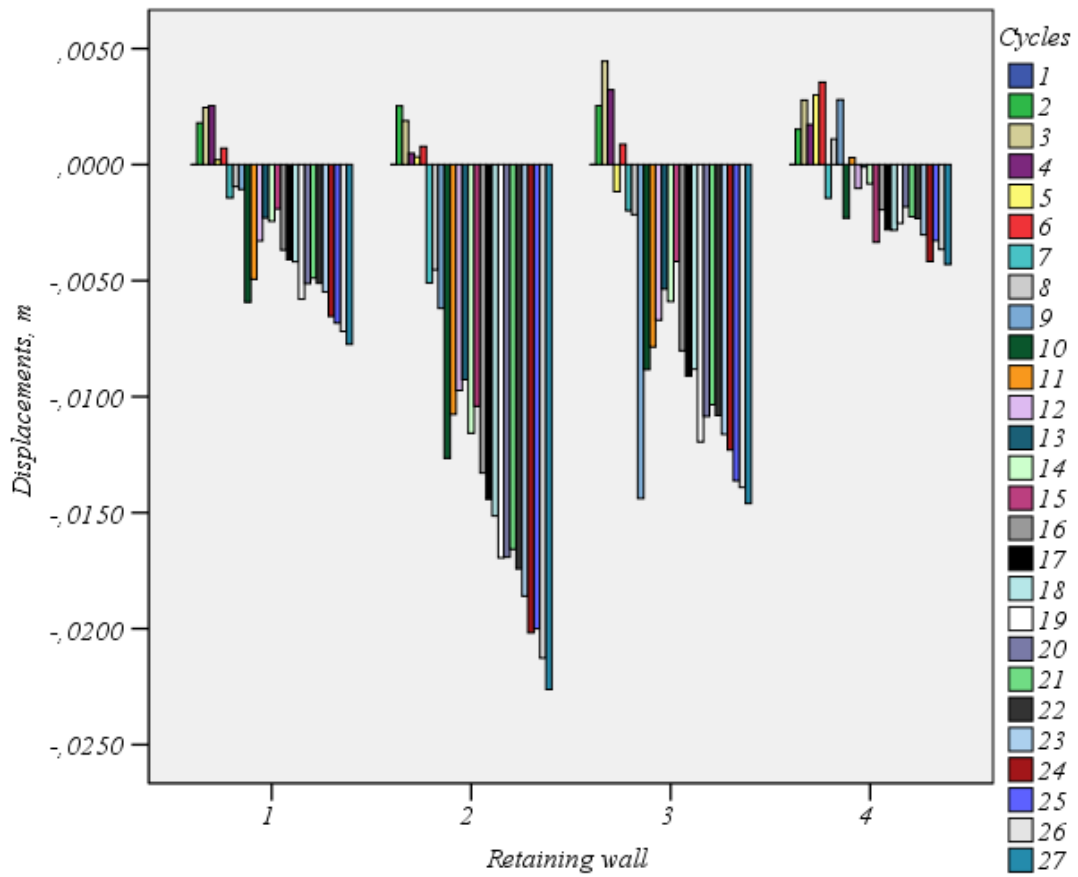


**Fig. 6.** Displacement on every retaining wall

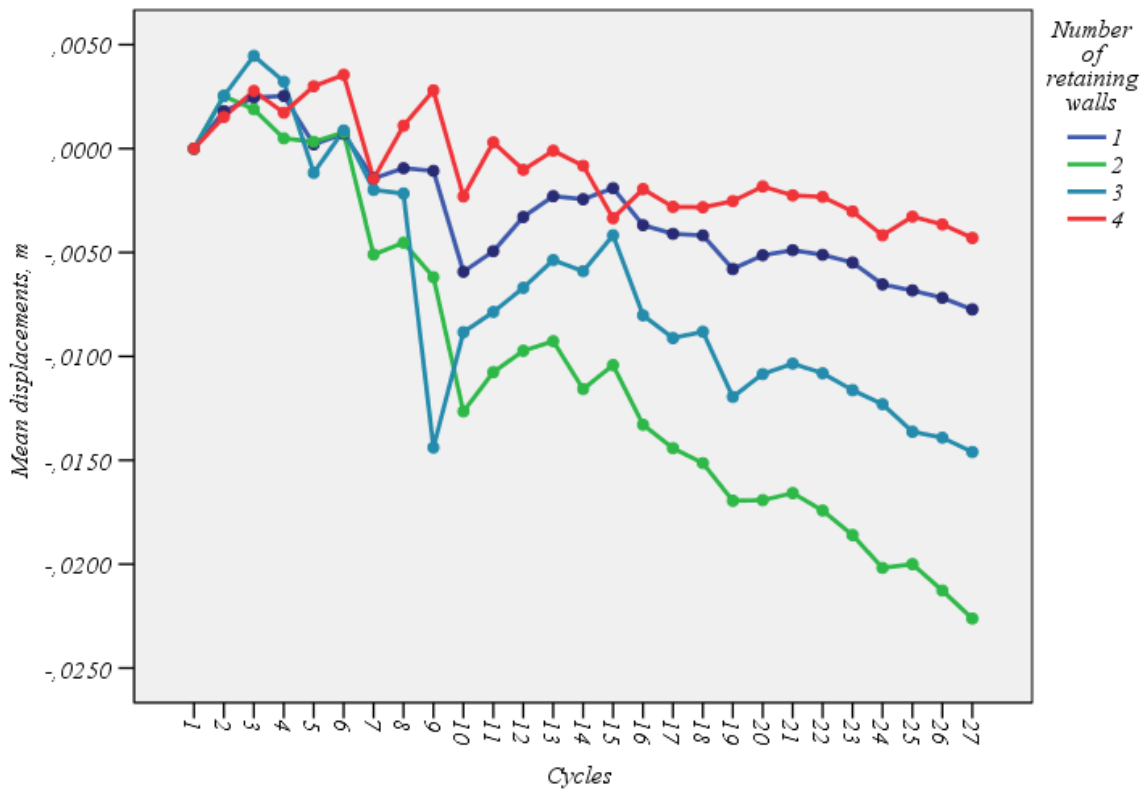


**Fig. 7.** Average displacement values for retaining walls in cycles

**Table 7.** Three-factor ANOVA (Displacement-Cycle-Number of retaining wall-Mark position)

Feature	DoF	The mean square	F	Significance level	$\eta^2$
$\alpha$	26	0,001	21,40	0,000	0,364
$\beta$	3	0,004	145,42	0,000	0,310
$\gamma$	1	0,000	10,339	0,001	0,011
$\alpha * \beta$	78	8E-5	2,686	0,000	0,177
$\alpha * \gamma$	26	7E-6	0,259	1,000	0,007
$\beta * \gamma$	3	0,000	6,740	0,000	0,020
$\alpha * \beta * \gamma$	78	5E-6	0,193	1,000	0,015
Error	972	3E-5			
Total	1188				

This result is very important, it confirms the complexity of the deformation process. From cycle to cycle different retaining walls change model of their displacement. Two-factor ANOVA (Displacement-Cycle-Number of retaining wall) shows the fundamental impossibility of the use of models deformation like a [3, 10], and speaks in favor of the use of models based on the theory of random functions.

At the analysis of the observations was paid a regard to circumstance that the displacement for marks, which is placed on the same vertical top and, bottom of each retaining wall differ. A hypothesis was pulled out that the displacement in the upper and lower parts of each retaining wall should be interpreted differently. According is pulled out hypothesis about necessity of verification a complex impact Displacement-Cycle-Number of retaining wall-Mark position. To test this hypothesis has been applied a three-factor ANOVA.

$$\left. \begin{aligned} F_{\alpha} &= \frac{m_{\alpha}^2}{m_r^2}, F_{\beta} = \frac{m_{\beta}^2}{m_r^2}, F_{\gamma} = \frac{m_{\gamma}^2}{m_r^2}, \\ F_{\alpha\beta} &= \frac{m_{\alpha\beta}^2}{m_r^2}, F_{\alpha\gamma} = \frac{m_{\alpha\gamma}^2}{m_r^2}, \\ F_{\beta\gamma} &= \frac{m_{\beta\gamma}^2}{m_r^2}, F_{\alpha\beta\gamma} = \frac{m_{\alpha\beta\gamma}^2}{m_r^2}. \end{aligned} \right\} (23)$$

In (23) factors are:  $\alpha$  (cycle observation),  $\beta$  (number of retaining wall),  $\gamma$  (mark position).

Three-factor analysis showed that significant is the contribution of the following groups of factors: Displacement-Cycle – 36%, Displacement-Number of retaining wall – 31%, Displacement-Mark position – 1%, Displacement-Cycle-Number of retaining wall – 18% Displacement-Number of retaining wall-Mark position – 2%.

Summarizing the results it is possible to pass to the conclusions about the executed research.

### THREE-FACTOR ANOVA

When the three-factor analysis of variance implementation checkup the following dispersion relation by analogy with (8) and (22):

### CONCLUSIONS

Analysis of variance was a powerful instrument to explore the displacements. Using analysis of variance revealed the following features of the measurements were made:

1. When unclear picture of nature of displacement found that displacements occurs between cycles of the whole landslide,

2. In different parts of the landslide retaining walls respond differently to each of them should be built its deformation model,

3. It is necessary to execute the detailed analysis of observations after every cycle because there is dependence between the cycles of observations and displacement of retaining walls, which indicate on the possible different terms of operation between cycles for every wall,

4. It is necessary separately consider displacement deformation marks at the top and bottom of each retaining wall.

The obtained results are more fully explained to the results of geodetic measurements and perform a correct construction of a predictive model of the deformation process. In future we plan to use the results and observations of atmospheric parameters (air temperature, soil temperature and humidity, amount of precipitation) to build a model of deformations by the regression analysis.

#### REFERENCES

1. **Brückl E., Brunner F.K., Lang E., Mertl S., Müller M., Stary U.** The Gradenbach Observatory—monitoring deep-seated gravitational slope deformation by geodetic, hydrological, and seismological methods. Technical Note Landslides. Published with open access at Springerlink.com.
2. **Draper N.R., Smith H. 1966.** Applied Regression Analysis John Wiley and Sons, Inc. New York, 394.
3. **Haberler-Weber M. 2005.** Analysis and interpretation of geodetic landslide monitoring data based on fuzzy systems. *Natural Hazards and Earth System Sciences*, 5, 755–760.
4. **Handbook** of Applicable Mathematics, Volume VI: Statistics, PART A, Chief Editor: Ledermann W., Edited by Lloyd E., John Wiley and Sons, Inc. New York, **1984**, 510, PART B, Chief Editor: Ledermann W., Edited by Lloyd E., John Wiley and Sons, Inc. New York, **1984**, 526.
5. **He X.F., Chen Y.Q., Zhou X.H. 2008.** Extraction of Deformation Signals of a Slope with Kalman Filtering Technique. 13th FIG Symposium on Deformation Measurement and Analysis, 4th IAG Symposium on Geodesy for Geotechnical and Structural Engineering Lisbon May 12-15.
6. **Mentes G. 2008.** Investigation of Different Possible Agencies Causing Landslides on the High Loess Bank of the River Danube at Dunaföldvár, Hungary. 13th FIG Symposium on Deformation Measurement and Analysis, 4th IAG Symposium on Geodesy for Geotechnical and Structural Engineering Lisbon May 12-15.
7. **Morozov V. 2012.** Work the front membrane of the membrane retaining wall at different angles of inclination. *Motrol: kom. Mot. Energ. Roln., OL PAN*, Vol. 14 (1), 42-46.
8. **Pavlovskaja O.G. 2012.** Analysis and Evaluation Geodetic Data Landslides Dynamics in the Blasting and Unloading Slopes 25.00.32 - "Geodesy" dissertation for the degree of candidate of technical sciences, Novosibirsk.
9. **Pirt A. 2012.** Evaluating The Repeatability Of RTK GPS Measurements Using Analysis Of Variance *Geodetski vestnik* 56/3, 427-442
10. **Pytharouli S.I., Kontogianni V.A., Nickitopoulou A., Psimoulis P.A., Stiros S.C. 2005.** Analysis of the Kinematics of a Deep-seated Landslide. From Pharaohs to Geoinformatics FIG Working Week 2005 and GSDI-8 Cairo, Egypt, April 16-21.
11. **Scheffe H. 1958.** The Analysis of Variance John Wiley and Sons, Inc. New York, 512.
12. **Schwieger V. 2006.** Sensitivity Analysis as a General Tool for Model Optimization - Examples for Trajectory Estimation. 3rd IAG 12th FIG Symposium, Baden, May 22-24, 12.
13. **Seber G.A.F. 1977.** Linear Regression Analysis John Wiley and Sons, Inc. New York, 460.

#### СТАТИСТИЧЕСКОЕ ИССЛЕДОВАНИЕ ПЕРЕМЕЩЕНИЙ ПОДПОРНЫХ СТЕНОК ПО РЕЗУЛЬТАТАМ ГЕОДЕЗИЧЕСКИХ ИЗМЕРЕНИЙ МЕТОДОМ ДИСПЕРСИОННОГО АНАЛИЗА

**Аннотация.** Выполнен анализ геодезических измерений за перемещениями подпорных стенок в жилом квартале города Киева. Для обработки наблюдений было предложено использовать метод дисперсионного анализа. Исследовано влияние изменения перемещений в зависимости от циклов наблюдений методом однофакторного дис-

персионного анализа. Метод однофакторного дисперсионного анализа позволил также определить, что для различных подпорных стенок деформационный процесс имеет различную динамику. Зависимость между циклами наблюдений и размещением подпорных стенок было определено с помощью двухфакторного дисперсионного анализа.

Метод трехфакторного дисперсионного анализа позволил дополнительно определить влияние расположения деформационных марок на величину перемещений. Подтверждено, что метод дисперсионного анализа имеет большие перспективы при анализе геодезических измерений, особенно при больших объемах наблюдений.

**Ключевые слова:** дисперсионный анализ, перемещения, дисперсионное отношение, уровень значимости, подпорная стенка, оползень, прогнозирование деформаций.



## Spiral Method of Concretion Mining from the Bottom Waters

*Mykhailo Sukach*

Kyiv National University of Construction and Architecture  
Povitroflotsky prosp., 31, Kyiv, Ukraine, 03680, e-mail: msukach@ua.fm

**Summary.** These features occurrence and distribution of deep-sea nodules. A development of the bottom of fossil spiral manner. Scheme is shown floating and complex trajectory carriage bottom of the unit. The basic technological calculation unit that moves around the base module and given recommendations on its use.

**Key words:** floating complex, iron-manganese minerals, spiral method of extraction, trajectory of motion, hose-cable.

### INTRODUCTION

The researchers conducted by oceanologists and marine geologists in the past decade have revealed patterns of occurrence of nodules based on landforms, direction of flow, sediment character, hydro chemical conditions and other factors [15, 17]. Usually deposits are elongated shape with compact placement areas where the concentration of nodules in 2...3 times the average [7, 10, 11]. Nodule deposits are characterized in terms of patchy structure with discrete zones of high placement concentrations [2, 3]. The above makes it necessary to justify the methods of ocean exploration, technology testing, research and industrial mining exploitation [9, 16].

### PURPOSE OF WORK

In order to save of resources need to set up a floating complex in such a way that the original data obtained in the pilot mining exploration mining complex would be representative for complex industrial exploitation.

### ANALYSIS METHODS OF EXTRACTION

The main element of the exploration mining complex for concretion mining, given the significant depth of development (4...6 km), is a system of concretions raising [1, 4]. Based on the results of tests in natural conditions, conducted by leading foreign companies, to be implemented in the first phase accepted as the most simple pipeline system recovery or airlift pump type [5]. Known technical solution patented by "Lockheed" (USA), which includes craft; descent gear unit pipeline; bottom platform located on its lower end; hose-cable flexible communication and data collection unit [6].

In such a system is extremely difficult to manage the orderly systematic treatment of a loose plot, given the significant difference in the length of the pipeline (6 km) and the width of the working body of the unit fee (a few meters), the masses craft (several hundred thousand tons) and aggregate collection (several tens of tons), the power of influence of natural factors (wind, flow rates of up to 2 m/s) on the pipeline during its movement by floating means (the pressure is several dozens, hundreds of tons) and the aggregate fee

(perturbation effects turbid bottom flows on submarine slopes inhibitory effect of flexible communications and ground soil) [8, 13, 14].

Deprived of such deficiencies on short-term fixation of the lower end of the pipe when lowering the bottom of the bottom platform – bottom base module interacting with flexible communication with the bottom end of the pipeline and shvydkoruhomoyu carriage carrying the tool "carrier" absorption (analog – cleaner containing unit and dust extraction head, interconnected corrugated hose).

SPIRAL WAY NATURE

The proposed technical solution is shown in a design setup is shown in Fig. 1. Bottom

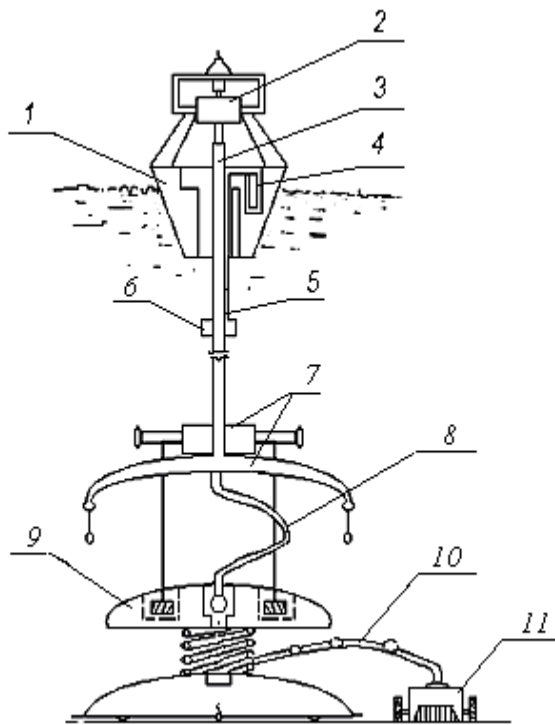


**Fig. 1.** Scheme complex floating:  
 1 – craft, 2 – descent gear unit, 3 – pipeline transport artery, 4 – compressor Station (airlift system recovery (ESR) or diesel generator – with pumping system recovery (PSR)), 5 – piping for compressed air at ESR or cable at PSR, 6 – mixer (ESR), submersible pumps (PSR), 7 – bottom base module; 8 – flexible pipe, 9 – donna coil, 10 – hose-cable, 11 – drive carriage

base module, which fixes the lower end of the pipeline to the processing area deposits (unit) includes a guided coil connected through hose cable Actuated of carriage, the latter performs a circular motion around the spiral path by bottom base module (Fig. 2).

Efficiency of up moving in spiral trajectories with respect to the bottom of the coil is determined as follows (Fig. 3). Carriage with free automatic hose-cable rewriter hose cableya coil describes involute circle, defined by equations in polar coordinates in the parametric form:

$$\rho = R_0 \left[ 1 + (\varphi + l_0/R_0)^2 \right]^{1/2},$$

$$\alpha = \varphi - \text{arctg}(\varphi + l_0/R_0),$$

where:  $\rho$  – polar radius of the point of attachment to the carriage hose-cable;  $\alpha$  – polar angle (phase) point of attachment;  $R_0$  – radius of the coil;  $l_0$  – length of the initial segment hose-cable, pulled coil;  $\varphi$  – phase separation of the coil hose cable.

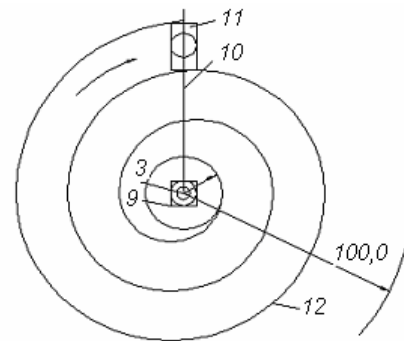


**Fig. 2.** Trajectory of motion of carriage: denotation 1 – 11 as on Fig. 1, 12 – carriage way

It is assumed that the value  $l_0$  depends on the size of the foundations of the bottom coil, which prevents the carriage freely maneuver close to the coil; apparently,  $l_0 \geq R_0$ . It is also assumed that the width of the carriage is connected with coil radius ratio  $b = 2\pi R_0$  to ensure complete overlap of the treated area between the two coils.

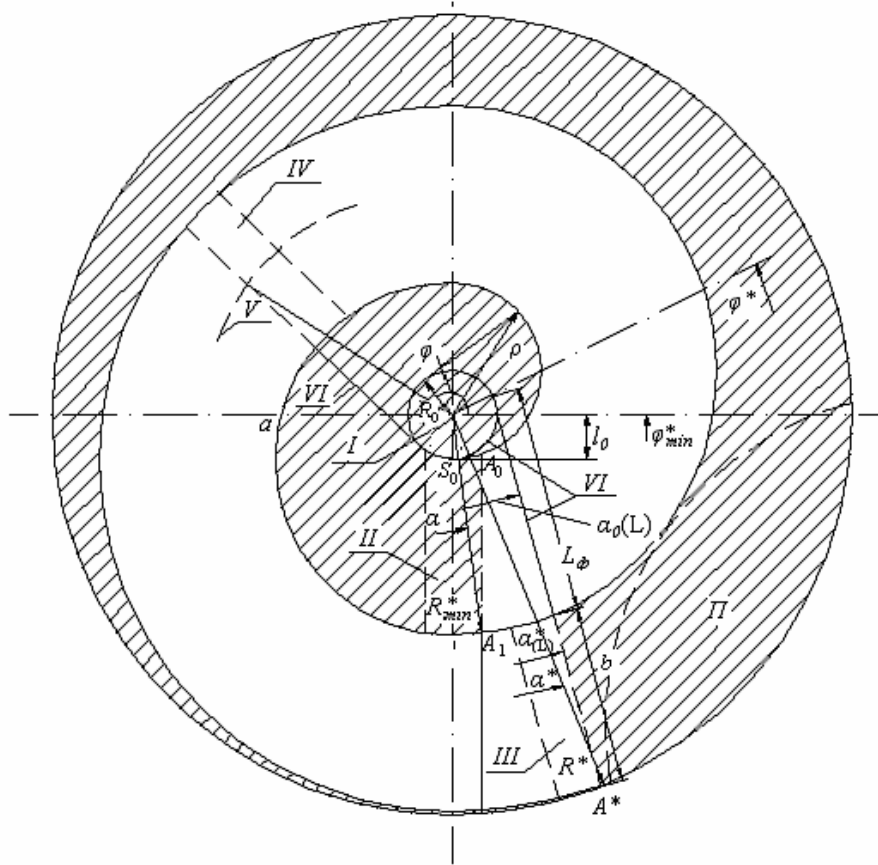


**Fig. 3.** Diagram spiral trajectory of up bound hose cable coil:  
 I – coil, II ... IV – caret position (II – original, III – end, IV – intermediate), V – trajectory of the carriage, VI – hose-cable, II – overlay zone adjacent blocks

Square shape  $A_0aA_1$  (uncultivated space inside the helix)  $S_0$  consists of the area covered by the polar radius  $\rho$  from the point  $A_0$  to point  $A_1$  when deploying hose-cable ( $S_0A_0aA_1$ ), and the area of a triangle ( $S_0A_0A_1$ ):

$$S_0 = S_0A_0aA_1 + S_0A_0A_1,$$

where:

$$\begin{aligned} S_0A_0aA_1 &= \frac{1}{2} \int_{\alpha_0}^{\alpha_1} \rho^2 \alpha \, d\alpha = \frac{1}{2} \int_0^{2\pi} \rho^2 \alpha^1 a \, d\alpha = \\ &= \frac{1}{2} R_0^2 \int_0^{2\pi} \left( \tau + \frac{l_0}{R_0} \right)^2 \alpha \, d\alpha = \frac{1}{6} \left( \tau + \frac{l_0}{R_0} \right)^3 \Big|_0 \end{aligned}$$

Denoting:

$$S(\varphi) = \frac{1}{6} R_0^2 \left( \varphi + l_0/R_0 \right)^3,$$

we obtain:

$$S_0A_0aA_1 = SR_0^2 = S(\Delta),$$

$$S_0A_0aA_1 = S(2\pi - S_0),$$

$$S_0 = S[2\pi - S_0 + S(\Delta)].$$

Let processed space is limited circle of radius  $R^*$ , associated with the maximum length hose-cable  $L_\phi$ , by ratio:

$$R^* = R_0 \left[ (L_\phi/R_0 + 2\pi)^2 + 1 \right]^{1/2}.$$

Limit setting  $R^*$  will be determined from the expression:

$$\varphi^* = (L_\phi - l_0)/R_0 + 2\pi.$$

Note:  $\varphi^*_{\min} = 2\pi$ , corresponding  $R^*_{\min}$ .  
Therefore, the number of complete rotations  
a carriage:

$$K^* = \lfloor \varphi^*/2\pi - 1 \rfloor.$$

The area that is maintained carriage, in  
which case:

$$S = \frac{1}{2} \int_{\tau^*-2\pi}^{\tau} \rho^2 \alpha^1 a \tau + S_{\Delta} - S_0 =$$

$$= S(\tau^*) - S(\tau^* - 2\pi) - S(2\pi) + S(0).$$

The area of a circle of radius  $R^*$ :

$$S^* = \pi R^{*2}.$$

Percentage of area processed,

$$E = (S/S^*) \cdot 100\%.$$

Trajectory, which makes the center of the  
carriage (see Fig. 2), is described by the equ-  
ations:

$$\rho = R_0 \left[ 1 + \left( \varphi + (l_0/R_0) + \pi^2 \right) \right]^{1/2},$$

$$\alpha = \varphi - \arctg(\varphi + (l_0/R_0) + \pi).$$

The path of movement of the carriage:

$$L = \frac{1}{2} \int_{\alpha_0(L)}^{\alpha_L^*} \rho^2 a_X = \int_0^{\varphi^*-2\pi} \rho \alpha^1 a \varphi =$$

$$\int_0^{\tau^*-2\pi} \frac{\left( \varphi + \frac{l_0}{R_0} + \pi \right)^2}{\sqrt{1 + \left( \varphi + \frac{l_0}{R_0} + \pi^2 \right)}} \alpha \varphi.$$

Denoting:

$$z = \varphi + (l_0/R_0) + \pi,$$

we obtain:

$P$ , mill.ton/year

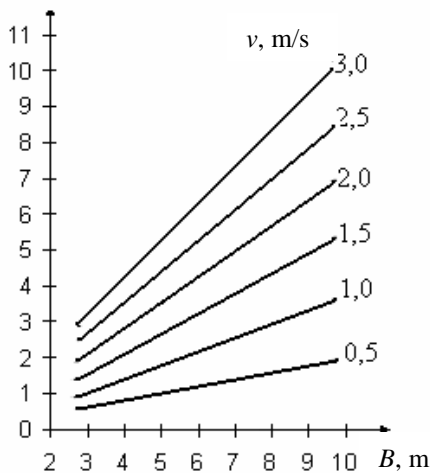


**Fig. 4.** Graph of the performance of the enterprise  $P$  from the width  $B$  and speed  $v$  of pickup

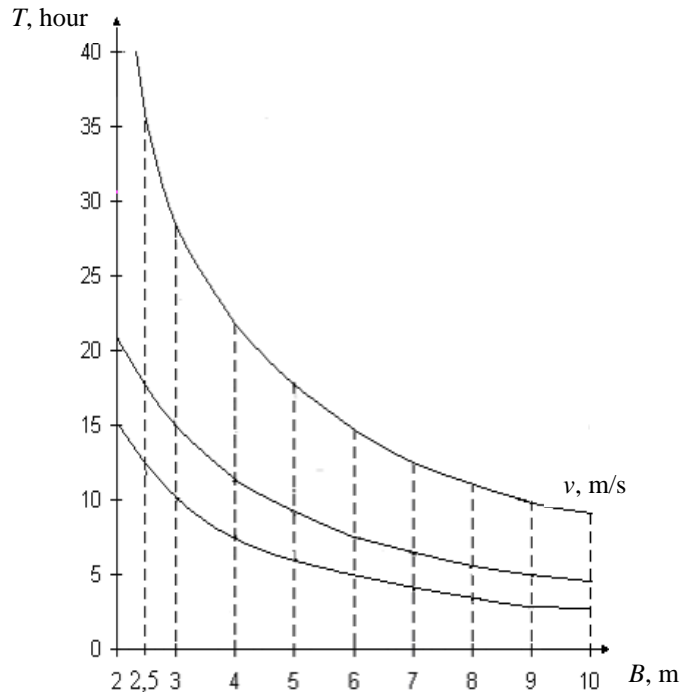


**Fig. 5.** Dependence term treatment areas  $T$  from the width  $B$  and speed  $v$  of pickup

$$L = R_0 \int_{\frac{l_0}{R_0} + \pi}^{\tau^* + \frac{l_0}{R_0} - \pi} \frac{Z^2}{\sqrt{1 + Z^2}} aZ =$$

$$= \frac{1}{2} R_0 \left[ Z\sqrt{Z^2 + 1} - \lg \left( Z + \sqrt{Z^2 - 1} \right) \right].$$

Then:

$$L = L(\varphi^* + (l_0/R_0) - \pi) - L(l_0/R_0) + \pi.$$

Specific treatment area, id the area that is treated as a unit path traversed by carriage:

$$D = S/L.$$

Using the computer program calculated the values  $R^*$ ,  $\varphi^*$ ,  $K^*$ ,  $S$ ,  $S^*$ ,  $E$ ,  $L$ ,  $D$  for different lengths of hose-cable ( $L_\Phi = 100 \dots 200$  м) and radiuses of the coil ( $R_0 = 0,2 \dots 1$  м) for a given width of the working body ( $B = 2,0 \dots 10$  м) and the length of the initial segment of hose-cable, pulled by coil ( $l_0 = 1 \dots 5$  м). According to our calculations, built feasibility dependency mining company (Fig. 4 and 5).

#### GUIDELINES FOR POOL DEVELOPMENT

Move the bottom platform – bottom base module in the next section area (block) is at a distance equal to twice the length hose cable. Thus, the deposits are processed by successive overlap of circular blocks in circuits where excavation is performed spiral (Fig. 6). The variant of the carriage passes through it forward and in reverse on the inside back-spiral.

To improve the efficiency of nodules slot scheme can be used with the trajectory of the carriage for reciprocal trajectories with a fixed rotation angle ( 210, 240, 270 ° etc. ) by operation of reversing switches or program laid down in the onboard memory computer bottom base module. Thus skate

chassis up (caret) must be reversed at a small angle ( $\sim 7^\circ$ ) at the outer side of the coil to create a constant tension in hose-cable that has neutral or slightly positive buoyancy.

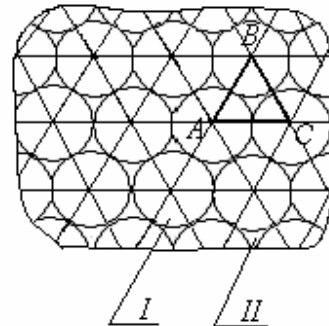


**Fig. 6.** Scheme working in field plots spiral circular trajectory carriage:

*I* – processed, *II* – uncultivated land

Moving the complex area of the new unit should be carried out by the pendulum movement of the lower end of the pipe at elevated above the bottom of the base module at a time when the craft is in the distance between the centers of adjacent range blocks (when included with the drivers, taxiing). More economic office hours – at moving of floating means taking into account influence of superficial flows and wind without including of main propulsion engines.

Lowering the bottom of the module should be performed at the time of stay of the craft center of a new unit (including the effects Angle undercurrents in trubop-rovid). Control mode switching engines, taxiing, carried out by the display location of the bottom base module based on signals received from the bottom sonar beacons.

As can be seen from the graph in Fig. 4 and productivity of industrial enterprises 1...3 million tons of nodules per year can be achieved with acceptable parameters of the speed range up to  $v = 1 \dots 2$  m/s and the width of the working body  $B = 2,5 \dots 3$  м. And working land area  $0,2 \text{ км}^2$  depending on these parameters extended from a few hours to 1,5 days (see Fig. 5). Losses in between a block areas can be substantially reduced by overlapping the blocks in slot pitch contours, for example in the area of “*II*” (see Fig. 3).

CONCLUSIONS

1. A block diagram of practicing deep deposits of ferromanganese nodules sedentary set of fixed at the bottom of the base module and quickly by a movable collector. The latter has a coordinating communication via hose cable with a drive carriage and performs a circular motion around the base module on a spiral trajectory.

2. Productive area of minerals in circular overlapping blocks, where excavation occurs spiral steps. Moving to the next set of traffic control unit and a collector carried by the installed program automatically includes data from sonar beacons.

REFERENCES

1. **Bakurov G. 1988.** Ships for deep-water mountain geological researches. Moscow, Shipbuilding, Nr 3, 12-16.
2. **Ferromanganese** concretions of the central part of the Pacific ocean, **1986.** Under editing I.O. Murdmaa, N.C. Skorniakova. Moscow, Nauka, 344.
3. **Fouco I. 1982.** Modern state of technique of booty of deep-water ferromanganese concretions. ВЦП, № E-41418, Moscow, 28.12.83, ist. Fusen, Vol.29, 99-167.
4. **Paschkin V., Iakovlev P., Cokolov V. 1999.** Dredging, refuliring- and gidromechanized works: train aid. Odesa, Astroprint, 432.
5. **Nurok G.A. 1985.** Processes and technology of hydromechanization of open mountain works. Moskov, Nedra, 471.
6. **Patent of the USA Nr 4232903, 1980.**
7. **Schniukov E., Ziborov A. 2004.** Mineral riches of the Black sea. Kyiv, NANU, 279.
8. **Sukach M. 2004.** Workflows of deep machines. Kyiv, Naukova dumka, 364.
9. **Sukach M. 2012.** Deep-water technique and technology for development of minerals of the World ocean. Labours VI ISTK "Energiya-2012", Simferopol-Alupka, 9.
10. **Sukach M. 2012.** Problems of booty of hard minerals from the bottom of the World ocean. Motrol: kom. Mot. Energ. Roln., OL PAN, Vol.14. Nr 1, 116-122.
11. **Sukach M., 2013.** Prospects of development of marine deposits of mineral raw material. Innovations in science are innovations in education: collection of labours. JuRGPU (NPI), Novocherkassk, 285-291.
12. **Sukach M. 2013.** Ukraine's prospects in development of marine mineral deposits. Econtechmod, OL PAN, Vol.2, Nr 2, 47-50.
13. **Sukach M., Lysak S., Sosnowski S. 2010.** Kinematic analysis of the working process of trencher. TEKA: kom. Mot. Energ. Roln., OL PAN, Vol.10, 425-431.
14. **Sukach M., Lytvynenko I., Bondar D. 2009.** System of the automated management and measuring of parameters of technological processes. Motrol: kom. Mot. Energ. Roln., OL PAN, Vol.11B, 186-189.
15. **Terms of education and conformity to law of placing of ferrimanganese concretions of the World ocean, 1987.** Edited O.D. Korsakov. Moskov, Nedra, 259.
16. **Ziborov A. 2006.** To obtain or not obtain the black Sea sapropels in Ukraine. Geology and minerals of the World ocean, Vol.1, 92-99.
17. **Ziborov A. 2008.** Prospects and tasks of mastering of marine deposits of mineral raw material. Geology and minerals of the World ocean, Vol.3, 5-18.

СПИРАЛЬНЫЙ СПОСОБ ДОБЫЧИ КОНКРЕЦИЙ СО ДНА АКВАТОРИЙ

**Аннотация.** Отмечены особенности залегания и распространения глубоководных конкреций. Предложена разработка донных ископаемых спиральным способом. Показана схема плавучего комплекса и траектория движения каретки донного агрегата. Приведены основные технологические расчеты агрегата, движущегося вокруг базового модуля, а также даны рекомендации относительно его применения.

**Ключевые слова:** плавучий комплекс, железомарганцевые конкреции, спиральный способ добычи, траектория движения, шлангокабель.

## Analysis of Modified Bitumen Difference Polymers

*Arthur Onischenko, Mykolay Kuzminets, Sergiy Aksenov*

National Transport University, str. Suvorova 1, Kyiv, Ukraine, 01001  
e-mail: Artur\_onish@bigmir.net, Vectra16i@i.ua, Kabysik@bigmir.net

**Summary.** An important step in the preparation of modified bitumen is selection of the composition and verification of various polymers' effectiveness. Therefore, paddle mixers are widespread in both industrial and laboratory conditions for efficient mixing of bitumen with polymers. The developed method allows to determine the completion time of modification process at various process parameters (temperature, mixing speed and content of the modifier) to complete stabilization of the properties and the homogenization of bitumen. The results of studies showed that optimal time for bitumen modification at which take place both stabilization of the properties and homogenization, ie astringent take the necessary level of uniformity with latex Butonal NS198, is about 3 hours.

**Key words:** cracking resistance, rutting resistance, shear resistance, water resistance, polymer-modified bitumen, laboratory blade mixer, homogenization.

### INTRODUCTION

Roads of Ukraine are characterized by high traffic volumes and intensity, and significant dynamic load on pavement of bridges and airfields require increased requirements to asphalt concrete, and, correspondingly, to bitumen. The most common and effective way to increase quality of asphalt is use of bitumens modified with polymers which significantly improve the properties of asphalt, namely cracking resistance, rutting resistance, shear resistance and water resistance, etc. [1-3, 7-14].

An important step in the preparation of modified bitumen is selection of the composition and verification of various polymers' effectiveness. These issues require availability of appropriate laboratory mixers for making polymer-modified bitumens. Modern practice of laboratory tests of modified bitumen shows lack of standardized procedures in the laboratory mixing and related laboratory equipment, which does not allow to get polymer-modified

bitumens in compliance with sole preparation technology, whereby it is possible to get no reliable laboratory test results [2-4].

The most simple and quite effective technical means of mixing low-viscosity liquids and liquids with solids that are in a state of near suspension are blade mixers. Therefore, blade mixers are widely used, in both industrial and laboratory conditions for efficient polymer bitumen modification.

### ANALYSIS OF RECENT RESEARCH

Objective to develop methodology for preparation of polymer modified bitumen with use of laboratory blade mixer with the purpose of selection of its composition and establishment of requirements to the process of mixing.

The authors developed method of preparation of modified bitumen using laboratory blade mixer Fig. 1. [1]). Method to determine the time of completion of modification process at different process parameters (tempera-

ture, mixing speed and amount of modifier) to complete homogenization and stabilization properties of bitumen.

The technique is to set a time during modified bituminous binder, wherein the stabilization properties will, and homogenization, i.e. binder acquires desired level of uniformity. At the beginning of bitumen modification process polymer is fed and time of modification completion is set. Estimation of bitumen stabilizing properties and homogenization when feeding polymer is carried out by the following criteria:

- rate of penetration change (with additional 1 hour of bitumen modification)  $\leq 2 \times 0,1$  mm / hour (modified bitumen acquired penetration stabilization),

- rate of elasticity change (with additional 1 hour of bitumen modification)  $\leq 2\%$  / h (modified bitumen acquired elasticity stabilization),

- variation coefficient in terms of penetration and elasticity (with additional 1 hour of bitumen modification)  $\leq 2\%$  (modified bitumen acquired penetration and elasticity uniformity).

Sampling schedule of modifying bitumen polymer is set taking into account stabilization properties of the binder and its homogenization. If the nature of such rates is not known for certain polymer-modified bitumen, it is recommended to carry out a trial modification, to establish nature and pace of modifications to select the appropriate sampling schedule.

Modification completion time is assumed to be the time at which all the processes of bitumen stabilization and homogenization have taken place. In order to define this time laboratory tests for definition of penetration and elasticity, their coefficients of variation at different sampling times are held. Based on the results changes of these indicators in each period between the time the mixing of sampling are assessed. Completion of the modification time is defined on the basis of the achievement of stability and uniformity properties of polymer-modified bitumen, in accordance with the scheme shown in (Fig. 2 – 5).

**Table 1.** Technical peculiarities of laboratory blade mixer

Peculiarities (conditions)	Technical data
Metal zinc container, dm3 (DSTU 3277)	7
Number of agitator blades	4
Angle of the blades, degrees	90
Helix angle of the blades, degrees.	22
Dimensions of blades, mm	L = 100, H = 20
The minimum distance between blades, at least, mm- Between the wall - Between the tank bottom	15 50
Frequency of rotation of blade shaft, rot / min.	10...30
Electric motor with speed control, power, kW	2
Oil electric tensor with electric temperature range, ° C (GOST 13268)	from 0 to 250
Thermocouples GOST R 8.585 with temperature range, ° C	from 0 to 300
Heating of the oil thermostat to a temperature T, ° C	220
Heat-resistant oil (GOST 18852) permissible temperature	250

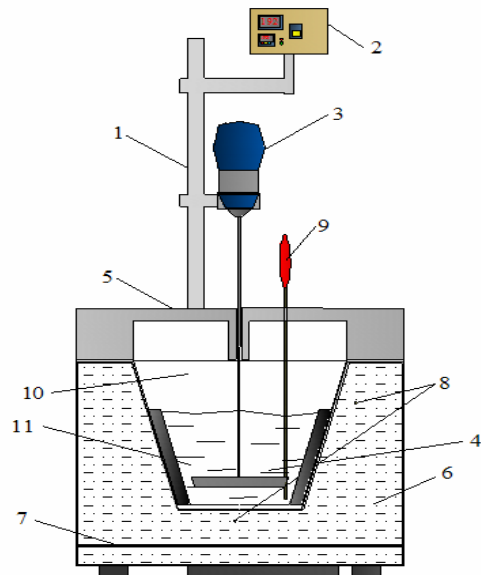


**Fig. 1.** Laboratory blade mixer (side-view)  
 1 - tripod, 2 - control unit, 3 - electric motor, 4 - blade agitator, 5 - oil thermostat 6 - oil tank 7 - electric tensor, 8 - thermocouple in the oil thermostat, 9 - thermocouple for modified bitumen, 10 - Metal container according to DSTU 3277, 11 - bitumen binder

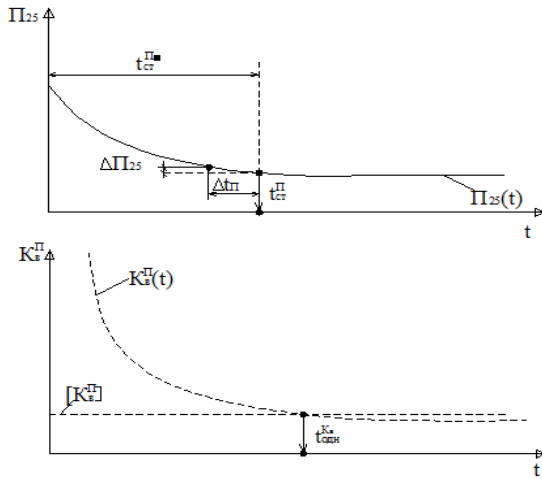
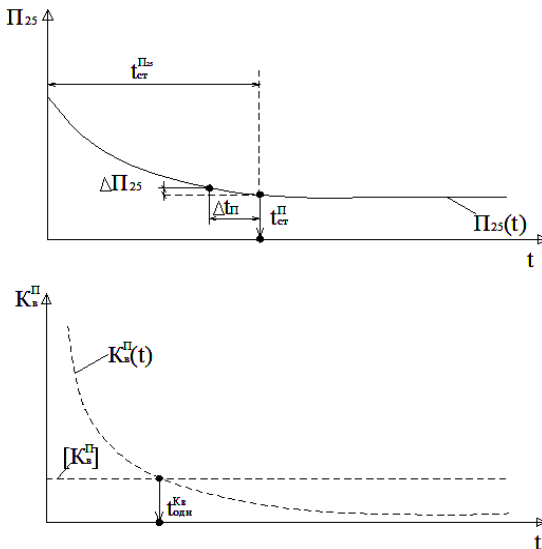


**Fig. 2.** Defining  $t_{3M}$  – time for mixing bitumen with polymer, using laboratory blade mixer on the basis of changes in penetration  $\Pi_{25}(t)$  and coefficient of penetration variation  $K_B^{\Pi}(t)$  depending on mixing time  $t_{3M}$  when  $t_{0DH}^{K_B} \geq t_{cr}^{\Pi_{25}}$

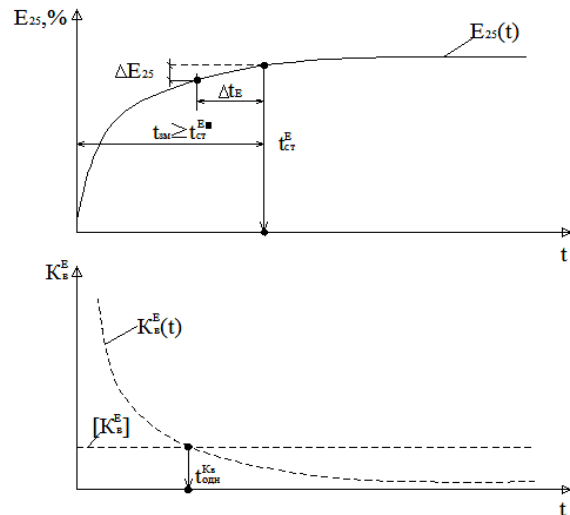
mers will be when the stabilization time for penetration  $t_{cr}^{\Pi_{25}}$  will be equal to or exceed mixing time  $t_{0DH}^{K_B}$ .

Fig. 3. presents a case where homogeneity of asphalt binder is reached faster than stabilizing of penetration properties. In this case, the time to achieve maximum coefficient of variation for penetration  $K_B^{\Pi}(t)$  corresponds to time  $t_{0DH}^{K_B}$ . It is smaller than the time which corresponds to the completion of penetration stabilization. Therefore, the process of completing of bitumen modification with polymers will be when mixing time is equal to or greater than penetration stabilization time  $t_{cr}^{\Pi_{25}}$ .

A similar scheme is used to determine process of completing of bitumen modification with polymers according to elasticity (Fig. 4 – 5).



**Fig. 3.** time for mixing bitumen with polymer, using laboratory blade mixer on the basis of changes in penetration  $\Pi_{25}(t)$  and coefficient of penetration variation  $K_B^{\Pi}(t)$  depending on mixing time  $t_{3M}$  when  $t_{0DH}^{K_B} \leq t_{cr}^{\Pi_{25}}$



**Fig. 4.** Defining time for mixing bitumen with polymer, using laboratory blade mixer on the basis of changes in elasticity  $E_{25}(t)$  and coefficient of elasticity variation  $K_B^E(t)$  depending on mixing time  $t_{3M}$  when  $t_{0DH}^{K_B} \leq t_{cr}^{E_{25}}$

Fig. 2. presents a case where penetration stabilization properties of bitumen are achieved faster than uniformity. In this case, the time to achieve maximum coefficient of variation for penetration  $K_B^{\Pi}(t)$  corresponds to time  $t_{0DH}^{K_B}$ . It is larger than the time which corresponds to the completion of penetration stabilization. Therefore, the process of completing of bitumen modification with poly-

The developed method of modified bitumen preparation using laboratory blade mixer allows to determine accurately time and accurate information concerning completion of stabilization properties and homogenization of the modified asphalt binder. After each sampling test results are input into record book and test results are processed [1-6].

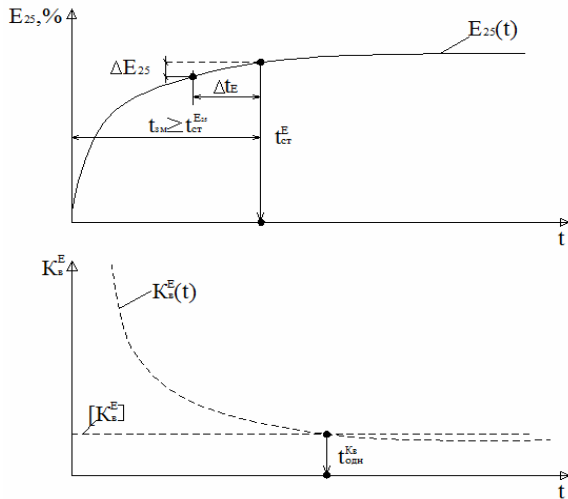


**Fig. 5.** Defining time for mixing bitumen with polymer, using laboratory blade mixer on the basis of changes in elasticity  $E_{25}(t)$  and coefficient of elasticity variation  $K_B^{E_{25}}(t)$  depending on mixing time  $t_{3M}$  when  $t_{ODH} \geq t_{CT}$

The authors conducted tests on Mozyrskogo bitumen BND 90/130, using different amounts of cationic polymer latex Butonal NS198. The test results are shown in Table 2.

**Table 2.** Physico-mechanical properties of bituminous binder according to amount of polymer and modification time

Initial bitumen type, type and amount of polymer, %	Mixing time, T, hour	Penetration $\Pi_{25}$ , mm <sup>-1</sup>	R&B $T_p$ , °C	Elasticity $E_{25}$ , %	Ductility $D_{25}$ , cm	Variation coefficient $K_B^{\Pi}$ , %	Variation coefficient $K_B^E$ , %
BND 90/130	-	97,0	47,0	-	>85	-	-
BND 90/130+ 2% Butonal NS198	1	80,0	52,0	62,0	>80	5,73	3,34
	2	73,0	53,0	67,0	77	3,34	3,09
	3	73,0	54,0	69,0	75	2,74	2,22
	4	72,0	55,0	69,0	72	1,39	1,45
	5	71,0	55,0	69,0	71	1,41	0,84
	6	70,0	55,0	69,0	71	0,82	0,72
BND 90/130+ 4% Butonal NS198	1	77,0	56,0	66,0	74	6,29	3,79
	2	67,0	57,0	70,6	61	4,45	3,56
	3	64,0	57,0	71,0	59	3,13	2,82
	4	62,0	60,0	71,7	59	2,48	2,13
	5	60,0	61,0	72,0	56	1,67	1,39
	6	59,0	61,0	72,3	56	1,30	0,80
BND 90/130+ 6% Butonal NS198	1	75,0	63,0	67,0	60	6,67	4,48
	2	69,0	65,0	71,0	47	2,51	4,23
	3	61,0	67,0	72,3	44	4,10	3,48
	4	57,0	67,5	72,6	43	3,51	2,86
	5	54,0	68,0	72,4	43	2,34	1,67
	6	53,0	68,0	72,5	43	1,89	1,38

PROCESSING OF TEST RESULTS IS CARRIED OUT ACCORDING TO FOLLOWING RULES

Average value and elasticity measurement of penetration for a given stage of the modification of the formula:

$$\bar{\Pi}_{25} = \frac{\sum_{i=1}^n \Pi_{25i}}{n}$$

and

$$\bar{E}_{25} = \frac{\sum_{i=1}^n E_{25i}}{n}, \tag{1}$$

where:  $\bar{\Pi}_{25}$ ,  $\bar{E}_{25}$  – mean value and flexibility for penetration measurements,

$\Pi_{25i}$ ,  $E_{25i}$  – the value of penetration and resilience of each measurement,

$n$  – number of measurements.

Standard deviation values measured from the mean value determined by the formula:

$$\Pi_{25} = \sqrt{\frac{\sum_{i=1}^n (\Pi_{25i} - \bar{\Pi}_{25})^2}{n-1}}$$

and

$$E_{25} = \sqrt{\frac{\sum_{i=1}^n (E_{25i} - \bar{E}_{25})^2}{n-1}}. \tag{2}$$

The coefficient of variation for penetration and elasticity is determined by the formula:

$$K_B^{\Pi_{25}} = \frac{\Pi_{25}}{\bar{\Pi}_{25}} \cdot 100\%$$

and  $K_B^{E_{25}} = \frac{E_{25}}{\bar{E}_{25}} \cdot 100\% . \tag{3}$

## CONCLUSIONS

1. Relative deviation of penetration bitumen at modification time (1-6 hr.) with feeding 2% Butonal NS198 varies from 1 to 6%, with 4% Butonal NS198 varies from 2 to 12% and with 6% Butonal NS198 from 1 to 13%, respectively.
2. Similarly determined relative deviation of bitumen elasticity at modification time (1-6 hr.) with feeding 2% Butonal NS198 varies from 0.5 to 8.0%, with 4% Butonal NS198 from 0.5 to 7, 0%, and with 6% Butonal NS198 varies between 0.5 and 6.0% respectively.
3. Test results are shown in Table 1 indicate that the obtained bituminous binders from initial material using series of different amounts of latex Butonal NS198 have different penetration parameters, but very similar parameters of softening temperature and elasticity. Significant difference of penetration, primarily associated with the rapid process of oxidation and aging of raw materials, as well as modification time and the amount of polymer.
4. The results showed that the optimal bitumen modification at which stabilization of properties and homogenization will be take place, i.e. binder acquires required level of uniformity with latex Butonal NS198, is about 3 hours. For other polymer modification time is set for the above described procedure.

- the properties of modified bitumen used in road construction. Bulletin of Prydniprovsk State Academy of Construction and Architecture. Dnepropetrovsk, PSABA, Nr 6-7, 14-17.
6. **Onishchenko A.M. 2008.** Improving durability of asphalt layers by the use of polymer latexes. Theses Candidate of sciences 05.22.11. Kyiv, 229.
  7. **DSTU B V.2.7-135:2007. 2007.** "Bitumen modified with polymers. Specifications" Zolotarev V.A., Mozgovoy V.V., Zhdanyuk V.K., and other.
  8. **Kulalaeva N., Mikhailyuk V., Petrov I. 2012.** Research of application of nanotechnology to clean oily water. MOTROL, Vol. 14, Nr 3, 74-84.
  9. **Gorbenko E., Streltsov V., Gorbenko N. 2013.** Innovative technology of production of vegetable oil. MOTROL, 125-131.
  10. **Polishchuk V., Lanovoi A. 2012.** Practical methods for evaluating the performance and the need for development of the road network. MOTROL, 69-78.
  11. **Chausov N., Wildemann V., Pilipenko A. 2012.** Modelling the behavior of plastic materials under complex loads. MOTROL, 191-200.
  12. **Anna Maria Klepacka, Jarosław Osiak, Małgorzata Powalka, Jacek Skudlarski. 2013.** Krajowe wykorzystanie surowców rolnych do produkcji biopaliw transportowych. MOTROL, 63-67.
  13. **Voitov V., Kravtsov, A., Sysenko I. 2013.** Prospects for the use of vegetable oils for the manufacture of lubricants and fluids. MOTROL, 54-61.
  14. **Sukach M., Filonov. Y. 2012.** Stand for research slit digging podgeosinteticheskim pressure. MOTROL, Vol. 14, Nr 3, 120-126.

## REFERENCES

1. **SOU 42.1- 37641918 - 100:2013. 2003.** " Bitumen, modified using laboratory blade mixer. Methods for process control modifications"
2. **Zolotarev V.A. 2009.** Polymer modified bitumen and asphalt polymer cements. Dorozhnaia tehnika. 88-95.
3. **King G.N., Radovskii B.S. 2004.** Properties of polymer bitumen binders in the U.S. and methods of testing. Scientific and Technical Information Kit. Novosti v dorozhnom dele - Issue 6. Moscow. 1-28
4. **Hochman L. M. 2004.** Complex organic binders based on block copolymers SBS type. Moscow, "Ekoinform" JSC, 510.
5. **Kirichek Y.A., Dem'yanenko V.V., Suhorebryy O.A. 2008.** Experimental study of

МЕТОДИКА МОДИФИКАЦИИ  
БИТУМА РАЗНЫМИ ПОЛИМЕРАМИ

**Аннотация.** Важным этапом процесса приготовления модифицированных битумов является подбор их состава и проверка эффективности действия разных полимеров. Поэтому, лопастные смесители нашли широкое применение, как в промышленных, так и в лабораторных условиях для эффективной модификации битума полимерами. Разработанная методика приготовления позволяет точно определить время завершения процесса модификации в различных технологических параметрах (температуры, скорости перемешивания и содержания модификатора) и достоверную информацию относительно завершения стабилизации свойств и гомогенизации

модифицированного битумного вяжущего. Результаты исследований показали, что оптимальное время модификации битумного вяжущего, при котором состоятся как стабилизация свойств так и гомогенизации, то есть вяжущее приобретет необходимый уровень

однородности латексом Butonal NS198 составляет около 3 часов.

**Ключевые слова:** трещиностойчивость, колеустойчивость, сдвигоустойчивость, водостойкость, битум модифицированный полимером, лабораторный лопастной смеситель, гомогенизация.

## Optimization of Motion Regimes for Machines and Mechanisms With a Mechatronics' Control

*Vjacheslav Lovejkin, Yuriy Chounyuk, Yuriy Romasevich*

National University of Life and Environmental Sciences of Ukraine  
Heroyv Oborony, 12, Kyiv, Ukraine, 03041, e-mail: d.um@mail.ru

**Summary.** Motion control of machines and mechanisms with a mechatronics control is now recognized as a key technology in mechatronics. The robustness of such motion control will be represented as a function of stiffness and a basic for practical realization, for example, in the precise agriculture. Target of such motion is parameterized by control stiffness which could be variable according to the task reference. However the system robustness of motion always requires very high stiffness in the controller. The paper shows that control of acceleration realizes specified motion simultaneously with keeping the robustness very high. The acceleration is a bridge to connect such robustness and variable stiffness. For practical applications, a technique to estimate disturbance is introduced to make motion controller to be an acceleration controller of machine/mechanism. Optimization of motion control of flexible structure and identification of mechanical parameters are also described.

**Key words:** optimization, motion, machines, mechatronics, control.

### INTRODUCTION

One of the most important elements in mechatronic technology is undoubtedly motion control (of machine/mechanism). However, the word „mechatronics”, registered as a trademark by Yaskawa Electric Co., in 1971 did not always include a concept of motion control [1].

In the 1970's, industries began to replace mechanical elements with electronic ones to achieve higher reliability and less maintenance. Also the mechatronic devices were designed to occupy smaller space in the final products. Totally junction of reliability, availability, and serviceability has been very much improved in relatively more compact products (and, for example, in the agricultural machines and mechanisms).

In the 1980's, a remarkable progress in mini- and micro- computers and power electronics technology made it possible to im-

prove the performance of motion regimes. For example, vector controlled induction motor has higher cut-off frequency almost up to three times in the speed control loop compared to the same-sized dc motor. Following these results, the novel theories of control were tested in such mechatronic systems. In the later 1980's and the early 1990's, mechatronic seemed slow case of various applications of control theories and of optimization theories of control as well.

The phenomena observed in the early 1990's [2] also came from the so-called „software-servo technology”. Generally major of software applied to motion control carries out the indispensable routines for diagnostics and sequential procedures. Only small area is assigned for programming control algorithms. The area was hardly sufficient for conventional PID controller. Recently the fast processor has gradually enabled more complicated algorithms within a shorter sampling time. Since the software-

servo technology has generated more room for control algorithms, higher performance and flexibility have been realized without additional investment. Than the novel algorithms have gained high evaluation from the practical viewpoint because the quality of motion was improved (in precise agricultural technologies as well). The motion control is now recognized as an important area in mechatronics [3]–[6].

This paper intends to show recent advances in motion regimes of machines/mechanisms control covering control and energy conversion [7] for a tutorial purpose. The physical meaning is emphasized rather than mathematical exactness. As is well known, control and estimation are twin aspect of system design. The fact holds in motion control of machines and mechanisms. The robust control and the estimation of parameters have the same basic. The several example shown later seen different approaches; however, the single interpretation is possible from the physical viewpoint.

The paper, at first, defines the stiffness in relation to various motion control. This concept leads to both the meaning of robustness and the general structure of motion control of machines and mechanisms. Then the paper points out the necessity of modification against flexible structure. Several examples will assure the concluded remarks at the end of the paper.

## MATERIALS AND METHODS

A mechanical system governed by the Lagrange equation is represented both geometrically and dynamically. The kinematics is represented as a set of algebraic equations which gives constrains of motion. The dynamics is a set of differential equations based on dynamic equilibrium of force. A motion controller generates a set of inputs to the actuators according to motion reference. A motions reference is synthesized in the reference generator. The sensor signal, the database and the commands from other motion systems and/or human operators are input signals for the reference generator. There will

be some intelligent process with composite structure in the reference generator. The general motion control totally consists of the motion controller and the reference generator. However, the paper lays stress on the motion controller.

From the control point of view, the output of the motions will be position and/or force. A simple case is continuous path tracking however, the need for force control is increasing because the industrial demand to the dexterous motion is growing up. A simplified index which covers various motion is preferable, though, there are various candidates of motion representation. One of such indices is stiffness.

Suppose that  $x$  is a position of motion of a controlled object (machine/mechanism) and  $f$  is a totally imposed force on that. From the kinematic and the dynamic equation, the following holds:

$$f = g(\ddot{x}, \dot{x}, x) \quad (1)$$

The stiffness  $k$  is defined in the partial differentiation:

$$k = \frac{\partial f}{\partial x} \quad (2)$$

The ideal position control inhibits any deviation of position against any deviation of force. That means  $k$  will be infinite in such a case. Naturally an integrator in the forward loop compensates the steady error and  $\delta x$  will be zero at infinite time. However, such function does not reflect in (2). On the other hand, the ideal force control inhibits any force deviation against any position deviation. Therefore,  $k$  is zero in the ideal force control. In the compliance control, there must be a relation between position and force. For instance, a virtual compliance control will have mechanical impedance computed in the controller according to the specified dynamics. Table 1 shows that  $k$  is a good parameter as an index which represents a target of motion.

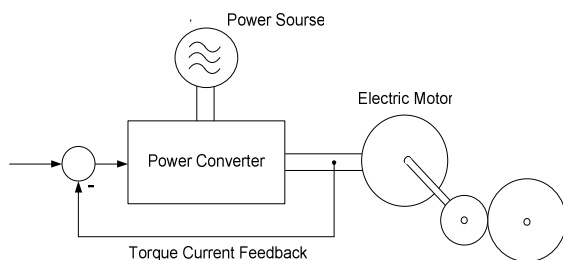
**Table 1.** Stiffness as a motion index

target of motion	stiffness $k$
position	$\infty$
compliant	finite
force	0

## RESULTS AND DISCUSSION

Various specifications for motion in industry require versatile ability in the controller. An efficient way to overcome this problem is to divide the function of motion control into two parts. Control flexibility is suitably realized in the motion reference generator since a kind of intelligence is indispensable in this part. It is necessary to track the motion reference accurately in the motion control part. The more intelligent a motion reference generator becomes, the more robust a motion controller should be. This is a kind of master-slave structure. There is an interpretation on robustness of motion controller, which makes the conception visible in mind. Suppose the moving body whose position is controlled along the predetermined path. Such a rigid body should knock down or break any obstacles on path and go forward to the end of part, if a motion controller is ideally robust. So called obstacle avoidance issue is solved in the motion reference generator by synthesizing an appropriate reference of trajectory. The robustness of the motion controller assures for the utmost the "high-fidelity" to the input reference.

The dynamical equation is excited by input force. Most of mechatronic systems adopt electrical actuator for the purpose. Fig. 1 shows a typical electric drive system.

**Fig. 1.** A typical electric drive system

Most of power converters use switching device for power control. The regulation of torque highly depends on the switching frequency. Since the recent power converter uses IGBT's, FET's, and so on, for fast switching, the current feedback includes high gain inside the feedback loop and the torque current follows the current reference with delay of less than from 50  $\mu$ s to 1 ms. The torque itself is produced by electronic interference of current and magnetic flux.

There are three types of the interference as shown in Table 2. The stepping motor, which is not in Table 2, is widely used for simple positioning. It has similar characteristics of synchronous motor, however, it generates high torque ripple and is not appropriate for fine and smooth motion. Each motor in Table 2 generates torque be the product of torque current by field. The field and the torque current is controlled to be orthogonal to each other [8]. Then by integrating all the torque par small piece of surface of rotor, the total generated torque  $T_m$  is given simply as:

$$T_m = K_t \cdot I_a, \quad (3)$$

where:  $K_t$  is a function of flux position and expanded in Fourier series and is called a torque coefficient.  $I_a$  is torque current. Fast switching devices make the power converter with feedback of torque current as a virtual current converter. In most cases, it is possible to regard  $I_a$  as  $I_a^{ref}$  (torque current reference). As a result, this chapter concludes that the actuation part is schematically represented in Fig. 2.

**Table 2.** Typical Electric Actuators

	dc motor	induction motor	synchronous motor
field	permanent magnet	field current by vector control	rotating permanent magnet with field orientation
torque	dc current	torque current by vector control	ac current with orientation

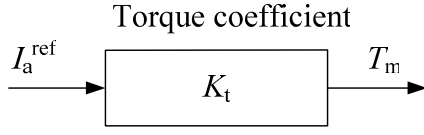


**Fig. 2.** Block diagram of actuator

It is necessary to define the equivalent disturbance in order to consider the robust control of motion actuated by electric motor. The explanation and the interpretation of robustness and stiffness in motion control lead to definition of disturbance. The general definition for single-input and single-output (SISO) linear system is discussed. Such system has the following transfer function between input  $U(s)$  and output  $Y(s)$ :

$$\frac{Y(s)}{U(s)} = K \cdot \frac{c_m \cdot s^m + c_{m-1} \cdot s^{m-1} + \dots + c_2 s + c_1}{s_n + a_n \cdot s^{n-1} + a_{n-1} \cdot s^{n-2} + \dots + a_2 s + a_1}. \quad (4)$$

Here  $y(t)$  is output variable and  $u(t)$  is input variable. If the disturbance  $d(t)$  is additive in the input side, the system is represented in the following state equation:

$$\begin{cases} \dot{x} = Ax + bu + e \cdot d \\ y = cx. \end{cases} \quad (5)$$

Here  $x = \begin{bmatrix} x_1 \\ x_2 \\ \vdots \\ x_n \end{bmatrix}$ ,  $A = \begin{bmatrix} 0 & 1 & 0 & \dots & 0 \\ 0 & 0 & 1 & \dots & 0 \\ \vdots & \vdots & \vdots & \dots & \vdots \\ 0 & 0 & 0 & \dots & 1 \\ -a_1 & -a_2 & -a_3 & \dots & -a_n \end{bmatrix}$ ,

$$b = \begin{bmatrix} 0 \\ 0 \\ \vdots \\ 0 \\ K \end{bmatrix}, \quad e = \begin{bmatrix} 0 \\ 0 \\ \vdots \\ 0 \\ 1 \end{bmatrix}, \quad c = [c_1 \quad c_2 \quad \dots \quad c_m \quad 0 \quad \dots \quad 0],$$

$x$  is a state vector,  $A$  is a system matrix,  $b$  is a distribution vector of input,  $e$  is a distribution vector of disturbance, and  $c$  is an observation column vector. Equation (5) is represented in Fig. 3.

The parameter variation and the disturbance should not give any significant effect

to output in robust control. At first, the parameters variation is evaluated. Suppose that the variation of system matrix  $A$  and the distribution vector  $b$  is additive to the nominal state denoted by lower suffix:

$$\begin{cases} A = A_0 + \Delta A, \\ b = b_0 + \Delta b. \end{cases} \quad (6)$$

where:  $\Delta A$  is a variation of  $A$  and  $\Delta b$  is a variation of  $b$ . The variation of dynamic matrix  $A$  is the same to the variation of the coefficients of the characteristic equation of (4). An extended disturbance is defined by modification of (5):

$$\begin{aligned} \dot{x} &= (A_0 + \Delta A) \cdot x + (b_0 + \Delta b) \cdot u + e \cdot d = \\ &= A_0 \cdot x + b_0 \cdot u + (\Delta A \cdot x + \Delta b \cdot u + e \cdot d). \end{aligned} \quad (7)$$

The third term in the right side is an extended disturbance defined to have the dimension of torque of force:

$$\tilde{d} = d + e^t \cdot (\Delta A \cdot x + \Delta b \cdot u). \quad (8)$$

By introduction of the extended disturbance, (5) is transformed to (9):

$$\begin{cases} \dot{x} = A_0 \cdot x + b_0 \cdot u + e \tilde{d}, \\ y = cx. \end{cases} \quad (9)$$

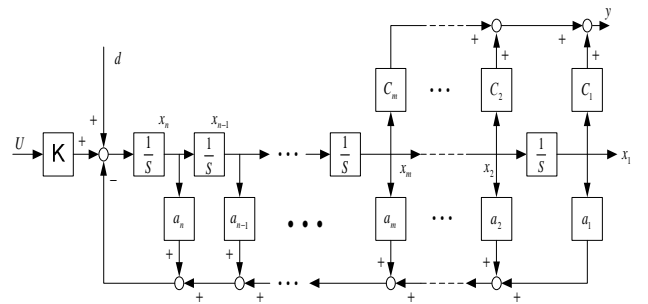


**Fig. 3.** Companion form of linear system

There are various proposals to estimate the disturbance. This chapter introduces a disturbance observer. Since the extended disturbance is the function of time, it is approximated by polynomials of  $(p-1)$  order [9]. Then (10) holds:

$$\frac{d^{(p)}\tilde{d}}{dt^p} = 0. \quad (10)$$

By putting (10) into (9), an augmented equation is obtained:

$$\begin{cases} \dot{\tilde{x}} = \tilde{A}_0\tilde{x} + \tilde{b}_0u \\ y = \tilde{c}_0\tilde{x}. \end{cases} \quad (11)$$

Here, the order of the matrix is  $(n+p)$  and  $\tilde{x}$  is as follows:

$$\tilde{x} = \begin{bmatrix} x_1 \\ x_2 \\ \vdots \\ x_n \\ \tilde{d} \\ \dot{\tilde{d}} \\ \ddot{\tilde{d}} \\ \vdots \\ \tilde{d}^{(p-1)} \end{bmatrix}, \tilde{A}_0, \tilde{b}_0, \tilde{c}_0 \text{ are as follows}$$

$$\tilde{A}_0 = \begin{matrix} & & & \overbrace{\hspace{2cm}}^{(n+p)} \\ \begin{bmatrix} 0 & 1 & 0 & \dots & 0 & 0 & 0 & \dots & 0 \\ 0 & 0 & 1 & \dots & 0 & 0 & 0 & \vdots & 0 \\ \vdots & \vdots & \vdots & \ddots & \vdots & \vdots & 0 & \vdots & 0 \\ 0 & 0 & 0 & \dots & 1 & 0 & 0 & \vdots & 0 \\ -a_{01} & -a_{02} & -a_{03} & \dots & -a_{0n} & 1 & 0 & \vdots & 0 \\ 0 & 0 & 0 & \dots & 0 & 0 & 0 & \vdots & 0 \\ \vdots & \vdots \\ 0 & 0 & 0 & \dots & 0 & 0 & 0 & \dots & 0 \end{bmatrix}, \end{matrix}$$

$$\tilde{b}_0 = \begin{bmatrix} 0 \\ 0 \\ \vdots \\ 0 \\ \frac{1}{K_0} \\ 0 \\ \vdots \\ 0 \end{bmatrix}, \tilde{c}_0 = \overbrace{[c_1 \ c_2 \ \dots \ c_m \ 0 \ \dots \ 0]}^{(n+p)}.$$

In (11), an equivalent disturbance defined by (8) seems a state variable. Clearly the system is uncontrollable, however, is observable. It is possible to construct an observed

which estimates state variables. The minimum order of observer is, therefore,  $n+p-m$ . Gopinath's method is a systematic way to construct such an observer [10]. Once  $\tilde{d}$  is estimated as  $\hat{\tilde{d}}$ , the input will be sum of two parts:

$$u = u^{ref} + u^{dis}. \quad (12)$$

The first term in the right side is a driving input to excite the system. The second term is a compensation to suppress the equivalent disturbance (and, by the way, to optimize the system as well), the compensation input is made by using the estimated equivalent – disturbance:

$$u^{dis} = -(b_0^t b_0)^{-1} b_0^t e \hat{\tilde{d}} = -\frac{1}{K_0} \hat{\tilde{d}}. \quad (13)$$

Since  $\hat{\tilde{d}}$  will be delayed by the lag poles in the disturbance observer, the compensation of the equivalent disturbance will be also delayed by the same amount. It is possible to design such delay as small as possible not to make robust stability deteriorate. The compensation input  $u^{dis}$  will change the original system without any disturbance.

Fig.4 visualizes a schematic diagram of the total system including the disturbance observer it is noted that the design of  $u^{ref}$  comes from the motion reference generator.

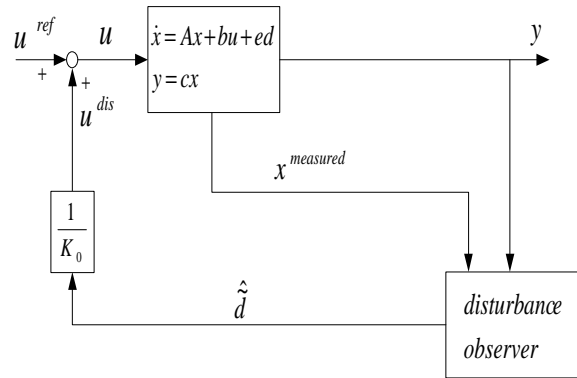


**Fig. 4.** Robust control based on disturbance observer

Generally total controller will have cascade of the outer loop to bring the desired

output and the inner loop by disturbance observer. The former will be a nest of the latter as shown in Fig. 5.

The previous design method is applied to the motion system described by (14):

$$I \frac{dw}{dt} = K_t I_a^{ref} - T_l, \quad (14)$$

Here  $I$  – inertia;  $K_t$  – torque coefficient of electric motor;  $T_l$  – load torque.

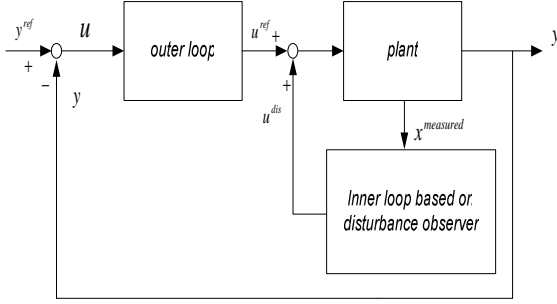


**Fig. 5.** Total system with robust control

The disturbance is load torque. The parameter variations are the change of inertia and the change of torque constant of motor. The output is position detected by position detector. The equivalent disturbance defined by (8) is:

$$\tilde{d} = -\frac{T_l}{I} + \left(\frac{K_t}{I} - \frac{K_{t_0}}{I_0}\right) I_a^{ref}. \quad (15)$$

Suppose the first derivative of  $\tilde{d}$  is zero. An augmented state equation corresponding to (11) is:

$$\frac{d}{dt} \begin{bmatrix} \theta \\ \omega \\ \tilde{d} \end{bmatrix} = \begin{bmatrix} 0 & 1 & 0 \\ 0 & 0 & 1 \\ 0 & 0 & 0 \end{bmatrix} \begin{bmatrix} \theta \\ \omega \\ \tilde{d} \end{bmatrix} + \begin{bmatrix} 0 \\ K_{t_0}/I_0 \\ 0 \end{bmatrix} I_a^{ref}. \quad (16)$$

By Gopinath's method, the following estimation process is obtained:

$$\hat{\tilde{d}} = k_1 \theta + z_1.$$

$z_1$  should satisfy (17), where  $k_1$  and  $k_2$  are free parameters:

$$\frac{d}{dt} \begin{bmatrix} z_1 \\ z_2 \end{bmatrix} = \begin{bmatrix} 0 & -k_1 \\ 1 & -k_2 \end{bmatrix} \begin{bmatrix} z_1 \\ z_2 \end{bmatrix} + \begin{bmatrix} -k_1 k_2 \theta \\ (k_1 - k_2^2) \theta + \frac{K_{t_0}}{I_0} I_a^{ref} \end{bmatrix}. \quad (17)$$

Equations (16) and (17) lead (18):

$$\hat{\tilde{d}} = \frac{k_1}{(S^2 + k_2 S) + k_1} (S^2 \theta - \frac{K_{t_0}}{I_0} I_a^{ref}) = \frac{k_1}{(S^2 + k_2 S) + k_1} \tilde{d}. \quad (18)$$

Two poles of the observer are  $\alpha$  and  $\beta$ , which are arbitrarily allocated in the complex plane. They satisfy (19):

$$\alpha + \beta = -k_2, \quad \alpha\beta = k_1. \quad (19)$$

It is worthwhile reconsidering (19). The parameters in (14) are the inertia and the torque coefficient. The inertia will change according to the mechanical configuration of motion system. The torque coefficient will vary according to the rotor position of electric motor due to irregular distribution of magnetic flux on the surface of rotor:

$$I = I_0 + \Delta I, \quad (20)$$

$$K_t = K_{t_0} + \Delta K_t. \quad (21)$$

By substituting (20) and (21) into (14), (22) holds:

$$I_0 \frac{dw}{dt} = K_{t_0} I_a^{ref} - (T_l + \Delta I \frac{dw}{dt} - \Delta K_t I_a^{ref}). \quad (22)$$

The second term of (22) is the disturbance torque  $T_{dis}$ :

$$T_{dis} = T_l + \Delta I \frac{dw}{dt} - \Delta K_t I_a^{ref}. \quad (23)$$

Comparing (14), (15), and (23), the following equation holds:

$$T_{dis} = I_0 (-\tilde{d}). \quad (24)$$

$T_{dis}$  contacts: 1) mechanical load(= $T_l$ ),

- 2) varied self-inertia torque  $\left[ = \Delta I \left( \frac{dw}{dt} \right) \right]$ ,
- 3) torque ripple from motor  $(= \Delta K_t I_a)$ .

The robust motion controller is designed to cancel the disturbance torque as quickly as possible.

The estimated disturbance torque is obtained from the position  $\theta$  and the current reference as shown in Fig. 6.

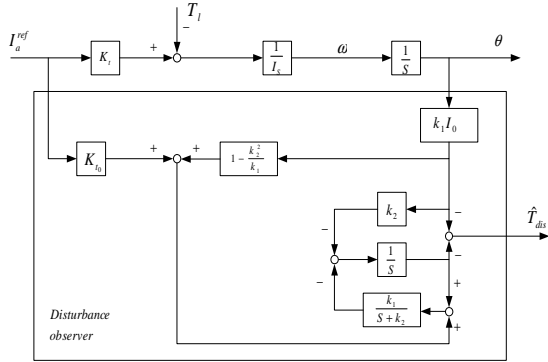


**Fig. 6.** Disturbance observed in motion system

According to the result of (12) and (13), compensation input is as follows:

$$I^{dis} = -\frac{I_0}{K_{t_0}} \hat{d} = \frac{1}{K_{t_0}} \hat{T}_{dis} \quad (25)$$

Robust motion controller has the schematic block diagram as shown in Fig. 7.

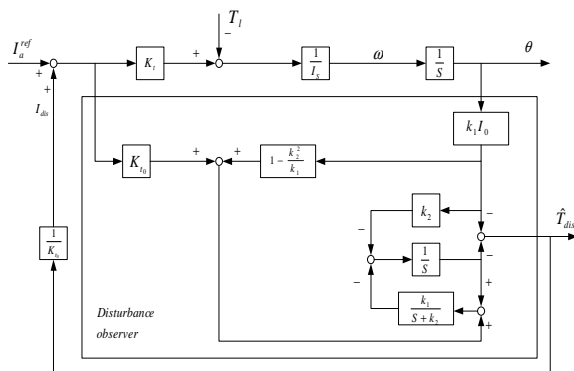


**Fig. 7.** A robust motion controller

There exists an integrator with high gain equivalently in the forward path as shown is

Fig.8. Therefore, the robust motion controller eliminates steady state error.

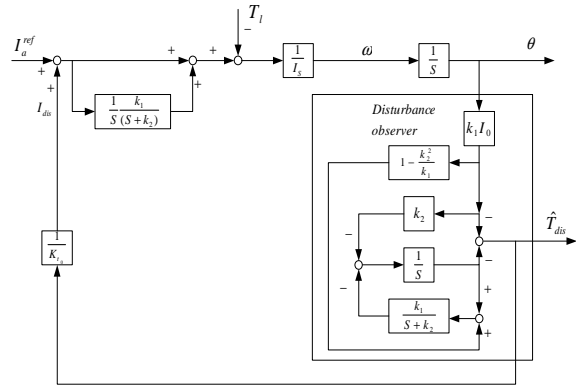


**Fig. 8.** Equivalent block diagram of Fig.7

Equation (18) shown that disturbance is estimated through low-pass filter. Generally there is such a low-pass filter in the observer structure. The poles of the observed determines the delay of the low-pass filter  $G_T(s)$ .

$G_T(s)$  gives a certain effect to the control performance. Fig.6 is also transformed into Fig.9.

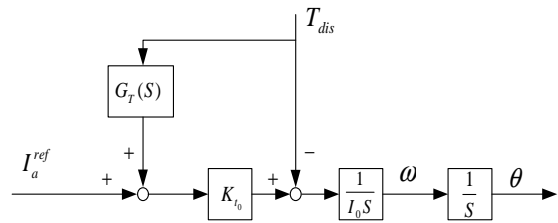


**Fig. 9.** A robust motion controller as an acceleration controller

Fig.9. transformed from Fig.6 clarifies the feedback effect of the disturbance. If there is no delay in the estimation process, the disturbance is completely canceled out. In fact, since there is definitely some time-delay in high frequency range determined by  $1 - G_T(s) = G_S(s)$ .  $G_S(s)$  is called a sensitivity function which shows a performance limit of robust control in high frequency range. In most of low frequency area covered by  $G_T(s)$ , the motion system is robust.

Fig. 9 shows another interpretation. It is possible to select nominal inertia and nominal torque coefficient as unity. This case

shows that a current reference is also an acceleration reference.

The chapter reaches that robust motion controller makes a motion system to be an acceleration control system. The result implies a versatility of robust motion controller for both position and force control. If position signal is fed back, a high-gain feedback in the robust controller makes stiffness very high. On the contrary, only pure force error feedback makes total stiffness zero since there is no gain to the position.

The disturbance estimated by (18) is used for a realization of robust mechanical system. In the actual application, the estimated disturbance is effective for not only the disturbance compensation but also the parameter identification in the mechanical system. As defined in (15), the equivalent disturbance  $\tilde{d}$ , which is estimated by the disturbance observer, includes the load torque  $T_l$  and the parameter variation torque  $[(K_t/I) - (K_{t0}/I_0)]I_a^{ref}$ . Here the load torque  $T_l$  consist of friction and external force effects in the mechanical system as follows:

$$T_l = \underbrace{T_c^{friction} + T_v^{friction}}_{\substack{\text{Coulomb and viscosity} \\ \text{friction effect}}} \omega + \underbrace{T_{ext}}_{\substack{\text{External} \\ \text{force effect}}} \quad (26)$$

This equation means that the output of the disturbance observed is only the friction effect under the constant angular velocity motion. This feature makes it possible to identify the friction effect in the mechanical system. Fig. 10 shows an example of the identified friction effect. In Fig.10, the friction effects are well identified as Stribeck friction model [11].

The external force effect is also identified by using the estimated disturbance. Here it is assumed that the friction effects are known beforehand by the above identification process. By implementing the angular accelerated motion, the system parameter  $K_{t0}/I_0$  is adjusted in the observer design so that it is close to the actual value  $K_t/I$ . As result, the disturbance observer estimates only the external force effect as follows:

$$\begin{aligned} \hat{\tilde{d}} &= \left( \frac{k_1}{s^2 + k_2 \cdot s + k_1} \right) \cdot \tilde{d} \Big|_{k_{t0}/I_0 \rightarrow K_t/I_0} = \\ &= \left( \frac{k_1}{s^2 + k_2 \cdot s + k_1} \right) \cdot \frac{T_{external}}{I_0}. \end{aligned} \quad (27)$$

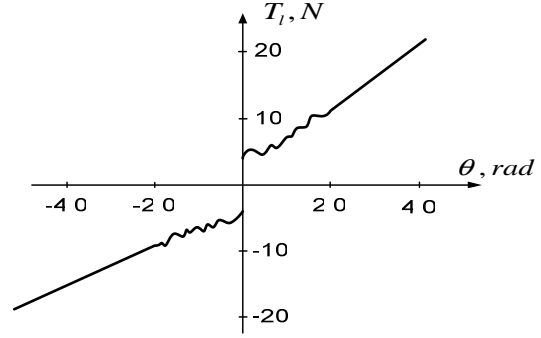
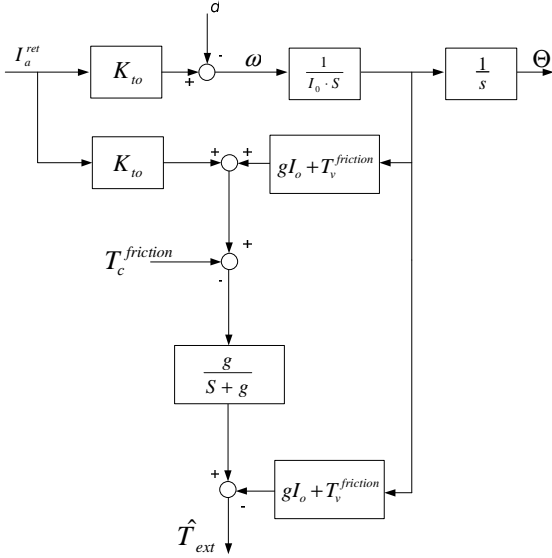


Fig. 10. An example of identified friction effect

The identification process of the external force is summarized in Fig. 11. The identified external force is applicable to senseless force feedback control in mechanical system [12] and is utilized for a realization of mechanical vibration control as shown in the next section.

As described before, the progress of robust control technologies makes it possible to realize high performance motion control of machines and mechanisms. In the industrial drive system such as a still rolling mill system and so on however, the development of technology is not enough to obtain the stable and high speed motion response since the mechanical vibration arises under the high accuracy positioning control. One may say such words about crane's systems as well. To address above issue, the mechanical vibration control is also taken up in the field of the motion control [13-15]. In particular a vibration control based on the external force feedback brings the sophisticated advantages to the mechatronic system. This section introduces a vibration control strategy based on the external force feedback called "resonance ratio control" in multiple resonance system. In this case, the external force may be obtained by using the identification process shown in Fig. 11.



**Fig. 11.** Identification process of external force

In general, the dynamical behavior of the mechanical resonance system is described as multiple mass spring model. Fig. 12 (a) shows a schematic illustration of the multiple mass spring system and Fig. 12 (b) is a block diagram.

In the vibration control, the disturbance effect imposed on the motor portion is suppressed by applying the robust control technique, which is based on the disturbance observer in this section. Then, the motion system seems an acceleration controller. Furthermore, the identified external force is fed back through the feedback gain  $K_r$ . Fig. 13 shows the total block diagram of the acceleration controller based on the external force feedback. Fig. 13 is transformed into Fig. 14 without any approximation. In the latter discussion, Fig. 14 is used for the analysis and the design of the vibration control for various mechanical systems, machines and mechanisms.

In Fig. 14, the following issues are considered to obtain the vibration suppression controller.

The controller of the motor portion is designed so that the poles of the system do not cancel the zeros by the motor state feedback.

The feedforward compensator is designed so that the location of the zeros is not changed.

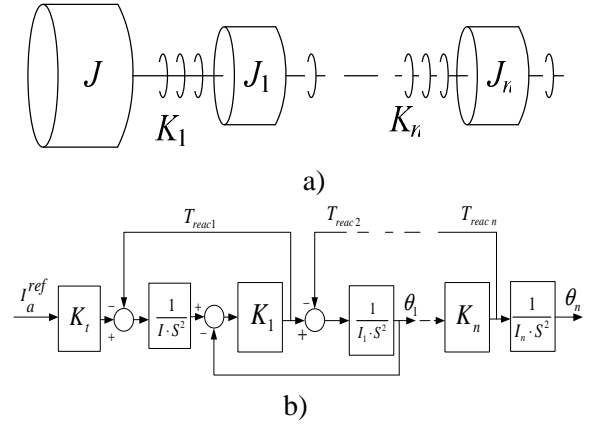


**Fig. 12.** A mode of mechanical resonance system  $K_f$ : Equivalent Total Stiffness of Load side;

$$I_a = I_1 + I_2 + \dots + I_n$$

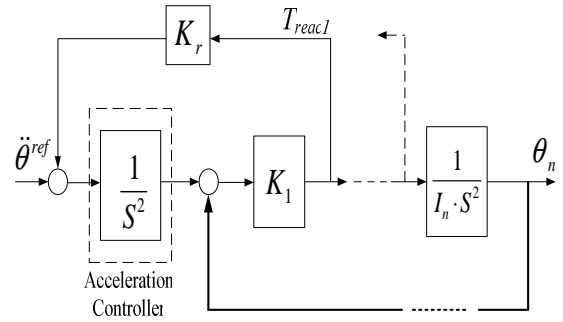


**Fig. 13.** Acceleration controller based on external force feedback

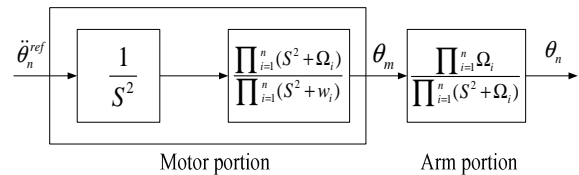


**Fig. 14.** Equivalent transformation of Fig. 13

In the vibration controller based on the external force feedback, PD control is applied to the motor position controller and the external force feedback gain is determined so that the above conditions are satisfied. To ensure the effectiveness of the external force feedback, the system stability is analyzed. In case PD control is applied to the motor portion of Fig. 14, the total block diagram of the mechanical system is rewritten as shown in Fig. 15. Fig. 16 shows the root loci of Fig. 15.

From Fig.16, starting angle of each oscillation pole  $\theta_i$  is obtained as follows:

$$\theta = 270^\circ - 2\alpha_i; \quad \theta_2 = 270^\circ - 2\alpha_2, \dots, \theta_{n-1} = 270^\circ - 2\alpha_{n-1}, \quad (28)$$

$$\theta \leq \alpha_j \leq 90^\circ; \quad 90^\circ \leq \theta_j \leq 270^\circ. \quad (29)$$

The above equations mean that the controller based on the external force feedback mares the oscillation poles stable. This is a basic concept of the proposed approach to obtain the stable motion response in the mechanical resonance system. In the actual design of the controller, only the first oscillation pole is considered to construct the vibration suppression controller (for example, for the crane's system). Then the controller gains  $K_p$ ,  $K_v$ ,  $K_r$  are determined according to the resonance ratio which shows the ratio of the natural frequency of the motor side and the load side. The vibration control strategy based on the resonance ratio is called "resonance ratio control" for machines, mechanisms and other mechanical systems.

As described before, all pole – loci of the mechanical resonance system move to the stable direction by the external force feedback. In the next step, the controller gains are determined according to the resonance ratio. Here it is asumed that the dominant oscillation pole of the mechanical system is the first oscillation pole. Then the transfer function of the system is described as follows:

$$\begin{aligned} \theta_m &= \frac{(s^2 + w_a^2)}{w_a^2} \cdot G_1(s) \cdot G_2(s) \cdot \theta^{cmd}, \\ \theta_a &= G_1(s) \cdot G_2(s) \cdot \theta^{cmd}; \quad w_a = \sqrt{\frac{K_f}{I_a}}, \\ w_m &= \sqrt{\frac{K_f}{I_a} \cdot (1 + K_r \cdot I_a)} = K \cdot w_a; \quad K = \sqrt{1 + K_r \cdot I_a}. \end{aligned} \quad (30)$$

Here  $w_a$  and  $I_a$  are the equivalent frequency and inertia of the load side in Fig. 13.  $w_m$  and  $K_f$  is the natural frequency of the motor side and the equivalent stiffness of the load side, respectively.  $K$  is the resonance ratio. The denominator  $D(s)$  of the transfer function of  $G_1(s) \cdot G_2(s)$  is given as follows:

$$\begin{aligned} D(s) &= s^4 + K_v \cdot s^3 + (K_p + w_m^2) \cdot s^2 + \\ &+ K_v \cdot w_a^2 \cdot s + K_p \cdot w_a^2. \end{aligned} \quad (31)$$

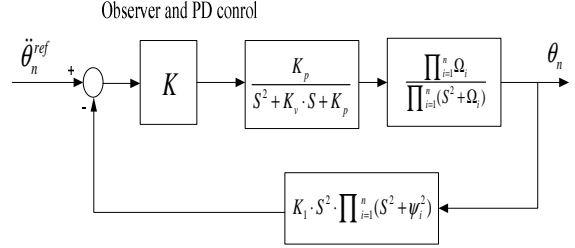


**Fig. 15.** Total block diagram of vibration suppression controller

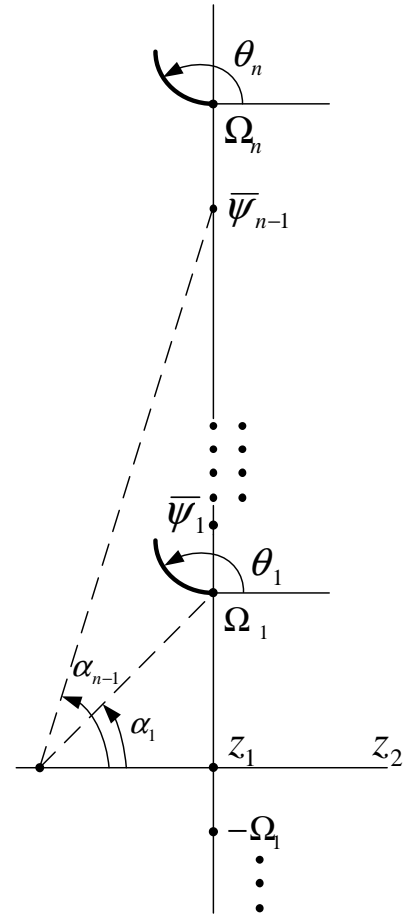


**Fig. 16.** Root locus of Fig. 15

To simplify the controller design,  $G_1(s)$  and  $G_2(s)$  are defined as second order system and  $\zeta_1$ ,  $\omega_1$ ,  $\zeta_2$ ,  $\omega_2$  - are introduced to describe the motion performance in each system. Then  $D(s)$  is also given us follows:

$$\begin{aligned} D(s) &= (s^2 + 2\zeta_1 \cdot \omega_1 \cdot s + \omega_1^2) \times \\ &\times (s^2 + 2\zeta_2 \cdot \omega_2 \cdot s + \omega_2^2). \end{aligned} \quad (32)$$

From (31) and (32), the following relations are obtained:

$$K_v = 2(\zeta_1 \cdot \omega_1 + \zeta_2 \cdot \omega_2), \quad K_p = \frac{\omega_1^2 \cdot \omega_2^2}{\omega_a^2},$$

$$\omega_m = \sqrt{-\frac{\omega_1^2 \cdot \omega_2^2}{\omega_a^2} + \omega_1^2 + \omega_2^2 + 4\zeta_1 \cdot \zeta_2 \cdot \omega_1 \cdot \omega_2}. \quad (33)$$

The important goal in the vibration control is to suppress the vibration, so that  $\zeta_1 = \zeta_2 = 1,0$  in (33). Also  $\omega_1 = \omega_2 = \omega_a$  to obtain the high speed motion response in the load side. Finally, the following control gains are obtained with resonance ratio of  $\sqrt{5}$ :

$$\begin{cases} K_r = 4 / I_a \\ K_p = w_a^2, \\ K_v = 4w_a. \end{cases} \quad (34)$$

By using a set of the gains shown in (34), the vibration of the mechanical resonance system is well suppressed. Fig. 17 and 18 are the experimental results of PD control and resonance ratio control respectively. These results clearly show that the resonance ratio control is effective for the vibration suppression in the mechanical resonance system, various machine and mechanisms as well.

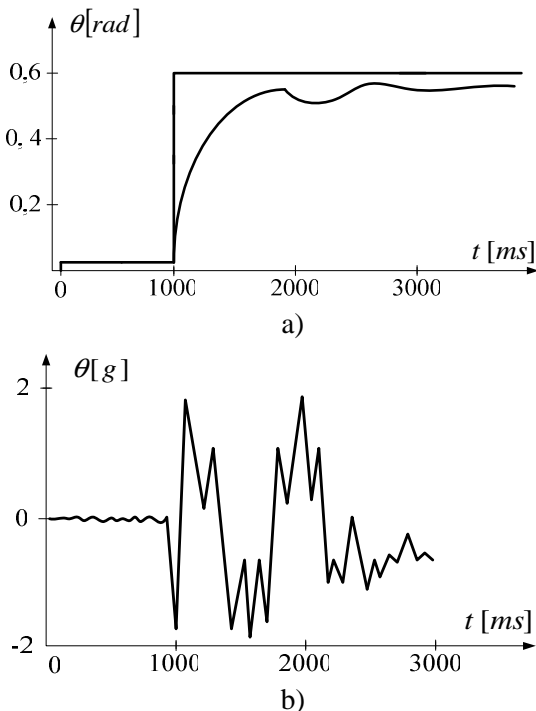


**Fig. 17.** PD control in mechanical resonance system

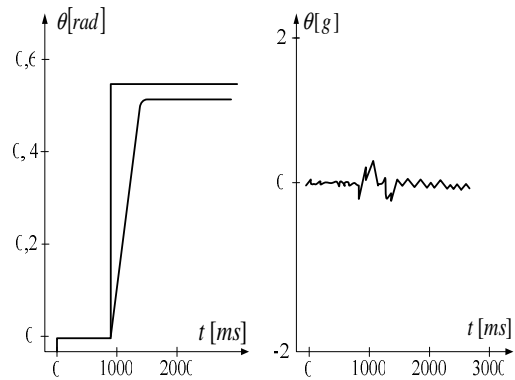


**Fig. 18.** Resonance ratio control in mechanical resonance system

## CONCLUSIONS

1. The paper intends to give a tutorial of motion control technology in mechatronics and in various machines and mechanisms as well. The robustness of the motion control makes the mechanical system more flexible. The stiffness of the motion, which correspond with the forward gain of the position, is defined to be a good index of robustness. The motion controller acquires robustness by estimating disturbance. The robustness and the identification is both sides of an optimal control each other. The resent – modern technique including two-degrees-of-freedom (optimal) control,  $H^\infty$  - control has proved the same structure from physical point of view [16]. The estimated disturbance includes reaction force from the environment. The information is used for estimation of mechanical parameters. By direct use of reaction force, an antivibration (optimal) control called a resonance ratio control for flexible structure is realized.

2. The paper little describes the reference generator. An intelligence in the reference generator is another key for intelligent mechatronics for mechanical systems, machines and mechanisms, however, it presuppose the robustness of the motion controller (for example, for crane's systems). From such point of view the role of robust motion controller will be more important in modern mechatronics.

3. The further development, particularly in the connection of reference generator and controller of motion for crane's systems, for agricultural machine and mechanisms, for various mechanical (resonance) systems, will be expected.

#### REFERENCES

1. **Yaskawa Electric Co. 1971.** Registered Trade Mark Nr 46, 32713.
2. **Ohnishi K.** Ed. in Proc. Int. Workshop an Advanced Motion Contr., Yokohama, Apr. **1990.**
3. **Carli A. De.** Ed. in Preprints, IFAC Workshop on Motion Contr. Intell. Automat, Perugia, Oct. **1992.**
4. **Okuma S.,** Ed. in Proc. 2nd Int. Workshop on Advanced Motion Contr., Nagoya Mar. **1992.**
5. **Kazerooni H., Hori Y. 1994.** Eds. in proc. 3rd Int. Workshop on Advanced Motion Contr., Berkeley, March, Oct.
6. **Pfeiffer F. and Brandenburg G. 1995.** Ed. in Proc. 3rd IFAC Workshop on Motion Contr., Munich, Oct.
7. **Ohishi K. 1993.** Eds., J. Robot. Soc. Jpn., Special Issue on Advanced Motion Control, vol. 11, Nr.4.
8. **Leonhard W. 1985.** Control of Electrical Drives. Berlin: Springer, Verlag
9. **Meditch J. and Hostetter G.H. 1974.** Observers for systems with unknown and inaccessible inputs, Int. J. Contr., Vol. 16, Nr 3, 473-480.
10. **Gopinath B. 1971.** On the control of linear multiple input – output systems, Bell Systems Tech. J., Vol. 50, Nr 3, 1063 – 1081.
11. **Southward S., Radcliffe C., MacCluer C. 1991.** Robust nonlinear stick – slip friction compensation, ASME J. Dynamics Syst., Measurement, Contr., Vol. 113, 639 – 645.
12. **Murakami T., Ohnishi K. 1993.** Torque sensorless control in multidegree of freedom manipulator, IEEE Trans. Ind. Electron, vol. 40, Nr 2.
13. **Murakami T. 1995.** Eds. Robot Soc. Jpn., Special Issue on Advanced Motion Control in Vibration System, Vol. 13, Nr 8.
14. **Seto K., Yoshida K., Nonami K. 1992.** Eds. in Proc. JSME First Int. Conf. Motion, Vibration Contr., Yokohama.
15. **Yoshida K., Ononami K. 1994.** Eds. in Proc. 2nd Int. Conf. Motion, Vibration Contr., Yokohama.
16. **Buja G., Fujita H., Ohnishi K. 1990.** Eds., Recent Advances in Motion Control. The Nikkan Kogyo Shimibun Ltd.

#### ОПТИМИЗАЦИЯ РЕЖИМОВ ДВИЖЕНИЯ МАШИН И МЕХАНИЗМОВ С МЕХАТРОННЫМ УПРАВЛЕНИЕМ

**Аннотация.** Управление движением машин и механизмов в настоящее время признается в качестве ключевой технологии в мехатронике. Робастность управления движением представлена в виде функции от жесткости и есть основной для практической реализации, например, в точном сельском хозяйстве. Цель движения параметризована жесткостью управления, которое, в соответствии с задачей, может быть переменной величиной. Однако, для достижения робастности движущейся системы необходима очень высокая жесткость управления. В работе показано, что управление ускорением системы реализуется одновременно с сохранением высокой робастности. Ускорение является переходом от робастности к переменной жесткости. Для практических применений введена методика оценки помех, что позволяет управляющему устройству движения управлять ускорением машины/механизма. Также описаны оптимизация управления движением гибкой структуры и идентификация механических параметров системы.

**Ключевые слова:** оптимизация, движение, машины, мехатроника, управление.

## The Hydraulic Quencher Dynamic Vibrations

*Leonid Pelevin, Mykola Karpenko*

Kyiv National University of Construction and Architecture  
Povitroflotskyi prosp., 31, Kyiv, Ukraine, 03680, e-mail: karpenko\_knuba@ukr.net

**Summary.** Carried out a review and analysis of the developed hydraulic system for quenching dynamic oscillations. Made the mathematical model for determining the time delay operation of the hydraulic system of the dynamic quenching of oscillations. Performed a period's calculation of cleavage of the soil and the time delay operation quencher dynamic oscillations from which it is possible in theory to establish the ability of the hydraulic system of dynamic quenching oscillations to operate in time. Developed hydraulic system dynamic quenching oscillations that occur inside the working unit to prevent the transmission of vibrations to the base of the machine. Conducted the analysis of the damper's means and the method of dynamic damping on which developed hydraulic system for quenching dynamic oscillations. Was built mathematical sequence for determination of the time delay operation of the quencher. Parameters allow you to construct experimental model hydraulic system quenching of dynamic oscillations.

**Key words:** quencher, the dynamic oscillations, hydraulic system, the time lag response, period cleavage soil.

### INTRODUCTION

The construction often includes works that cannot be performed by conventional machines. In this case, using a special technique, which is equipped by active action engines and used for ground operations can be consider as a solution.

One of the disadvantages of this special technology – transmission of vibrations from the working body to base machine, accompanied by the premature wearing down of the parts of the basic machine which do not participate in the destruction of the ground.

To solve the problem mentioned above will help amortizable equipment to isolate vibrations from the movement of the working body to the base machine.

Given that the current cushioning devices are not effective enough and demand a construction a new hydraulic system dynamic quenching oscillations and mathematical

model for determination of the one of the main characteristics of the new system, namely: determining the time delay in the operation of the hydraulic system dynamic quenching oscillations for evaluation, timeliness, triggering of on specified dynamic fluctuations.

### PURPOSE OF WORK

Based on the results of the analysis of the method of the dynamic analysis and vibration cushioning devices to develop:

– A mathematical model for determining the time delay in the operation of the hydraulic system dynamic quenching oscillations;

– Own hydraulic construction for extinguishing dynamic oscillations that arise inside the working organ for impossible their transmission to the base machine.

## THE MAIN MATERIAL

In engineering is often necessary to damp the vibration transmitted to the machine from its working equipment. Basically – it is machines with dynamic (active) working tools. As a result of work, the vibrations can be transmitted to the machine and cause destruction. For impossibility transmit the vibrations from the working body to the base machine used so-called springy elements that are trying to put out vibrations transmitted to the base machine. The main method of vibration damping is called – a method of dynamic vibration damping [3, 4, 5, 15, 19].

The method of dynamic vibration damping is based on the accession to the object's vibration protection additional devices to change its vibration's condition. A work of the dynamic quencher is based on putting out the force transmitted to the object. This dynamic quenching differs from another method of reducing vibration, characterized by imposition of the additional kinematic object linkages, such as fixing some of its points [2, 19].

Changing the base machine a vibrating condition when joining a dynamic quencher can be achieved by the redistribution of vibrational energy from the object to the quencher and in the direction of the increasing energy dissipation fluctuations [13, 20]. The first from mentioned is implemented by changing the system's settings of the object-quencher over the frequencies of the vibration excitation by correcting the elastic-inertial properties of the system. In this case, attachable to the object devices are called the inertial dynamic quenchers. The inertial quencher is used to suppress harmonic mono or narrowband random fluctuations.

During a vibration's load of the wider frequency range the second method is preferred. It is based on increasing dissipative properties of the system by attaching to the object additional specific damping elements. Dynamic quencher dissipative types are called absorbers vibrations [3]. The combined ways of the dynamic quenching using both correction elastic-inertial and dissipative properties of the system are also possible. In such cases

we talk about the dynamic quencher of friction [7, 16].

When implementing dynamic quencher counteraction fluctuations the object carried by reactions that are passed to it attached bodies. For this reason, considerable efforts with limited amplitudes masses adjusted, can be achieved only by large mass (moment of inertia) connected bodies, typically  $\approx 5...20\%$  of the reduced mass (moment of inertia) primary system appropriate form of vibrations within the frequency quenching which is performed respectively [3].

Typically, dynamic quencher is used to achieve a local effect: a reduction of the object's vibration in parts where the quencher is fastened. Often it may be associated even with the deterioration of the object's vibration in the other – less appropriate places.

Dynamic quencher can be constructively implemented based on the passive elements (Fig. 1) (masses, springs, shock absorbers, dampers) and the active ones, which have their own power sources.

In the last case, we are talking about the use of the automatic control systems that use electric, hydraulic and pneumatic driven el-



**Fig. 1.** The overall look of shock absorbing passive elements:

*a* – spring (of vehicle), *b* – spring

ements. Successful is their combination of passive devices, an example of which is the shock absorber shown in Fig. 2.

The utilization of the active elements expands the possibilities dynamic vibration's suppression, because allows to conduct continuous adjustment of the parameters of dynamic quencher as a function of excitation

acting, and thus perform quenching in conditions of changing vibration loads. A similar result can be achieved sometimes by means of passive devices with nonlinear characteristics.



**Fig. 2.** General view of the shock absorber

Shock absorber – the device which converts the mechanical energy in the thermal and is used for vibration damping (damping) and shock absorption and bumps acting on the casing (frame). Shock absorbers are used in conjunction with elastic elements: springs(of vehicle) or springs, pillows, etc.

Hydraulic shock absorbers became the most commonly used. In hydraulic shock absorber the resistance force depends on the speed of movement of rod. Working medium – oil. The principle of operation of the shock absorber is based on the reciprocating movement of the piston shock absorber, which through a small hole puts an oil from one chamber to another, converting mechanical energy in the heat energy.

Today, the generally used solutions for vibration damping devices are those which utilize the hydraulic elements. Hydraulic dampers as opposed to friction ones, have the longer duration of work and can demperfering a small oscillation amplitude.

In Fig. 3 is shown the design of the damper, which contains the adjusting screw. This allows to increase the resistance value of the flowing liquid through the channel and thus governed by a calming according to [9, 12, 13].

Nowadays, the most promising is the hydraulic vibration damping system, which is designed based on hydraulic shock absorbers and dampers.

In the design of hydraulic systems blanking dynamic fluctuations must be considered

dynamic characteristics of systems, which, in particular, the transfer speed signals and the total system performance, pressure fluctuations in various points of the system (including hydraulic shocks), sustainability and quality of system transients [1, 11].

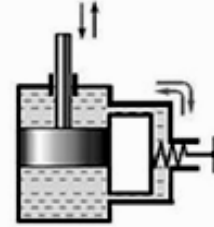


**Fig. 3.** Liquid dampers adjusting screw

Movement of actuating mechanism always comes with some delay in relation to the input signal. The identification of the delay's amount allows to perform the dynamic system's, the total response time and the need to introduce appropriate units to compensate for the delay calculation, depending on the frequency control signal and set when the corresponding pulses [8, 17, 9].

To perform the system's calculations it is necessary to know the basic system parameters, including the size of pipelines, hydraulic and mechanical resistance properties of the working fluid and hydraulic machines, hydraulic power source characteristics [6].

Total delay time of the system's response can be defined as a first approximation by the formula:

$$t_d = \frac{\Delta V + V_1}{Q_h + 0,5Q_b}, \quad (1)$$

where:  $\Delta V$  – reduces the volume of liquid in the system by increasing the pressure on the value of  $\Delta p$ ,  $m^3$ ,  $V_1$  – volume of fluid required to filled-tion of additional volumes in the system,  $m^3$ ,  $Q_b$  – leak in the system for working pressure,  $m^3/s$ ,  $Q_h$  – the nominal flow rate in the system,  $m^3/s$ .

In this case  $Q_h$  and  $V_1$  determined from the formula:

$$Q_h = \frac{17,1N_h}{P_h}, \quad (2)$$

where:  $N_h$  – hydraulic drive power, kW,  $P_h$  – nominal pressure hydraulic system MPa.

The volume of the fluid required to fill the additional volume in the system  $V_1$ , is 5...10% of the total volume of fluid in the hydraulic system  $V$ ,  $m^3$ . The total volume of fluid in the hydraulic system is calculated as follows:

$$V = V_c + V_e \quad (3)$$

where:  $V_e$  – the amount of hydraulic fluid that is equipped in hydraulic system,  $m^3$ ,  $V_c$  – the amount of hydraulic fluid that is in the pipeline hydraulic system Eq. (3), which is calculated by the equation:

$$V_c = \frac{\pi D^2}{4} L, \quad (4)$$

where:  $L$  – total length of pipelines, m,  $D$  – internal diameter hydraulic of the pipeline,  $m^2$ , calculated by the formula:

$$D = 4,5\sqrt{Q_h/W}, \quad (5)$$

where:  $W$  – speed liquid is in the hydraulic system at a prescribed pressure, m/s.

$$V_1 = (0,05...0,1)V. \quad (6)$$

At first approaching the delay operation of the system Eq. (1) we obtain the equation:

$$t_d = \frac{\Delta V + V_1}{Q_h} \cdot \frac{1}{1 - \frac{Q_b}{2Q_h}}. \quad (7)$$

In the view of that:

$$Q_b = K_b P, \quad (8)$$

where:  $P$  – operating pressure in the system, MPa,  $K_b$  – the coefficient of leakage of liquid, received from the equation:

$$K_b = j \frac{61,2N_h}{P^2}, \quad (9)$$

where:  $j$  – coefficient of that changes the units of measurement of l/min in  $m^3/s$  and 0.278 matter.

In this case, reduce the volume of liquid in the system while increasing pressure on the value of  $\Delta p$  is calculated as follows:

$$\Delta V = \delta S_1 L, \quad (10)$$

where:  $\delta$  – coefficient of decrease of the liquid, which depends on the operating pressure;  $S_1$  – cross-section inner diameter hydraulic of the pipeline,  $m^2$ .

Moreover,  $S_1$  is calculated as follows:

$$S_1 = \frac{\pi D^2}{4}. \quad (11)$$

In the final order determining equations will get simplified the delay triggering, performance, which will look like:

$$t_d = \frac{\delta S_1 L + V_1}{Q_h - 0,5K_b P}. \quad (12)$$

From dependence is obvious that to reduce the delay's time triggering it is necessary:

1. Working channels and pipelines should be as short and rigid,
2. Volume losses should lowered to a minimum,
3. Pump capacity should be significant.

In general, the performance of the quencher dynamic oscillations is determined for each a particular system, provided that the signal can be transmitted with a specific delay, but performance must be such as not to violate the stability of the all circuit [18].

To achieve the stated conditions, we need to know period the cleavage of soil that need to find the time at which the dynamic working organ ripper makes one complete cycle of the movement  $T_c$  [14], and is inversely to the

average oscillation frequency maxima of cutting the soil, and is given by:

$$T_c = \frac{1}{\bar{n}_m} \text{ s}, \quad (13)$$

$$\bar{n}_m = \frac{\bar{n}_0}{0,63...0,87} \text{ 1/s}, \quad (14)$$

where:  $\bar{n}_0 = (2,0...2,8) \frac{W_w}{H}$  1/s – the average oscillation frequency of cutting soil  $H$  – loosening depth, m,  $W_w$  – speed of the working body.

Determine the dependence of time the delay triggering quencher dynamic fluctuations of hydraulic parameters [2, 19].

Suppose that a dynamic body of work in rocky soil at a depth of  $H = 0,3$  m, in which case the rate of dynamic body is

$$W_w = 2 \text{ m/s}.$$

First of all determine the period shearing soil:

$$T_c = \frac{1}{\bar{n}_m} = \frac{1}{15,3} = 0,09 \text{ s}. \quad (15)$$

Determine a relationship Eq. (14) middle frequency oscillation cutting forces:

$$\bar{n}_m = \frac{\bar{n}_0}{0,63...0,87} = \frac{13,3}{0,87} = 15,3 \text{ 1/s}, \quad (16)$$

$$\bar{n}_0 = 2 \cdot \frac{2}{0,3} = 13,3 \text{ 1/s}. \quad (17)$$

Initial data hydraulic system blanking dynamic oscillations:  $N_h = 100$  kW,  $P_h = 25$  MPa,  $P = 30$  MPa,  $L = 20$  m,  $W = 4.25$  m/s.

Carry out a calculation:

$$Q_h = \frac{17,1 \cdot 100}{25} = 68,1 \text{ m}^3/\text{s}, \quad (18)$$

$$D = 4,5 \cdot \sqrt{68,1/4,25} = 18 \text{ mm}, \quad (19)$$

$$V_{\text{con.}} = \frac{3,14 \cdot 0,018^2}{4} \cdot 20 = 0,0051 \text{ m}^3, \quad (20)$$

$$V_1 = (0,0051 + 0,0549) \cdot 0,1 = 0,006 \text{ m}^3, \quad (21)$$

$$S_1 = \frac{3,14 \cdot 0,018^2}{4} = 0,00026 \text{ m}^2, \quad (22)$$

$$K_b = 0,278 \frac{61,2 \cdot 100}{30^2} = 1,89 \text{ kW/MPa}^2, \quad (23)$$

$$t_d = \frac{30 \cdot 0,00026 \cdot 20 + 0,006}{68,1 - 0,5 \cdot 1,89 \cdot 30} = 0,004 \text{ s}. \quad (24)$$

From the resulting example we can conclude that the system performance satisfies oscillation quenching specified condition of this dynamic organ as triggering delay is less than 15 % of the period shearing soil.

By changing parameters of the hydraulic system dynamic quenching fluctuations – namely the supply hydraulic fluid in the system and reduce fluid volume ratio, and substituting in the present calculation, we plot the dependence of the delay in operation of the hydraulic system dynamic quenching oscillation (speed) of hydraulic fluid supply system (Fig. 4) and from coefficient reduction of fluid (Fig. 5).

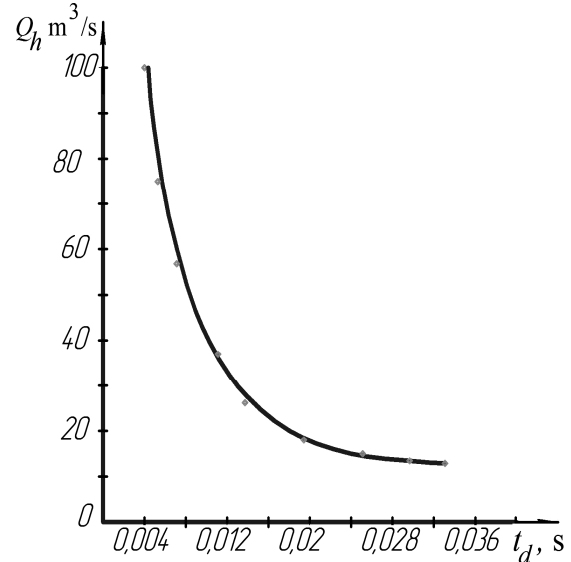


**Fig. 4.** Graph of the time delay operation hydraulic blanking dynamic fluctuations of supply of hydraulic fluid

The hydraulic quencher dynamic fluctuations was developed to improve the effi-

ciency of dynamic quenching of oscillations, it is based on the use of the system mentioned above.

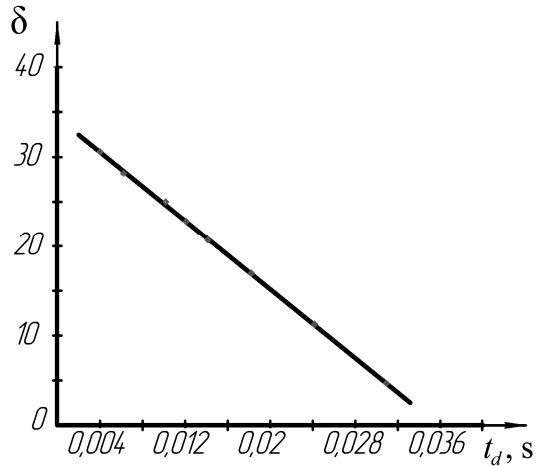


**Fig. 5.** Graph of the time delay operation hydraulic blanking dynamic fluctuations of coefficient reduce the amount of fluid

Quencher dynamic oscillations (Fig. 6, 7) works as follows [10].

Vibrations that are transmitted from the working body to the base machine blanked with the help dynamic fluctuations quencher 1. At active work oscillatory body rod 3 tries to reproduce vibrational motion in the housing 2. However, when the direction of the vibrational motion is reproduced, for example, left by movement of fluid through the the holes throttled 6 plunger 4, 8 rods blocking valve and plunger valve 11 moving blocking right. Thus blocking rods 8 pressed to valve rods washer 7. Meanwhile blocking plunger valve 11 pressed to plunger 4, blocking throttling holes 6, so that the liquid begins to flow through passage the holes 12, which extinguished the movement of the rod 3 left. Once

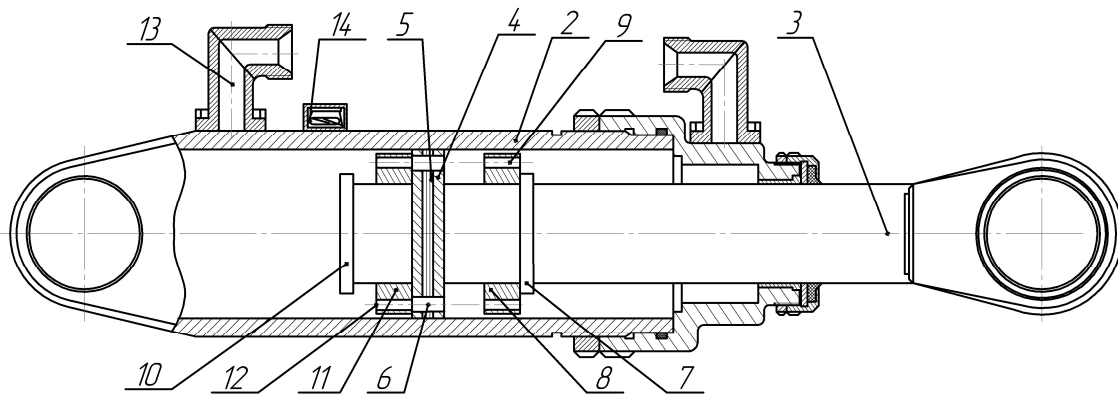


**Fig. 6.** Quencher dynamic fluctuations

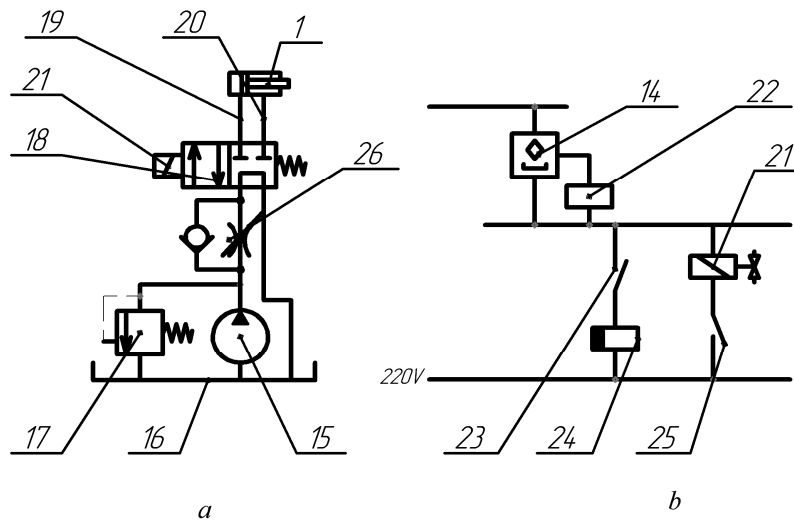


**Fig. 7.** The hydraulic circuit control quencher dynamic oscillations *a* and electrical circuit control distributor *b*

the plunger 4 reaches the reed switch 14, the magnetic field of the magnet constant step 5 shut reed contacts 14 (Fig. 7, b). The signal will go to detention relay 22, which shut normally open contact 23. He, in turn, turned on the delay relay exclusion 24. After that delay relay exclusion shut 24 contact 25, which starts the electromagnetic control 21. The electromagnetic control 21 toggles the distributor 18 in the left position. Hydraulic pump 15 through a variable orifice with check valve 26, which regulates the supply of hydraulic fluid distributor 18 and pressure line 19 takes an additional portion of the fluid in the plunger cavity quencher dynamic fluctuations 1. Excess fluid flows out of rods quencher dynamic cavity oscillations 1 through the drain line 20 and distributor 18 to a tank of hydraulic fluid 16. When plunger 3 moves to the right by moving the working fluid through the throttling holes 6, 8 rods blocking valve and plunger valve 11 blocking move left. Plunger blocking valve plunger 11 pressed to washer 10 and rods blocking valve 8 pressed to plunger 4 blocking throttling holes 6. As a result, the liquid begins to flow through passage 9 the holes, putting the movement of the rod 3 right. Once the plunger 4 moves away from the reed switch 14 and the magnetic field of the magnet constant step 5 stops to influence the reed switch 14 (reed switch contacts open up 14), the signal ceases to be submitted normally open contact 23. He, in turn, relay switching delay open up exclusion 24. It will work for a while, allowing the hydraulic pump 15 to submit several additional portions of the liquid in the plunger cavity oscillations quencher 1-for-4 plunger removal of reed switch 14. After exclusion of 24 delay relay contact will turn off 25, 21 control the electromagnetic switch distributor 18 in the far right position, then feed additional portion of the liquid to the quencher dynamic fluctuations 1 end. Hydraulic fluid is fed to the quencher through the pipe 13.

Because of the dynamic fluctuations quencher 1 reduced dynamic fluctuations in the base machine, during the working bodies active action.

## CONCLUSIONS

1. Based on the analysis of dynamic cushioning devices for vibration in the hydraulic system, the mathematical model of the process of determining the delay's time of their operation, which allows you to design these systems.
2. Based on the values built dependency graphs: time delay operation of the hydraulic system dynamic oscillations on quenching koefitsiyenta reduction of fluid and supply of hydraulic fluid. By changing these parameters the system designed adjustable hydraulic damping system dynamic oscillations.
3. A new design of hydraulic blanking dynamic fluctuations with the ability to change the parameters of the filing.
4. The design provides adjustable vibro base machine from vibrations attachments.

## REFERENCES

1. **Bud'ko V. 2003.** Dynamics and regulation hidropnevmosystem. Kyiv, NAU, 64 (in Ukraine).
2. **Cândeia I., Popescu S. 2003.** Theoretical and experimental study on soil vibrators used for the germinal layer preparation. Motrol: kom. Mot. Energ. Roln., OL PAN, vol. 3. (6), 55-62 (in Poland).
3. **Chelomej V.N. 1981.** Vibrations in Technology: Handbook: in 6 volumes. Red. Soviet: (pred.). Moscow, Mashinostroenie, Vol. 6, 456 (in Russian).
4. **Emtsev B. 1987.** Technical hydromechanics.: M.: Mashinostroenie, 439 (in Russian).
5. **Gavrilenko B. Minin V. 1958.** Hydraulic drive. Moscow, Mashinostroenie, 240 (in Russian).
6. **Gijom M. 1964.** Investigation and calculation of hydraulic systems. Moscow, Mashinostroenie, 387 (in Russian).
7. **Korobochkin B. 1976.** dynamics of hydraulic machines. Moscow, Mashinostroenie, 240 (in Russian).
8. **Lewis E., Sterh H. 1966.** Hydraulic control system. Moscow, Mashinostroenie, 407 (in Russian).
9. **Nagorniy V., Denisov A. 1991.** Devices of automation and hydro pneumatic. Moscow, Mashinostroenie, 367 (in Russian).

10. **Patent** Ukraine № 90197 from May 12.2014 (in Ukraine).
11. **Popov D. 1987.** Dynamics and regulation of hydraulic and pneumatic systems. Moscow, Mashinostroenie, 464 (in Russian).
12. **Schokdemper. 2014** Available at: <http://nl.wikipedia.org/wiki/Schokdemper>, accessed 20 Jul. 2014 (in Nederlands).
13. **Shorin V. 1980.** Elimination of fluctuations in air pipes. Moscow, Mashinostroenie, 156 (in Russian).
14. **Vetrov Ju., Vlasov V. 1995.** Machines for excavation. Sample calculation: Teach. user. Kyiv, ISDO, 304 (in Russian).
15. **Vilde A., Cesnieks S., Rucins A. 2004.** Minimisation of Soil Tillage. Motrol: kom. Mot. Energ. Roln., OL PAN, vol. 4. (30), 237-243 (in Poland).
16. **Vilde A., Rucins A. 2004.** The Impact of Soil Physical and Mechanical Properties on Draft Resistance of Ploughs. Motrol: kom. Mot. Energ. Roln., OL PAN, vol. 4. (31), 243-249 (in Poland).
17. **Vilde A., Tanaś W. 2005.** Determination of the soilfriction coefficient and specific adhesion. Motrol: kom. Mot. Energ. Roln., OL PAN, vol. 5. (24), 212-217 (in Poland).
18. **Walusiak S., Dziubiński M., Pietrzyk W. 2005.** An analysis of hydraulic braking system reliability. Motrol: kom. Mot. Energ. Roln., OL PAN, vol. 5. (25), 217-226 (in Poland).
19. **Zakharchuk B., Telushkin V. 1987.** Bulldozer and rippers. Moscow, Mashinostroenie, 240 (in Russian).
20. **Zipkin Ya. 1977.** Foundations of the theory of automatic systems. Moscow, Mashinostroenie, 560 (in Russian).

#### ГИДРАВЛИЧЕСКИЙ ГАСИТЕЛЬ ДИНАМИЧЕСКИХ КОЛЕБАНИЯХ

**Аннотация.** Проведен обзор и анализ существующих амортизирующих устройств. Рассмотрен метод динамического гашения колебаний. Составлена математическая модель определения времени запаздывания срабатывания гидроавтоматической системы гашения динамических колебаний, значение которого позволяет создавать гидроавтоматические системы гашения колебаний вовремя реагирующих на динамические внешние возмущения. Проведен расчет периода скальвания грунта при работе рыхлителя и времени запаздывания срабатывания гасителя динамических колебаний, на основе которых устанавливается способность гидроавтоматической системы гашения динамических колебаний вовремя срабатывать обеспечивая предотвращение передачи колебаний к базовой машине. Разработана гидроавтоматическая система гашения динамических колебаний, возникающих на рабочем органе, для предотвращения передачи этих колебаний к базовой машине.

**Ключевые слова:** гаситель, динамические колебания, гидроавтоматическая система, время запаздывания срабатывания, период скальвания грунта.

## Development of Ukraine Territory Flooding Processes; Its Parameters and the Influence on the Environmental Safety Level

*Olena Voloshkina, Julia Bereznitska*

Kyiv National University of Construction and Architecture  
Povitroflotskyy prosp., 31, Kyiv, Ukraine, 03680, e-mail: juli\_mmm@ukr.net

**Summary.** Shows the present state of development of flooding processes of Ukraine territory. Given filtration stages in the flooding the process of and methods of their calculation. The method of filtration resistance for calculating of the filtering in flooding process is analyzed. Shows the dependence between the development of flooding process and intensifying processes of landslides on Ukraine territory.

**Key words:** environmental safety, flooding process, groundwater level, method of filtration resistance, process of landslide.

### INTRODUCTION

Spread areas of flooding is one of the major environmental problems on the territory of modern Ukraine, in connection with which there is a need to study the causes of its origin and determine the level of environmental safety with regard to the factors that cause it.

Essential factors of the regional flooding development are:

- increase of rainfall in the last decade as a result of global climate change,
- almost total underregulation of the river network on plain areas with groundwater level's skids from 1,5-4 m to 8-10 m and a substantial reduction in the volume of water unsaturated rocks above soil water-bearing horizon, which increased the rainfall influence on the above-lying rocks water saturation,
- forming of zones of an increase technogenic feed of subsoil waters within the limits of the irrigatory systems etc.

### THE CURRENT STATE OF UKRAINE'S TERRITORY FLOODING PROCESS

From data of Government geological service the general area of flooding for 20 last the on territory of Ukraine grew twice. General data about the number of the impounded settlements and flooding areas in the Ukraine's administrative regions are listed in Table 1.

Depending on the main source of flooding and the complex of influential factors, the flooded areas of Ukraine's territory are divided into three types:

- flooding in natural conditions, according to the source natural – precipitation (thawed snow, flood and rainwater), when balance of groundwater is not broken. This type pertains Polissya (Volyn, Zhytomyr, Rivne areas and the northern part of Kyivarea), as well as the northern part of Lviv and Ternopil areas,
- naturally-technogenic flooding when groundwater balance slightly disturbed or disrupted due to increase their power, which is associated with a decrease in the natural

**Table 1.** The flooding areas in the administrative regions Ukraine

№	Administrative area	Area of flooding, ths. km <sup>2</sup>			The ratio indicators, 1982 to 2013
		1980	2010	2013	
1	Vinnytsia	0,3	0,005	0,005	2,96
2	Volyn	-	9,14	9,14	-
3	Dnipropetrovsk	1,04	7,29	7,29	7,0
4	Donetsk	0,35	0,23	1,66	8,67
5	Zhytomyr	-	0,04	0,04	-
6	Zakarpattia	-	0,001	0,001	-
7	Zaporizhia	0,73	0,01	0,01	4,37
8	Ivano-Frankivsk	-	-	-	-
9	Kiev	0,21	0,02	0,021	-
10	Kirovohrad	0,01	0,057	0,057	4,2
11	Luhansk	0,48	0,02	0,035	0,34
12	Lviv	0,15	0,25	0,261	1,43
13	Mykolaiv	0,74	17,03	17,03	17,5
14	Odessa	1,37	20,6	20,6	9,9
15	Poltava	0,81	0,15	8,5	10,4
16	Rivne	-	11,7	11,7	-
17	Sumy	0,4	0,07	0,07	1,8
18	Ternopil	-	-	-	-
19	Kharkiv	0,77	3,0	3,0	3,9
20	Kherson	0,62	11,3	11,3	16,85
21	Khmelnyskyi	0,01	0,06	0,06	-
22	Cherkasy	0,35	0,06	0,06	0,22
23	Chernivtsi	0,26	-	4,1	16,0
24	Chernihiv	0,03	0,15	0,15	5,0

territory drainage. This type occurs in the Central and southern regions of Ukraine in Dnipropetrovsk, Zaporizhya, Kharkiv, Lugansk, Donetsk and to the North of Odessa, Nikolaev and Kherson areas,

- technogenic flooding with violation of groundwater balance under the influence of economic activity, when man-made sources of flooding are dominating (irrigation systems, canals, reservoirs, ponds, in settlements – water supply and sewerage network). Plot of technogenic underflooding exist on the almost all Ukraine`s territory. The most impounded areas are: Kherson, Odesa, Mykolaiv, Dnipropetrovsk, Zaporizhia, Poltava, Kharkiv and Donetsk areas. This type of flooding is one of the most dangerous, since even in years with a low rainfall, the situation does not change.

#### STAGES OF FILTRATION IN THE FLOODING PROCESS

The forecast of raising of the ground waters when flooding and a water loss estimate on filtering from natural and artificial reservoirs on agricultural areas, requires study the main filtration stages with taking into account of the area hydrogeological conditions.

The first filtration stage is characterized by conditions of the aeration zone water saturation and achievement by a filtrational flow of ground waters level. Conditions of the such schemes existence provides an estimated water level on a surface, which is set in a fairly short time period and some time remains variable.

The first stage of filtration is characterized by the following parameters:

- time of the homogeneous soil saturation to the ground waters surface:

$$t = \frac{\mu}{k} (h_g + H_\kappa) \varphi(\alpha), \quad (1)$$

where: the function  $\varphi(\alpha)$  is defined by the equation:

$$\varphi(\alpha) = \frac{h_0}{h_g + H_\kappa} - \ln \left( 1 + \frac{h_0}{h_g + H_\kappa} \right), \quad (2)$$

where:  $k$  i  $\mu$  – the coefficient of soil filtration and the coefficient of soil insufficient saturation,  $H_c$  – the overall height of capillary water rise in the soil,  $H_\kappa$  – the height of capillary soil vacuum,  $h_g$  – the height of the soil surface flooding:

$$H_\kappa \approx (0,5 - 0,7) H_c. \quad (3)$$

The time of soil saturation by water depends on the its type (height of aeration zone in the soil) and the water level on the flooded areas.

In the absence of the outflow on the flooded areas, the time of soil saturation by water in general is pretty short.

In the outflow presence on the borders of the filtration area, groundwater motions stabilization can ensue in the lower soil layer, and groundwater level lifting to the bottom border of an upper saturated soil layer may not ensue.

In the outflow absence and in condition of infiltration stable mode presence the at the free soil surface, which may be defined by the equation:

$$\varepsilon = k_1 \frac{h_g + h_{01}}{h_{01}}. \quad (4)$$

The next filtration stage after saturation of soil aeration zone is observed for a long term of the time and is characterized by the continuing drainage structures functioning or natural outflow from territory.

The estimated scheme of the given stage is presented as the completely flooded territory, within which is located a systematic drain.

Filtration flow for such drain is calculated by the equation:

$$q = \frac{k_1 (h_g - h_g)}{\Delta L}, \quad (5)$$

where:  $\Delta L$  - filtration resistance of the drain imperfection according to the degree of opening of the aquifer thickness,  $h_g$  - water pressure (water level) in the drain.

Prediction of groundwater level rise is an important task in the calculations of territory flooding process. This is especially concerns to the territories, where surface water bodies are located, because they are the main source of groundwater supply. One of the methods of calculating the groundwater level rising near canals and reservoirs is a method of filtration resistance, which allows to bring imperfect by the type of opening of the aquifer thickness aquifer reservoirs to perfect and greatly simplify the filtration calculation technique.

In the case of the lateral outflow in open drain transient filtering mode can be observed. In this case, groundwater level lowering the in the soil slope at any moment of time can be calculated by the proposed simplified equation obtained by analytic solutions:

a) homogeneous aquifer soil layer:

$$y(x,t) = H_0 - \frac{2H_0^2}{L} \sum_{n=1}^{\infty} \left( e^{-\alpha_n C \frac{tk}{\mu H_h} t \theta \alpha_n} - 1 \right) \times \sin \alpha_n \frac{x}{H_0}, \quad (6)$$

b) two-layer aquifer soil structure:

$$y(x,t) = H_0 - \frac{2H_0^2}{L} \sum_{n=1}^{\infty} \left( R_2 - \frac{k_2}{k_1} R_1 \right) e^{-\alpha_n C t \theta \alpha_n \frac{tk_1}{\mu H_0}} \times \sin \alpha_n \frac{x}{H_0}, \quad (7)$$

where:

$$C = 1 - \frac{\varepsilon}{k_1}; \alpha_n = \frac{(2n-1)\pi H_0}{2\left(L + \frac{b}{2}\right)},$$

where:  $L$  – the distance from the drain to the filtration area boundary,  $R_2$  and  $R_1$  – dimensionless quantities, which depend on the parameters of the filtration,  $H_0$  – groundwater level on the flooded territory.

#### FEATURES OF FILTRATION RESISTANCE CALCULATING FOR FLOODING PROCESS

Definition values of the filtration resistance in the case of enclosed drains and small canals are pretty detailed researched, and there is the defined methods of their precise calculation. However, for cases of wide open reservoirs when there is a disparity:  $\frac{B_k}{m} > 2$  (where:  $B_k$  - width of the reservoir on the bottom,  $m$  - aquifer layer thickness), the value of the filtration resistance offered to accept by the approximate dependencies, that overstate the real value of the filtration resistance, which in its turn lead to a decrease in the calculated values of the groundwater levels.

Thus, there is a need of delineate of recommended in the literature formulas use, depending on hydrogeological conditions of the filtration area, for which it is necessary to investigate the changing values of the filtration resistance of the drain imperfection according to the degree of opening of the aquifer thickness calculated by the recommended formulas (1)-(4) under different hydrogeological conditions of filtering for the further their use in forecasting groundwater level on the flooded territories.

The equations for filtration resistance calculating the in cases of wide water reservoir are next:

- for the case of homogeneous aquifer soil layer:

$$\Delta L = 0,44m, \quad (8)$$

- for the case of two-layer aquifer soil structure:

a) under condition of  $k_2/k_1 \geq 10$ :

$$\Delta L = \sqrt{\frac{k_2 m_2 m_e}{k_1}}, \quad (9)$$

b) under condition of  $1 \leq k_2/k_1 < 10$ :

$$\Delta L = 0,5(h_e + m_2 + m_e \sqrt{\frac{k_2}{k_1}}), \quad (10)$$

c) under the condition of:  $\frac{k_2}{k_1} \leq 1$ ,

d)

$$\Delta L = 0,5(h_e + m_e + m_2 \frac{k_2}{k_1}), \quad (11)$$

- for the case of three-layer aquifer soil structure:

$$\Delta L = \frac{T}{T_1} \Delta L_1 - 0,5 \frac{T_3}{T_1} B_k + \frac{T_3}{T_1 c} (1 - c \overline{B_k} \Delta L_1). \quad (12)$$

In these equations:  $\Delta L$  - filtration resistance of water reservoir;  $m_e$  - upper aquifer layer thickness;  $m_2$  - the thickness of the second aquifer layer;  $h_e$  - the depth of the water in the reservoir;  $k_1, k_2$  - filtration coefficients of the first and second aquifer layers.

On the basis of the analysis of existing methodologies for determining filtration resistance have been constructed dependences, presented in Fig. 1-3.

#### ENVIRONMENTAL SAFETY LEVEL OF FLOODED TERRITORIES IN DEPENDENCE WITH LANDSLIDE PROCESS

Development of the territory flooding processes is one of the leading factors of reduce of the bearing capacity of soil slope upper part, which activates landslides. In recent years there has been a rapid increase of landslide processes on the territory of Ukraine – up to the 23100 objects with the doubling of its number in the last 30 years.

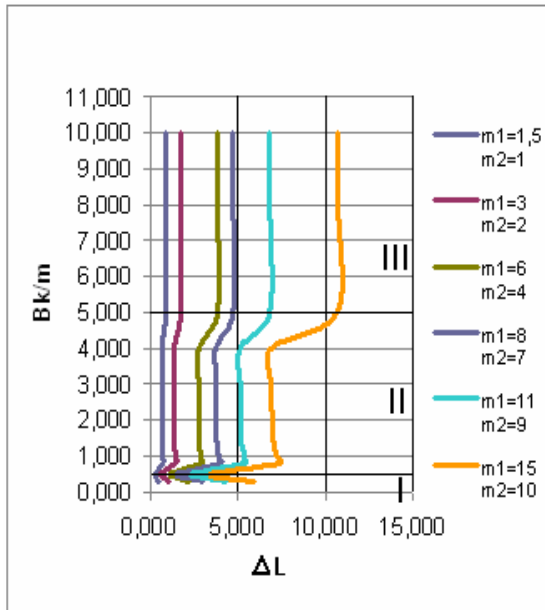


**Fig. 1.** Value of the filtration resistance for case of homogeneous aquifer soil layer

In this figure: zone I - water flow is calculated by analogy with round drain for a case of open channels with the small width of the channel on the bottom under condition of the  $B_k/m \leq 0,5$ ; zone II - for medium-sized channels under condition of the  $0,5 < B_k/m < 5$ ; zone III - for channels with large sizes for under condition of the  $B_k/m \gg 5$ .

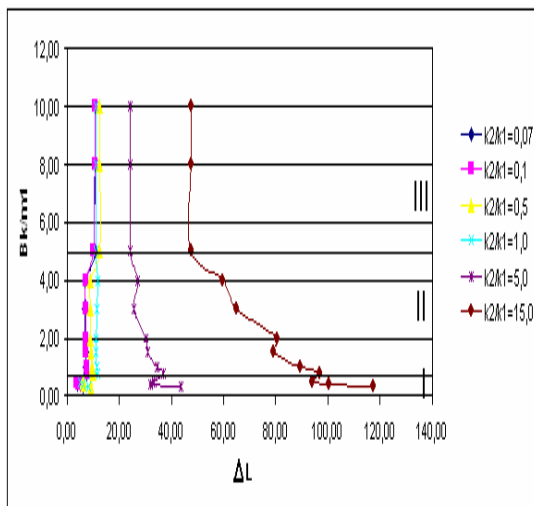


**Fig. 2.** Value of the filtration resistance for the case of the two-layer aquifer soil structure with the different ratios of filtration coefficients

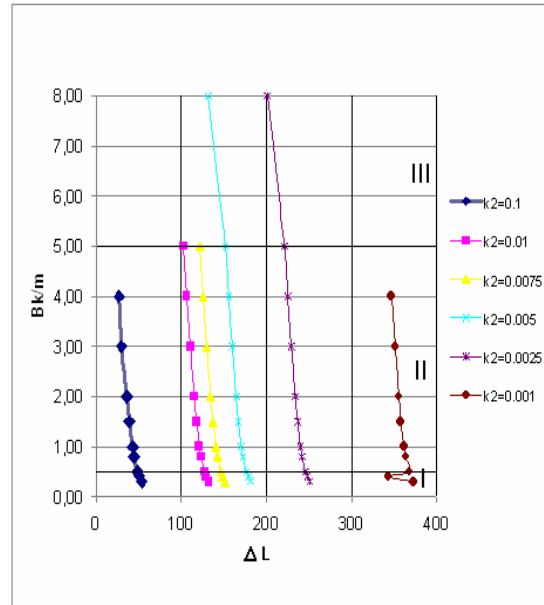


**Fig. 3.** Value of the filtration resistance for the case of the three-layer aquifer soil structure with the different ratios of filtration coefficients

When considering the risk of landslide processes in time, it should be noted that under the condition of other immutable weight coefficients the largest impact on the slopes sustainability has a process of regional water-balance equilibrium breaking in the upper zone of the geological environment, i.e. the regional revitalization of flooding processes. There is a direct dependence between the generalized data about progress of landslides depending on progress of territory flooding processes.

The Table 2 shows data on areas of flooding and landslides on the administrative distribution on the Ukraine territory of for 1982-2013.

The annual probability of dangerous geological processes such as landslides, within a 1 km<sup>2</sup> is defined by the formula:

$$K_{dgp} = K_{sc} K_t, \quad (13)$$

where:  $K_{sc}$  – the factor of spatial areas contamination (% of total landslide areas  $f_{tl}$  within the general area that is considered):

$$K_{sc} = \frac{f_{tl}}{f}, \quad (14)$$

**Table 2.** The data on areas of flooding and landslides on the administrative distribution on the Ukraine territory of for 1982-2013

№	Administrative area	1982-1984		1997 pik		2006 pik		2013 pik	
		Area of flooding, ths. km <sup>2</sup>	The number of land-slides	Area of flooding, ths. km <sup>2</sup>	The number of land-slides	Area of flooding, ths. km <sup>2</sup>	The number of land-slides	Area of flooding, ths. km <sup>2</sup>	The number of land-slides
1	2	3	4	5	6	7	8	9	10
1	Vinnitsia	0,3	234	0,895	225	8,96	338	0,05	339
2	Volyn	-	-	12,9	-	13,91	-	9,14	-
3	Dnipropetrovsk	1,04	214	7,28	303	7,3	382	7,29	382
4	Donetsk	0,35	123	3,03	125	3,04	188	0,23	189
5	Zhytomyr	0,02	10	19,75	11	20,13	10	0,04	10
6	Zakarpattia	-	1278	3,02	1596	3,02	2880	0,01	3274
7	Zaporizhia	0,73	244	3,19	218	3,2	205	0,01	206
8	Ivano-Frankivsk	-	487	0,008	1005	0,008	769	-	805
9	Kiev	0,21	764	8,1	816	8,1	790	0,02	814
10	Kirovohrad	0,01	99	0,14	95	0,142	143	0,01	140
11	Luhansk	0,48	564	0,16	593	0,164	1138	0,03	769
12	Lviv	0,15	421	0,21	524	0,116	1289	0,25	1347
13	Mykolaiv	0,73	707	12,82	985	17,767	1150	17,3	1148
14	Odessa	1,37	938	13,52	5167	19,685	5885	20,6	5835
15	Poltava	0,81	732	8,5	761	8,5	824	0,15	824
16	Rivne	0,01	-	12,79	-	12,8	-	11,7	-
17	Sumy	0,4	397	0,42	490	0,474	567	0,07	567
18	Ternopil	-	54	-	119	-	117	-	117
19	Kharkiv	0,77	518	3,02	851	3,02	1659	0,12	1615
20	Kherson	0,62	37	10,45	63	11,945	43	11,3	43
21	Khmelnyskyi	0,02	364	-	203	0,014	425	0,06	420
22	Cherkasy	0,35	685	0,08	810	0,08	1034	0,06	1033
23	Chernivtsi	0,03	1272	0,42	1435	0,4	1622	-	1468
24	Chernihiv	0,4	8	4,4	11	4,4	11	0,15	9

t - the coefficient of the temporal landslides development dynamics, or frequency activation processes for a specific period of time T, determined by the formula:

$$K_t = \frac{1}{T}, \quad (15)$$

and depends on the complex of effects and anthropogenic factors within territory that is considered. Taking into account the impact of stabilization systems and engineering protection measures (which are calculated, as a rule, for a period of up to 30 years), in formulas also introduced the corresponding coefficient:

$$K_e = \frac{30}{T^t}, \quad (16)$$

where:  $T^t$  – small cycle of landslides activation.

For the conditions of the development of geographically distributed dangerous exogenous geological processes should be taken into account the density of the building on the landslide territories  $K_{poi}$  and population density within the territorial estimation.

When calculating the individual risk of landslide processes activation on built-up flooded territories it is necessary to consider differentiated approach of build-

ing density landslide areas  $K_{pol}$  in the areas. Its value is offered to be taken by the formula:

$$K_{pol} = \frac{S_{a.f.}}{S_{t.a.}}, \quad (17)$$

where:  $S_{a.f.}$  – the area of flooding in the localities of the oblast,  $S_{t.a.}$  – total area of the flooding area.

The value of the coefficient  $K_{pol}$  built in Table 3.

Individual life risk from dangerous exogenous processes is calculated by the formula:

$$R_{ind} = d \times K_{sc} \times K_t \times K_{pol} \times K_{SF} / (K_c N),$$

where:  $d$  i  $N$  – the density of population and the total citizen number in the territory which is considered,  $K_{SF}$  - the activation of landslides due to flooding process.

Using the data given in Table 3, were calculated the rates of increase in the flooded areas and landslides in years for those Ukrainian areas, where landslide process is most active (Table 4). Based on these calculations,

**Table 3.** The value of the coefficient  $K_{pol}$

№	Administrative area	The value of the coefficient $K_{\text{заб}}$
1	Vinnitsia	0,1
2	Volyn	0,012
3	Dnipropetrovsk	0,013
4	Donetsk	0,04
5	Zaporizhia	0,22
6	Kirovohrad	0,0065
7	Luhansk	0,61
8	Mykolaiv	0,03
9	Rivne	0,018
10	Khmelnyskyi	0,96
11	Chernihiv	0,005
12	Ukraine	0,014

**Table 4.** The rates of increase flood areas and landslides

Administrative area	Odessa	Mykolaiv	Zakarpattia	Ukraine
Increasing the area of flooding, attitude indicators 1997. indicators in 1982, times	9,89	17,56	3	13,6
Increasing the number of landslides, attitude indicators 1997. indicators in 1982, times	5,5	1,39	1,25	1,58
Increasing the area of flooding, attitude indicators 2006. indicators in 1997, times	1,46	1,38	1	1,01
Increasing the number of landslides, attitude indicators 2006. indicators in 1997, times	1,14	1,17	1,8	1,32
Increasing the area of flooding, attitude indicators 2013. indicators in 2006, times	1,04	0,96	1,0	0,6
Increasing the number of landslides, attitude indicators 2013. indicators in 2006, times	1,0	0,99	1,14	0,99
Increasing the area of flooding, attitude indicators 2013. indicators in 1982, times	15,0	23,33	3,0	8,26
Increasing the number of landslides, attitude indicators 2013. indicators in 1982, times	6,22	1,62	2,56	2,1

it is possible to deduce dependence between an increase of landslips quantity and an increase of the flooding area through coefficient  $K_{\text{IIA}}$ . The coefficient of landslips activation of due to flooding process  $K_{\text{SF}}$  is determined separately for each area.

## CONCLUSIONS

Progressive development of the flooding process on the Ukraine territory leads to a further study of the causes of its occurrence, as well as the impact of this process on the quality of the major life-supporting resources in order to increase the level of environmental safety.

The analysis of existing methods of calculating filtration stages of flooded territories indicates the need for further and more detailed study of this process.

A method of filtrational resistance used for calculation of filtering on flooded territories in detail studied for closed drains and narrow channels, whereas for broad channels this method amounts to a simplified formula. According to the calculations on these formulas with increasing the width of the channel increases the filtration resistance, and thus the value calculated levels of groundwater will fall.

In the case of  $k_2/k_1 \leq 1$  the simplify of aquifer structure to the homogeneous leads for inflating the values of filtration resistance which is undesirable, because when calculating the level groundwater it will lead to underestimated values of them; in the case of  $k_2/k_1 > 1$  the simplify of the aquifer structure to homogeneous leads the understatement of the value of the filtration resistance and in such cases groundwater levels are calculated with some margin.

A preliminary analysis showed that taking into account the magnitude of the filtration resistance for coastal areas flooded by water reservoir requires further studies under different hydrogeological conditions and different modes of filtration.

The process of regional flooding in its turn is one of the leading factors boosting landsliding processes on the territory of Ukraine. Analysis of annual monitoring data of flooded territories and activating of landslides on the administrative areas allowed to enter an additional factor, which takes into account the increased risk of landslides caused by raising the groundwater level in built-up areas.

## REFERENCES

1. **Oleynik A.Y., Voloshkina E.S. 1985.** Calculation of a non-stationary filtration to a slope of the imperfect channel in view of инфильтрации on a free surface. Moscow, Reports of the Academy of Sciences of the Ukrainian SSR, Nr 5, 43-45.
2. **Oleynik A.Y. 1981.** Geohydrodynamics of a drainage, Kiev, Naukova dumka, 283.
3. **Trofimchyk A.N., Khakyuh Y.I., Glebchuk H.S. 2008.** Mathematical modeling of the slope sustainability at rise of the groundwater levels, Ecology and resources, Kiev, Institute of problems of national security of Ukraine, Vol. 18, 51-58.
4. **Voloshkina E.S. 1987.** Definition of filtrational parameters of inflow to the open drainage channels working in conditions of a variable water level in a vein of. Irrigation and Water Management, Kiev, Vol. 66, 67-70.
5. **Iakovlev E.O., Voloshkina O.S., Khopkha P.M. 2005.** Impact factors of modern regional flooding of Ukraine territory in the formation of national threats. Ecology and resources, Kiev, Institute of problems of national security of Ukraine, Vol. 12, 15-36.
6. **Voloshkina O.S., Bereznitska Y.O. 2010.** Application of the method of the filtration resistance when calculating groundwater level of the flooded areas. Environmental safety and management, Kiev, Kiev national university of construction and architecture, National academy of sciences of Ukraine, Institute of telecommunications and global information space, Vol. 5, 75-83.
7. **Mellander P.-E., Jordan P., Wall D.P. 2012.** Delivery and impact by pass in a Karst aquifer with high phosphorus source and pathway potential. Water Research, Vol. 46, 2225-2236.
8. **Bychenok M.M., Rohogin O.G., Iakovlev E.O. 2004.** On the assessment of risk of life

- and management in the natural and man-made environment. Ecology and resources, Kiev, Institute of problems of national security of Ukraine, Vol. 10, 136-143.
9. **Glebchuk H.S. 2005.** Investigation of the influence of the hydrographic network density and regional flooding process on the dynamics of landslides in Kharkiv area. Ecology and resources, Kiev, Institute of problems of national security of Ukraine, Vol. 11, 174-179.
  10. **Bereznytska Y.O., Iakovlev E.O., Voloshkina O.S. 2013.** Environmental risk of the landslide process in the flooded slope. Ecological safety and balanced natural resources management, Vol. 1(7), 85-19.
  11. **Vetrova N.** Ecological audit and ecological monitoring in environmental safety of a region. Motrol: kom. Mot. Energ. Roln., OL PAN, Vol. 14 (1), 80-85.

РАЗВИТИЕ ПРОЦЕССОВ ПОДТОПЛЕНИЯ  
НА ТЕРРИТОРИИ УКРАИНЫ;  
ОЦЕНКА ЕГО ПАРАМЕТРОВ И ВЛИЯНИЯ  
НА УРОВЕНЬ ЭКОЛОГИЧЕСКОЙ  
БЕЗОПАСНОСТИ

**Аннотация.** Рассмотрено современное состояние развития процесса подтопления на территории Украины; приведены стадии фильтрации в процессе подтопления и методы их расчета. Проанализирован метод фильтрационных сопротивлений при расчете фильтрации в процессе подтопления. Показана зависимость развития процесса подтопления и оползневых процессов на территории Украины.

**Ключевые слова:** экологическая безопасность, процесс подтопления, уровень грунтовых вод, метод фильтрационных сопротивлений, оползневые процессы.



## The Risk Assessment of Threats from Biological Objects in Environmental Safety

*Tetiana Kryvomaz, Olena Voloshkina*

Kyiv National University of Construction and Architecture  
Povitroflotskyy prosp., 31, Kyiv, Ukraine, 03680, e-mail: ecol@i.ua, stf@knuba.edu.ua

**Summary.** Necessity to present results of scientific research in an accessible form for proper interpretation by public and environmental safety experts has been shown. Myxomycetes ecology and metabolism to verify their safety for human health has been evaluated as an example. Bayesian methods for probability analysis is proposed to be used for risk assessment. The "Environmental safety passports of species" are recommended for evaluation of impact of each species on the environment, humans and other living organisms.

**Key words:** environmental safety, risk assessment, myxomycetes, ecological passport.

### INTRODUCTION

Improvement of methods for evaluation and display of environmental risk is necessary for operational changes analysis in the environment, to show the dynamics and predict the possible consequences on the health of the population. Living organisms play a key role in the transformation in nature, they are able to enhance and reduce the impact of negative factors on the environment, human and other natural objects [6]. Also living organisms can be of danger for environment or people health so it is very important to make correct evaluation of threat from them. The problem is that biological scientific information not always has correct interpretation in ecological safety study. For example, the article about dangerous properties of slime mold for human health [13] was surprising for all scientists who study myxomycetes. Slime molds (myxomycetes) are fungus-like protozoa, which is mainly associated with remains of woody microhabitats [4], but was never found in human body. That article has not presented verification of reliable proof

base about pathogenic internals of myxomycetes, so scientists are unlikely to perceive such information seriously. But because these organisms are poorly-known by public, people were very amazed by the idea about a new causer of "all illness" and wrong information is quickly spread through mass-media and Internet. As a result some patients take treatment against "very dangerous" myxomycetes, insist to found the real cause of their illness and have a proper treatment. This example shows the necessity to present results of scientific research in an accessible form for public display in order to avoid ambiguity. The proper interpretation of investigations is especially important in environmental safety, because it may affect the accuracy of decision-making measures to ensure the safety of the population and environment.

### PURPOSE OF WORK

The objective of this study is found the way of evaluation of threats from biological objects to environment, human and other

living organisms. According with this purpose, myxomycetes are used as a model organism to find the way of risk assessment of environmental safety threats. For assessment of their danger for human health Bayesian methods are used for probability analysis that studies their distribution, ecology and metabolism.

## MATERIAL AND METHODS

Material for this study is result of myxomycetes research for more than 20 years in their native habitats in Ukraine: 1643 samples from field collections, herbarium of M.G. Kholodny Institute of Botany NAS of Ukraine and literature sources about distribution of myxomycetes in Ukraine (278 species total) [4]. There are near a thousand species of myxomycetes total known in over world.

Bayesian rule is used for analysis probability to find species of myxomycetes on reputed substratum used:

$$P(M | E) = \frac{P(E | M)}{\sum_m P(E | M_m)P(M_m)} * P(M), \quad (1)$$

where:

$|$  – a conditional given probability,

$E$  – the evidence corresponds to new data that were not used in computing the prior probability,

$M$  – event represented model,

$P(E | M)$  – the conditional probabilities are specified to define the models,

$P(M_m)$  – the degree of belief in  $M_m$ .

For discover possibility to find myxomycetes on before unknown substratum use additive Laplace smoothing is a technique used to smooth categorical data. Given an observation  $x = (x_1, \dots, x_d)$  from a multinomial distribution with  $N$  trials and parameter vector  $\theta = (\theta_1, \dots, \theta_d)$ , a "smoothed" version of the data gives the estimator:

$$\hat{\theta}_i = \frac{x_i + \alpha}{N + \alpha d} \quad (i=1, \dots, d), \quad (2)$$

where:

$\alpha > 0$  is the smoothing parameter ( $\alpha = 0$  corresponds to no smoothing). Additive smoothing is a type of shrinkage estimator, as the resulting estimate will be between the empirical estimate  $x_i / N$ , and the uniform probability  $1/d$  [18].

The control action generally is represented in the form of a functional:

$$R = F\left(x_i, v_i, \frac{dx_i}{dt}, \dots, \frac{dv_i}{dt}, \dots, \int x_i dt, \dots, \int v_i dt\right), \quad (3)$$

where:

$x$  – a controlled variable,

$v$  – parameter of external influences,

$dx/dt$  and  $dv/dt$  – derivatives on a time from parameters of regulating and external influences, accordingly, that is velocities of a modification of parameters,

integrals on a time from parameters of regulating and external influences, that is the accumulated modifications of parameters [14].

## RESULT OF RESEARCH

Myxomycetes (slime molds) in different stages of their life cycle are presented as spores, myxamebaes, flagellate cells, plasmodium and fruiting bodies. Myxomycetes tend to be rather inconspicuous in their occurrence. This stage also includes myxamebaes and flagellate cells. From plasmodium after a period of feeding and growth then fruiting bodies develop in a drier and more exposed location. Fruiting bodies of most species are relatively ephemeral and do not persist in nature for very long. These fruiting bodies containing numerous spores which can be dispersed by wind and will eventually germinate and develop into a plasmodium under suitable conditions. Myxomycetes spend a portion of their life cycle in a state where their very presence in a given habitat can be exceedingly difficult if not impossible to determine.

Analyses of substratum where fruiting bodies of myxomycetes in Ukraine were find

show the following distribution: 42% - on destroying dead wood (xylophilic), 20% - on forest floor litter (litterophilic or deciduophilic), 20% - on bark of living trees (corticolous), 7% - on mosses (bryophilic) and 2% - on living herbal plants (herbophilic). Sometimes myxomycetes fruiting bodies (until 1% of total biota) possible to found on dung of herbivorous animals (coprophilic), on fungi fructifications (mycophilic), on lichen (lichenophilic), and even on soil or stone (geophilic). Also 8% of myxomycetes species belong to nivicolous ecological group, occurring at the edge of melting snow in mountain high altitude in the Carpathians in early spring [5]. This ecological group divides by phenology and physiology, but substratum preference show nivicolous myxomycetes as deciduophilic and herbophilic. The diagram of myxomycetes fruiting bodies distribution by type of substratum was made according with these data (fig. 1). Nivicolous myxomycetes were divided equally between deciduophilic and herbophilic, then substratum groups of herbophilic and bryophilic were integrated.

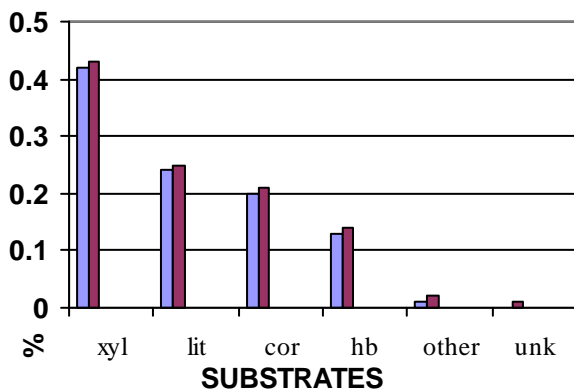


**Fig. 1.** The distribution of myxomycetes fructifications by type of substratum: xyl – xylophilic, lit - litterophilic (deciduophilic and half of nivicolous), cor – corticolous, hb - herbophilic (includ bryophilic and half of nivicolous), other - coprophilic, mycophilic, lichenophilic, geophilic et al.; unk – unknown substratum up to now; ■ – real data; ■ – data with additive Laplace smoothing

As we can see, myxomycetes sporocarps have never been found on or inside human body. Additive Laplace smoothing (2) gives 1% probabilities to find myxomycetes on be-

fore unknown substratum. Also the same frequency added to the each substratum types where myxomycetes sporocarps were really found. Calculation according to Bayesian analysis (1) gives around  $10^{-5}$  probability for all unbelievable substrates for myxomycetes. This probability includes volcano, vacuum, human body and other millions of habitats, where fruiting bodies of myxomycetes were never found before. Each of hypothetical microhabitats reduces such events probability by exponentially. So chance to find myxomycetes sporocarps on or inside human organism is negligibly small. Even this tiny chance can't be used, because for creating fruiting bodies myxomycetes need more or less dry substratum and sun shine, but inside human body there are no suitable conditions for this. Any organism can't become parasitic without effective reproducing strategy inside of host body, so myxomycetes can't be dangerous for people. For hundreds of years of myxomycetes study only a few very exotic cases were registered of finding myxomycetes sporocarps on living animals: *Physarum pusillum* on lizard, *Arcyria stipata* on snail shell and *Diderma effusum* on aquarium fish. The *Corytophanes cristatus* belongs to the lizard who most part of their life don't move waiting for prey and as a result on the skin of this animal not only myxomycetes sporangia is found, but also moss and other vegetation [21]. Sporangium of *Arcyria stipata* on shell can't make damage to snail, because it even doesn't touch the body of snail. Phaneroplasmodia of *Diderma effusum* were observed feeding on green algae and diatoms submerged in water in an aquarium as result of a laboratory experiment. This species submerged in water and growing on agar culture. Portions of the plasmodium were also observed adhering to the skin surface of an eel-like fish in the aquarium [19]. All these exceptional cases only prove the rule that myxomycetes don't have a habit to create fruiting body on living animals and it is absolutely impossible for them to do it inside human body.

Sporocarp stage is short and ephemeral for slime molds. Most part of their life cycle

myxomycetes exist as vegetative stage presented by mobile free-living plasmodium and as spores. Myxomycetes are fundamentally terrestrial organisms and they have a significant impact on the species diversity of soil microorganisms. Plasmodium typically lives in cool and shady moist places and feed on bacteria, protozoa, yeast cells, fungi, organic remains, and etc. It is very inconspicuous in their occurrence inside destroyed wood and in soil and it is rather difficult to find plasmodium in nature. Plasmodium can't crawl into human body itself being unnoticed, only if people eat them especially. In Mexico people prepare exotic food from big plasmodium *Fuligo septica* [16]. In 4 Amazonian communities of Ecuador mythical, food, medicinal and recreational use of 3 myxomycetes species recorded: *Arcyria denudata*, *A. cinerea* and *Lycogala epidendrum*. They are used *Lycogala epidendrum* medicinally by rubbing the myxomycetes aethalia in skin infections and also they call this species "fungus for eating" and is eaten raw [3]. The plasmodium can't live and give fructification in human body, because it is quickly destroyed by enzymes. On myxomycetes feed insects, fungi, slime and invertebrates. Some spores go through beetles guts and it is example of mutual advantage, because it help to myxomycetes distributions. But slime molds spores never grow up in guts of living animals [10]. A few myxomycetes spores can be got by breathing with air, but human immune system has very strong protection against bioactive metabolites of myxomycetes. It was confirmed by allergy prick testing, which shows sensitization to myxomycetes [7]. But myxomycetes can't become strong allergen, because concentration of their spore in air is so low, that it is very difficult to inbreathe enough number of spores to cause allergy reaction. The best focus group for study allergy from myxomycetes is myxomycetologists, people who permanently work with these organisms in the field and in laboratories. Preliminary study of their allergy reaction on myxomycetes spores found is only one real case of sensitization. It confirms that myxomycetes

have no chance to become real dangerous allergen.

Almost 100 natural compounds were described from myxomycetes including their chemical structures and biological activities: lipids, fatty acid amides and derivatives, alkaloids, amino acids and peptides, naphthoquinone pigments, aromatic compounds, carbohydrate compounds, terpenoid compounds [2]. Myxomycetes plasmodia and sporocarps have biological activity against micro-pathogens *Candida* [8]. Red colored sporophores of *A. denudata* contain major pigments alkaloids arcyriarubins and arcyriaflavins, which are new lead structures for the synthesis of biologically active substances and show highly potent biological effects. Arcyriaflavin derivatives have antimicrobial activity against *Bacillus cereus* and antitumor activity against leukemia cells [2]. Arcyriaflavin analogues are currently being evaluated in human clinical trials as anticancer drugs [15].

All these dates show that myxomycetes can be classified to the group of the living organisms with lowest danger probability for human health.

## DISCUSSION

This research is to show that myxomycetes are not dangerous for humans. Also on this example we can see that even such innocuous organisms can be under distrust. Such situation is not unique only for myxomycetes and can happen with any living organisms. Wrong evaluation of dangerous level can have unpredictable and far-reaching effects on safety of human, other living organisms and on environment in general. It shows necessity of scientific information to be presented in the way which can be understandable for all stakeholders of groups to avoid improper interpretations. For this reason we propose to implement a system of safety certification of all living organisms. The myxomycetes were proposed to be used as model objects to develop patterns of environmental safety passports of species. The

reason of such a choice is justified by morphology, physiology, biochemistry and phylogeny of myxomycetes and by their wide distribution in different habitats of different regions of the world.

These organisms combine inherent features of fungi and protozoa, but now there is general agreement that their true position is among the protozoa. However they are covered by the same nomenclatural code, and are listed in mycology's main reference work. So it is give possibility to work out of certification structure for both kingdoms.

It is possible to see most myxomycetes species by naked eye, but special equipment is needed for studying details of their morphology and for discovering species of the size less than 1 mm. So they have intermediate position between macroscopic and microscopic organisms. This factor also supports choosing myxomycetes as a model organism for certification, because it helps to find the universal common model for certification.

Myxomycetes are easy to be cultivated in a laboratory on agar and other substrates. This gives possibility to study their reactions on different influences. Their full life cycle takes rather short time and transformation from plasmodium to mature sporocarps can last for just a few days. These features make myxomycetes excellent model objects, which are very often used for a wide range of scientific researches.

Myxomycetes occur in all spheres of nature on different stage of their life cycle: soil, air and less in water. Study DNA from soil shows that myxomycetes (including protostelids and dictyostelids) are dominating group of protists in this habitat, where they are presented as spores, plasmodium and myxamoebas. DNA analyses show also presence of myxomycetes in water, probably in stage of spores [17]. Lower atmospheric levels with vegetation give best condition for the development of myxomycetes fruiting body and to distribute their spores by air. So data for environmental certification of slime molds can be extrapolated to other organisms living in soil, air and even water. Myxomycetes are distributed nearly in all terrestrial

ecosystems worldwide from Antarctica to desert. Approximately 30% of the species are cosmopolitan, but they are the most common in temporary zones of North Hemisphere, where moisture and decaying organic matter are available [17]. Temperature and humidity are the main factors that regulate myxomycetes distribution and abundance. They are widespread in various habitats in the world, which is also a significant argument for choice slime molds as a model object for environmental certification.

The role of myxomycetes role in ecosystems is not studied enough yet. They help to keep bacterial levels and are important for nutrient cycling and forest productivity. Slime molds have ability to decompose plant matter and absorb nitrogen and heavy metals. This shows their potential use for bioremediation and pollutant removal. Myxomycetes can be used as air quality indicators of natural ecosystems and urban areas. Also they are indicators for evaluation of forest ecosystem condition. As we can see from this research, myxomycetes are not dangerous for human health and it gives possibility to discover their internals, which can be useful for people.

Myxomycetes are excellent model for genetic, biochemistry, biophysics, bionic, bioengineering and other researches. For example, *Physarum polycephalum* is an extensively studied system in biophysics. The plasmodial stage is of particular interest, since it exhibits, despite the relatively simple organization of this unicellular organism given an external stimulus, the plasmodium optimizes its cell shape, vein network and growth with respect to transport efficiency, robustness with respect to link deletion and avoidance of unfavorable conditions. Also remarkable phenomenon is the synchronization of the contraction patterns in the tubular vein network that generates shuttle streaming to distribute nutrients efficiently throughout the organism. From the perspective of biophysics it is natural to consider these phenomena in the framework of self-organized complex systems [11].

The plasmodium of *Physarum polycephalum* changes its shape as it crawls over a plain agar gel and, if food is placed at two different points, it will put out pseudopodia that connect the two food sources. Plasmodia were able to find the shortest path between two food sources placed at the exits of a labyrinth. Here we show that this simple organism has the ability [9].

Plasmodium creates networks to connect food sources with incredible efficiency to reproduce public transport networks on the scale of a petri dish. *Physarum polycephalum* forms networks with efficiency, tolerance and cost comparable to those of real-world infrastructure networks (Tokyo rail system). The core mechanisms needed for adaptive network formation can be captured in a biologically inspired mathematical model that may be useful to guide network construction in other domains [20].

Recently an interest in technological developments started to move away from solid materials to soft matter implementations and bio-inspired and hybrid implementations: bio-mimetic sensors which employ a conductive fluid encapsulated in elastic container and use deformation of the elastic container in transduction, carbon nanotube filled elastomers, polymer hair cell sensors. An experimental laboratory implementation of *Physarum polycephalum* was designed based on tactile bristles. The plasmodium responds to repeated deflection of bristle by an immediate high-amplitude spike and a prolonged increase in amplitude and width of its oscillation impulses. The signal strength of myxomycetes tactile bristle sensor averages near six for an immediate response and two for a prolonged response [1].

Myxomycetes use an externalized spatial memory to navigate in complex environments. *Physarum polycephalum* constructs a form of spatial memory by avoiding areas it has previously explored. This mechanism allows the slime mold to solve the U-shaped trap problem — a classic test of autonomous navigational ability commonly used in robotics requiring the slime mold to reach a chemoattractive goal behind a U-shaped bar-

rier. Drawn into the trap, the organism must rely on other methods than gradient-following to escape and reach the goal. The spatial memory enhances the organism's ability to navigate in complex environments. It is a unique demonstration of a spatial memory system in a nonneuronal organism, supporting the theory that an externalized spatial memory may be the functional precursor to the internal memory of higher organisms [22].

All these examples show that myxomycetes are very popular model objects in various researches. Their unique characteristics give possibility for slime molds to be used for working-out with structure of “Environmental safety passports of species” as a biological system model. This structure can be adapted for certification of other groups of organisms, in accordance with their morphology and characteristics of metabolism.

#### ENVIRONMENTAL SAFETY PASSPORT OF SPECIES

“Environmental safety passports of species” (ESPS) are necessary for effective monitoring and management of environmental safety. Implementation of species certification will increase the level of control in the system of ecological safety and effectiveness of protection actions for environment and humans. The main purpose of the introduction of passports is to systematize scientific information for determination of effect of this species on the environment, humans and other living organisms. The new system will enhance control level of species metabolism and improve the effectiveness of environmental protection. ESPS is a comprehensive document which is necessary for all species of living organisms. Such passport describes relationship between these species, other organisms and human with evaluating threatens from all sides. There are also analyses of impacts of abiotic factors from habitat to species vital activity to show range of tolerance, optimum, minimum and maximum value of each factor. The conclusion will be

made about real and potential risks associated with this species for other organisms, human and environment. The recommendations will be designed for reduction or prevention of such risks. Also threats will be evaluated for this species from other organisms, human and different environmental factors. According to them the strategy plan of species protection will be developed.

ESPS summarize data of scientific researchers from different fields of science in any accessible way. Certification will provide the most comprehensive information about safety aspects of the species from reliable sources of information. All available data about each species of living organisms will be conveniently structured in such passport. ESPS will have an open structure for addition of new data from experts. In such way scientific information becomes available to a wide range of stakeholders and it helps to avoid wrong interpretations and systematization of environmental safety will be reinforced.

This minimizes the possibility of incorrect interpretation of scientific data and the conditions for constructive interaction between scientists and managers.

Introduction of ESPS will improve the system of environmental safety for the effectiveness of measures enhancement to protect the nature and people.

## CONCLUSIONS

1. Correct evaluation of threats from biological objects to environment, human and other living organisms is very important for environmental safety.

2. Analysis of myxomycetes habitats, ecology, distribution and metabolism show that these organisms can't be really dangerous for health of people.

3. In environmental safety Bayesian methods for probability analysis is perspective methodology for evaluation of risk assessment of threats from biological objects to environment, human and other living organisms.

4. For proper interpretation of results of biological research in environmental safety the implementation of "Environmental safety passports of species" is proposed, which include veracious scientific information about these organisms and evaluation of risk probability.

5. Myxomycetes are suitable for being used as a model organism in process of development of "Environmental safety passports of species" structure.

## REFERENCES

1. **Adamatzky A. 2014.** Tactile Bristle Sensors Made With Slime Mold. *IEEE Sensors journal*, vol. 14, Nr 2, 324-332.
2. **Dembitsky V. M., Rezanka T., Spízek J., Hanus L.O. 2005.** Secondary metabolites of slime molds (myxomycetes). *Phytochemistry*, Nr 66(7), 747-769.
3. **Gamboa-Trujillo P., Grefa G., Uwinjin P., Piyaguaje D., Cavalcanti L.H. 2011.** Myxomycetes of Ecuador: Ethnomycological Notes. *Proc. 7th International Congress on Systematics and Ecology of Myxomycetes*, Recife, Brazil, 119.
4. **Krivomaz T.I., Dudka I.O. 2011.** Myxomycetes of Ukrainian forests. *Proc. 7th International Congress on Systematics and Ecology of Myxomycetes*, Recife, Brazil, 87.
5. **Krivomaz, T.I., Michaud, A. & Minter, D.W. 2010.** Nivicolous Myxomycetes. *IMI Descriptions of Fungi and Bacteria*, Set 184, Nr 1831-1840, 1-37.
6. **Krivomaz T.I. 2014.** First steps in myxomycete conservation activities. *Fungal Conservation*, Nr 4, 35-39.
7. **Lierl M.B. 2013.** Myxomycete (slime mold) spores: unrecognized aeroallergens? *Ann Allergy, Asthma & Immunology.*, Nr 111(6), 537-541.
8. **Lima V.H.M., Guimarães L.L., Albuquerque S.S.M.C., Cavalcanti L.H. 2011.** *Proc. 7th International Congress on Systematics and Ecology of Myxomycetes*, Recife, Brazil, 110.
9. **Nakagaki T., Yamada H., Tóth Á. 2000.** Maze-solving by an amoeboid organism. *Nature*, № 407, 470.
10. **Perkovsiy E.E., Krivomaz T.I. 2000.** Features of myxomycetes feeding on beetles of subgenera *Cyphocele* and *Neocele* of genus

- Agathidium* (Coleoptera, Leioididae). Bulletin of Zoology, vol. 34, Nr 1–2, 103–108.
11. **Radszweit M., Engel H., Bär M. 2014.** An active poroelastic model for mechanochemical patterns in protoplasmic droplets of *Physarum polycephalum*. PLoS ONE, 9(6), 1-32.
  12. **Reid C.R., Beekman M., Latty T., Dussutour A. 2012.** Slime mold uses an externalized spatial “memory” to navigate in complex environments. PNAS, Vol. 109, Nr 43, 17490-17494.
  13. **Sacharchuk I.I. 2009.** Epidemiology of lihogala slime mold fungus in terms of predicting cancer in Ukraine. Internal Medicine, Nr 3(15).
  14. **Saliev E. 2013.** Reliability of the functioning of the water supply and sewerage system. Model, Vol 15, Nr 5, 53-60
  15. **Steglich W. 1989.** Slime moulds (Myxomycetes) as a source of new biologically active metabolites. Pure & Appl. Chem., Nr 61 (3), 281–288.
  16. **Stephenson S.L., Stempen. H. 1994.** Myxomycetes: a Hand-book of Slime Molds. Portland, Timber Press, 183.
  17. **Stephenson, S.L. Novozhilov, Yu.K., Schnittler, M. 2000.** Distribution and ecology of myxomycetes in high-latitude regions of the northern hemisphere. J. Biogeogr., Nr 4, 741–754.
  18. **Stone J.V. 2013.** Bayes’ Rule: A Tutorial Introduction to Bayesian Analysis. Sebtel Press, 170.
  19. **Tamayama M. Keller H.W. 2013.** Aquatic Myxomycetes. Fungi, Nr 6 (3), 18–24.
  20. **Tero A. Takagi S., Saigusa T., Ito K., Beber D.P., Fricker M.D., Yumiki K., Kobayashi R., Nakagaki T. 2010.** Rules for biologically inspired adaptive network design. Science, Nr 327 (5964), 439–442.
  21. **Townsend J.H., Aldrich H.C., Wilson L.D., Cranie J.R. 2005.** First report of sporangia of a myxomycete (*Physarum pusillum*) on the body of a living animal, the lizard *Corytophanes cristatus*. Mycologia, Nr 97(2), 346–348.
  22. **Umedachi T., Idei R., Nakagaki T., Kobayashi R., Ishiguro A. 2012.** Fluid-Filled Soft-Bodied Amoeboid Robot Inspired by Plasmodium of True Slime Mold. Advanced Robotics, Nr 26 (7), 693-707.

#### ОЦЕНКА РИСКА УГРОЗ СО СТОРОНЫ БИООБЪЕКТОВ В СФЕРЕ ЭКОЛОГИЧЕСКОЙ БЕЗОПАСНОСТИ

**Аннотация.** Обоснована необходимость предоставления результатов научных исследований в форме, доступной для правильной интерпретации общественностью и экспертами в сфере экологической безопасности. В качестве примера была доказана безопасность миксомицетов для здоровья человека, путем анализа особенностей их экологии и метаболизма. Для оценки рисков предложено использовать Байесовские методы анализа вероятности возникновения угроз. Рекомендовано внедрение «Паспортов экологической безопасности видов» для оценки воздействия каждого вида на окружающую среду, человека и другие живые организмы.

**Ключевые слова:** экологическая безопасность, оценка рисков, миксомицеты, экологический паспорт.

## Protection of Building Materials Against Biodeterioration Using Energy Saving Nanotechnology

*Nataliya Zhuravska*

Kyiv National University of Construction and Architecture  
Povitroflotskyy prosp., 31, Kyiv, Ukraine, 03680, e-mail: nzhur@ua.fm

**Summary.** The advances in energy-efficient nanotechnologies in construction has been considered. The harmful effects of building materials, the impact of pollution in violation of indoor climate on human activity have been analyzed. The author has proposed a hypothesis that has been confirmed for using the method of concrete protection from biological damage.

**Key words:** nanotechnology, biological damage, concrete strength, indoor climate, life safety.

taking into account the examined further problems.

### INTRODUCTION

High rates of urban development requires a recovery, "wellness" works for buildings conservation, with safe conditions for people's life, using effective ways of dealing with biodeterioration of building materials and structures. Energy saving nanotechnologies allow to solve these tasks.

Nanotechnologies are developing very rapidly in construction. From a present-day perspective nanoscience is the creation of nanomaterials and nanosystems, modification of objects that include components with size less than 100 nm in at least one dimension [9]. Energy saving nanotechnologies are aimed at creating more durable, affordable building materials of interest,

### THE MAIN PART

The European citizens spend more than 90% of their time in a confined space. More than 40% of people in enclosed spaces complain of the worsening state of health and various inconveniences (European Construction Technology Platform, 2005). Scientific studies have shown that the deformation process of nonmetallic building materials such as concrete, plaster, dry mixes of different origin is connected with the action of microorganisms. These structures damage is caused by the influence of microorganisms leading to a synergy of different types of corrosion.

Microbiological corrosion of concrete is found in residential and industrial buildings. The external manifestations of damage of building materials, products and designs by microorganisms are blistering, cracking, delamination of entire fragments of plaster,

on the floor, ceiling and walls the presence of dark spots (Fig. 1, 2). Often these phenomena are accompanied by a variety of climatic conditions (high humidity, temperature extremes). Air pollution can cause respiratory and cardiovascular



**Fig. 1.** The microbiological corrosion in industrial building



**Fig. 2.** The microbiological corrosion in residential building

diseases, cancer, premature birth, increased infant mortality, neurological and psychiatric disorders, decreased immunity. 72% of residents of contaminated areas suffer from chronic bronchitis, diseases of the respiratory system. There is a clear link between air pollution and extensive myocardial infarction [9].

For prevention and creating a safe environment it is necessary to:

- reduce consumption of energy and material resources throughout the life cycle of buildings and structures, ranging from the manufacture of materials for buildings (based on strength increase) and materials biodegradation problems, site selection and further during design, construction and operation (creation of microclimate conditions, including in the working area of buildings and structures),

- expand and complement the classical building design with concepts of saving, serviceability, durability, impact on the environment and human health due to the resource saving (electricity, water and other resources usage taking into account progressive methods, including nanotechnologies as well),

- use innovative approaches, software (Autodesk, Graphisoft) effectively for various tasks, in particular, the calculation and optimization of the environmental buildings profiles already at the early stages of architectural design.

At residential, public and industrial buildings and structures, agricultural buildings, meat and dairy and livestock complexes the use in the operation of too high or low indoor temperatures, humidity, lighting, air quality (carbon dioxide, smoke, hazardous fine and coarse particles, dangerous radiation, microorganisms, etc.), noise, allergens, harmful gas, the improper disposal of waste water (Fig. 3), a solid or liquid waste have a detrimental effect. They are dangerous to human health and adversely affect the quality components in the operation of building materials [8, 15, 16].

The adverse effect on the human body is caused by a set of interactions between the material, environment and man, according to the dynamics of possible current state of relations "environment-man" [9, 11].

About 20% of the European citizens have an allergic reaction to the mites and lower fungi (caused by biodegradation of materials and structures, and others.). The dominance

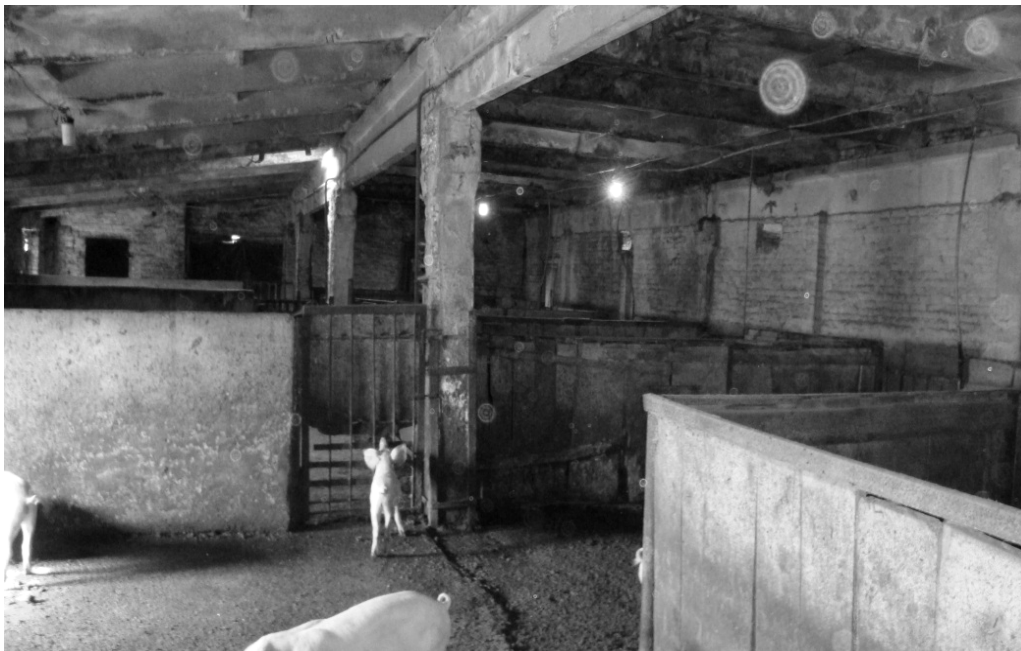


**Fig. 3.** Biological corrosion in animal farm

of asthma and allergies in residential buildings is also increasing [17, 18]. In Europe one of seven children suffers from asthma and in Western Europe the number of such children is ten times higher than in Eastern Europe (European Construction Technology Platform 2005). The main factors of concrete deterioration or corrosion are the environmental effect, aggressive atmosphere, changes of the indoor climate. At the same time the main threat to concrete is the same thing that contributes to concrete hardening – water and gas. Today it is accepted to distinguish several types of concrete corrosion depending on the characteristics of its triggering processes [7, 13, 10].

Chemical corrosion of concrete is most widely spread. Most often it is caused by the interaction of the surface layers of the concrete with atmospheric moisture and carbon dioxide contained in the air. Ensuring an effective response to biological corrosion of various building materials, products and structures caused by the vital activity on them or in them of various microbes and fungi [14], is becoming more and more acute scientific and practical problem in the field of construction and operation of residential and industrial buildings and structures (biological corrosion). Currently, more than 40...50% of the total number of recorded in the world injuries are related to the activity of micro-organisms [13].

In Kiev National University of Construction and Architecture various buildings, including recently renovated ones, have been examined for over 17 years. They have shown that 80...90% of buildings are struck by various organisms, bacteria, protozoa and other microscopic fungi, algae, lichens and even higher plants. Inside many buildings (hospitals, kindergartens, schools, institutions state) the pollution of the area with, for example, a variety of microscopic fungi (micromycetes) exceeds ten or over hundred times the maximum permissible limits, if you focus on the regulations of the European Union. Microscopic fungi tend to degrade the performance of construction

materials, on which they grow, causing the biological damage and biodegradation of the latter. They can cause mycetogenic allergy, mycoses, mycotoxicosis and other diseases. Everything is connected with high risk to human health and life in general [8, 9, 12].

The possibility of concrete corrosion is determined by its initial porous structure and the presence in it of so-called capillaries on which the moisture and other substances can penetrate into concrete causing destructive processes. Therefore, the main task to prevent or stop concrete corrosion is to protect its pores from potentially harmful elements. This can be done at various stages, including using nanotechnologies.

Measures of protection against corrosion can be divided: passive and active. Passive protection measures are intended to protect concrete from the damaging effects of harmful carriers (application of coatings and leveling compounds, synthetic lining films and plates, the use of energy-efficient nanotechnologies (magnetic water) to increase concrete strength and biological stability during production) [13]. Special protective additives for water resistance and high density concrete structure may also be included in its composition at the time of manufacture. The technology of concrete manufacture may include the addition of special protective layers, providing it with additional protection, and after its manufacture processing its surface with special hydraulic, vapor and gas barrier compositions, applying the protective coating (membrane) by sputtering products against bacteria, mold and other microorganisms. The goal of active protection measures is to minimize the conditions leading to the formation of harmful carriers (compliance with indoor climate requirements (ventilation, drying, waterproofing buildings, monoblock devices out letting condensate, mechanical cleaning and etc.).

Active researches on the use of various nanomodifiers in the production of concrete are of much interest for developers. The obtained results show a significant increase in consumer characteristics, such as strength,

PROTECTION OF BUILDING MATERIALS AGAINST BIODETERIORATION  
USING ENERGY SAVING NANOTECHNOLOGY

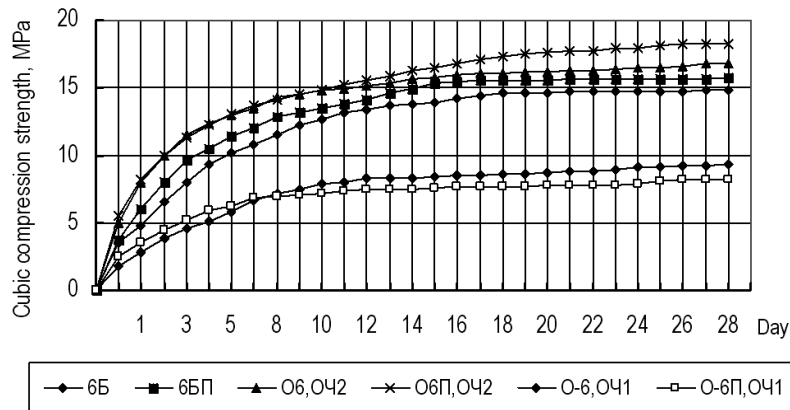


**Fig. 4.** The dependence of the strength of concrete samples series "6" on time: Series "6" W/C = 0,76; 6БП, 6Б – samples prepared by classical technology, respectively using steaming and without it; 6ОП, ОЧ1; 6ОП, ОЧ2; 6О, ОЧ1; 6О, ОЧ2 – samples prepared using magnetic water respectively using steaming and without it; ОЧ1, ОЧ2 – installation modes with different characteristics

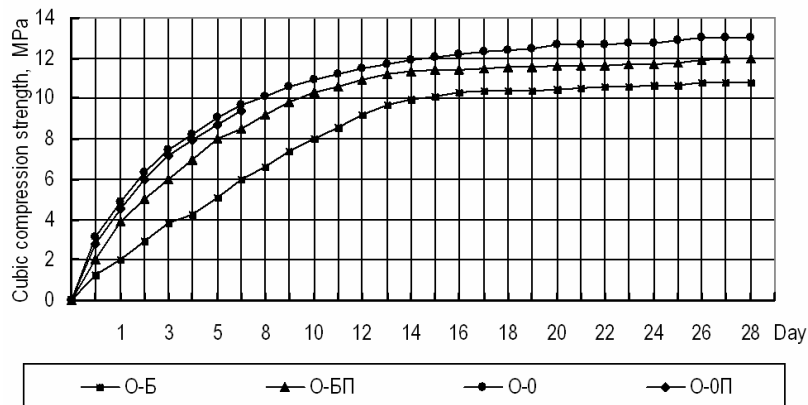


**Fig. 5.** Dependence of the strength of concrete samples Series "O" on time: Series - "O", W/C = 0,77 (with a broken structure of cement); ОЧ2 – setting mode; О-БП; О-Б – samples prepared by classical technology, respectively, using steaming and without it; О-0П; О-0 - samples prepared using magnetic water, respectively, using steaming and without it

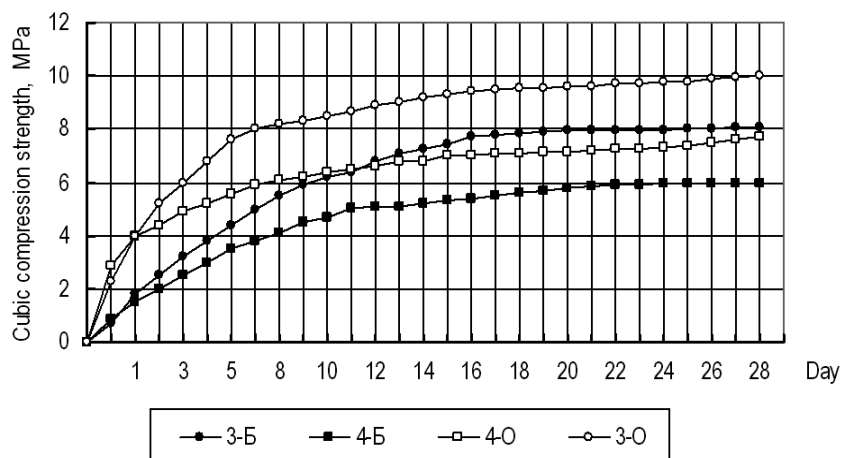


**Fig. 6.** Dependence of the strength of concrete samples Series "3" and "4" on time: Series - "3", W/C = 0,66; 3-Б – samples prepared by classical technology; 3-0 – samples prepared using magnetic water (ОЧ2 – setting mode), Series - "4", W/C = 0,74 (with addition of bischofite 0,14%); 3-Б – samples prepared by classical technology; 3-0 – samples prepared using magnetic water (ОЧ2 – setting mode)

from 10...20%, fracture resistance of concrete blocks energy to fracture, its hardening acceleration (Fig. 4, 5, 6). Energy saving nanotechnologies help considerably save energy resources, reducing the time spent on grinding clinker [9].

Currently the technology based on the practical implementation of biocidal materials (Kimry city) is quite widely applied. Our energy-efficient nanotechnologies thanks to the ultra small particle size reach the high strength and resistance of the coating to external influences to maintain the indoor climate. On the basis of biochemical method the technology of synthesis of silver nanoparticles with a broad spectrum of antimicrobial action, etc. has been created.

The kinetics, mechanism and nature of materials hardening are complicated and the action of magnetic water treatment is shown not only in the process of samples setting and strength development, but also in the quality of obtained products [19]. According to industrial tests, the strength of concrete and other building materials has growing by 10...30% (We take into account this fact in recommendations for biodeterioration mitigation of building materials, products and structures during their operation). It becomes possible to reduce the consumption of cement and water during manufacture [20].

1962, the USSR, B.A. Neiman – the beginning of magnetic water application in the production of concrete in construction. Now magnetic water is used by the leading manufactures of concrete, cement, plaster, tiles using gypsum binders.

The effectiveness of water treatment by the magnetic field, starting from the first devices of the Belgian company EPURO brand Capi, is determined largely by the magnetic field intensity in the gap, water velocity, the angle between the water directions and the magnetic field lines, and the number of intersections and the contact time of water with magnetic field.

It is described in literature that the initial use of magnetic water contributes to the intensity of the components interaction,

which leads to the reduction of the manufacturing processes and increase in the products strength [3]. Since the process with ordinary water can be insufficiently effective, our goal is to develop technologies to activate this process by the method of using magnetic water.

According to current scientific hypotheses [1, 2, 3, 4, 14], the magnetic field affects the water molecules. There is a spin flip of protons of these molecules' nuclei with the release of the molecular energy. This leads to water clusters destruction and turns magnetic water into liquid with unbalanced H<sub>2</sub>O molecules that tend to interact with other active substances. Due to the small size of the monomolecules, this leads to a strong speed growth of diffusion processes of such water transfer, including in ultramicropores capillary-porous bodies, in which ordinary water can not penetrate.

The hypothesis about nanotechnologies is used by the author to solve the problem of concrete biodeterioration as a capillary-porous body. For this a series of experiments have been conducted and 150 samples of cubes have been analyzed.

The author investigated and presented (Fig. 4, 5, 6), the samples with dimensions 70x70x70, series "6", "O", "3", "4". The magnetic water was prepared during the tap water flow through the pipeline using magnets "Ilios-M", company "Votali", Donetsk. The filed characteristics were 230...430 mT operating at setting mode: cleaning – 1, 2 (OЧ1, OЧ2 – with different service programs).

Samples in the forms of cubes were prepared in batches (with or without steaming (up to 28 days.) The steaming chamber was used for steaming ( $t = 80^{\circ}\text{C}$ ,  $\tau = 6 \text{ h}$ ).

The determination of the samples compression breaking strength was performed on the press in accordance with current standards.

On the 7...11th day samples prepared with the magnetic water (characterized by decreased pore structure uniformly distributed in the material) gain strength

while the samples with ordinary water – on the 28th day. On the 7th date the strength of the samples prepared with the magnetic water is 20...40% more than the strength of samples prepared with ordinary water. The samples prepared with the use of magnetic water on the 14th day gain strength equal to the strength of the samples with steaming with ordinary water on the 28th day. On the 28th day the strength of the samples prepared with magnetic water is 7 ... 12% more than that of the samples prepared with plain water. Further series of experiments on the physico-chemical characteristics of concrete are planned.

## CONCLUSIONS

Our studies confirm the practicability of the magnetic water use as an activator in the production of construction materials, which will let use energy-efficient nanotechnologies in the production. This requires a deep study of complex physical and chemical systems, which is scheduled by the author in the following series of experiments.

## REFERENCES

1. **Minenko V.I. 1970.** Magnetic treatment of water-dispersed systems. Technika, 168.
2. **Klassen V.I., 1973.** Water and magnet. Moscow, Publishing House Nauka, 112.
3. **Stukalov P.S., Vasiliev E.V., Glebov N.A. 1969.** Magnetic Water Treatment. Leningrad, Publishing House Sudostroitel-stvo, 192.
4. **Pople I.A. 1951.** Molecular association in liquid II. A theory of the structure of water, Proc. Roy. Soc., Vol. A250, No 1081, 163-178.
5. **Ivanov F.M., Gorshin S.N., Waite J. et al 1984.** Biodegradation in the Construction. Ed. By. F M. Ivanov, S.N. Gorshina, Moscow, Stroyizdat, 320.
6. **National** report on the state of environment in Ukraine in 2010, **2011.** Kyiv, Center for environmental education and information, 254.
7. **Figovski O., Magarshak Y. 2005.** Objectives of mankind in the coming millennium. Environmental and human health. Protection of air and water. Waste disposal: in 2 Vol. Vol.1, Collection of scientific articles to the XIII international Scientific-Practical Conference. Kharkov, Rayderukrgntts Energostal, 360.
8. **Zhuravskaya N.E. 2014.** Ways to create a safe environment for human life. Human environment: natural, technological, and social. Materials to the iii international scientific-practical conference of students and young scientists. Bryansk, Publishing house BGITA, 122-124.
9. **Zhuravska N.E. 2014.** The question of biodeterioration of concrete and reinforced concrete. Resource saving materials, structures, buildings and structures. Collection of scientific works. Vol. 28, Rivne, NUVGP, 181-187.
10. **Krilenkov V.A., Vlasov D.Y., Dashko R.E., Elders S.A. 2003.** Problems of preservation of residential and industrial infrastructure of the cities from biodegradation. Infstroy, No 5, 3-13.
11. **Andreyuk B.I., V.I. Bilan, Z.Z. Koval, I.A. Kozlova. 1980.** Microbial corrosion and its pathogens. Kyiv, Naukova Dumka, 184.
12. **Tsublova E.G. 2013.** Research of biodestructors' communities in urban ecosystems. Biosphere compatibility: people, region, technology, No 4, 83-86.
13. **Malkyn E.S., Furtat I.E., Zhurav-skaya N.E., Usachyov V.P. 2014.** Prospects for resource saving technologies through magnetic treatment of water and aqueous solutions. Ventilation, lighting and heat. NTRP, Ed. 17, Ed. E.S. Malkin. Kyiv, KNUBA, 120-127.
14. **Dorfman Y.G. 1955.** Magnetic properties and structure of the substance. Moscow, State publishing house technical and technical literature, 377.
15. **Kovtun G.L., Veryovkin A.L. 2010.** Nanomaterials: Materials Science and Technology: Overview. Kharkov, KIPT, 73.
16. **Middendorf B., Singh N.B. 2007.** Research and technology of cement and materials based on it at the nanoscale. Building Materials, No 1, 50 - 51.
17. **Belichenko E.A., Tolmachev S.N., Misko T.M., Duka A.G. 2011.** Effect of carbon nanoparticles on the properties of extruded cement-sand concrete. Concrete and reinforced concrete in Ukraine, No 6, 2 - 8.
18. **Novitskiy A.V., Banniy O.M. 2011.** Analiz

nadiynosti zasobiv dlya prigotuvannya i rozdavannya kormiv metodoi dereva vidmov. Motrol. Motoryzacja i energetyka rolnictwa. Vol. 13B, Lublin, 117-124.

19. **Pezarski F. 2011.** Innowacyjna technologia produkcji bentonitu odlewniczego z wykorzystaniem wyselekcjonowanych frakcji powstajacych przy wytwarzaniu sorbentow. Motrol. Motorization and power industry in agriculture, Vol. 13. Lublin, 269-280.
20. **Punagin V. 2013.** Study of structural stresses in the monolithic concrete of natural hardening. TEKA: kom. Mot. Energ. Roln., OL PAN, Vol. 13, No 4, 201-207.

## ЗАЩИТА СТРОИТЕЛЬНЫХ МАТЕРИАЛОВ ОТ БИОПОВРЕЖДЕНИЙ С ИСПОЛЬЗОВАНИЕМ ЭНЕРГОСБЕРЕГАЮЩИХ НАНОТЕХНОЛОГИЙ

**Аннотация.** Рассмотрены достижения энергосберегающих нанотехнологий в строительстве. Проанализированы вредные воздействия строительных материалов, влияние биологического загрязнения вследствие потенциально возможного биологического оброста на жизнедеятельность человека. Автором предложена гипотеза, которая нашла подтверждение для использования метода защиты бетона от биоповреждений.

**Ключевые слова:** энергосберегающие нанотехнологии, биологическое обрастание, прочность бетона, биологические загрязнения, безопасность жизнедеятельности.

## Table of contents

<b>Petro Kulikov, Vitaliy Ploskiy, Volodymyr Skochko</b> The principles of discrete modeling of rod constructions of architectural objects.....	3
<b>Valery Chybiryakov, Anatoly Stankevich, Dmitro Levkivskiy, Volodymyr Melnychuk</b> Application of generalized “method of lines”, for solving problems of thermoelasticity of thick plates.....	11
<b>Victor Bazhenov, Sergii Pyskunov</b> A finite element technique and results of continual fracture process modeling.....	21
<b>Victor Bazhenov, Sergii Pyskunov, Oleksiy Shkryl</b> Modeling of crack growth process in spatial bodies under cyclic loading condition.....	29
<b>Volodymyr Sakharov, Veronika Zhuk, Liudmyla Skochko</b> Interaction study of the frame building with foundation weakened by the underground mines under the seismic load.....	37
<b>Dmytro Smorkalov</b> Calculation of deflection of one- and two-layer slabs supported on four sides.....	45
<b>Pavel Krivenko</b> Progress in cement science - why alkaline activation?.....	55
<b>Kateryna Pushkarova, Maryna Sukhanevych, Kateryna Bondar</b> Penetrability waterproofing mortar based on slag-contain compositions, modified by zeolites.....	67
<b>Maksym Klys</b> Analysis of space planning and design decisions modern cottage.....	73
<b>Roman Schultz, Andriy Annenkov, Andriy Khailak, Valentyna Strilec</b> Statistical research of retaining walls displacement on the results of geodetic measurements by analysis of variance.....	81

<b>Mykhailo Sukach</b>	
Spiral method of concretion mining from the bottom waters.....	95
<b>Arthur Onischenko, Mykolay Kuzminets, Sergiy Aksenov</b>	
Analysis of modified bitumen difference polymers.....	101
<b>Vjacheslav Lovejkin, Yuriy Chovnyuk, Yuriy Romasevich</b>	
Optimization of motion regimes for machines and mechanisms with a mehatronics' control.....	107
<b>Leonid Pelevin, Mykola Karpenko</b>	
The hydraulic quencher dynamic vibrations.....	119
<b>Olena Voloshkina, Julia Bereznitska</b>	
Development of Ukraine territory flooding processes; Its parameters and the influence on the environmental safety level.....	127
<b>Tetiana Kryvomaz, Olena Voloshkina</b>	
The risk assessment of threats from biological objects in environmental safety.....	137
<b>Nataliya Zhuravskaya</b>	
Protection of building materials against biodeterioration using energy saving nanotechnology.....	145

## LIST OF THE REVIEWERS

1. Andriy Babenko
2. Sergiy Bilyk
3. Vitaliy Chernenko
4. Yuriy Doroshenko
5. Viktor Gaydaychuk
6. Olexander Gondlyakh
7. Iryna Klimova
8. Volodymyr Kovbasa
9. Olexander Marchuk
10. Ivan Nazarenko
11. Vitaliy Ploskiy
12. Raisa Runova
13. Leonid Sheinich
14. Olexander Trofimchuk
15. Stepan Voytenko

Editors of the “MOTROL” magazine of the Commission of Motorization and Power Industry in Agriculture would like to inform both the authors and readers that an agreement was signed with the Interdisciplinary Centre for Mathematical and Computational Modelling at the Warsaw University referred to as “ICM”. Therefore, ICM is the owner and operator of the IT system needed to conduct and support a digital scientific library accessible to users via the Internet called the “ICM Internet Platform”, which ensures the safety of development, storage and retrieval of published materials provided to users. ICM is obliged to put all the articles printed in the “MOTROL” on the ICM Internet Platform. ICM develops metadata, which are then indexed in the “Agro” database.

Impact factor of the “MOTROL” journal according to the Commission of Motorization and Energetics in Agriculture is 1,41 (Vol.16, No. 8).

## GUIDELINES FOR AUTHORS (2014)

The journal publishes the original research papers. The papers (min. 8 pages) should not exceed 12 pages including tables and figures. Acceptance of papers for publication is based on two independent reviews commissioned by the Editor.

Authors are asked to transfer to the Publisher the copyright of their articles as well as written permissions for reproduction of figures and tables from unpublished or copyrighted materials.

**Articles should be submitted electronically to the Editor and fulfill the following formal requirements:**

- Clear and grammatically correct script in English,
- Format of popular Windows text editors (A4 size, 12 points Times New Roman font, single interline, left and right margin of 2,5 cm),
- Every page of the paper including the title page, text, references, tables and figures should be numbered,
- SI units should be used.

**Please organize the script in the following order (without subtitles):**

Title, Author(s) name (s), Affiliations, Full postal addresses, Corresponding author's e-mail

Abstract (up to 200 words), Keywords (up to 5 words), Introduction, Materials and Methods, Results, Discussion (a combined Results and Discussion section can also be appropriate), Conclusions (numbered), References, Tables, Figures and their captions.

Note that the following should be observed:

An informative and concise title; Abstract without any undefined abbreviations or unspecified references; No nomenclature (all explanations placed in the text); References cited by the numbered system (max 5 items in one place); Tables and figures (without frames) placed out of the text (after References) and figures additionally prepared in the graphical file format jpg or cdr.

Make sure that the tables do not exceed the printed area of the page. Number them according to their sequence in the text. References to all the tables must be in the text. Do not use vertical lines to separate columns. Capitalize the word 'table' when used with a number, e.g. (Table I).

Number the figures according to their sequence in the text. Identify them at the bottom of line drawings by their number and the name of the author. Special attention should be paid to the lettering of figures – the size of lettering must be big enough to allow reduction (even 10 times). Begin the description of figures with a capital letter and observe the following order, e.g. Time(s), Moisture (% vol), (% m<sup>3</sup>m<sup>-3</sup>) or (% gg<sup>-1</sup>), Thermal conductivity (W m<sup>-1</sup>K<sup>-1</sup>).

Type the captions to all figures on a separate sheet at the end of the manuscript.

Give all the explanations in the figure caption. Drawn text in the figures should be kept to a minimum. Capitalize and abbreviate 'figure' when it is used with a number, e.g. (Fig. 1).

Colour figures will not be printed.

Make sure that the reference list contains about 20 items. It should be numbered serially and arranged alphabetically by the name of the first author and then others, e.g.

7. Kasaja O., Azarevich G. and Bannel A.N. 2009. Econometric Analysis of Banking Financial Results in Poland. Journal of Academy of Business and Economics (JABE), Vol. IV. Nr 1, 202–210.

References cited in the text should be given in parentheses and include a number e.g. [7].

Any item in the References list that is not in English, French or German should be marked, e.g. (in Italian), (in Polish). Leave ample space around equations. Subscripts and superscripts have to be clear. Equations should be numbered serially on the right-hand side in parentheses. Capitalize and abbreviate 'equation' when it is used with a number, e.g. Eq. (1). Spell out when it begins a sentence. Symbols for physical quantities in formulae and in the text must be in italics. Algebraic symbols are printed in upright type.

Acknowledgements will be printed after a written permission is sent (by the regular post, on paper) from persons or heads of institutions mentioned by name.